

5. RESEARCH ACTIVITIES

5.1 NUCLEAR PHYSICS

During last year, the Charged Particle Detector Array (CPDA) at IUAC has been extensively used in coincidence with GDA for the study of reaction dynamics for Complete Fusion and Incomplete Fusion reactions. It has been observed in the reaction $^{16}\text{O} + ^{169}\text{Tm}$ at 90 MeV that the spin distribution of (αxn) and ($2\alpha xn$) channels in coincidence with fast α -particles emitted in forward direction are significantly different from the spin distributions observed from the equilibrated compound nucleus. The yields for residues in coincidence with fast α -particles are constant up to $J \sim 10\hbar$ and then fall off with higher spin, indicating the absence of side-feeding to the lowest members of the yrast band. In contrast, the same residual nuclei in coincidence with α -particles emitted in the backward direction show an exponential fall with high spin states.

In order to understand the population of yrast band as a function of the entrance channel angular momentum, the reaction $^{12}\text{C} + ^{169}\text{Tm}$ has been studied in the energy range 55-90 MeV. As expected, the relative population of high spin states for the ^{177}Re ($4n$) fusion-evaporation channel increases with increasing bombarding energy. The spin distributions at all energies show an exponential fall off with spin, indicating the importance of side-feeding for Complete Fusion reactions.

High spin states of ^{129}Cs , ^{135}Ba and ^{141}Nd have been studied using GDA. In some of the experiments, a Clover detector was used at $\sim 90^\circ$ in coincidence with HPGe detectors for polarization measurements.

The energy and angular distribution of neutrons produced in the fission of ^{228}U have been studied in the reaction $^{19}\text{F} + ^{209}\text{Bi}$ near the barrier. Pre- and post-scission component of neutron multiplicity and the mass distribution of fission fragments have been extracted. The compound nucleus $^{200}\text{Pb}^*$ has been populated in two reactions $^{16}\text{O} + ^{184}\text{W}$ and $^{19}\text{F} + ^{181}\text{Ta}$ near the barrier. Spin distribution of the residual nuclei have been measured to study the entrance channel effect on fission-hindrance.

The role played by transfer channels in sub-barrier fusion enhancement is an open question. Fusion excitation function and the angular distribution of fusion-evaporation residues for the reaction $^{40}\text{Ca} + ^{70}\text{Zn}$ have been measured near the barrier. Direct detection of transfer channels using HIRA was unsuccessful due to poor beam rejection.

The importance of breakup channel in near-barrier fusion enhancement has been studied using the radioactive ^7Be beam from HIRA. Elastic scattering angular distribution for $^7\text{Be} + ^9\text{Be}$ and $^7\text{Li} + ^9\text{Be}$ have been measured at various bombarding energies. The elastic scattering cross sections for the two systems were found to be of comparable magnitude at same $E_{\text{cm}}/V_{\text{B}}$. Similar set of optical potential parameters gave reasonably good description of elastic scattering angular distributions for both the systems. The extracted fusion cross section σ_{fusion} for the system $^7\text{Li} + ^9\text{Be}$ was significantly smaller than the corresponding total reaction cross section reaction.

Two collaborative experiments have been carried out at GSI this year for the study of neutron-rich nuclei. The B(E2) values of shell model calculations for the even Sn isotopes $^{102-130}\text{Sn}$ show a parabolic trend which agrees well with the experimental measurements for heavier Sn iso-

topes. For lighter Sn isotopes ($A = 114$), the $B(E2)$ values deviate significantly from this systematics but have large error bars. Coulomb excitation of ^{114}Sn beam of 3.4 MeV/A at GSI on a ^{58}Ni target has been measured experimentally by detecting the Doppler-broadened γ -rays in coincidence with the target/projectile like fragments. Clover electronics developed at IUAC were used in this experiment with super-Clover detectors. A complementary Coulomb-excitation experiment at IUAC using a ^{58}Ni beam on enriched Sn targets is planned later this year. A scattering chamber for the detection of back-scattered Ni in coincidence with γ -rays in the GDA setup has been developed.

For the study of β -decay of stopped radioactive beams at GSI, a double-sided Si-strip detector has been developed as an active stopper. A fast fragment implant will deposit more than 1 GeV energy in the detector, while an emitted β -particle would deposit less than 1 MeV in the same detector. In beam test of the setup at GSI indicates that both the implanted radioactive beam and the β -particles associated with the decay of the beam could be identified.

A large-basis shell model program has been developed for the study of the properties of nuclei in the sd-shell region. The behaviour of $T=0$ and $T=1$ pairing as a function of spin and temperature has been studied using this program. Unlike mean-field theories of pairing where the correlations tend to vanish above a critical spin, a smooth transitional behaviour has been observed in the present approach. The correlations derived in the neighbouring even-even, odd-mass and odd-odd systems are observed to be quite similar.

It is planned to setup a facility at IUAC for the study of g -factors of high-spin states using Transient Magnetic Field technique. To study the feasibility of using inverse kinematics to produce the heavy recoils at energies above 2 MeV/A, we have carried out an experiment to measure the life times of states in ^{75}Br using the reaction $^{51}\text{V} + ^{27}\text{Al}$ at 150 MeV. The extracted lifetimes are comparable to the values obtained by using conventional method.

The mechanical structure for holding the Clover detectors in INGA setup at beam hall II is currently under construction. All the detectors with anti-Compton shields have been received and commissioned. Adequate number of Clover electronics and spectroscopy ADCs are under fabrication. The array is expected to be commissioned by the end of this year.

The Recoil Separator HYRA has now been tested in beam. In the reaction $^{16}\text{O} + ^{197}\text{Au}$ at 100 MeV, the beam rejection improved from $4 \cdot 10^6$ (vacuum mode) to 10^9 after introduction of 0.5 Torr of He gas in the magnet. In a separate experiment, ^{204}Fr recoils produced in the reaction $^{27}\text{Al} + ^{181}\text{Ta}$ at 148 MeV were detected at the focal plane. Apart from the recoils, 7 MeV α -particles from the α -decay of ^{204}Fr could also be detected in the focal-plane detector. Further tests are planned to correlate the α -particles with the corresponding recoils.

The NAND neutron array with provision for mounting up to 48 neutron detectors at a distance of 2 m from the target has been commissioned. The target is mounted inside a spherical scattering chamber of 60 cm diameter. A feasibility run has been carried out to study fusion-fission reaction dynamics using neutron array set up. Fission fragments were detected in two large area position sensitive MWPCs placed at folding angle. Neutron time of flights was measured in 16 neutron detectors. Currently the time of flight resolution is limited by the beam pulse width of $\sim 2\text{ns}$ which can be improved below $\sim 500\text{ps}$ with the installation of the rebuncher in the beam line.

5.1.1 High Spin States in ^{129}Cs

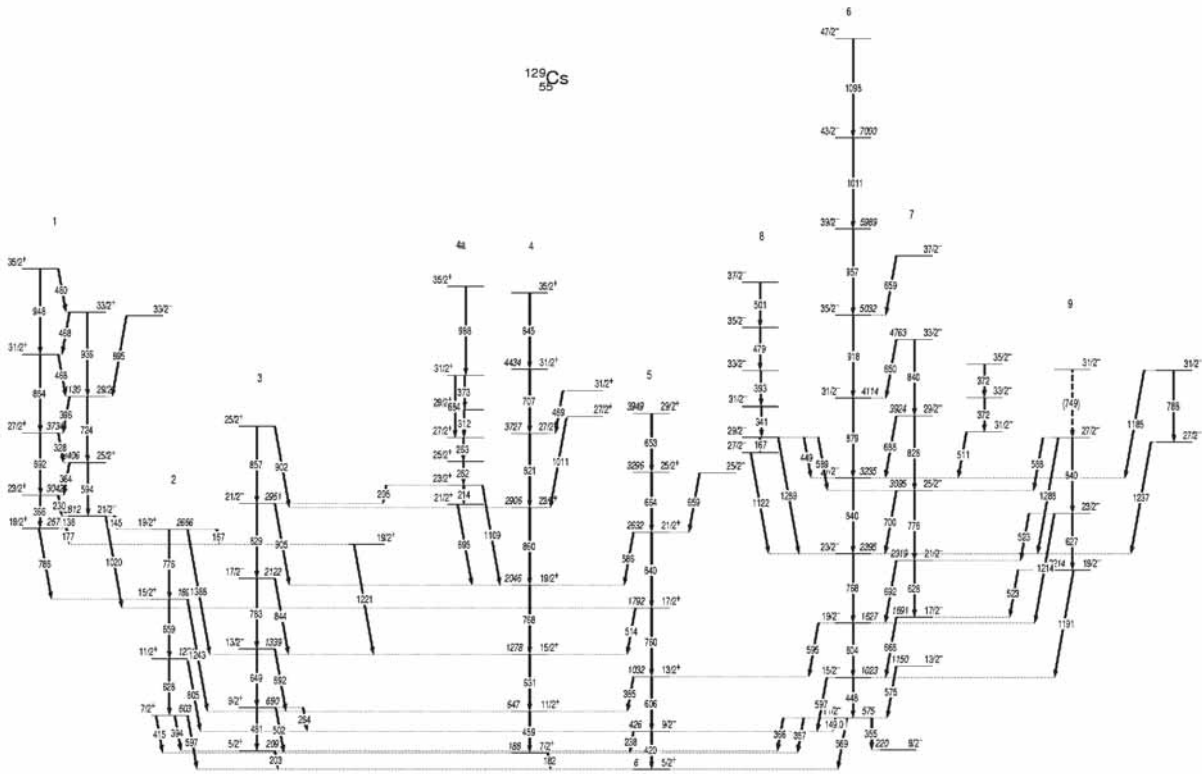
S. Sihotra¹, Kuljeet Singh¹, J. Goswamy², D. Mehta¹, Nirmal Singh¹, Rakesh Kumar³, S. Muralithar³, R.P. Singh³, R.K Bhowmik³

¹Department of Physics, Panjab University, Chandigarh - 160 014

²UIET, Panjab University, Chandigarh 160 014

³Inter-University Accelerator Centre, Aruna Asaf Ali Marg, New Delhi 110 067

The $_{55}\text{Cs}$ nuclei are expected to display a rich variety of band structures as the deformation remains well-developed across a large range of the neutron Fermi surface. For the odd-Z nuclei, the shape at low rotational frequencies is mainly influenced by the valence quasiproton. At higher frequencies, additional rotationally-aligned $\nu(h_{11/2})^2$ quasiparticles are expected to polarize the γ -soft core depending upon the position of the neutron Fermi surface in the $h_{11/2}$ shell. The triaxial deformation in this mass region has been evidenced by the interpretation of observed crossing frequencies, staggering behavior and $\Delta=1$ doublet bands, which have been explained in the manifestation of chirality. Chiral bands has been observed in various odd-A and odd-odd nuclei with multi-quasiparticle configurations that have substantial angular momentum components along the three principal axes. Another important feature is the magnetic dipole bands generated through the shear mechanism and have also been reported in the odd-A ^{131}Cs and doubly-odd ^{132}Cs isotopes. In continuation to our earlier investigations in this region [1, 2], we have done experiment to study high spin states in ^{129}Cs nuclei.



High spin states in ^{129}Cs populated in the fusion-evaporation $^{122}\text{Sn} (^{11}\text{B}, 4n)$ reaction at $E_{\text{lab}} = 55, 60$ and 63 MeV, respectively, have been investigated through in-beam g-ray spectroscopic techniques. The ^{11}B ion beam was delivered by the 15UD Pelletron accelerator at Inter-University Accelerator Centre (IUAC), New Delhi. The target, ^{100}Sn , had a backing of 12mg/cm^2 Pb, in order to stop the recoiling nuclei without stopping the evaporated charged particles. The emitted g-rays were detected using the Gamma Detector Array (GDA) equipped with 8 Compton suppressed Ge detectors and a 14-element BGO multiplicity filter. The Ge detectors were mounted in three groups of four each making angles of 45° , 90° and 153° with the beam direction and having an inclination of $\pm 23^\circ$ with the horizontal plane. A total of 300 million events were collected for the reaction $^{122}\text{Sn} (^{11}\text{B}, 4n)$. The data were subsequently sorted offline using INGASORT program to produce a symmetrized $4k \times 4k$ matrix of Eg vs Eg. RADWARE graphical-analysis package is being used to establish coincidence and intensity relationships for various gamma transitions. The preliminary level scheme obtained from the analysis done so far is shown in fig.1 with the band structures labeled 1-9. The new bands 4a, 8 and 9 have been established while band 1 is modified by adding more new transitions. The earlier level scheme of ^{129}Cs [1] has been extended substantially.

The support of Pelletron Scientific and technical staff at IUAC and financial support from UGC, CSIR (India) are duly acknowledged.

REFERENCES

- [1] L.Hildingson et al., Z.Phys.A-Hadrons and nuclei 340,29-33 (1991)
 [2] Y.Liang et al., Physics Review C42,890-901 (1990)

5.1.2 Low and Medium Energy States in ^{141}Nd

Samit Bhowal¹, Rajarshi Rout², A.Goswami², Sudeb Bhattacharya², S.Muralithar³, G.Gangopadhyay⁴

¹Surendranath Evening College, 24/2 M.G. Road, Kolkata-9

²Saha Institute of Nuclear Physics, Block-AF, Sector 1, Bidhan Nagar, Kolkata-64

³Inter University Accelerator Centre, Aruna Asaf Ali Marg, New Delhi 110067.

⁴University College of Science, University of Calcutta, 92 A.P.C Road, Kolkata-9.

Nuclei near closed shell display a variety of excitation mechanisms. Single particle structures exist side by side with collective excitations. A number of nuclei near $N=82$ shell closure has been under investigation in recent years. Particular attention has been given to Nd nuclei with evolution from single particle structure to stable triaxiality observed in ^{139}Nd [1] and ^{140}Nd [2]. Triaxiality is difficult to prove experimentally. One unambiguous signature of triaxiality is the existence of wobbling mechanism at high spins. However, in ^{141}Nd , even the low energy structure is almost completely unknown. Thus, it is very important to first study the structure of this nucleus at low and medium excitation energy.

The present experiment was done at the 15UD Pelletron accelerator of Inter University Accelerator Centre in which we used 80 and 85 MeV ^{16}O beam to irradiate a target of ^{130}Te

(~1.5 mg/cm² thickness) with 5 mg/cm² gold backing. The target was prepared in SINP, Kolkata. The gamma-gamma coincidence spectra were taken using a modest array of nine HPGe detectors and a CLOVER detector and a multiplicity ball of fourteen BGO elements. The beam energy was decided upon doing an excitation function study. Data was collected for about one hundred hours. Approximately 15 million good events were recorded.

The analysis of the acquired data is in progress. The analysis packages INGASORT, RADWARE and CANDLE has been used. Preliminary results indicate the existence of a number of possible new bands. Already more than 25 new gamma rays has been placed in the level scheme. A partial level scheme is shown in figure 1.

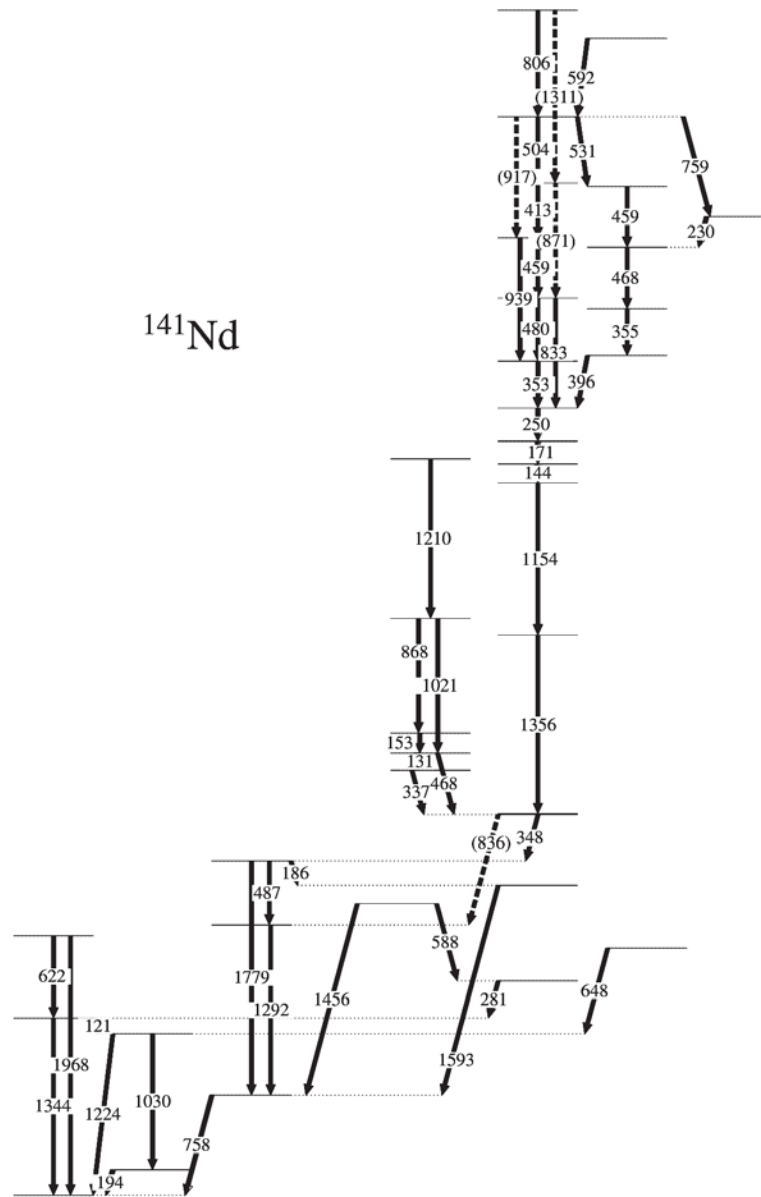


Fig. 1. Partial level scheme of ¹⁴¹Nd

REFERENCES

- [1] C.M. Petrache et al, Phys. Rev. C 61, 011305 (R) (1999)
[2] C.M. Petrache et al, Phys. Rev. C 72, 064318 (2005)

5.1.3 High spin states and Shape Coexistence in ^{135}Ba

S. Kumar¹, R. Palit², H. C. Jain², I. Mazundar², P. K. Joshi², A. Y. Deo², Z. Naik², A. Dhal³, A. Goel⁴, A. Devi⁵, T. Tarkeswar⁵, I. Mehrotra⁵, G. Jnaneshwari⁶, A. Babu⁶, D. Negi⁷, V. Kumar⁷, R. Kumar⁷, R. P. Singh⁷, S. Muralithar⁷, R. K. Bhowmik⁷, S. C. Pancholi⁷, L. Chaturvedi⁸, S. S. Malik⁹ and A. K. Jain¹

¹Department of Physics, Indian Institute of Technology, Roorkee 247667.

²Department of Nuclear and Atomic Physics, Tata Institute of Fundamental Research, Mumbai

³Department of Physics, Banaras Hindu University, Varanasi221005.

⁴Department of Physics, Amity University, Noida201303.

⁵Department of Physics, University of Allahabad, Allahabad211002.

⁶Department of Nuclear Physics, Andhra University, Visakhapatnam530003.

⁷Inter University Accelerator Centre, Aruna Asaf Ali Marg, New Delhi110067.

⁸Department of Physics, Pandit Ravishankar Shukla University, Raipur492010.

⁹Department of Physics, Guru Nanak Dev University, Amritsar143005.

Introduction

The nuclei around the $A=135$ mass region form a transitional region where the collectivity is characterized by a moderate deformation and softness with respect to the triaxiality. Evidence for characteristics such as the shape coexistence and gamma-softness has been observed during the last two decades for many nuclei from Xe to Nd. In particular, the study of odd-mass nuclei in this region provides important information on the quasiparticle excitations in such conditions of the deformation.

In the odd-mass even Z nuclei ($N = 77$), collective structures based on the $h_{11/2}$ and $g_{7/2}$ neutron configurations have been systematically observed and characterized as having triaxial prolate shape. Nilsson diagrams indicate that in this mass region there are several positive parity neutron orbitals originating from the $g_{7/2}$, $d_{3/2}$, $d_{5/2}$ and $s_{1/2}$ spherical shell model states which determine the low excitation energy structures, whereas for the negative parity states there is only the $h_{11/2}$ orbital. Many of these nuclei show interesting spectroscopic properties both at low and high spins [1, 2]. The ^{135}Ba nuclei lies near the neutron shell closure at $N = 82$ and in the proton midshell between $Z = 50$ and $Z=64$ shell closures. In this nucleus, an interplay of quadrupole collectivity and single-particle degrees of freedom could exist even in the relatively low-lying states.

In the previous works, some lower spin levels have been reported by the $(^9\text{Be}, xn)$ [3] and (n, γ) [4] reactions. Thus, this work is done for complete structure information at low and high spin in ^{135}Ba . In this paper, we report on the complete spectroscopy in ^{135}Ba to understand the $N=79$ systematics and shapes changes from low spin state to high spin states.

Experimental Details

The high spin states of ^{135}Ba were populated in the $^{130}\text{Te} (^9\text{Be}, 4n)^{135}\text{Ba}$ reaction at a beam energy of 42.5 MeV obtained from the 15UD Pelletron at Inter University Accelerator Centre (IUAC),

New Delhi. A 99.90% isotropically enriched target of ^{130}Te , with a thickness of $\sim 750 \mu\text{g}/\text{cm}^2$ deposited on $6 \text{ mg}/\text{cm}^2$ backing of ^{197}Au was used. The gamma-gamma coincidence data were collected using an array of twelve Compton HPGe detectors along with a multiplicity filter of fourteen BGO detectors. The HPGe detectors, at approximately 18 cm from the target, were arranged in three groups, each consisting of four detectors, at angles of 50° , 98° and 144° with respect to beam direction. For polarization measurements, the Clover detector was used at 98° , placed at 25cm from the target. The HPGe detectors had an energy resolution of about 2.4 keV at 1332 keV and relative efficiencies of $\sim 23 \%$. The energy calibrations and efficiencies were obtained from the energy of the known gamma-ray lines in ^{152}Eu and ^{133}Ba . A total of 340 million gamma-gamma events corresponding two or higher fold were collected in the list-mode data. The raw data was sorted out into a $E_\gamma.E_\gamma$ ($4\text{k} \times 4\text{k}$) matrix after gain matching of all spectra to a dispersion of 0.5 keV per channel using CANDLE program (an acquisition system developed at IUAC). The analysis of the matrix to generate gated spectra is done using RADWERE program. Another $E_\gamma.E_\gamma$ matrix with events recorded at 98° along x-axis and those recorded at 144° along the other axis was generated in order to determine the direction correlation of oriented nuclei (DCO) ratio for spin assignment.

Results

The partial level scheme of ^{135}Ba developed in the present work is shown in Fig. 1. It was constructed from gamma-gamma coincidence, intensity and directional correlation measurements. The earlier known level scheme has been substantially extended to 6 MeV excitation energy and $37/2^+$ spin with addition of about 25 new transitions. The gamma rays except at 682.6 and 1052.4 KeV have been observed for the first time. A typical coincidence spectrum with gate on 682.6 keV transition is shown in Fig. 2. Fig. 3 represents the coincidence spectrum with gate on 204.7 keV gamma line, which shows

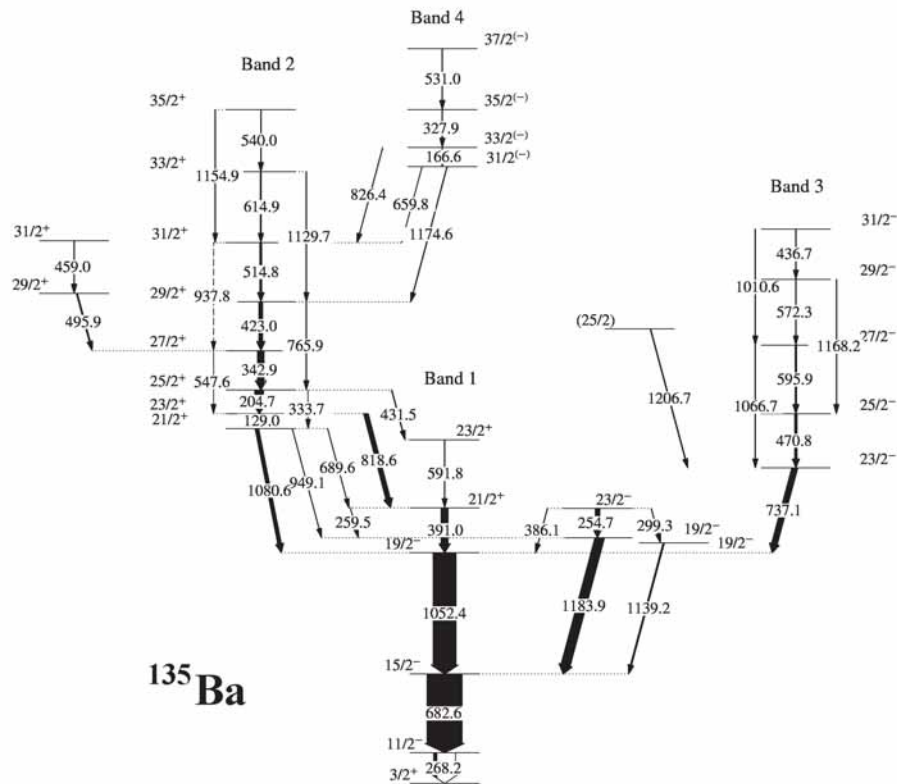


Fig. 1. Partial level Scheme of ^{135}Ba .

the new transitions. The low spin states upto $19/2 \hbar$ indicate a triaxial shape. A dipole positive parity band and a Collective Dipole band have been identified in the present work.

The shape coexistence of prolate and oblate deformations have been observed (Band 3 and Band 4). Theoretical calculations to understand the experimental results are in progress.

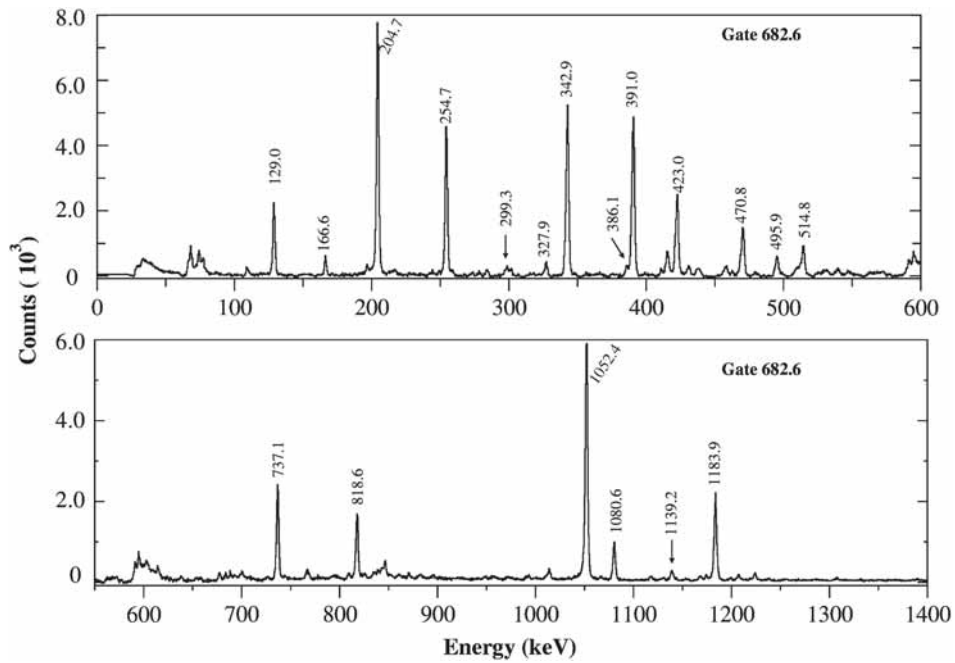


Fig . 2. The coincidence gated spectrum on 682.6 keV transition showing the new transitions.

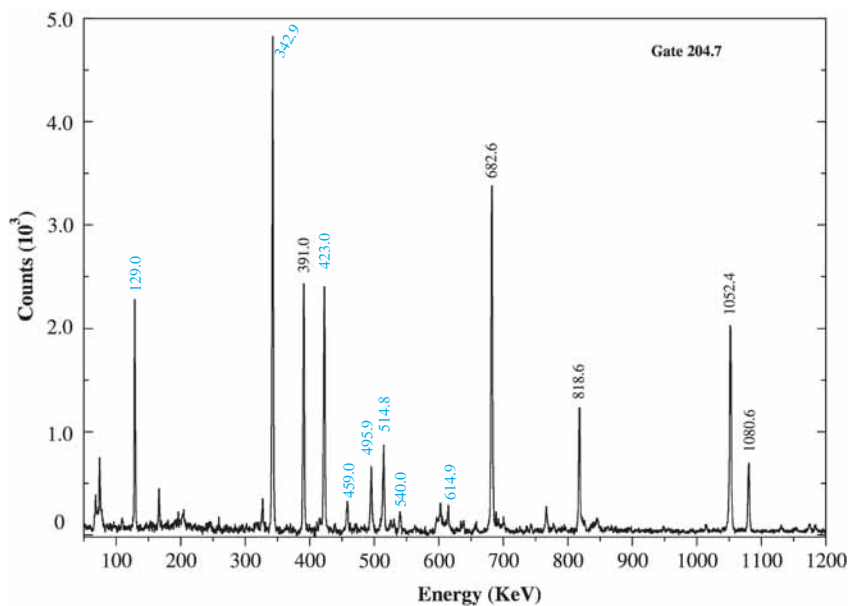


Fig . 3 The coincidence gated spectrum on 204.7 keV transition showing the transitions of Band 3 (blue colour label) .

Acknowledgment

The authors are thankful to the Pelletron accelerator staff of IUAC for their support during the experiment. The help from the target laboratory is highly appreciated. Financial support from the Ministry of Human Resources and the Department of Science and Technology (Govt. of India) at Roorkee is gratefully acknowledged.

REFERENCES

- [1] C. M. Petrache, et. al., Nucl. Phys. A615, 228 (1997).
- [2] C. M. Petrache, et. al, Phys. Rev. C 72, 064318 (2005).
- [3] E. Dragulescu, et. Al, Rev.Roum.Phys. 32, 743 (1987).
- [4] V. A. Bondarenko et al, Nucl. Phys. A551(1993)54

5.1.4 Lifetime measurement of excited states of ^{75}Br

D.Negi¹, V.Kumar¹, T.Trivedi², S.Appan.Babu³, Ranjeet⁴, V.Kumar⁵, P.Singh⁶, R.Kumar¹, S.Muralithar¹, R.P.Singh¹, A.K.Bhati⁵, R.K.Bhowmik¹

¹Inter University Accelerator Centre, Aruna Asaf Ali Marg, New Delhi 110067

²University of Allahabad, Allahabad

³Andhra University

⁴University of Delhi, Delhi

⁵Punjab University, Chandigarh

⁶Aligarh Muslim University, Aligarh

Nuclei in the mass region $70 < A < 80$ of the nuclear chart have been the study of interest due to their peculiar place in the nuclear chart. These nuclei are not far from the shell closure and there exists a strong competition of single and collective modes, thus exhibiting all the phenomenon of transitional nuclei, like shape coexistence [1,2] and shape competition [3,4]. When the number of both protons and neutrons lie close to ($Z = N = 38$) high deformation is observed, and rigid rotational behavior is found in these nuclei. As one goes away from this number in either direction, transitional effect shows up. Nuclei studied extensively in this region are Kr and Sr isotopes.

Odd A nuclei possess special interest, of how the extra nucleon effects the nearby core, thus adding information to the study of nearby even-even nucleus treated as core. Of these odd Bromine isotopes are good example to study as they lie between Kr and Se isotopes, and thus can be treated as either particle-core or hole-core coupling.

Lifetime of excited states, 718 keV ($13/2^+$) and 518 keV ($7/2^-$) in ^{75}Br have been remeasured using the reaction $^{51}\text{V}(^{27}\text{Al}, 2np)^{75}\text{Br}$ with beam energy 150 MeV from 15UD Pelletron at IUAC. Inverse reaction has been used in order to have high recoil velocity, which gives a well resolved shifted peak from un-shifted one (fig1). The ultimate aim of the experiment was to check the feasibility of this reaction to study g-factors of excited states by transient magnetic field technique.

RDM setup at IUAC was used for measuring the stopped and unstopped components

of the γ -line for different target-stopper distances. Gamma rays were detected by GDA array with 10 HP Ge detectors in singles mode. Data was taken at 19 distances for the time duration of 4hrs each. Calibration of distance was done both in air as well on-line and an offset of 7mm is obtained. Preliminary analysis of the spectrum with singles data were done using ingasort and lifetime program. Lifetime of 10 ± 0.3 ps and 15.1 ± 0.5 ps for 563keV and 518 KeV transition respectively is obtained. Further interpretation of results will be done.

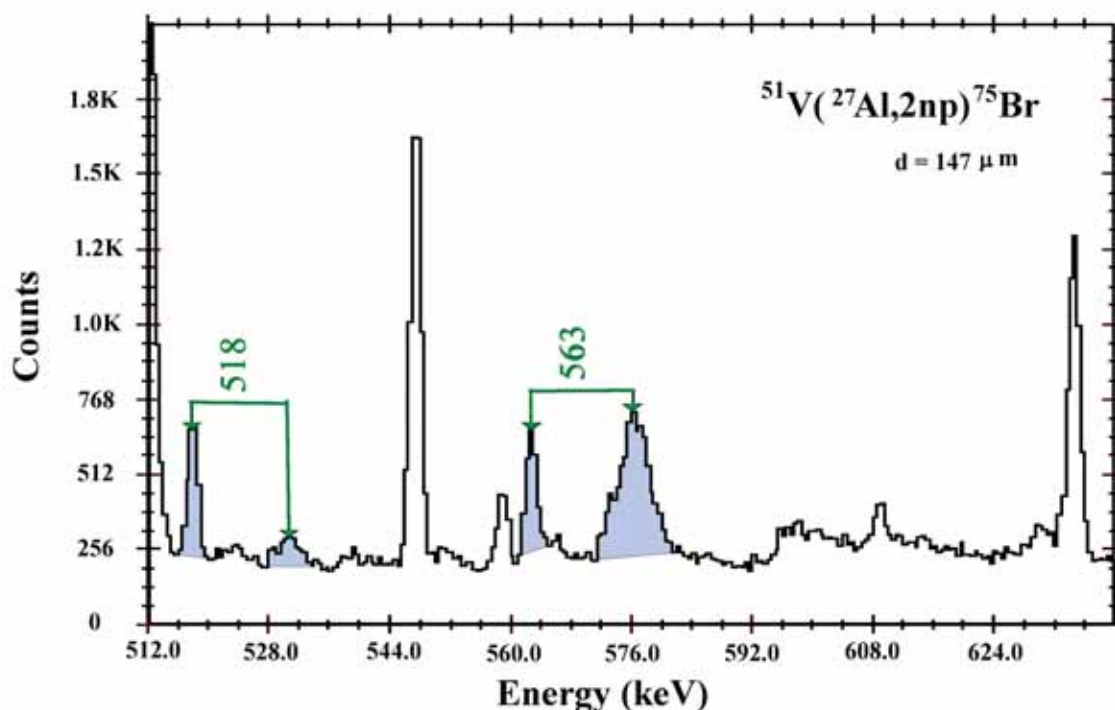


Fig. 1. Shifted and unshifted peaks of 518 & 563 keV transitions in ^{75}Br

REFERENCES

- [1] E.F. Moor et.al, PRC 38, 696 (1988).
- [2] B.J. Varley et.al., Phy Lett B 194, 463 (1987).
- [3] R.B. Peircey et.al., PRL 47, 1514 (1981).
- [4] P.D. Cottle et.al., PRC 42, 1254 (1990).

5.1.5 Pre-scission neutron emission from the fission of ^{228}U

Hardev Singh¹, Golda K. S.², Akhil Jhingan², R. P. Singh², P. Sugathan², Ranjeet³, S. Mandal³, P. D. Shidling⁴, Mihir Chatterjee⁵, S. K. Datta², Santanu Pal⁶ and I. M. Govil¹

¹Department of Physics, Panjab University, Chandigarh-160014, India

²Inter University Accelerator Centre, Aruna Asaf Ali Marg, New Delhi 110067

³ Department of Physics and Astronomy, Delhi University, India

⁴ Department of Physics, Karnatak University, Dharwad, India

⁵ Saha Institute of Nuclear Physics, Kolkata-700064, India

⁶ Variable Energy Cyclotron Centre, 1/AF, Bidhan Nagar, Kolkata

In recent years, pre-scission neutron multiplicity from heavy ion induced fusion-fission reactions has been used as a tool to investigate the reaction dynamics [1-3]. The experimental pre-scission neutron yield, in general, was found to be much larger as compared to the statistical model predictions and this excess yield is used to estimate the time scale of the fusion-fission process. In the present experiment, we have measured the pre-scission yield of neutrons from $^{19}\text{F} + ^{209}\text{Bi}$ reaction at various lab energies.

The Experiment was performed at Inter University Accelerator Centre, New Delhi using 100, 104, 108, 112 and 116 MeV pulsed ^{19}F beam in General Purpose Scattering Chamber (GPSC). Self supporting ^{209}Bi target of thickness $300 \mu\text{g}/\text{cm}^2$ was used in the experiment. Fission fragments were detected using two large area position sensitive multiwire proportional counters. Detectors were placed on both sides of the beam so as to cover the folding angle for symmetric fission. Four neutron detectors consisting of organic liquid scintillator cells (BC501) were placed outside the chamber at a distance of 100 cm from the target to detect the fission coincident neutrons. Detectors were placed at angles of 30° , 60° , 90° and 120° with respect to the beam direction. Two silicon surface barrier detectors were used at $\pm 11^\circ$ for beam flux normalization purpose. Pulse Shape Discrimination (PSD) technique was employed to discriminate gammas and neutrons detected. The observed TOF of neutrons was converted into energy and was corrected for neutron detector efficiency.

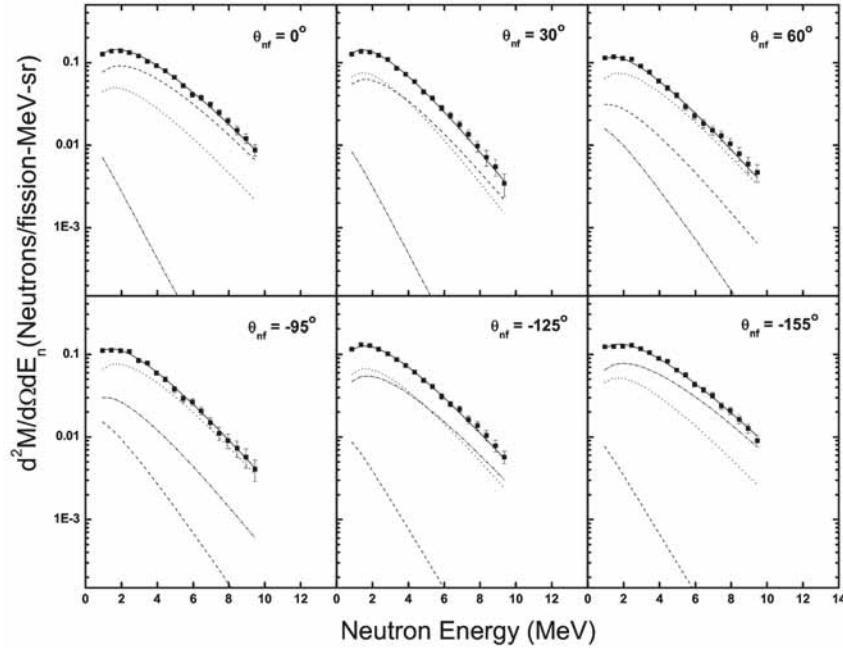


Fig. 1. Neutron energy spectra along with fits for pre-scission (dotted line), post-scission-1 (dashed), post-scission-2 (dash dotted) components. The total contribution is represented by solid line.

Pre and post-scission component of neutron multiplicity was extracted by least square fitting of observed neutron energy spectrum with Watt expression [4] at various angles as shown in fig. 1. We have also measured the masses of fission fragments from flight paths and time difference between complementary fragments assuming symmetric fission and no particle emission before scission as shown in fig.2. The FWHM of mass distribution is 30 u.

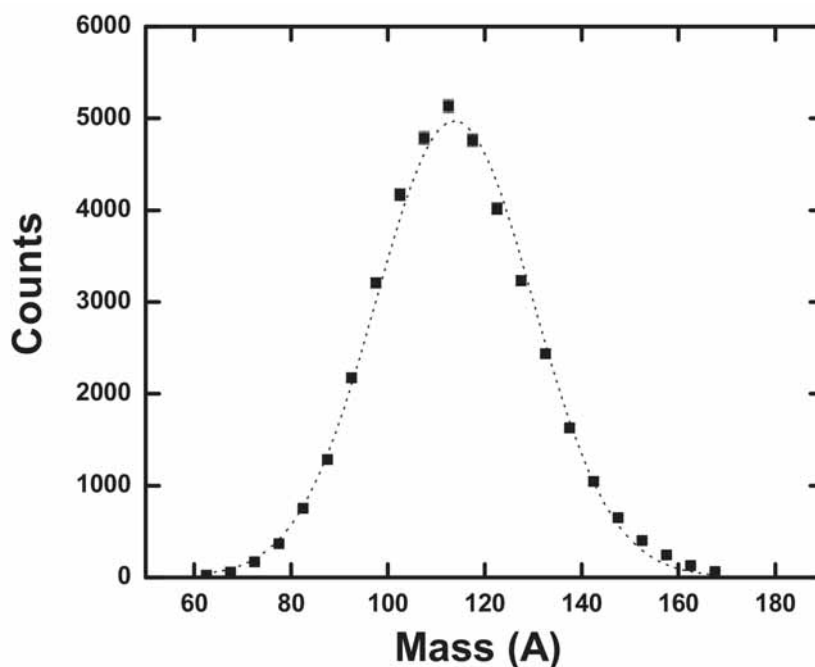


Fig. 2. Mass distribution (filled squares) along with the Gaussian fit (solid line).

REFERENCES

- [1] D. J. Hinde et al., Phys. Rev. C 45, 1229 (1992)
- [2] A. Saxena et al., Phys. Rev. C 49, 932 (1994)
- [3] L. M. Pant et al., Eur. Phys. J. A 16, 43 (2003)
- [4] D. Hilscher et al., Phys. Rev. C 20, 576 (1979).

5.1.6 Evaporation residue cross section and spin distribution measurements for $^{19}\text{F} + ^{181}\text{Ta}$ system

P. D. Shidling¹, N. M. Badiger¹, S. Nath², N. Madhavan², S. Muralithar², A. Jhingan², J.J. Das², J. Gehlot², P. Sugathan², R. P. Singh², A. K. Sinha³, Santanu Pal⁴, S. Kailas⁵, Ranjeet⁶, S. Mandal⁶, R. Singh⁶, B. R. Behera⁷, Devaraj¹, Prasad E.⁸, K.M. Varier⁸, M.C. Radhakrishna⁹

¹Department of Physics, Karnatak University, Dharwad - 580003.

²Inter University Accelerator Centre, Aruna Asaf Ali Marg, New Delhi 110067.

³UGC-DAE, CSR, Kolkata Centre, Kolkata - 700098.

⁴Variable Energy Cyclotron Centre, Kolkata - 700064.

⁵Nuclear Physics Division, Bhabha Atomic Research Centre, Mumbai - 400085.

⁶Department of Physics and Astrophysics, Delhi University, Delhi - 110007.

⁷Department of Physics, Punjab University, Chandigarh - 160014.

⁸Department of Physics, Calicut University, Calicut - 673635.

⁹Department of Physics, Bangalore University, Bangalore - 560056.

The time scale of fission for highly excited heavy nuclei resulting from a heavy ion induced fusion reaction has been extensively studied by measuring multiplicities of neutrons [1], charged particles [2] and GDR γ - rays [3]. These experiments have shown that the fission process is strongly hindered relative to expectation based on the standard statistical model description of the process. However, Frobrich et al. [4] pointed out that evaporation residues (ERs) are the most sensitive probes for studying the dynamics of fusion-fission process. Formation probability of ERs in heavy ion induced fusion reaction is sensitive to the dissipation strength inside the fission barrier. Hence, direct measurement of ERs alone can provide the desired separation between pre-saddle and post-saddle dissipation. Suppression of fission also enhances population of evaporation residues with the occurrence of higher spin values. Therefore, the combined study of evaporation residue and its spin distribution gives more insight into fusion-fission dynamics, as seen in our earlier measurements (S.K.Hui et al.[5] & P.D.Shidling et al.[6]). In the present experiment we have measured evaporation residue cross section and spin distribution for $^{19}\text{F} + ^{181}\text{Ta}$ system leading to the same compound nucleus $^{200}\text{Pb}^*$ studied earlier by us using $^{16}\text{O} + ^{184}\text{W}$ [6]. Another motivation for carrying out same kind of measurements for two different channels was also to study the entrance channel effect on fission hindrance via evaporation residue cross section and spin distribution. Present measurements were carried out in the laboratory energy range 82 MeV to 125 MeV.

The experiment was performed using Heavy Ion Reaction Analyzer (HIRA) [7] and 14 element BGO multiplicity filter. ^{19}F pulsed beam with the pulse separation of 4 μsec was taken from 15UD Pelletron and bombarded on enriched ^{181}Ta target of thickness 250 $\mu\text{g}/\text{cm}^2$ with carbon backing of 30 $\mu\text{g}/\text{cm}^2$. ERs were detected at the focal plane by a large area (50 \times 50 mm^2) 2D position sensitive Si detector. 14 BGO detectors were mounted at the target chamber in a close geometry for detecting gamma rays in coincidence with ERs. The BGO array covered 48% of 4 π solid angle but taking energy response into account we had an effective solid angle of \approx 30% at $E_\gamma \sim$ 660 keV. Elastically scattered fluorine ions were registered in two Si surface barrier detectors placed at $\pm 25^\circ$ w.r.t. beam direction. A carbon foil of 30 $\mu\text{g}/\text{cm}^2$ thickness with large surface area was placed 10 cm downstream from the target to reset the charge state of ERs to statistical distribution after internal conversion processes, if any. Measurements were performed at laboratory beam energies of 82, 85, 89, 93, 97, 101, 104, 109, 114, 117.5, 121.5 and 125 MeV. The time of flight (TOF) setup (with ERs detected at the focal plane as start and RF of beam pulsing system as stop) helped in separating ERs from the beam-like particles. Fig.1 shows the 2D plot of energy vs TOF. To further confirm that there is no low energy beam contamination in ERs, a gold foil of thickness 250 $\mu\text{g}/\text{cm}^2$ was placed at the target position keeping HIRA settings unchanged. Hardly any particle was observed in the focal plane of HIRA in the region of interest of ERs as shown in E vs TOF plot(Fig.2). This implied that our method of using TOF setup gave very clean identification of ERs.

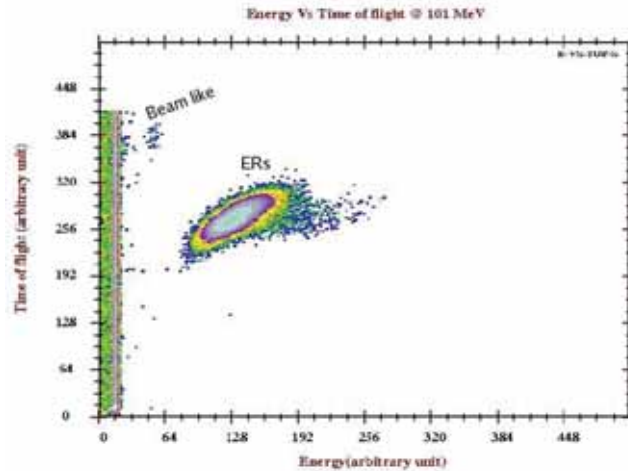


Fig.1 Two-dimensional plot of energy vs time of flight. The evaporation residues are seen at the centre, while scattered beam-like particles are seen at top left corner of the plot.

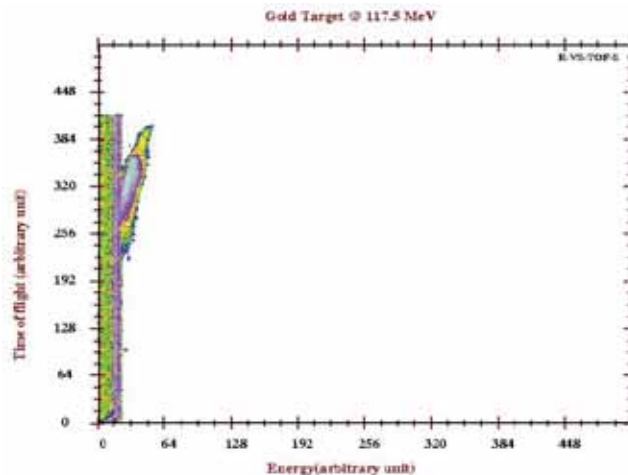


Fig.2 Two-dimensional plot of energy vs time of flight for gold target at 117.5 MeV beam energy, showing the absence of beam-like particles in the region of ERs.

Time-to-digital converter (TDC) signals from the individual BGO detectors were also recorded. These spectra helped us in constructing the bitpattern spectrum of γ rays. Fold distribution was constructed from the bitpattern spectrum. Offline analysis has been carried out using CANDLE software [8]. Generated fold distribution was inturn gated with 2D spectrum of energy vs time of flight. Generated fold distribution was converted into the moments of the multiplicity distribution by following the procedure adopted by Vander Werf [9]. Multiplicity distribution was generated by incorporating the extracted moments into the skewed gaussian multiplicity distribution [6]. Transformation of multiplicity distribution to spin distribution is made by assuming the ERs to be good rotor with two units of angular momentum being carried out by each non statistical

gamma ray, Fig. 3 shows the probability spin distribution for one beam energy. Extracted evaporation residue yield was converted into cross section. Fig. 4 shows the plot of evaporation residue cross section vs beam energy. To understand the entrance channel effect, experimental evaporation residue cross sections of both the system are compared in reduced coordinates as shown in Fig. 5. Similarly, first three moments of gamma multiplicity distribution are compared for both the systems (Fig. 6 to Fig.8). The first moment do not show any difference but as we compare higher moments which are more sensitive to higher spin population, we see some evidence of entrance channel effect (Fig. 7 & Fig. 8). This is reflected in the comparison of cross section too. Theoretical calculations are in progress to estimate the fission hindrance and also the entrance channel effect on fission hindrance, if any.

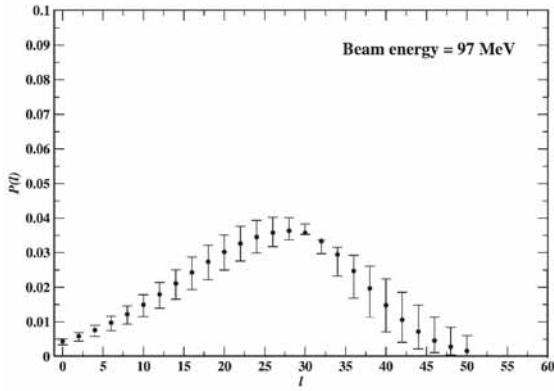


Fig.3 Plot of $P(l)$ vs l for 97 MeV beam energy

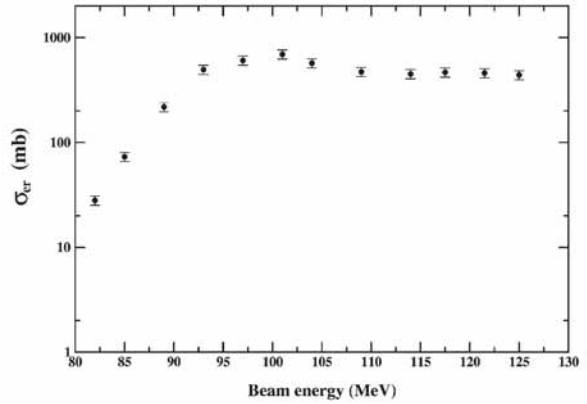


Fig.4 ER cross section vs Beam energy (MeV)

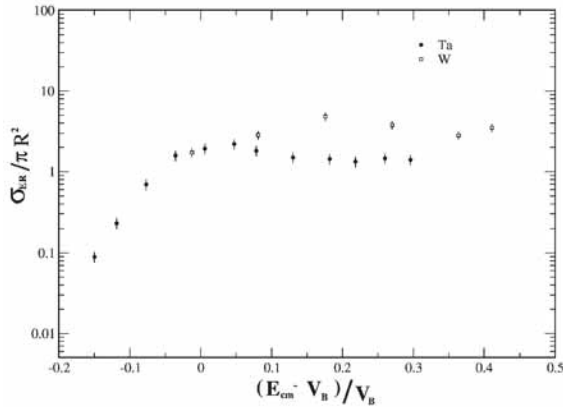


Fig. 5. Plot of evaporation residue cross section in reduced coordinates for $^{19}\text{F} + ^{181}\text{Ta}$ & $^{16}\text{O} + ^{184}\text{W}$ system.

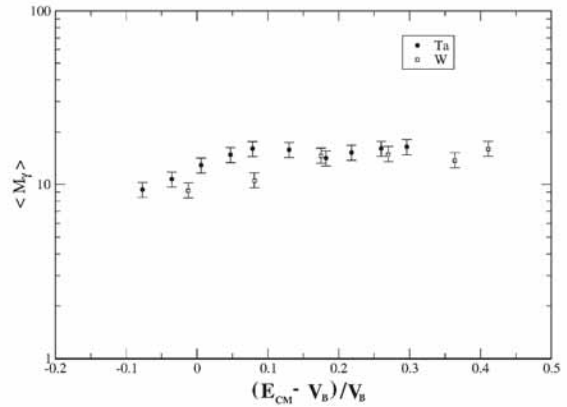


Fig. 6. Plot of average gamma multiplicity in reduced coordinates for $^{19}\text{F} + ^{181}\text{Ta}$ & $^{16}\text{O} + ^{184}\text{W}$ system

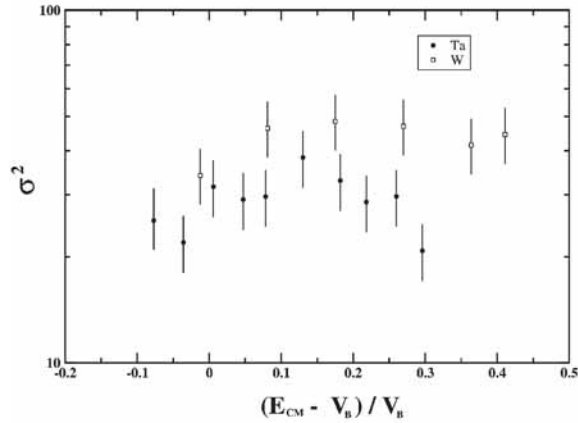


Fig. 7. Plot of second moments in reduced coordinates for $^{19}\text{F} + ^{181}\text{Ta}$ & $^{16}\text{O} + ^{184}\text{W}$ system.

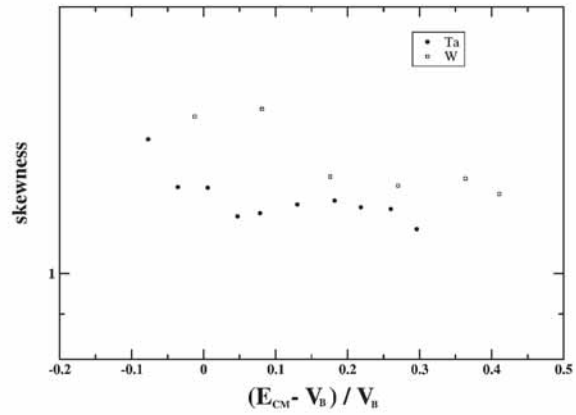


Fig. 8. Plot of third moments in reduced coordinates for $^{19}\text{F} + ^{181}\text{Ta}$ & $^{16}\text{O} + ^{184}\text{W}$ system.

REFERENCES

- [1] D.J. Hinde et al. Phys. Rev. C. 45(1992)1229.
- [2] J. P. Lestone et. al., Phys. Rev. Lett. 67 (1991)1078.
- [3] I. Diószegi et al. Phys. Rev. C. 63 (2000) 014611
- [4] P. Frobrich et al. Nucl. Phys. A. 563 (1993) 326.
- [5] S. K. Hui et al. Phys. Rev. C 62 (2000) 054604
- [6] P. D. Shidling et al. Phys. Rev. C 74 (2006) 064603.
- [7] A. K. Sinha et al., NIMA 339 (1994) 543
- [8] CANDLE Version 2.2, developed at Inter University Accelerator Centre , New Delhi.
- [9] S.Y. Vander Werf, Nucl. Instr. And Meth. 153 (1978) 221.

5.1.7 Spin distribution studies at $E/A \approx 4\text{-}7\text{MeV}$: a sensitive probe for in-complete fusion dynamics

Pushpendra P. Singh¹, B. P. Singh¹, Unnati¹, Manoj K. Sharma¹, D. P. Singh¹, Rakesh Kumar², P. D. Shidling³, D. Singh¹, J. K. Rana¹, P. S. Rao⁴, R. Ali¹, R. P. Singh², S. Muralithar², M. A. Ansari¹, H. D. Bhardwaj⁵, R. Prasad¹ and R. K. Bhowmik²

¹Accelerator Laboratory, Department of Physics, A. M. University, Aligarh-202 002

²Inter-University Accelerator Center, Aruna Asaf Ali Marg, New Delhi 110 067

³Department of Physics, Karnataka University, Dharwad-580 003

⁴Department of Physics, M. S. University, Vadodara-390 002

⁵Department of Physics, D. S. N. College, Unna-202 331

In recent years, there has been a renewed interest in exploring the reaction dynamics of heavy ion interaction leading to the production of fast projectile-like fragments (PLFs) in forward cone. The production possibility of PLFs was first investigated by Britt and Quinton [1], in the bombardment of ^{197}Au and ^{209}Bi by ^{12}C , ^{14}N and ^{16}O projectiles at ≈ 10.5 MeV/nucleon. These reactions were referred to as massive transfer reactions. Later, Galin et. al. [2], also observed fast PLFs in forward cone and termed these PLFs as a consequence of in-complete fusion (ICF) reaction dynamics. In order to explain some of the characteristics of ICF, several models viz; Sumrule model [3], break-up fusion model [4], promptly emitted particles (PEP's) model [5], etc., have been proposed. The Sum rule model of Wilczynski et al., predicts that ICF mainly occurs in the peripheral interactions and are localized in the angular momentum space above the critical angular momentum for the complete fusion. The break-up fusion model of Udagawa and Tamura explained the ICF reaction dynamics in terms of the break-up of projectile into its clusters in the nuclear force field of the target nucleus. One of the fragments is assumed to fuse with target nucleus to form an in-completely fused composite system and the remnant continues nearly un-deflected in forward cone with almost same velocity as that of incident projectile. However, in PEP's the particles transferred from the projectile to target nucleus may get accelerated in the nuclear force field of target nucleus and hence acquire extra velocity to escape. As a matter of fact all these models have been used to fit the experimental data at projectile energy $E/A \geq 10$ MeV with rare earth targets, but not perfectly consistent with the experimental data at relatively low bombarding energies, i.e., $E/A \sim 5-7$ MeV and for medium mass targets. As such for perfect modeling of ICF dynamics, it is essential to have experimental data for several projectile-target combinations. The advances in the ICF reaction dynamics took place after the measurement of the spin distribution for different reaction products by T. Inamura et al. [6], using particle-gamma coincidence technique.

In order study the CF and ICF processes, experiments have been carried at the Inter-University Accelerator Center (IUAC), New Delhi using Gamma Detector Array (GDA) alongwith Charged Particle Detector Array (CPDA), employing particle gamma-coincidence technique. The target projectile-combinations used in the present experiments were; (i) $^{16}\text{O}+^{169}\text{Tm}$, and (ii) $^{12}\text{C}+^{169}\text{Tm}$. The beam energies were ≈ 90 MeV (^{16}O) and $\approx 55-90$ MeV (^{12}C) with beam current ≈ 4 pnA. The scattered beam was removed by an Aluminum absorber of appropriate thickness placed in front of each CPD. Fourteen detectors in the CPDA were divided into the three angular rings, (i) Forward angle (F) $10^\circ-60^\circ$, (ii) Sideways (S) $60^\circ-120^\circ$ and (iii) Backward angle (B) $120^\circ-170^\circ$. Depending on the fast component of the CPDA signal, proton and α -particles in each angular ring can be identified. Due to the extra absorber thickness required for stopping the scattered beam, only protons and fast α -particles ($E_\alpha > 17$ MeV) could be detected in the forward ring. Coincidences were demanded between particles ($Z=1,2$) and prompt γ -rays emitted as a result of heavy ion interaction with target nucleus. Data analysis has been carried out using INGASORT. Selection of specific exit channels in forward, backward and 90° angles were achieved by looking into various gated spectra. The main reaction channels that were identified in the forward ring in coincidence with fast α -particles are $^{169}\text{Tm}(^{16}\text{O}, \alpha xn) ^{181-x}\text{Re}$, $^{169}\text{Tm}(^{16}\text{O}, \alpha pxn) ^{180-x}\text{W}$, $^{169}\text{Tm}(^{16}\text{O}, 2\alpha xn) ^{177-x}\text{Ta}$ and $^{169}\text{Tm}(^{16}\text{O}, 2\alpha pxn) ^{176-x}\text{Hf}$. The residues which have been identified in backward ring are $^{169}\text{Tm}(^{16}\text{O}, xn) ^{181-x}\text{Re}$ and $^{169}\text{Tm}(^{16}\text{O}, pxn) ^{184-x}\text{Os}$. Some neutron channels $^{169}\text{Tm}(^{16}\text{O}, xn) ^{185-x}\text{Ir}$ have also been identified from the singles spectra and confirmed

from decay γ -lines.

The spin distributions for different reaction products have been measured by studying the relative population of different levels in a rotational band to understand the side feeding pattern intensities for different reaction channels. As a representative case, the relative intensities of different levels of the residual nuclei produced in $^{16}\text{O}+^{169}\text{Tm}$ system in coincidence with α -particles is shown in Fig. 1. As can be seen from this figure, the spin distributions are distinctly different for direct- α emitting channels as that of fusion-evaporation channels. It may, however, be pointed out that, the yield for the residues in coincidence with α -particles emitted in forward direction is constant up to $J=11\hbar$ and then falls with high spin states, indicating the absence of side-feeding to the lowest members of yrast line transitions or lower spin states are not populated. In contrast, the same residual nuclei ^{177}W in coincidence with α -particles emitted in backward direction shows an sharp exponential fall with high spin states, an indication of strong side-feeding. Moreover, spin at half yield for ^{177}W ($\alpha p3n$) and ^{172}Ta ($2\alpha 5n$) reaction products populated via ICF in forward cone are found to be $13\hbar$ and $15\hbar$. Further, in case of ^{177}W ($\alpha p3n$), populated via fusion-evaporation channel in backward cone, the spin at half yield is found to be around $10\hbar$, indicating the population of direct- α channels at higher input angular momentum as compared to the fusion-evaporation channel in peripheral interactions. Several such channels have been compared. On the basis of above results, it can be inferred that, input angular momentum increases with fusion in-completeness [7].

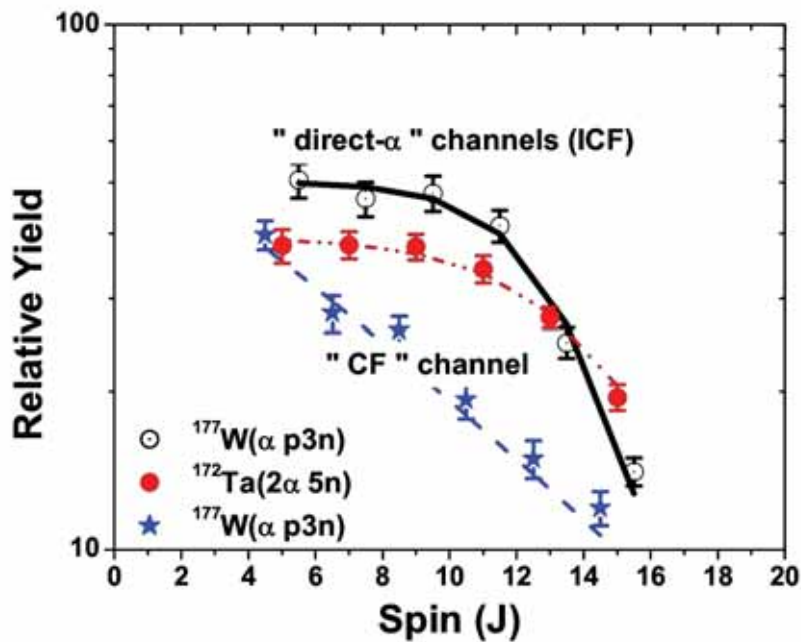


Fig. 1. Typical spin distribution for (i) ^{177}W ($\alpha p3n$), populated both via direct- α emission and fusion-evaporation channel, and (ii) ^{172}Ta ($2\alpha 5n$), populated via direct- 2α emitting channel.

In order to have a more detailed picture of spin distributions associated with direct-a emitting channels and to see the effect of projectile energy (input angular momentum), an complementary experiment has been performed for $^{12}\text{C}+^{169}\text{Tm}$ system in the energy range 55-90 MeV, using similar experimental conditions. The projectile has been chosen in such a way, so that all the direct-a channels in $^{16}\text{O}+^{169}\text{Tm}$ system will be the pure neutron channels in $^{12}\text{C}+^{169}\text{Tm}$ system. The spin distributions may therefore be compared to know the difference in the fusion-evaporation and direct-a emitting channels. Typical spin distribution for ^{177}Re ($4n$) residue at several beam energies is shown in the Fig.2. As can be seen from this figure, the yield is remarkably increasing with projectile energy. It may also be pointed out that, at low bombarding energies the yield is indicating sharp exponential fall with spin but at higher energies yield is not decaying so fast, which indicate that the low bombarding energies are not able to produce high spin states significantly. It may however be pointed out that, the high input angular momentum, which is a function of projectile energy is not contributing to produce high spin states in the final reaction products. As such, it is expected that the population of high spin states in fusion-evaporation channels is some what hindered by other reaction channels like ICF dynamics at these energies. Data analysis is still in progress.

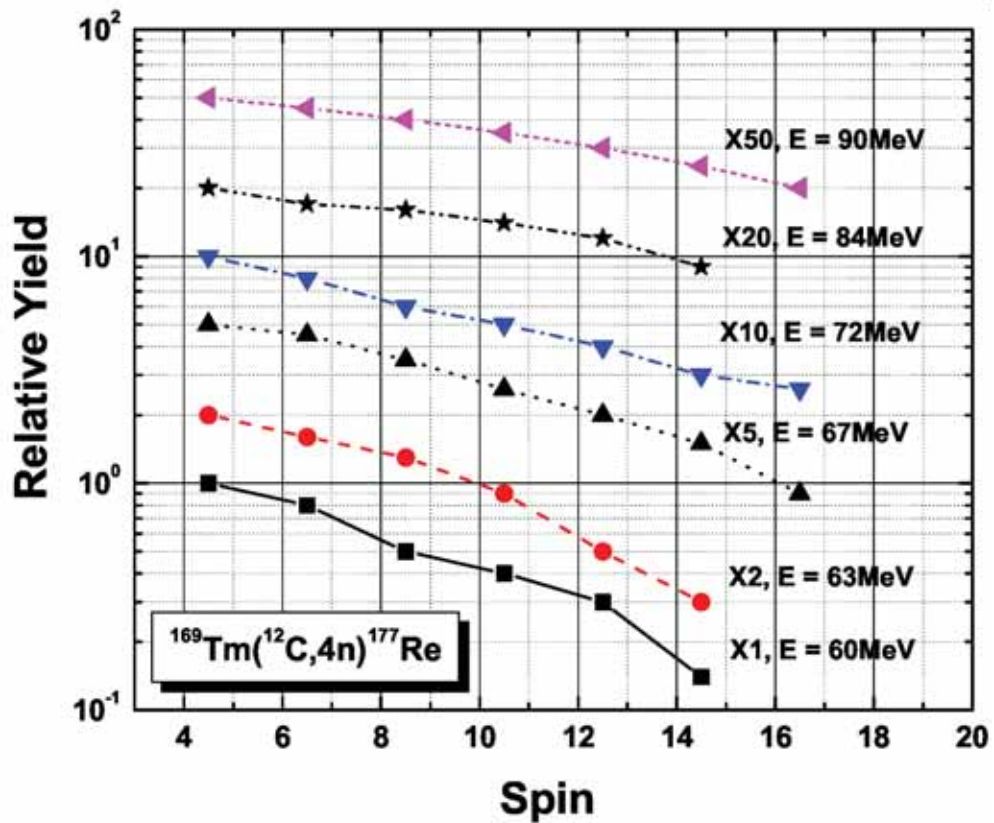


Fig. 2. Typical spin distribution for ^{177}Re ($4n$) populated via fusion-evaporation in $^{12}\text{C}+^{169}\text{Tm}$ with in the energy range 60-90 MeV.

REFERENCES

- [1] H. C. Britt and A. R. Quinton, Phys. Rev. 124 (1961) 877.
- [2] J. Galin et. al., Phys. Rev. C9 (1974) 1126.
- [3] J. Wilczynski., et al., Nucl. Phys. A373 (1982) 109.
- [4] T. Udagawa and T. Tamura, Phys. Rev. Lett. 45 (1980) 1311.
- [5] J. P. Bondroff, et al., Nucl. Phys. A333 (1980) 285.
- [6] T. Inamura et. al., Phys. Lett. B 68 (1977) 51.
- [7] Pushpendra P. Singh, et al., Nucl. Phys. Symp. V51 (2006) 361.

5.1.8 Transfer and Fusion measurements for $^{40}\text{Ca} + ^{70,66}\text{Zn}$ around Coulomb Barrier

Ranjeet¹, S. K. Mandal¹, R. Singh¹, N. Madhavan², S. Muralidhar², J. J. Das², S. Nath², A. Jhingan², B. Behera³, Shashi Verma¹, Hardev Singh³, K. Kalita⁴, P.D. Shidling⁵, J. Gehlot², Suneel¹, E. Prasad⁶

¹Department of Physics and Astrophysics, Delhi University

²Inter University Accelerator Centre, Aruna Asaf Ali Marg, New Delhi 110067

³Department of Physics, Panjab University, Chandigarh

⁴Department of Physics, Guwahati University, Assam

⁵Department of Physics, Karnataka University, Dharwad

⁶Department of Physics, Calicut University, Kerala

Nuclear reaction mechanism is a very exciting and not well understood area of nuclear physics. Main cause of this limitation is that nuclear interaction is not known exactly till now. Moreover, nucleus itself is a multi-particle system whose solutions are impossible to obtain exactly, even with known potentials. One of the interesting problems in nuclear reaction mechanism is fusion of heavy ions around Coulomb barrier and coupling of the internal degrees of freedom to the relative motion of colliding nuclei (1). This coupling, below barrier, influences the quantum tunneling that leads to fusion thereby resulting in large enhancement of fusion cross section. Three factors can play vital role in sub-barrier fusion: (i) static nuclear deformation, (ii) coupling to low lying nuclear excitations and (iii) coupling to nucleon transfer reactions (2). The role of first two is firmly accepted based on very compelling experimental evidences while the role of transfer is still not conclusive.

To probe the role of transfer in fusion and to study the various interesting features of transfer itself in heavy ion collisions, we have chosen $^{40}\text{Ca} + ^{70,66}\text{Zn}$ systems. In the present experiment, using the recoil mass spectrometer HIRA (3) at Inter University Accelerator Center, New Delhi, we have measured (i) fusion excitation function for $^{40}\text{Ca} + ^{70}\text{Zn}$ from 106 MeV to 146 MeV lab energy (~12% below to ~13% above Coulomb barrier), (ii) angular distribution of evaporation residues (0° to 10° in steps of 2°), (iii) transmission efficiency for evaporation residues at 0° and 130 MeV of beam energy. Feasibility study of transfer for this system, using HIRA, is also investigated. ^{40}Ca pulsed beam, with pulse separation of 250 ns, was delivered by 15UD Pelletron accelerator at IUAC.

Evaporation residues are forward focused and it is not possible to study them without proper beam rejection which, in this case, is effectively done by HIRA. A target of ^{70}Zn ($\sim 95\%$ enriched and thickness of $\sim 670 \mu\text{g}/\text{cm}^2$) was used for fusion excitation function. A carbon foil of thickness $\sim 40 \mu\text{g}/\text{cm}^2$ was placed 10 cm downstream from the target to reset the charge state of evaporation residues to statistical distribution after possible internal conversion processes. Two monitor detectors were placed symmetrically at 25° on either side of beam for normalization purposes. At focal plane of HIRA, a large area MWPC detector was used (15 cm x 5 cm window) with isobutane gas at low pressure (~ 2 mbar), for position and timing information. A segmented, ionization chamber of entrance window size 7cm x 3.5 cm (with active lengths of 3 cm - 5.8 cm - 13 cm) was placed after MWPC and operated at pressure ~ 30 mbar for Z identification of particles arriving at focal plane. For efficiency run, in addition, we used a HPGe detector at 90° , at target chamber. Angular distribution data was taken with 1 mSr solid angle of acceptance while fusion excitation and efficiency data were taken with 5 mSr solid angle of acceptance. The transmission/detection efficiency for ERs (all charge states reaching focal plane) are $\sim 7.79\%$ (for MWPC) and $\sim 4.07\%$ (for IC) at 130 MeV. The offline analysis is being carried out using CANDLER (4) software. Some of the gated spectra and preliminary results are shown in Figs. 1 to 5.

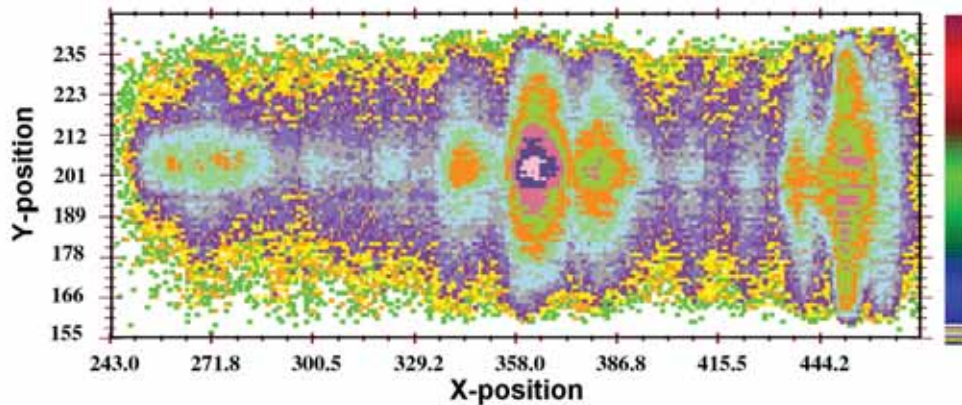


Fig. 1. ER mass (m/q) distribution at focal plane for lab energy of 130 MeV (obtained with MWPC energy gating)

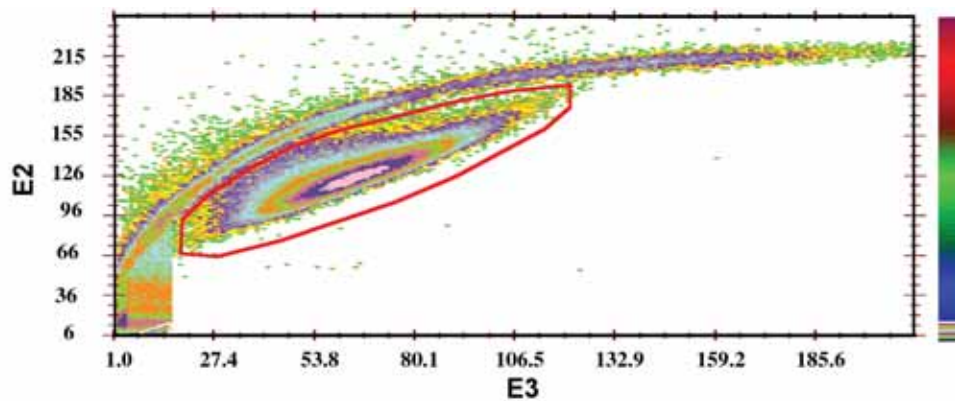


Fig. 2. E3 vs. E2 (IC energy signals) 2D spectrum for lab energy of 130 MeV showing ER separation from beam-like contaminants

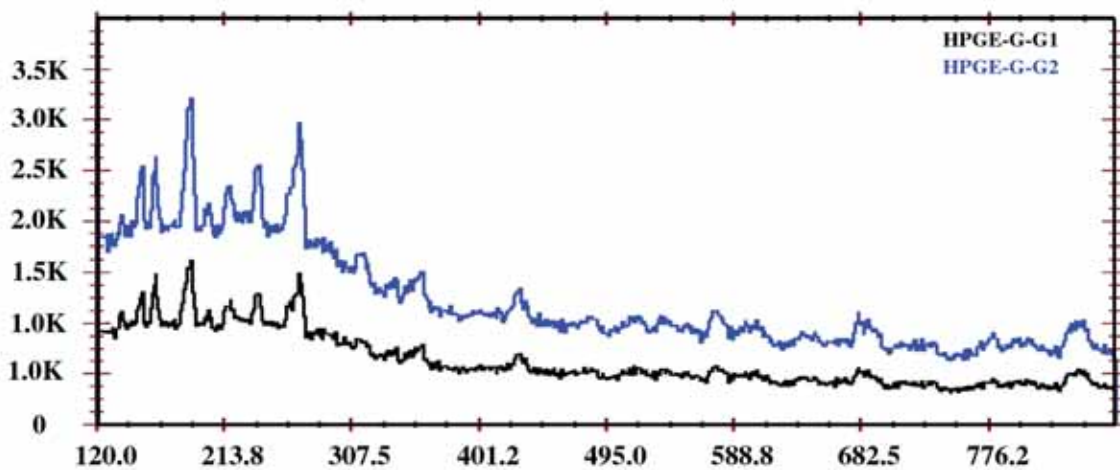


Fig. 3. Gamma energy spectra from HPGe (a) singles and (b) gated by ERs reaching MWPC (upper spectrum, 15cm-5cm) & ERs reaching IC (lower spectrum, 7cm-3cm)

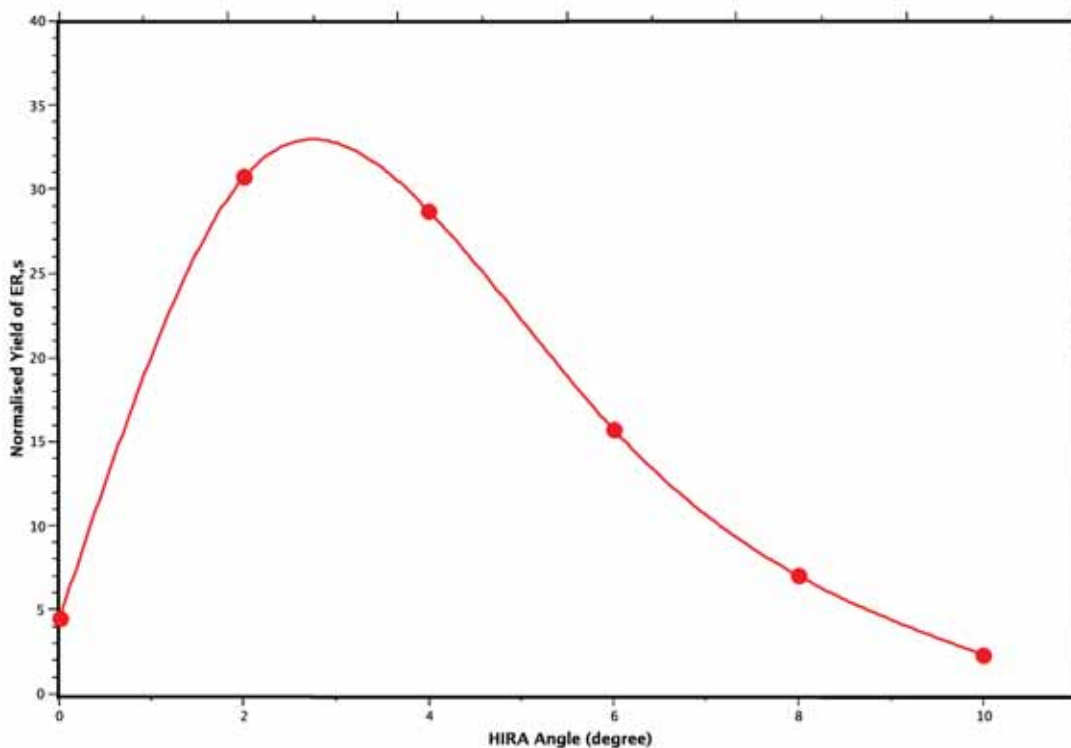


Fig. 4. Angular distribution of ERs (all masses of ERs reaching focal plane at 130MeV)

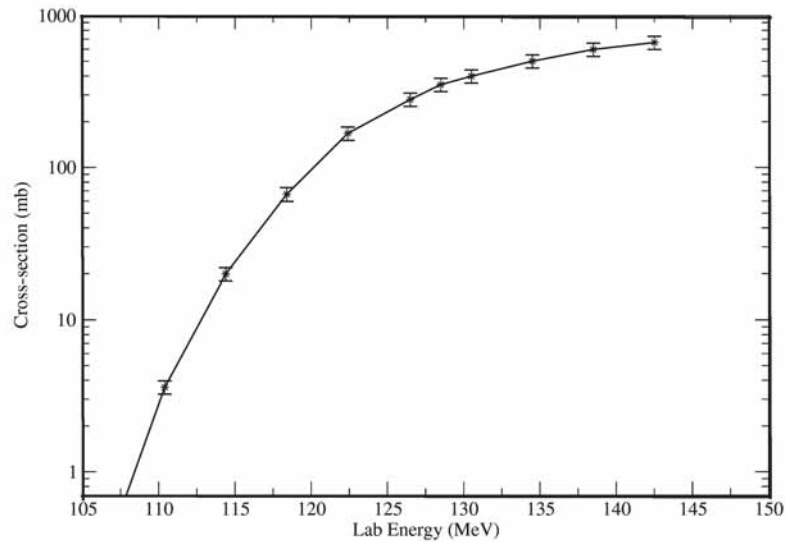


Fig. 5. Fusion cross-section from extracted transmission/detection efficiencies of HIRA

REFERENCES

- [1] A. M. Stefanini et al., *Phy. Rev. C* 41 (1018) 1990
- [2] W. von Oertzen et al., *Rep. Prog. Phys.* 64 (2001) 1247-1337
- [3] A.K. Sinha et al., *NIMA* 339 (1994) 543
- [4] CANDLE 2.1 version developed at IUAC, New Delhi

5.1.9 Influence of breakup of weakly bound projectiles ${}^7\text{Be}$, ${}^7\text{Li}$ on interaction with ${}^9\text{Be}$

Shashi Verma¹, J. J. Das², A. Jhingan², K. S. Golda², S. Mandal¹, K. Kalita⁴, N. Madhavan², P. Sugathan², J. Gehlot², Ranjit¹, S. Nath², T. Varughese², S. Barua⁴, B. K. Nayak³, P. K. Sahu³, B. John³, V. Jha³, A. Saxena³, S. K. Datta², R. Singh¹

¹Department of Physics and Astrophysics, Delhi University, Delhi - 110007

²Nuclear Science Centre, Aruna Asaf Ali Marg, New Delhi 110067

³Nuclear Physics Division, BARC, Mumbai - 400085

⁴Department of Physics, Gauhati University, Guwahati-781014

Considerable amount of experimental and theoretical efforts have been devoted over past few decades to understand the effect of break-up of weakly bound stable and radioactive nuclei on fusion cross sections for a range of systems over different energy spans [1]. The effect of break-up on fusion cross sections has been predicted to be different in different energy regimes and masses. Such investigations are of more relevance in case of light systems in context of astrophysics. The existing data in the literature for light systems show results which are at variance. The coupling of collective degrees of freedom to the fusion channel usually tends to lower the effective potential barrier and consequently enhances its cross sections at near and sub-barrier energies. On the other hand findings in light heavy ion fusion reactions, surprisingly showed that the break-up

channel was able to inhibit the fusion process when weakly bound nuclei were involved as projectiles because of the larger probability of the projectile dissociation along the collision. An alternative approach to study the influence of break-up on fusion cross section is through the elastic scattering measurements. The recent availability of radioactive ion beams has further triggered a good number of studies to investigate reactions induced by unstable nuclei like ${}^6\text{He}$, ${}^7\text{Be}$ etc. In view of the similarities of weakly bound stable systems with their radioactive associates, the comprehension of the reactions induced by intense beams like ${}^{6,7}\text{Li}$ and ${}^9\text{Be}$, should be very important for understanding reactions induced by low intensity radioactive ion beams. ${}^7\text{Be}$, being the mirror nucleus of ${}^7\text{Li}$, has a bound $(1/2)^-$ state at 0.430 MeV, similar to that of ${}^7\text{Li}$ at 0.478 MeV.

In order to extend our understanding on this subject, we have carried out elastic and transfer measurements for loosely bound radioactive ${}^7\text{Be}$ and elastic scattering and fusion measurements for the stable ${}^7\text{Li}$ with ${}^9\text{Be}$ target. The experimental measurements on ${}^7\text{Be} + {}^9\text{Be}$ and ${}^7\text{Li} + {}^9\text{Be}$ systems were performed using 15 UD pelletron accelerator facility at Inter-University Accelerator Centre (IUAC).

Elastic scattering angular distributions have been measured for ${}^7\text{Be} + {}^9\text{Be}$ system at $E_{\text{lab}} = 17, 19$ and 21 MeV in the angular range $24^\circ - 57^\circ$ (c.m.). An optical model (OM) analysis of these data has been carried out in order to extract optical potential parameters and reaction cross sections using the optical model code SNOOPY. One proton stripping cross sections were also measured for this system at $E_{\text{lab}} = 19$ and 21 MeV. These transfer angular distribution data were compared with the finite range Distorted Wave Born Approximation (FRDWBA) calculations. For the ${}^7\text{Li} + {}^9\text{Be}$ system elastic scattering angular distributions were measured and emitted light charged particles were detected at $E_{\text{lab}} = 15.75, 24$ and 30 MeV in the angular range $7^\circ - 70^\circ$ (c.m.). Shown in Fig. 1 and Fig. 2, are the optical model calculations for the elastic scattering angular distributions for ${}^7\text{Be} + {}^9\text{Be}$ and ${}^7\text{Li} + {}^9\text{Be}$ systems respectively, at the indicated energies.

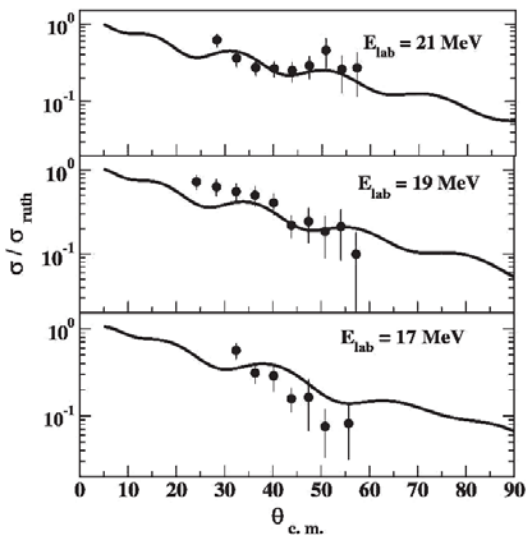


Fig. 1. Elastic scattering angular distributions for ${}^7\text{Be} + {}^9\text{Be}$ system

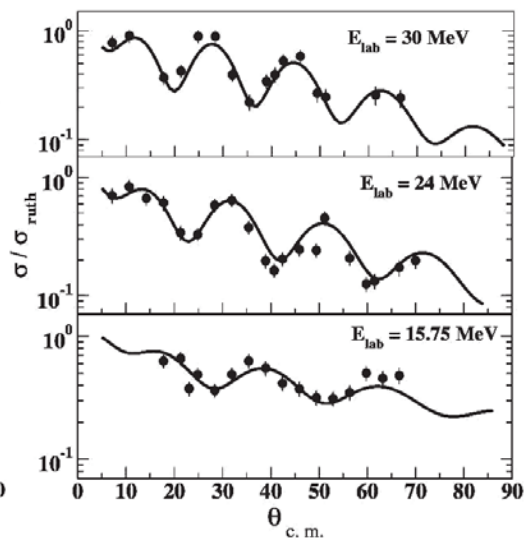


Fig. 2. Elastic scattering angular distributions for ${}^7\text{Li} + {}^9\text{Be}$ system

The elastic scattering cross sections for the two systems were found to be of comparable magnitudes at same $E_{c.m.}/V_{C.B.}$ i.e, 21 MeV for ${}^7\text{Be}$ corresponds to 15.75 MeV of ${}^7\text{Li}$. It may be mentioned that the optical model analysis of the elastic scattering angular distribution data for ${}^7\text{Be} + {}^9\text{Be}$ system yields 1298, 1445, 1562 mb for the reaction cross sections at $E_{lab} = 17, 19$ and 21 MeV respectively. It was found that the similar set of optical potential parameters give reasonably good description of elastic scattering angular distributions for both the systems. However, for ${}^7\text{Be} + {}^9\text{Be}$ system slightly larger value of diffuseness was needed as compared to ${}^7\text{Li} + {}^9\text{Be}$ system.

The resulting optical potential parameters are given in Table below for both the systems.

Set	System	E_{lab} (MeV)	V_o (MeV)	r_o (fm)	a_r (fm)	W_{surf} (MeV)	r_i (fm)	a_i (fm)
I	${}^7\text{Be} + {}^9\text{Be}$	17	60	1.35	0.88	8.4	1.96	0.83
		19	60	1.35	0.88	12.4	1.96	0.83
		21	60	1.35	0.88	16.4	1.96	0.83
II	${}^7\text{Li} + {}^9\text{Be}$	15.75 - 30	60	1.28	0.88	24.40	1.90	0.88

The ${}^9\text{Be}({}^7\text{Be}, {}^6\text{Li}) {}^{10}\text{B}$ angular distributions at $E_{lab} = 19$ and 21 MeV are shown in Fig. 3 along with the corresponding FRDWBA calculations made using the FRESKO code. For entrance channel the optical model parameters used were the same as obtained from the analysis of the elastic scattering data. FRDWBA calculations provide a good description of the data at $E_{lab} = 19$ MeV and 21 MeV.

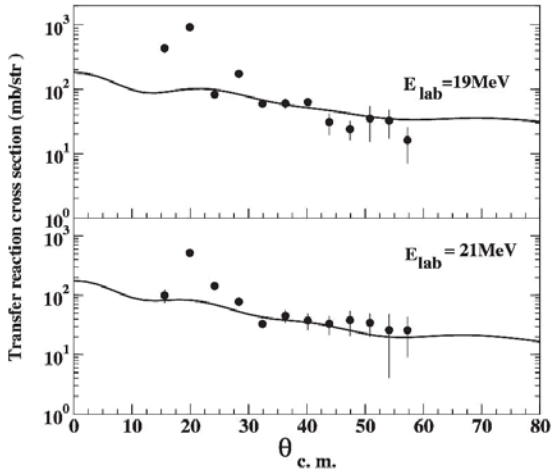


Fig. 3. ${}^9\text{Be}({}^7\text{Be}, {}^6\text{Li}) {}^{10}\text{B}$, One proton transfer angular distributions at $E_{lab} = 19$ and 21 MeV. The continuous curves result from FRDWBA calculations.

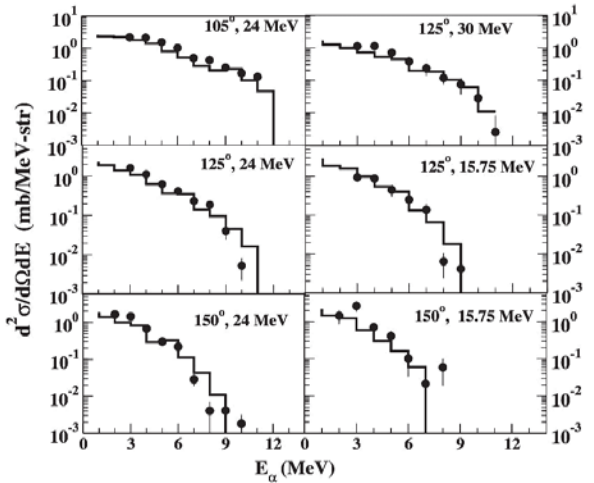


Fig. 4. alpha-energy spectra from the reaction ${}^7\text{Li} + {}^9\text{Be} \rightarrow {}^{16}\text{N}^*$ at energies and angles indicated in the panels. The histograms represent the results of PACE calculations.

Fusion cross sections were obtained by reproducing the measured alpha-evaporation spectra from the compound nucleus at backward angles with the statistical model calculations. The evaporated alpha-particles were detected at lab angles of 125° and 150° at 15.75 MeV; 105°, 125° and 150° at 24 MeV; and 125° at 30 MeV. The measured alpha-energy spectra were integrated over 1 MeV energy bins. The alpha-energy spectra from PACE calculations were corrected for the thick target. The energy spectra of alpha particles would get significantly affected due to the energy loss of incident beam in the target and the energy loss of emergent charged particles. Therefore, the experimental yield can be compared with the PACE calculations only after these energy corrections are incorporated. This was done by treating the total target thickness as a combination of number of thin target slabs and the PACE calculations were performed for each slab with corrected beam energy. By adjusting σ_{fus} cross section and hence l_{max} we could reproduce the experimental alpha-spectra and therefrom obtained fusion cross sections at measured energies. The agreement between the experimental alpha-spectra and the ones obtained from PACE calculations can be noted in Fig. 4.

For the ${}^7\text{Li} + {}^9\text{Be}$ system, the fusion cross sections, σ_{fus} , were found to be much lower than the reaction cross sections, σ_{reac} at all the three measured energies as Tabulated in the following table.

E_{lab} (MeV)	σ_{fus} (mb)	σ_{reac} (mb)	$\sigma_{\text{fus}}/\sigma_{\text{reac}}$
15.75	677.4 ± 80.6	1333	0.51 ± 0.06
24	669.5 ± 79.7	1370	0.49 ± 0.06
30	655.2 ± 77.9	1431	0.46 ± 0.05

The present results on fusion cross sections show good agreement with the ones obtained by Takahashi et al. [2] using evaporation residue technique. A comparison of the measured fusion cross sections with those reported by Takahashi et al. [2] is shown in fig. 5. These authors concluded that the suppression of σ_{fus} in collision between two very light weakly bound nuclei is strongly correlated to the value of the binding energy of projectile. Fusion reaction cross sections for ${}^9\text{Be} + {}^9\text{Be}$ system at an energy much above the Coulomb barrier were also found to be much lower than the reaction cross sections as measured by Omar et al. [3] following the evaporation residue technique. These results were interpreted in terms of the loosely bound alpha-particle structure of ${}^9\text{Be}$ nucleus.

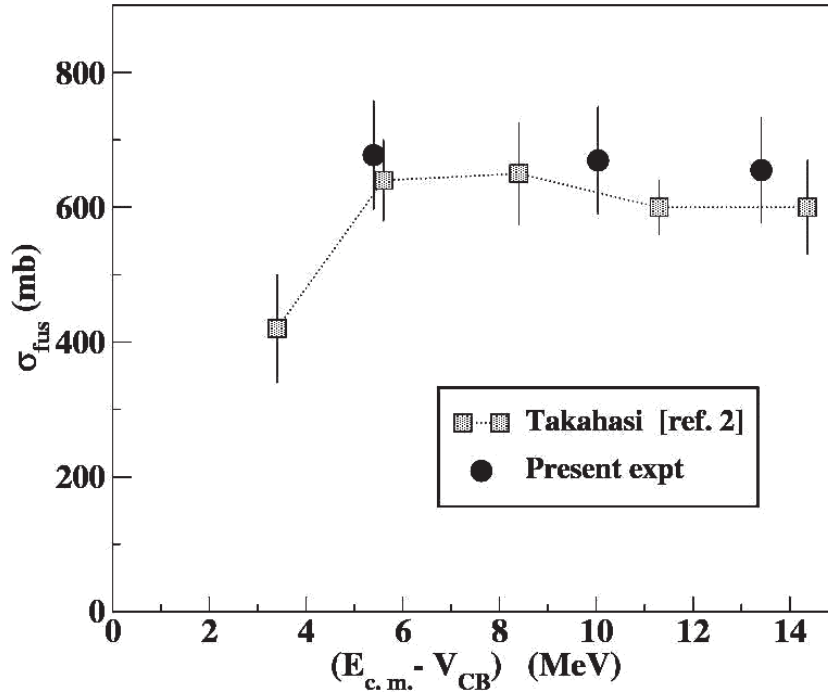


Fig 5. Energy dependence of the fusion cross section for ${}^7\text{Li} + {}^9\text{Be}$. The lines are drawn to guide the eye.

The energy spectra of emitted protons, deuterons, tritons and alpha particles were also measured in the angular range of 7° - 70° (c.m.) using a pair of telescopes having different thicknesses. The inclusive measurement of light charged particle spectra may also shed some light on the influence of break-up on fusion process. In the present measurement for ${}^7\text{Li} + {}^9\text{Be}$ system the alpha-spectra at forward angles show relatively much larger cross sections than expected from the PACE calculations. However, this deviation of the experimental cross sections decreases with the increase in emission angles. The measured larger cross sections for alpha-particles and tritons at small angles could possibly be because of the contributions from direct channels or break-up of ${}^7\text{Li}$ into alpha + t. The detailed analysis of the charge particle distributions may provide a better insight into the processes playing a dominant role in the larger cross sections at forward angles.

REFERENCES

- [1] L. F. Canto et al., Phys. Rep. 424, 1 (2006) and references therein.
- [2] J. Takahashi et al., Phys. Rev. Lett. 78, 30 (1997).
- [3] A. R. Omar, J. S. Eck, T. R. Ophel and J. R. Leigh, Phys. Rev. C 30, 1516 (1984).

5.1.10 Coulomb excitation of ${}^{114,116}\text{Sn}$

P. Doornenbal^{1,2}, P. Reiter¹, P. Bednarczyk², L. Caceres², J. Cederkäll^{3,4}, A. Ekström³, J. Gerl², M. Górska², A. Jinghan⁵, R. Kumar⁵, R.P. Singh⁵, H. J. Wollersheim²

¹Institute for Nuclear Physics, University of Cologne, Germany

²Gesellschaft für Schwerionenforschung, Darmstadt, Germany

³PH Department, CERN, Geneva, Switzerland

⁴Physics Department, University of Lund, Sweden

⁵Inter University Accelerator Centre, Aruna asaf Ali Marg, New Delhi 110067

The $B(E2)$ values of shell model calculations for the even tin isotopes $^{102-130}\text{Sn}$ show a parabola-like trend, as can be seen in figure 1, which resembles the typical behavior of a one-body even tensor operator across a shell in the seniority scheme[1]. Thus, for a seniority changing transition, the $B(E2)$ values increase at first, then flatten, peak at midshell and fall off thereafter. Existing experimental data show an almost perfect agreement with this plot for tin isotopes heavier than $A = 114$ [3,4], hence only if at least half of the major shell $N = 50 - 82$ is filled.

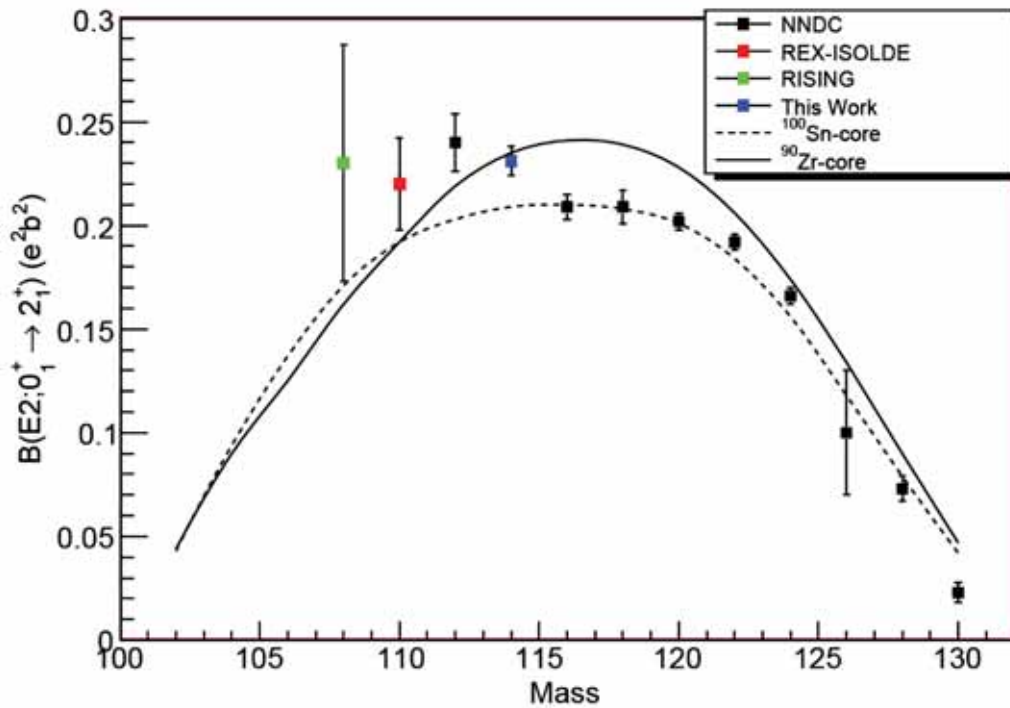


Fig. 1. $B(E2)$ values for first 2^+ states of even Sn isotopes. The solid and dashed curves are shell model predictions assuming ^{90}Zr and ^{100}Sn core. The result of the present measurement is shown as blue square.

In the case of lighter stable tin isotopes, which have a natural abundance of less than 1%, the publications for ^{112}Sn [5-7] and ^{114}Sn [8-10] yield higher $B(E2)$ values than expected. This may indicate the increasing role of core polarization when approaching the doubly magic ^{100}Sn . However, until now big experimental errors prohibit further theoretical interpretations. One main reason for these errors is that these experiments either have used enriched targets, then the uncertainty stems from the impurity of the target, or used the recoil distance Doppler-shift (RDDS) method which is error prone for lifetimes lower than 1ps.

The Coulomb excitation experiment was performed with an isotopic pure $^{114,116}\text{Sn}$ UNILAC beam at 3.4 MeV/u in the X7 area at GSI. The gamma decays were measured with two Super-Clover and two Cluster Ge-detectors. The distance of the Ge-detectors to the target was 20 cm, which resulted in a photo peak efficiency of 3% at 1.3 MeV. The experimental setup is shown in fig 2.

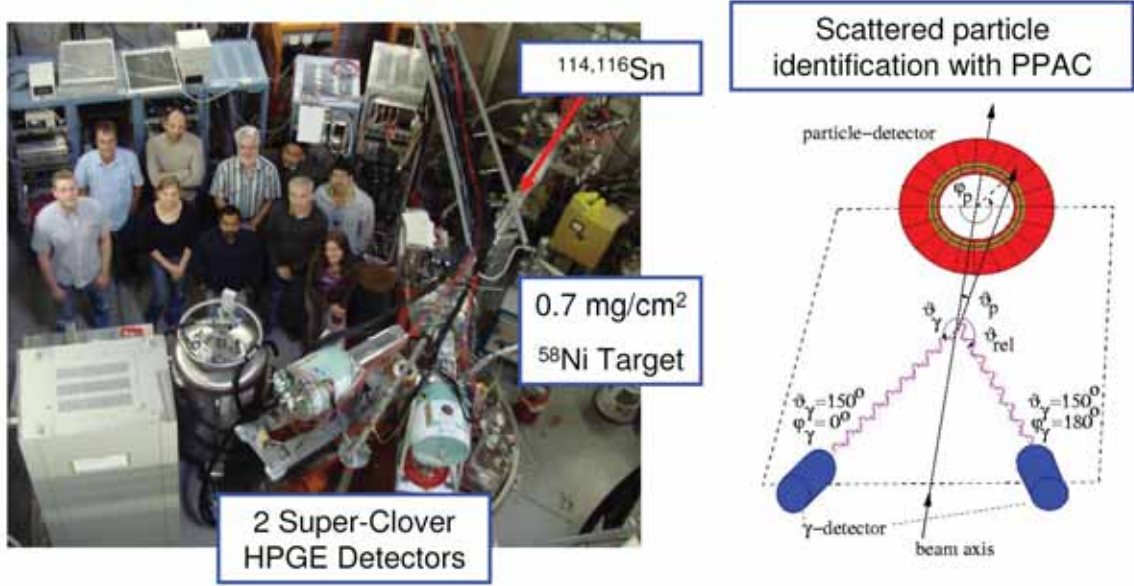


Fig. 2. Experimental setup for the B(E2) measurements at GSI.

The scattering angle determination of the heavy ions was done with a position sensitive annular parallel plate avalanche counter (PPAC), which covers scattering angles of $\theta_{\text{lab}} = 12 - 45^\circ$ and $\phi_{\text{lab}} = 0 - 360^\circ$ as the projectile as well as the target nucleus were detected in the PPAC (fig 3).

To determine the B(E2) values Contributions from higher lying states were taken into account. Literature value for ^{116}Sn is $0.209(6) e^2b^2$ and for ^{58}Ni is $0.0493(7) e^2b^2$. There are two possibilities to determine B(E2) of ^{114}Sn : one relative to ^{58}Ni and other relative to ^{116}Sn .

$$\begin{aligned}
 B(E2, ^{114}\text{Sn}) &= B(E2, ^{116}\text{Sn}) \frac{\sigma_{^{116}\text{Sn}} I_\gamma(^{114}\text{Sn}) I_\gamma(^{58}\text{Ni})}{\sigma_{^{114}\text{Sn}} I_\gamma(^{58}\text{Ni}) I_\gamma(^{116}\text{Sn})} \\
 &= 0.231(7) e^2b^2
 \end{aligned}$$

B(E2) of ^{114}Sn determined to be $0.231(7) e^2b^2$ (figure 5) This value is higher than expected from state of the art LSSM calculations using a ^{110}Sn or ^{90}Zr core (fig 1) and Supports the observed high B(E2) values for $^{108,110}\text{Sn}$. The next step is to perform a precise measurement of the B(E2) of ^{112}Sn at IUAC New Delhi.

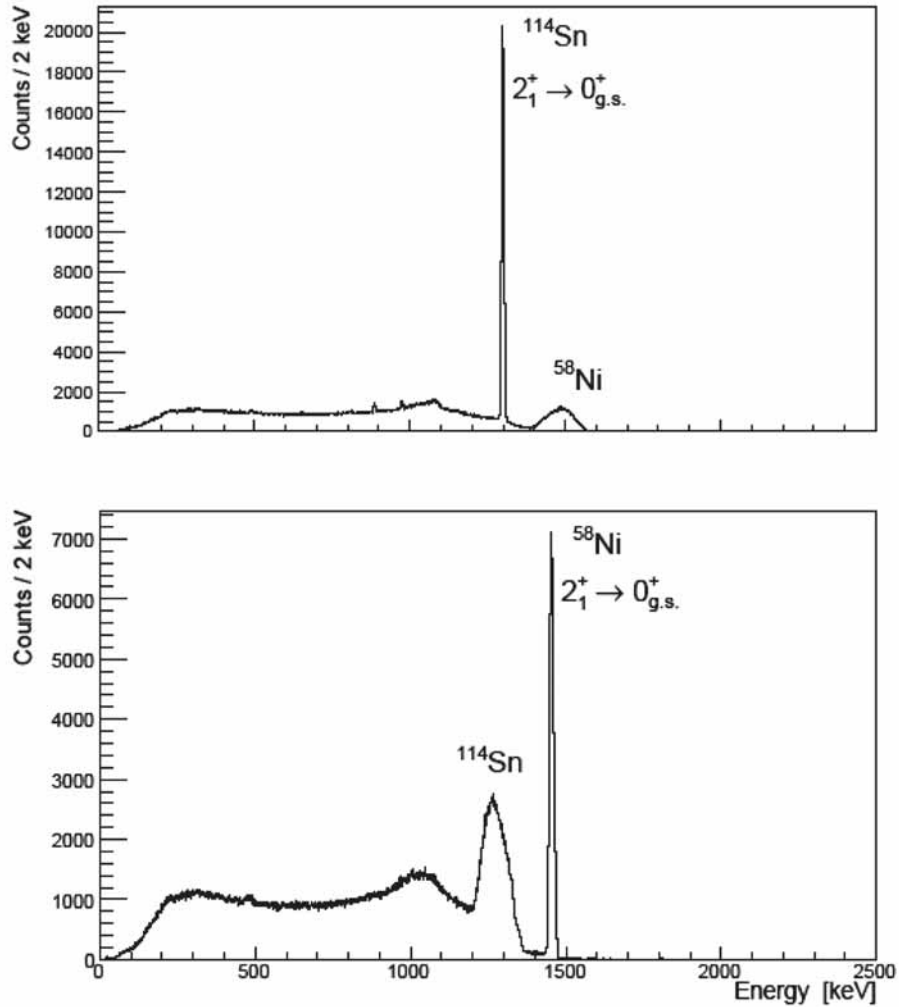


Fig. 3. Doppler Corrected g-spectra for ^{58}Ni and ^{114}Sn

REFERENCES

- [1] R. Casten, Nucl. Structure from a Simple Perspective. Oxford University Press Inc., N New York (2000).
- [2] A. Banu, PhD. Thesis, 2005
- [3] S. Raman, Atomic Data and Nuclear Data Tables 78, 1-129 (2001)
- [4] D.C. Radford et al., Nucl. Phys. A 746, 83c-89c (2004)
- [5] Atomic Data and Nuclear Data Tables, Volume 36, Issue 1, 1987, 1-96
- [6] R. Greatzer et al., Phys. Rev. C 12, 1462-1468 (1975)
- [7] P.H. Stelson et al., Phys. Rev. C2, 2015-2022 (1970)
- [8] D.S. Andreev et al., Izvest. Akad. Nauk SSSR, Ser.Fiz 25, 832 (1961)
- [9] J. Gableske et al., Nucl. Phys. A, Vol. 691, (2001) 551-576
- [10] I.N. Vishnevsky et al., Proc. 41st Ann. Conf. Nucl. Spectrosc. Struct. At. Nuclei, Minsk, p. 71 (1991)
- [11] G.M. Temmer and N. P. Heydenburg, Phys Rev. 104, (1956) 967-980

5.1.11 Stopped beam experiments at RISING : active stopper measurements

R. Kumar^{1,2}, F.G. Molina³, S. Pietri⁴, P. Doornenbal^{2,5}, I. Kojouharov², W. Prokopowicz², H. Schaffner² and H.-J. Wollersheim²

¹Inter-University Accelerator Centr, Aruna Asaf Ali Marg, New Delhi 110067

²GSI Darmstadt

³Univ. Valencia

⁴Univ. Surrey

⁵Univ. Köln

A new beta counting system has been developed for the RISING (Rare Isotope Spectroscopic INvestigation at GSI) project to study the beta decay of exotic nuclei produced by fission and fragmentation. This system employs the Micron Semiconductor Ltd.[1] Model W1(DS)-1000 DC coupled double-sided silicon strip detector (DSSSD) with 16 front strips and 16 back strips, each of width 3mm, to detect both fragment implants and their subsequent beta decays. One of the challenges in designing electronics for the beta counting system is the range of charged particle energies that must be measured. A fast fragment implant will deposit more than 1GeV total energy in the DSSSD, while an emitted beta particle will deposit less than 1MeV. As can be seen in fig.1, implantation and decay events are directly correlated within each pixel of the detector, providing a measurement of the β -decay time in the seconds range.

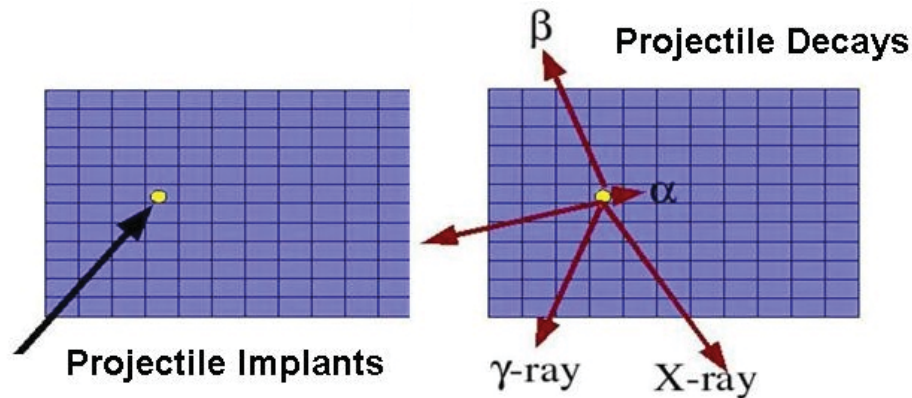


Fig.1. Schematic drawing of the position correlation between the projectile implant and the subsequent β -decay measured with the double-sided silicon strip detector (DSSSD).

The mesytec MPR-32 multi-channel preamplifier is available in a linear and logarithmic mode. A typical application of the logarithmic one is decay spectroscopy which allows the measurement of both the β -energy (in MeV range) and the implantation of heavy ions (in GeV range) with the silicon detector. The MPR-LOG series provides a linear range, which covers 70% of the total range. The last 30% covers the range up to 3GeV. Fig.2 shows the characteristics of the logarithmic MPR-32 preamplifier which was measured with a research pulser using the correct pulse shape. The pulse height can not be directly related to the implantation energy because of the pulse height defect. The MPR-32 can easily be combined with two mesytec STM-16 shaping-/

timing filter/ discriminator modules when the differential input version is used. A shaping time of $1\mu\text{s}$ (FWHM) was selected for the following measurements. Each analogue signal (34 pin male connector) was fed directly to a CAEN V785AF ADC. The trigger signal of STM-16 was used to produce the ADC gate. The detection limit for low energy b-particles is at $\sim 150\text{keV}$.

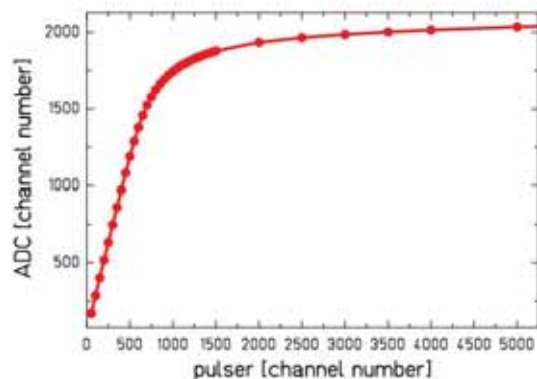


Fig.2. The characteristics of the logarithmic MPR-32 preamplifier was measured with a 10MeV linear range setting and the STM-16 spectroscopy amplifier (gain=1, threshold=5 and shaping time $2.5\mu\text{s}$ FWHM).

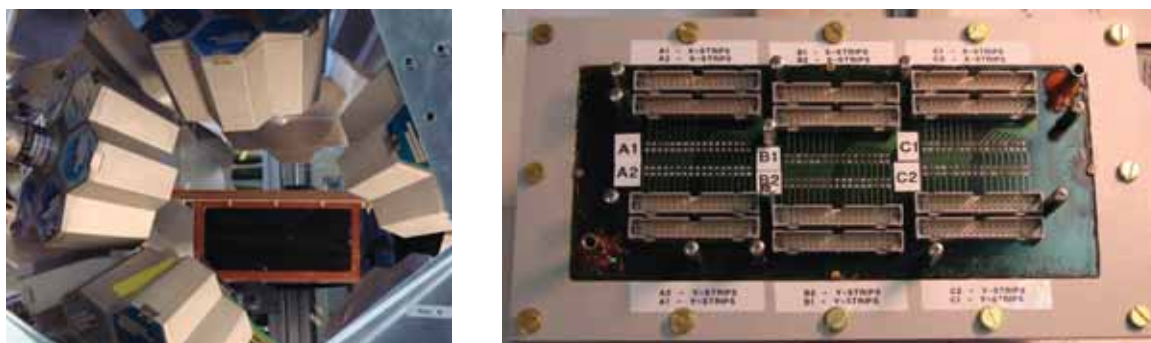
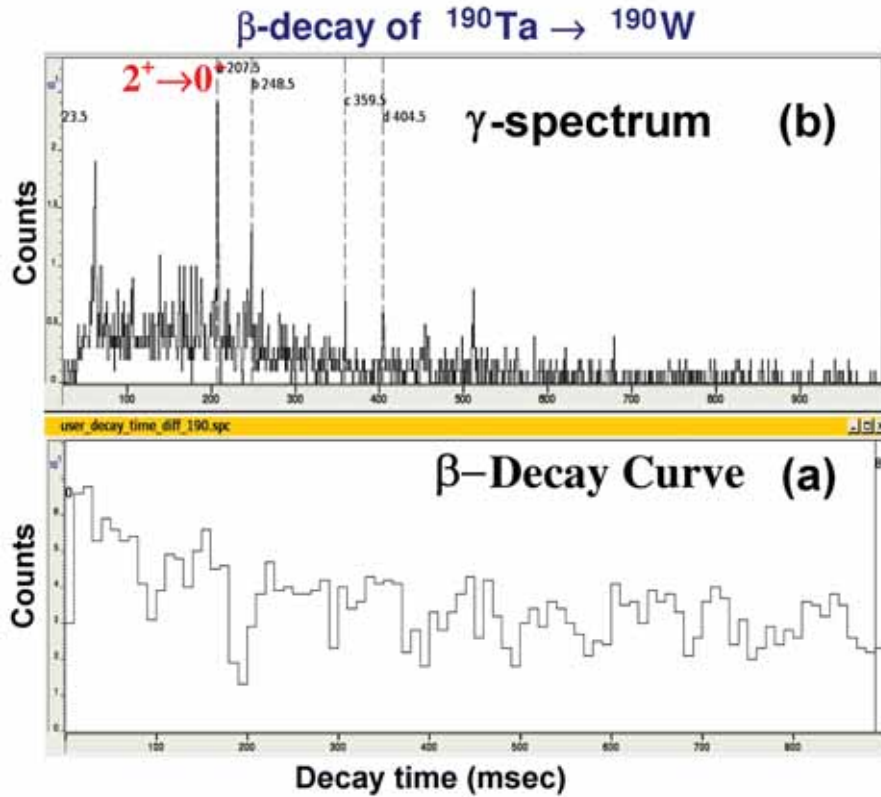


Fig.3. The Cluster array of the stopped beam RISING experiments with the active stopper vessel made out of Pertinax (left) and the top cover of the active stopper chamber with the cable connectors (right) for six DSSSD arranged in two rows.

For the in-beam experiments, the DSSSD was operated in dry nitrogen at atmospheric pressure. A test measurement has been performed with the RISING set-up in the S4 area of the fragment separator (FRS) at GSI to investigate the heavy ion implantation in the double-sided Si-strip detector. Initial test of the setup was carried out with a primary beam of 136Xe with 400MeV/A which was slowed down in the S4-degrader and finally implanted in the silicon detector. The active stopper vessel for the DSSSD (fig. 3) is surrounded by the Cluster array of the stopped beam RISING experiments. The chamber is produced out of 2mm Pertinax with an entrance and exit window covered by a thin black Pocalon C foil ($20\mu\text{m}$). The top cover of the chamber shows

the cable connectors for six DSSD which can be arranged in two rows. Although the implanted beam produced signals in more than one strip, their position could be identified from the energy deposited on neighbouring strips.



**Fig. 4. (a) Time difference between implantation and β -decay of $^{190}\text{Ta} \rightarrow ^{190}\text{W}$
(b) γ -rays in coincidence with the β -particles**

For the first β -decay experiments with the RISING setup, ions of $^{198,202}\text{Ir}$, ^{168}Dy , $^{190,192}\text{Ta}$, ^{194}Re and $^{203,205}\text{Au}$ of ~ 50 MeV/A energy were produced in the reaction $^{208}\text{Pb} + ^9\text{Be}$ at 1 GeV/A. Typical implantation time was for 1.5 sec followed by 18 sec beam off period. Fig 4a shows the time correlation of β -particles with the stopped ion implanted in the same pixel. The energy spectra of γ -rays detected in the Cluster array in coincidence with β -particles are shown in fig 4b. The know transition energy at 207 keV in ^{190}W [3] can now be assigned to the $2^+ \rightarrow 0^+$ transition, based on the present coincidence measurement. The experimental setup also allowed lifetime measurements of high spin isomers populated in heavy ion fragmentation reaction.

REFERENCES

- [1] Micron Semiconductor Ltd www.micronsemiconductor.co.uk
- [2] mesytec www.mesytec.com
- [3] Zs. Podolyak et al, Phys. Lett 491B (2000) 225
- [4] J.I. Prisciandaro et al., Nucl. Instr. Meth. A505 (2003), 140

[5] J. Elson, Pico Systems, 543 Lindeman Rd., Kirkwood, MO 63122, USA

5.1.12 Shell model study of the pairing correlations

J.A. Sheikh ^{1,2}, P.A. Ganai ¹, R.P. Singh ², R.K. Bhowmik ² and S. Frauendorf ³

¹Department of Physics, University of Kashmir, Srinagar, 190 006, India

²Inter University Accelerator Centre, Aruna Asaf Ali Marg, New Delhi 110067

³Department of Physics, University of Notre Dame, Notre Dame, IN 46556, USA

It is well established that the pairing field is an important component of the nuclear mean-field potential. The interplay between the deformation driving forces and the pairing field determines most of the properties of a nuclear system. The relevance of the pairing field for the nuclear many-body system was proposed in the seminal work of Bohr, Mottelson and Pines in 1958 [1]. During the last nearly 50 years, the effects of the pairing field has been primarily studied in the mean-field approximation [2, 3]. In this approach, the pairing correlations are finite up to a certain rotational frequency or temperature [4, 5] and then these correlations suddenly vanish above this transitional point. The empirical analysis of the experimental data, however, shows a smooth transition from one phase to the other. The reason for this discrepancy is known to arise from the neglect of the fluctuations in the mean-field models [6-10].

For a finite system, the fluctuations are important and need to be incorporated for an accurate description of these systems [11, 12]. The particle number projection methods are now readily available at zero temperature [13] to incorporate the fluctuations quite accurately. The projection at finite temperature is more important as it is known that the mean-field or BCS wave function for an even or odd particle system has admixtures from both even and odd neighbouring particle numbers [12, 14]. It has been demonstrated recently in an exactly solvable model that the pairing correlations re-appear at finite temperature after they are quenched at zero temperature and high rotational frequency [8, 15]. This surprising result, which completely contradicts the mean-field predictions, needs to be studied in more realistic models.

The purpose of the present work is to study the pairing correlations in a realistic space using the spherical shell model (SSM) approach. A new shell model program has been developed by two of the present authors [16]. This new program completely works in the *j*-representation [17] and is quite similar in structure to that of ANTONIE code developed by the Madrid-Strasbourg group [18]. The shell model approach provides the most accurate description of nuclear properties and incorporates all the possible modes of excitations.

RESULTS AND DISCUSSIONS

The shell model calculations have been performed in the middle of the *sd*-shell for 'USD' interaction. The calculations have been carried out in mid-SD shell region for the nuclei ²⁸Si, ²⁷Si and ²⁶Al. A Comparison of these nuclei provides information about pairing correlations in even-even, odd-A and odd-odd nuclei. The pairing correlations have been calculated using the canonical ensemble approach [8, 11] since the exact solutions have well defined particle number. A few

thousand states for each angular momentum have been calculated to evaluate the statistical partition function from which the pair gaps are extracted.

The results of the neutron (Δ_n), proton (Δ_p) and neutron-proton (Δ_{np}) monopole pair gaps for ^{28}Si are shown as a function of temperature (T) in Figs. 1 and 2 for even- and odd-spin values. Even- and odd-spin values are plotted separately since they have different intrinsic structures.. In order to investigate, in detail, the variation of the pairing correlations with spin (I), the correlations are plotted separately for different value of spin.

For $I=0$ in Fig. 1, Δ_n , Δ_p and Δ_{np} are identical and quite large at low temperatures. The ground-state in even-even systems is a paired configuration with maximum correlations. These correlations are almost unchanged till $T \approx 2$ MeV and then these correlations are observed to be reduced with increasing temperature. However, in comparison to the mean-field models which predict a sudden transition from the paired to the unpaired state, the exact analysis depicts a smooth drop in the pair correlations. The most unexpected observation in Fig. 1 is that at large temperatures Δ_{np} deviates considerably from Δ_n and Δ_p . It seems that there is a break down of the isospin symmetry at higher temperatures, although the two-body interaction used in the present work obeys isospin symmetry. This isospin symmetry breaking is also observed in the ref.[19]

For even-spin values of $I=2, 4, 6, 8$ and 10 , it is observed that the pair correlations drop in a step wise manner and the pairing gaps for these spin values at $T=0$ are approximately 2, 1.8, 1.6, 1.45 and 1.30. The temperature dependence of the pairing gaps for $I=2$ and 4 depict a similar behaviour as that of $I=0$. For $I=8$ and 10 , it is noted that at low temperatures there appears a slight increase in the pair correlations and for higher temperatures the correlations drop as in the earlier cases.

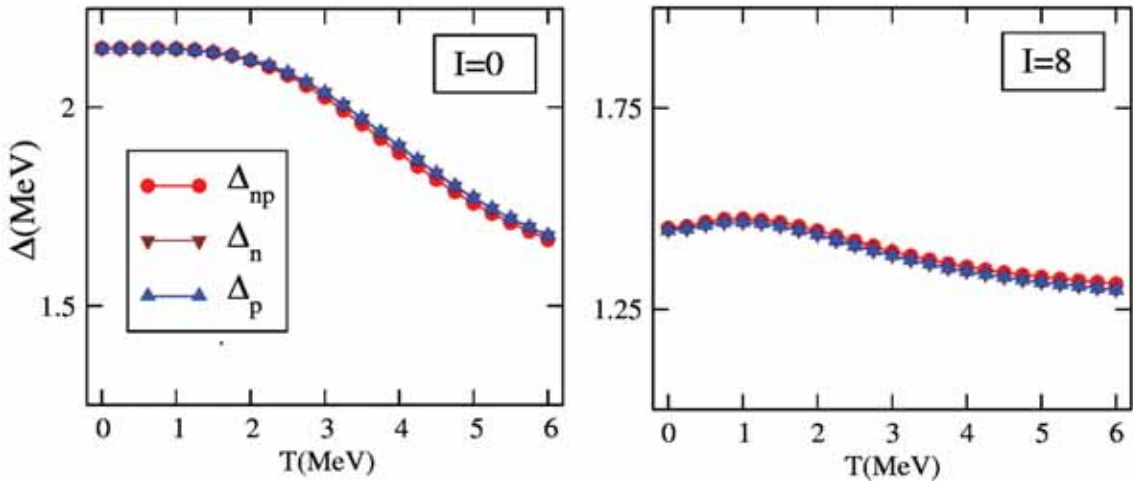


Fig.1. Temperature dependence of pair-gaps for ^{28}Si . The results are shown for even-spin values of $I = 0$ and 8

For odd-spin values, shown in Fig. 2, pair gaps depict a different behaviour as compared to the even-spin values and show a drop at very low temperatures. This is easily understood by noting that the odd-spin band is a two quasi-particle band with reduced pairing. It is also noted that for $I=1$, the isospin symmetry breaking appears to be maximum which is not easily comprehensible. For odd-spin states of $I=7, 9$ and 11 , it is observed that for low temperatures, the pair correlations increase with increasing temperature. In particular, for $I=11$, Δ_{np} pair correlations seem to increase considerably.

For the odd-odd ^{26}Al system, results for low spin values are quite different from those of even-even and odd-systems. It is noted that for $I=0$, Δ_{np} is quite large as compared to Δ_n and Δ_p . The ground-state for the odd-odd system is a neutron-proton paired state rather than the identical particle paired state. For $I=2$, Δ_{np} is still larger as compared to identical particle pairing, but with increasing spin the results are similar to the even-even system. The isospin symmetry seems to be preserved at low temperatures, but is violated at higher temperatures. For odd-spin values, isospin symmetry seems to be preserved for all spin values and there is only slight violation at higher temperatures.

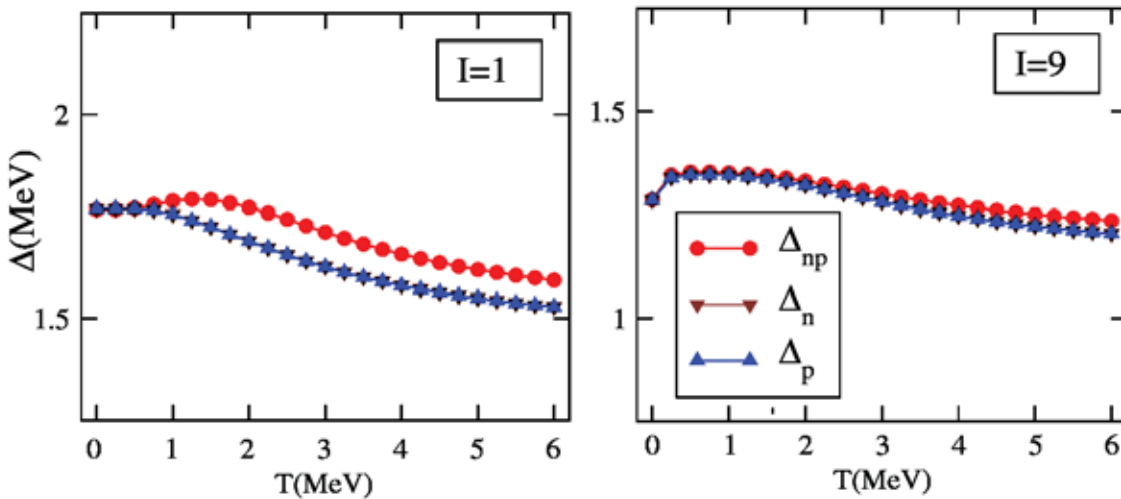


Fig. 2. Temperature dependence of pair-gaps for ^{28}Si . Pair-gaps are shown for odd-spin values with $I = 1$ and 9 .

The pairing correlations for odd-system and odd-odd system are only a few percent lower than the even-even system. This again contradicts the mean-field prediction that the pairing in the odd and odd-odd systems is substantially lower than the even-even system.

REFERENCES

- [1] A. Bohr, B.R. Mottelson and D. Pines, 11 (1958) 936
- [2] A. Bohr and B.R. Mottelson, Nuclear Structure, Vol. 2 (Benjamin Inc., New York, 1975)
- [3] P. Ring and P. Schuck, The Nuclear Many Body Problem (Springer, New York) 1980.
- [4] A.L. Goodman, Nucl. Phys. A352 (1981) 30

- [5] A.L. Goodman, Phys. Rev. C38 (1988) 1092
- [6] J.L. Egido and P. Ring, J. Phys. G 19 (1993) 1
- [7] N. Dinh Dang, P. Ring and R. Rossignoli, Phys. Rev. C47 (1993) 606
- [8] S. Frauendorf, N.K. Kuzmenko, V.M. Mikhajlov and J.A. Sheikh, Phys. Rev. B68 (2003) 024518
- [9] M. Anguiano, J.L. Egido and L.M. Robledo, Nucl. Phys. A696 (2001) 467
- [10] J.A. Sheikh, P. Ring, E. Lopes and R. Rossignoli, Phys. Rev. C66 (2002) 044318
- [11] L.D. Landau and E.M. Lifshitz, Statistical Physics, Butterworth-Heinemann, (1999)
- [12] R. Balian, H. Flocard and M. Veneroni, Phys. Rep. 317 (1999) 251
- [13] J.A. Sheikh and P. Ring, Nucl. Phys. A665 (2000) 71
- [14] H. Flocard and N. Onishi, Ann. Phys. (N.Y.) 254 (1996) 275
- [15] J.A. Sheikh, R. Palit and S. Frauendorf, Phys. Rev. C72 (2005) 041301(R)
- [16] J.A. Sheikh and R.P. Singh, to be published
- [17] J.B. French, E.C. Halbert, J.B. McGrory and S.S.M. Wong, Advances in Nuclear Physics, edited by M. Baranger and E. Vogt, Plenum, New York, 1969, Vol. 3
- [18] E. Caurier, G. Martinez-Pinedo, F. Nowacki, A. Poves, A. P. Zuker, Rev. Mod. Phys. 77 (2005) 427
- [19] D.J. Dean, S. L. Koonin, K. Langanke, P. B. Radha, Phys. Lett. B 399 (1997) 1
- [20] C. Baktash, J.D. Garrett, D.F. Winchell and A. Smith, Phys. Rev. Lett. 69 (1992) 1500, and references therein

5.2 MATERIALS SCIENCE

There have been a large number of experiments in materials science with energetic ion beams. The experiments have been on various type of materials such as polymers, metal semiconductor interfaces, oxide materials, magnetic materials etc. The problems were related to electronic sputtering, ion beam mixing, nanostructuring of the materials, surface modifications, materials modification, ion beam induced epitaxial crystallization etc.

On-line ERDA using large area position sensitive detector was effectively used for the electronic sputtering measurements in LiF and graphite. The electronic sputtering of LiF clearly showed the dependence on the grain size which were qualitatively explained by thermal spike model assumptions. Characterization studies by ERDA were performed in some cases. The ion beam mixing experiments in Ti/Si, Mo/Si and Au/Ge systems were performed.

In a first experiment of in-situ XRD in phase 2 beam hall, the growth of Au nanoparticles with ion beam irradiation was investigated and explained by temperature spike mechanism. Formation of Ge nanocrystals in SHI irradiated GeO_2 was observed. Sub-micron pores generated by chemical etching of SHI irradiated polymers, were filled with Ag nanoparticles and electronic properties of the same were studied. The field emission characteristics of the C nanowire created by SHI irradiation of fullerene were studied. Creation and alteration in nanostructures of Co, ZnO and SnO_2 were studied by different groups. The effect of SHI irradiation on the PVDF/silicate nanocomposite were studied. The effect of SHI irradiation on the phase transition of nano orthoferrites were studied and was compared with the effect of hydrostatic pressure. The nano ripple and nano dot formation in keV atoms irradiated InP was shown to be dependent on the angle of incidence. Nano ripples in 6H-SiC were formed by 100 keV Ar ion irradiation.

In-situ transport properties were studied in the ion irradiated Au/n-Si Schottky structures. Ex-situ transport studies were performed in irradiated Au/n-GaAs Schottky structures. In IBIEC experiments, it was shown that lower mass ions are more effective in recrystallization at lower temperatures. The semiconductors studied for irradiation effects were InGaAs/InP, Cu_xS and ZnO. The content of magnetic carbon in the ion irradiated fullerene was shown to be dependent on the energy loss of the ions. It was shown that the band gap in CdS:Mn system can be increased by ion irradiation. Phase transformation from amorphous TiO_2 to a mixed rutile and anatase phase was observed by ion irradiation. CdTe and CdZnTe based gamma detectors were studied for radiation damage response.

SHI induced modifications were studied in NiO, Al_2O_3 , YBCO, ferrites, ferroelectrics, Li Zinc silicate glass, borosilicate glass, ThGeO_4 , LiNbO_3 , Benzimidazole crystals, pyrochlores, Hydroxyapatite, polyanalin composite, metal polymer nanocomposite, polyimide, poly methylthiophene etc. Apart from these, the memory devices used in spacecraft were tested for radiation damage.

5.2.1 On-line study of Hydrogen loss from Passivated Mercury Cadmium Telluride under intense electronic excitation

Anjali¹, P. Srivastava¹, S. Ghosh¹, S A Khan²

¹Department of Physics, IIT Delhi, Hauz Khas, New Delhi - 110016

²Inter-University Accelerator Centre, Aruna Asaf Ali Marg, New Delhi 110 067

Mercury cadmium telluride (MCT) is a key material at the heart of advanced IR detector systems. Introduction of atomic hydrogen into semiconductors has attracted wide interest as it can significantly passivate the electrical activity of dangling or defective bonds as well as provides atomically smooth surfaces [1]. It is also found that hydrogen can passivate both shallow acceptor and donor impurities in several technologically important semiconductors. The improvement of the electrical and optical properties of the MCT based IR devices has been observed from AFM [1], RHEED [1], infrared transmission [2], Hall [3], and C-V measurements etc. The AFM and RHEED studies of hydrogen etched MCT wafers confirm the removal of the oxides and the Te overlayer from the Br- etched MCT wafers. The hydrogenation of MCT reduces the below band gap absorption [2], improves the resistivity by two orders of magnitude [3] and increases in minority carrier lifetime [4,5] by passivating the deep traps. Based on these measurements, a few mechanisms have been suggested to explain hydrogenation process in MCT. Apart from this, our RBS investigations on CdTe/MCT and CdTe/h-MCT suggest that hydrogenation results in drastic improvement in the compositional stability of MCT passivated by CdTe [6]. But, there is no direct evidence for these mechanisms. Therefore, it becomes very important to study the distribution of hydrogen in the MCT substrate as well as on the passivant - MCT interface to understand the actual role of hydrogen in this improvement. An important step in this direction would be to quantify H content in hydrogenated MCT and find its concentration profile as a function of depth. For this purpose, we employed on-line Elastic Recoil Detection Analysis (ERDA) technique, which has been established as an important tool in this respect.

The MCT wafers were hydrogenated using a Photo-CVD set-up. Details are described elsewhere [7]. ERDA measurement of hydrogenated MCT for studying the hydrogen distribution was done at Inter University Accelerator Centre (IUAC), New Delhi. For performing the ERDA measurements, 80 MeV Ni⁺⁹ ions were used as projectile. The beam spot was 2 mm × 2mm. The Si surface barrier detector was used for detection of recoiled hydrogen atoms. The detector was placed in the forward direction and the scattering angle was 45°. The sample was also tilted at an angle of 30°. The solid angle of the detector was 1.98 mSr. To prevent the recoiled atoms other than that of hydrogen, a stopper foil is generally placed in front of the detector. For this purpose, a 22.6 mm thick stopper foil of Al was used. The thickness of the Al foil was optimized to block the penetration of abundantly recoiled heavier atoms (Hg, Cd, Te, O etc.) while permitting the passage of the hydrogen atom. The estimation of the thickness of Al foil was done using SRIM [8].

The recoil spectrum profile shown in figure 1 suggests that the hydrogen is mainly present near the surface of the sample and the areal concentration of hydrogen falls as we move deeper. The hydrogen signal from channel number 1031 to 557 was selected for the calculations of hydrogen concentration, as the signal is almost negligible beyond channel number 557. ERD analysis

shows that about 11% hydrogen is present in the hydrogenated samples. Hydrogen present near surface may somehow satisfy the Hg vacancies and reduce their mobility either by changing the surface morphology or by forming complexes with the Hg vacancies present in the near surface region. Also the formation of Hg and Cd hydrides has been suggested which can reduce further movement of Hg vacancies in the MCT wafer.

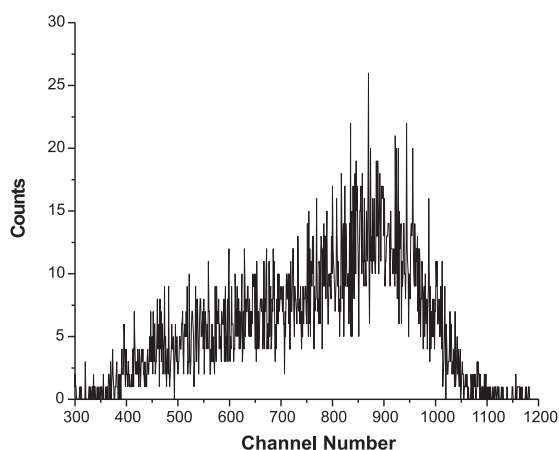


Fig. 1. Distribution profile of hydrogen in hydrogenated MCT wafer. Channel no. along x-axis represents the recoil energy and hence the depth of H in the wafer and the count along y axis represents recoil yield of H.

REFERENCES

- [1] K. S. Ziemer, C. D. Stinespring, L. S. Hirsch, T. H. Myers, J. Crys. Grow. 191 (1998) 594.
- [2] Y. F. Chen, and W.S. Chen, Appl. Phys. Lett. 59 (6), (1991) 703.
- [3] S. Sitharaman, R. Raman, L. Durai, S. Pal, M. Gautam, A. Nagpal, S. Kumar, S. N. Chatterjee, S. C. Gupta, J. Crystal Growth, 285(3) (2005) 318.
- [4] H. Kim, S. H. Bae, C. K. Kim, H. C. Lee, H. Chul, Proc. SPIE, 3436 (1998) 98.
- [5] A. I. Evstigneev, V.F. Kuleshov, G.A. Lubochikova, M. V. Pashkovskii, E. B. Yakimov, N. A. Yakin, Sov. Phys. Semicond. 19 (1988) 562.
- [6] Anjali, P. Srivastava, S. Mohapatra, R. Pal, H.P. Vyas, B.R. Sekhar, and H.K. Sehgal, Semiconductor Science & Technology, 21 (2006) 998.
- [7] O. P. Agnihotri, H. K. Sehgal, R. Pal, V. Gopal, Appl. Phys. Lett. 77(9) (2000) 1330.
- [8] J. F. Ziegler, SRIM - 98.01, The stopping range of ions in matter, IBM research, 28-0 York Town Heights, NY 10598, USA, 1998.

5.2.2 Influence of Grain Size on Electronic Sputtering of LiF Thin Films

M. Kumar¹, S. A. Khan², F. Singh², A. Tripathi², D. K. Avasthi² and A. C. Pandey¹

¹Department of Physics, University of Allahabad, Allahabad 211 002

²Inter-University Accelerator Centre, Aruna Asaf Ali Marg, New Delhi 110 067

The electronic sputtering from LiF thin films is investigated using 120 MeV Ag^{25+} ions in equilibrium charge state as projectiles. The sputter yield of Li and F from 160 nm thin polycrystalline LiF films with different grain sizes (22-58 nm) is measured with online elastic recoil detection analysis technique. The sputtering yield is of the order of 10⁵ atoms/ion. A reduction in sputter yield is observed with increasing grain size [1] as shown in figure 1.

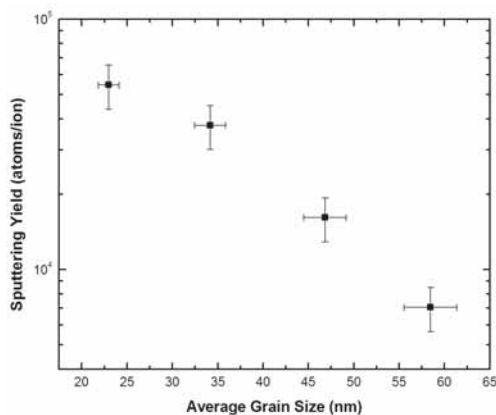


Fig. 1. Variation of electronic sputter yield with grain size of the film. The yield increases with reduction in the grain size.

The results are explained in terms of size effect along with inelastic thermal spike model as discussed for thickness dependence electronic sputtering of LiF thin films [2]. According to thermal spike model, the mean diffusion length of the excited electrons strongly influences the electron phonon interaction resulting in high energy transfer to the lattice from projectile. The electrons liberated in different directions from the ion track have different diffusion length depending on their energies. Now, there are two factors that affect the mean diffusion length, one is the thickness of the film and other one is grain size of the film. But as the film thickness is same for all the cases, the only factor is grain size of the film, which affects the electronic sputtering process.

The grain boundaries in the films have all the possible orientations and become electron scatterer. In this respect they behave like film interface [3] and influence electron motion. As the grain sizes become smaller, scattering of electrons from the grain boundaries effectively reduces mean diffusion length of electrons. A smaller mean diffusion length of electrons may result in a stronger localization of the electronic excitation energy within the nano-crystallites. A thermal spike calculation performed for different grain sizes in tin oxide by Berthelot et al. showed a strong size effect on the temperature evaluation in the grains [4]. On the other hand, the thermal energy, which diffuses out of the grain boundaries, will be higher in larger grains than in smaller grains [4]. Higher temperature spikes and a reduced out diffusion of thermal energy in smaller grains result in confinement of more thermal energy in the lattice and hence in higher sputtering.

REFERENCES

- [1] M. Kumar, S. A. Khan, F. Singh, A. Tripathi, D. K. Avasthi and A.C. Pandey, Nucl. Instrum. and Methods B (in press, doi:10.1016/j.nimb.2006.12.021).
- [2] M. Kumar, S. A. Khan, F. Singh, A. Tripathi, D. K. Avasthi and A.C. Pandey, IUAC Annual Report 2005-2006, page 150.

- [3] A F Mayadas and M Shatzkes, Phys. Rev. B 1 (1970) 1382.
 [4] A. Berthelot, S. Hémon, F. Gourbilleau, C. Dufour, E. Dooryhée and E. Paumier, Nucl. Instrum. Meth. B 146(1998)437.

5.2.3 Swift heavy ion induced modification in Ti/Si system studied with sub-nanometre resolution

Parasmani Rajput¹, Ajay Gupta¹, V R Reddy¹ and D. K. Avasthi²

¹UGC-DAE Consortium for Scientific Research, Indore, 452 017, India

²Inter-University Accelerator Centre, Aruna Asaf Ali Marg, New Delhi 110 067

X-ray waveguide structures have attracted considerable interest because of the possibility of using them for the study of the structural properties of the guiding layer itself. We use an x-ray waveguide structure to study the changes occurring in a Si/Ti/Si tri-layer upon swift heavy ion irradiation. The tri-layer Si/Ti/Si embedded in a planar waveguide can provide detailed information about the position and thickness of the Ti marker layer with sub-nanometre resolution using x-ray fluorescence measurements [1].

A multilayer with a nominal structure: substrate (float glass)/Pt (70 nm)/Si (16 nm)/Ti (3 nm)/Si (8 nm)/Pt (2 nm), was deposited using ion beam sputtering. Two Pt layers form the walls of the planar waveguide, while the tri-layer Si/Ti/Si forms the cavity of the planar waveguide. Waveguide modes can be excited in the cavity, whenever the following condition is satisfied:

$$D = n\lambda/2 \sin\theta,$$

where λ is the wavelength of the x-rays, θ is the angle of incidence of the x-rays, D is the thickness of the waveguide cavity, and n is the order of the mode. The Ti fluorescence exhibits peaks at angles of incidence corresponding to the waveguide modes due to resonance enhancement of the x-ray intensity inside the cavity. The relative intensities of various peaks depend upon the exact position and width of the Ti marker layer, and the sensitivity of the technique is enhanced by positioning the Ti layer asymmetrically with respect to the centre of the cavity [1]. X-ray reflectivity and x-ray fluorescence measurements were performed using a Bruker AXS D8 Advance diffractometer using Cu K α radiation. Reflected x-rays were collected using a scintillation detector, while the Ti K α fluorescence from the sample was measured using an Amptek XR100T PIN diode detector (with an energy resolution of 250 eV) kept vertically above the sample. Samples were irradiated with 120 MeV Au ions to fluences ranging from 5×10^{12} to 5×10^{13} ions /cm² using the 15UD Pelletron at IUAC. Raman measurements were performed on a Horiba JY HR800 micro-Raman system using an argon 488 nm laser as an excitation source and a CCD detector.

The Raman spectra of pristine and irradiated samples provide quantitative information about the mixing of Ti with Si. Figure 1 shows the x-ray reflectivity of pristine sample as well as irradiated samples to fluences of 5×10^{12} to 5×10^{13} ions /cm². Three sharp dips in the x-ray reflectivity patterns between the critical angles (q_c) of Si and Pt indicate the excitation of the TE₀, TE₁ and TE₂ modes of the waveguide. Figure 2 gives the x-ray fluorescence from the Ti marker layer for a pristine sample as well as the samples irradiated sample. Possible intermixing at various interfaces induced due to irradiation is in general manifested in terms of an increased

interface roughness. Since the intermixing of the Ti layer with Si is very strong, it was taken into account by assuming a change in its composition (i.e. a decrease in its electron density) accompanied by a proportional increase in its effective thickness. The resulting electron density profiles after fitting of fluorescence and reflectivity are shown in figure 3. For the electron density profile, one may note that the Ti layer broadens considerably with irradiation fluence. At the same time, centroid of the peak exhibits a small shift towards the surface. The profile of the top Pt layer also exhibits a small broadening, which may be partly due to surface roughness and partly due to some intermixing with Si. The electronic energy loss (Se) in Ti is above the threshold value and therefore one expects large damage creation in Ti layer, which would result in intermixing with Si. Shift in the position of the centroid of Ti layer with irradiation can be understood in terms of an asymmetric mixing at the two interfaces.

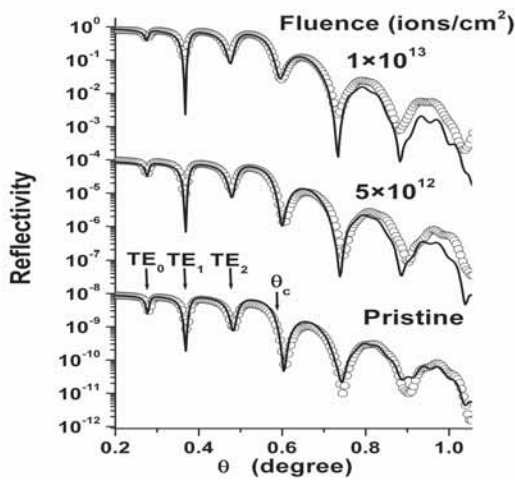


Fig. 1. X-ray reflectivity of pristine and irradiated samples as a function of angle of incidence

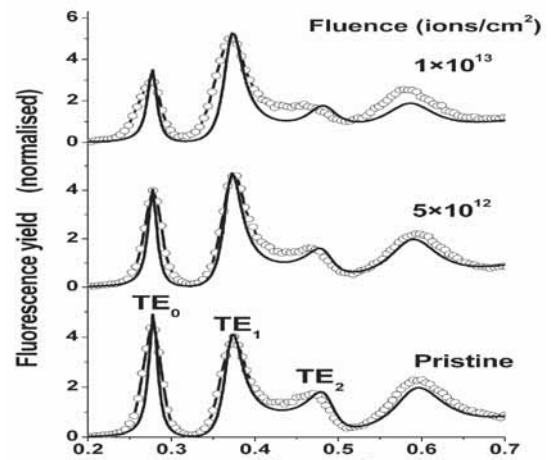


Fig. 2. Ti fluorescence from pristine and irradiated samples as a function of angle of incidence

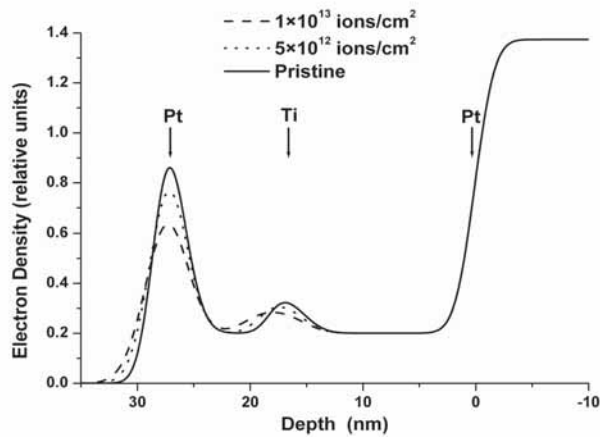


Fig 3. The electron density profile of pristine and irradiated samples as obtained from simultaneous fitting of x-ray reflectivity and Ti fluorescence data.

REFERENCE

- [1] A. Gupta, P. Rajput, A. Saraiya, V. R. Reddy, M. Gupta, S. Bernstorff, and H. Amenitsch, Phys. Rev. B 72 (2005) 075436.

5.2.4 Mixing induced by Swift Heavy Ions at Metal/Si interface

I.P.Jain¹, Garima Agarwal¹, Shivani Agarwal¹, Pratibha Sharma¹, Chhagan Lal¹, Rajkumar Jain¹, Renu Dhunna, Devendra Vyas, D.Kabiraj² and Akhilesh Pandey³

¹Centre for Non-Conventional energy Resources, University of Rajasthan, Jaipur

²Inter-University Accelerator Centre, Aruna Asaf Ali Marg, New Delhi 110 067

³Solid State Physics Laboratory, New Delhi

Ion Beam Mixing (IBM) has been considered as an alternated means to form metal contacts in microelectronic devices using ion beam to trigger the reaction at the interface of metal and Si [1]. A number of studies on reaction kinematics between Mo and Si have been done by solid-state reaction, ion implantation techniques [2-5] and by SHI irradiation [6].

Electron beam evaporated Mo/Si thin film system has been irradiated with 120 MeV Au ions using 15 UD Pelletron Accelerator at IUAC New Delhi, India, in Material Science Chamber at different fluences from 10^{12} to 10^{14} ions/cm². The electronic and nuclear energy losses were 36.6 keV/nm and 0.7 keV/nm for Mo and 12.9 keV/nm and 0.21 KeV/nm for Si have been calculated using SRIM 2003 program. X-Ray Reflectivity (XRR) studies were undertaken to measure the deposited thickness in pristine system. Measurements were performed using CuK α radiation. Grazing incidence X-Ray diffraction (GIXRD) measurements were performed using CuK α radiation. The elemental distribution in all samples was determined by Rutherford Back-scattering Spectroscopy (RBS) using 3 MeV He⁺ ion beam at backscattering angle 170^o. Fits to the spectra were obtained with the help of the RUMP computer code.

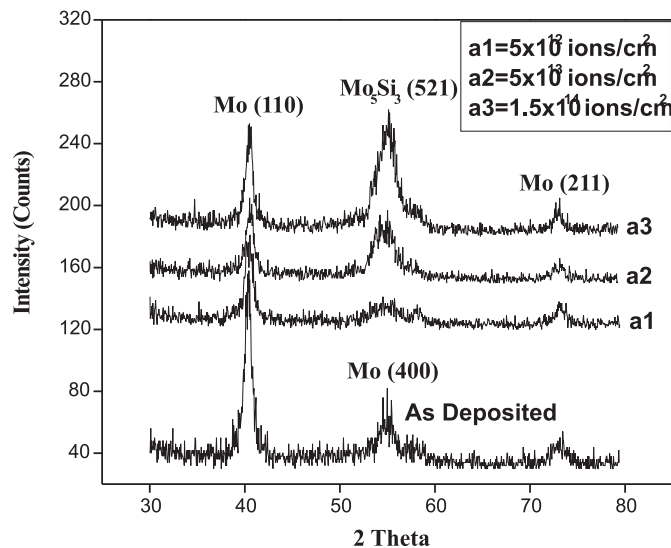


Fig. 1. GIXRD curves of as-deposited and irradiated Mo/Si system

Fig. 1 shows the X-Ray Diffraction patterns of the as-deposited as well as irradiated thin films with different fluences. This system is irradiated at different fluences as $a_1=5 \times 10^{12}$, $a_2=5 \times 10^{13}$ and $a_3=1.5 \times 10^{14}$ ions/cm². The sample irradiated at lowest dose 5×10^{12} ions/cm² shows a broad peak of Mo₅Si₃ with minimum intensity and it increases with increasing the fluence. At highest dose of 1.5×10^{14} ions/cm², a sharp peak of tetragonal-Mo₅Si₃ was formed. The diffraction peak at $2\theta=55.13^\circ$ corresponding to (521) plane allows the identification of Mo₅Si₃ phase.

It is to be noted that the weak peak of Mo₅Si₃ is also observed in the films irradiated at lowest fluence 5×10^{12} ions/cm². The dominant peaks of Mo₅Si₃ phase confirms that films are mainly composed of Mo₅Si₃. The Mo₅Si₃ is a tetragonal structure with the same **a** and **b** axes ($a=b=9.648 \text{ \AA}$, $c=4.913 \text{ \AA}$). From the evaluated microstructural parameters (Table 1), it is clear that the crystallite size of Mo increases in the irradiated sample in comparison of pristine one while the dislocation density decreases on the increase in crystallite size. Also the crystallite size of Mo₅Si₃ increased in case of irradiation reaching to higher fluences. This may be due to the sudden increase in temperature at the irradiation regime. Hence XRD measurements revealed that irradiation promotes the movement of atoms at the interface leading to the formation of new mixed compound in the form of metal silicide.

The RBS spectra of as-deposited and irradiated Mo/Si thin film system at various fluences were recorded. Sample irradiated at lowest dose 5×10^{12} ions/cm² shows a very little shift in the peaks of Mo and Si, which are not clearly observable but with the help of RBS data and its calculation using RUMP code determines a little mixing of the order of 1.5nm. In case of irradiation at fluences 5×10^{13} and 1.5×10^{14} ions/cm² a little decrease in the slope and shift towards the lower edge of Mo peak and in front edge of Si peak indicated that the mixing occurred at these interfaces. The concentration profiles for Mo/Si system were extracted from the RBS spectra with the help of RUMP simulation code. They were fitted with a Gaussian error function and the values for mixing length, interface variance, mixing rate and mixing efficiency corresponding to each irradiation fluence are calculated.

The mixing rate was calculated from the slope of the linearly fitted line of Fig. 2. In assumption of thermal spike model for semiconductor system [7] each incident ion loses its energy during its transit across the material mainly by electronic excitation. Temperature of electronic system rises for a typical time span of 10-15 s which is followed by transfer of energy from electrons to the target via the electron - phonon coupling, inducing the local temperature rise (= 1000K) in a very narrow zone. The rise and decay of the lattice is governed by two coupled differential equations [8]. For the temperatures above the melting point the lattice melts followed by fast quenching. The melting of lattice facilitates atomic motion through this zone and an enhanced diffusion takes place dominantly in each cylindrical melt zone. Thermal spike model has also been used previously to explain ion beam mixing in Metal/Si system [9,10].

REFERENCES

- [1] X.Q. Cheng, R.S. Wang,, X.J. Tang, B.X. Liu, Nucl. Instr. and Meth. Phys. Res. B 207 (2003) 301.
- [2] F.M. d'Heurle, M.Y. Tsai, C.S. Petersson, B. Stritzker, J. Appl. Phys. 53 (1982) 3067.
- [3] D.L. Kwang, D.C. Mayers, N.S. Alvi, L.W. Li E. Norbeck, Appl. Phys. Lett. 47 (1985) 688.
- [4] J.Y. Cheng, H.C. Cheng, L.J. Chen, J. Appl. Phys. 62 (1987) 3722.

- [5] J. H. Liang, C.T. Tsai, Nucl. Instr. and Meth. Phys. Res. B 242 (2006) 598.
- [6] D. Bhattacharya, G. principi, A. Gupta, D.K. Avasthi, Nucl. Instr. and Meth. Phys. Res. B 244 (2006) 198.
- [7] D.K. Avasthi, W. Assman, A. Tripathi, S.K. Srivastava, S. Ghosh, F. Grüner, M. Toulemonde, Phys. Rev. B 68 (2003) 153106.
- [8] Z.G. Wang, C. Dufour, E. Paumier and M. Toulemonde, J Phys.: Condens. Matter 6 3 (1994) 6733.
- [9] K. Diva, D. Kabiraj, B.R. Chakraborty, S.M. Shivaprasad, D.K. Avasthi, Nucl. Instr. and Meth. Phys. Res. B 222 (2004) 169.
- [10] G. Agarwal, P. Sharma, I.P. Jain, Appl. Surf. Sci. 252 (2006) 1165.

5.2.5 Effect of swift heavy ion irradiation in FePt system

S.Kavita¹, V.Raghavendra Reddy¹, Ajay Gupta¹, D.K.Avasthi²

¹UGC-DAE Consortium for Scientific Research, University Campus, Indore

²Inter University Accelerator Centre, Aruna Asaf Ali Marg, New Delhi 110 067

Swift heavy ions lose their energy in the target mainly via inelastic collisions leading to the excitation of the target electrons. The electronic energy loss has been found to create various modifications in the target material, which include creation of point defects, latent track formation, sputtering and intermixing at the interfaces. While the material modification in insulators using swift heavy ion irradiation has been studied quite extensively [1] The effects of swift heavy ion irradiation are shown to be different in bulk as compared to thin films and multilayers [2,3] Aim of the study is to elucidate the effect of reduced dimensionality of the system (i.e., homogeneous alloy film, multilayer film and nano-particles) on the swift heavy ion induced modifications. Such studies are expected to through light on the mechanism of material modification due to electronic energy loss. The FePt system due to its high magnetic anisotropy value is considered to be the best candidate for the future recording industry.

The equi-atomic FePt homogeneous alloy and [Fe (1.9 nm)/ Pt(2.5 nm)]·8 multilayer films are vacuum annealed at 450°C for 1 h for obtaining the L10 structure (hereafter referred as alloy thin film and multilayer, respectively). The FePt nano-particles with L10 structure in silver matrix (henceforth referred as nano-particles) are prepared by thermal annealing at 450°C of [FePt(1 nm)/Ag(1.6 nm)]·35 multilayer. The FePt layer with thickness values of 1 nm is not expected to form continuous film and annealing at high temperature should form FePt nano-particles in Ag matrix. The alloy thin film and nano-particles with L10 structure are irradiated with Au⁺ ions of 120 MeV to fluencies 10¹³ and 5 x 10¹³ ions/cm². The multilayer film with L10 structure is irradiated with Ag⁺ ions of 120 MeV to a fluence of 5 x 10¹³ ions/cm² using 15UD Pelletron at Inter University Accelerator Centre, New Delhi. X-ray Diffraction (XRD) and the magneto optical Kerr effect (MOKE) in longitudinal mode are used for the characterization. It is observed that irradiation results in partial destruction of L10 ordering. Fig. 1 gives the XRD spectra of deposited, annealed and irradiated samples. Detailed analysis is in progress. Irradiation effects are more pronounced in the case of nano-particles and multilayers as compared to that of continuous alloy film.

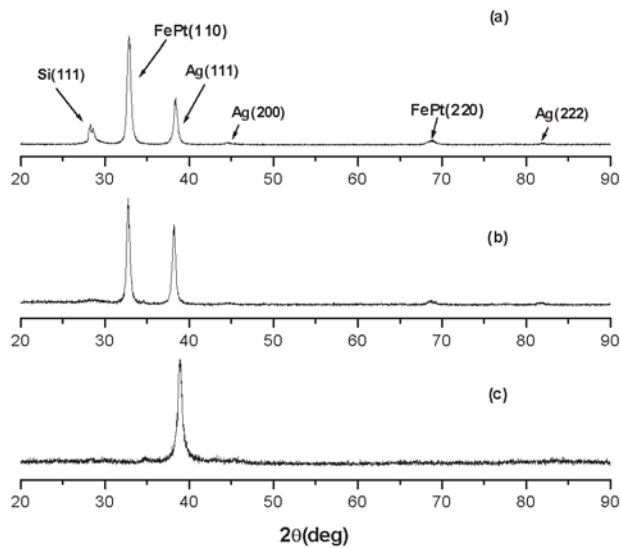


Fig. 1. XRD patterns in the theta-2theta mode and MOKE loops in longitudinal mode (a) Ag 16 film annealed at 450°C and irradiated with 120 MeV Au⁺ ions to 1x10¹³ ions/cm² (b) Ag16 film annealed at 450°C (c) As-deposited Ag16 film

REFERENCES

- [1] R.L.Fleischer, P.B.Brince and R.M.Walker., J.Appl.Phys. 36 (1965) 2645
- [2] C.Dufour, Ph.Bauer, G.Marchal, J.Grilhe, C.Jaouen, J.Pacaud and J.C.Jousset., Europhys.Lett, 21 (1993) 671
- [3] Pratima Dhuri, Ajay Gupta, S.M.Chaudhari, D.M.Phase and D.K.Avasthi., Nucle.Instrum.Methods Phys.Res.B 156 (1999) 148

5.2.6 Phase formation within Au and Ge nanoislands by room-temperature ion irradiation

T. Som¹, B. Satpati¹, F. Prokert², V. Cantelli², D. Kabiraj³

¹Institute of Physics, Sachivalaya Marg, Bhubaneswar - 751 005

²Research Center Rossendorf, P.O. Box 510119, D-01314 Dresden, Germany

³Inter-University Accelerator Centre, Aruna Asaf Ali Marg, New Delhi 110 067

Embedded metal/semiconductor nanocrystals have stimulated scientific interest because of the potential applications utilizing their unique electrical and optical properties. So far as ion beam modification of nanocrystals is concerned, the recent observations of ion-induced burrowing of Pt and Ag could be good cases for studying the single electron tunneling phenomenon. It has also been demonstrated that nanocrystals can undergo shape transition by ion irradiation [1], which has potential application in photonics.

Au and Ge layers (each having 1 nm of nominal thickness as indicated by a digital thickness monitor) were evaporated on a native oxide covered Si(100) substrate using a deposition

rate of 0.01 nm s^{-1} . In this case, the films are expected to grow in the form of nanoislands. Later on, the sample was cut into small pieces and they were irradiated by 1.5 MeV Au^{2+} ions at room temperature (RT) under a vacuum of $3 \times 10^{-7} \text{ mbar}$. Irradiation was performed at normal incidence with different fluences in the range 1×10^{13} to $1 \times 10^{15} \text{ ions cm}^{-2}$. The XRR and the GIXRD results presented here were obtained from the ROBL-CRG beamline BM 20 at the ESRF, Grenoble (France). The samples were also analysed by using a JEOL 2010 UHR transmission electron microscope (TEM) under planar and cross-sectional geometries.

The microstructure of the pristine sample is studied by TEM (shown in Fig. 1). This low magnification micrograph indicates that the average particle size of $\sim 5\text{-}7 \text{ nm}$. The inset represents the corresponding high-resolution cross sectional TEM (XTEM) micrograph of the same sample. This shows the presence of both crystalline and amorphous islands at the surface of the substrate. Calculation of d-spacings from the lattice fringes of the islands matches well only with the Au reflections.

In case of a specimen irradiated to a fluence of $1 \times 10^{14} \text{ ions cm}^{-2}$, it is observed that the island sizes and the shapes are quite different here. Many bigger islands with a large size distribution ($5\text{-}30 \text{ nm}$) are formed, whose d-spacing ($0.309 \pm 0.01 \text{ nm}$) matches well with the (225) plane of metastable $\gamma\text{-Au}_{0.6}\text{Ge}_{0.4}$. We have performed high-resolution lattice imaging from many big islands to observe the close proximity of their d-spacings to that of tetragonal $\text{Au}_{0.6}\text{Ge}_{0.4}$ alloy

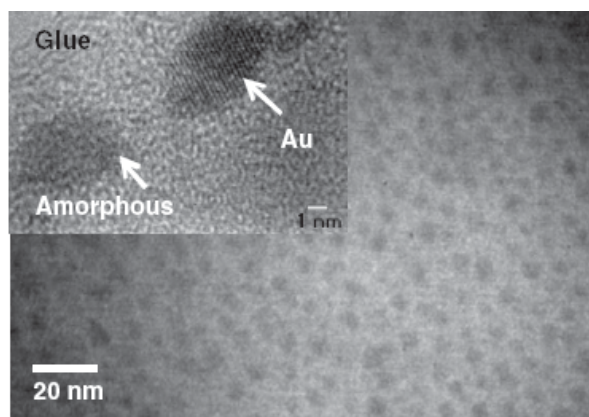


Fig. 1. Bright-field plan-view TEM micrograph of a pristine Au/Ge island thin film sample. The inset shows a high-resolution cross-sectional view of the same sample

phase. Thus, irradiation of Au/Ge nanoislands thus, leads to the formation of nano-dimensional Au-Ge alloy islands at the surface due to RT irradiation of 1.5 MeV Au^{2+} ions using a fluence of $1 \times 10^{14} \text{ ions cm}^{-2}$. XTEM image (not shown) obtained from the Au/Ge island thin film irradiated to a fluence of $1 \times 10^{15} \text{ ions cm}^{-2}$ shows the formation of a nearly single continuous layer ($6\text{-}8 \text{ nm}$). However, at some places bigger islands (up to 50 nm) are seen to be on the verge of coalescence to form a nearly continuous layer. The HRTEM studies performed from such areas also indicate the formation of the $\text{Au}_{0.6}\text{Ge}_{0.4}$ alloy. In addition, the presence of the native oxide below the alloy layer is still evident; this works as a barrier to avoid mixing of the Au and/or Ge islands with the substrate. The surface free energy of the Au-Ge alloy is not available and, therefore, it is difficult to predict its interfacial behaviour with the native oxide layer under ion bombardment. However, the

fact that $\text{Au}_{0.6}\text{Ge}_{0.4}$ alloy islands grow parallel to the oxide surface indicates the wetting of the substrate because of their sufficiently smaller surface energies [2].

Let us now discuss the possible mechanism leading to the mixing of the nanoislands of Au and Ge. In case of ion-atom collisions, primary knock-ons (recoils) will be generated followed by secondary collision cascades. Thus, Au and Ge atoms not only get displaced within the respective layers but also a fraction of these atoms are pushed into the other layer across the interface. As a matter of fact, others have observed recoil implantation for irradiation of elemental nanoclusters [2,3]. At a later stage, a molten state is expected to develop [4], which upon quenching may lead to the nucleation of metastable crystalline Au-Ge phase formation as discussed above.

REFERENCES

- [1] E. Snoeks, A. van Blaaderen, T. van Dillen, C.M. van Kats, M.L. Brongersma, and A. Polman, *Adv. Mater.* 12 (2000) 1511; S. Roorda, T. van Dillen, A. Polman, C. Graf, and A. van Blaaderen, *Adv. Mater.* 16 (2004) 235.
- [2] X. Hu, D. G. Cahill, and R.S. Averback, *J. Appl. Phys.* 92 (2002) 3995.
- [3] G.C. Rizza, M. Strobel, K.H. Heinig, and H. Bernas, *Nucl. Instr. Meth. Phys. Res. B* 178 (2001) 78.
- [4] R. Kissel and H.M. Urbassek, *Nucl. Instr. Meth. Phys. Res. B* 180, 293 (2001).

5.2.7 Electron beam assisted growth of silver nano-wires in etched ion tracks

K. A. Bogle¹, S. A. Gangal¹, V. N. Bhoraskar², Tejashree M. Bhav¹ and D. K. Avasthi³

¹Department of Electronic Science, University of Pune, Pune - 411 007

²Department of Physics, University of Pune, Pune - 411 007

³Inter University Accelerator Center, Aruna Asaf-Ali Marg, New Delhi - 100 067

Latent tracks were created in self supporting polyimide films of thickness ~ 50 μm , by 150 MeV Si ion irradiation at a fluence of 1×10^6 ions/ cm^2 . The ion tracks were suitably etched using 4 M NaOCl solution, to obtain conical shaped pores in the polymer matrix. The variation in the track size at NaOCl solution temperature, $T = 60, 70, 80$ and 90°C , and etching time $t = 45^\circ\text{C}$ are shown in Figure 1.

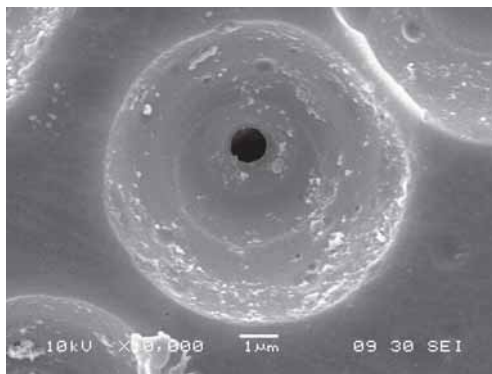


Fig. 1. Ion tracks size at an etching time of $t = 45$ min for temperature of etchant at 90°C (NaOCl)

It was observed that with increasing the etchant temperature the size of the conical ion track increases along with a large bulk etching. At lower temperature ($T = 60^{\circ}\text{C}$), the etching did not clear the ion track. At an etchant temperature of $T = 70^{\circ}\text{C}$, the conical ion tracks are found to be clear with an average pore size of 150 nm. With further increase in the etchant temperature to 80°C and 90°C the tracks size nearly reached to 1 mm, with a large bulk etching, which increases the top diameter of the cone to few mm.

The minimum size open ion track (~ 150 nm, obtained at $T = 70^{\circ}\text{C}$, $t = 45$ min) were filled with silver particles using electron beam assisted electroless deposition technique. The size of these filled particles was confirmed from the Scanning electron microscopy along with Energy dispersive X-ray spectroscopy. Figure 2 gives few SEM micrographs of filled ion tracks with Ag particles.

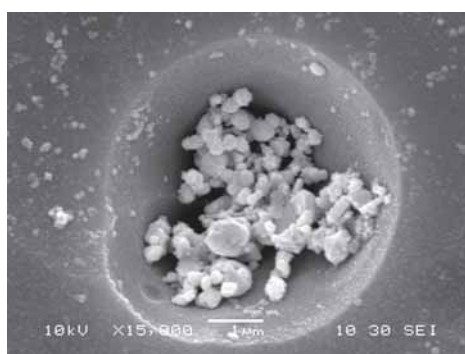


Fig. 2. Filled ion tracks at different stages using electron beam assisted electroless deposition technique.

It was seen that the pores in the polymer samples are filled with silver clusters of average size ~ 40 nm. This indicates that the tracks are filled with silver nanoparticles. The conductivity of the filled tracks with silver nanoparticles in polyimide film was measured using a Frequency dependent I-V technique. A contact was formed on the film of about 1 mm diameter and the frequency dependent I-V measurements were carried out and the variation in the resistance with frequency is shown in Figure 3. Due to a contact of 1 mm diameter, the measurement exhibited a behavior of an array of Ag nanowires.

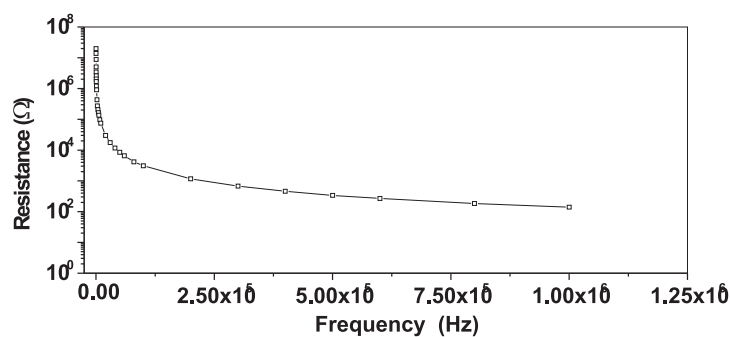


Fig. 3. The variation in resistance with frequency for the filled ion tracks with silver nanoparticles.

It can be observed from Figure 3, that current increases from μA to mA as the frequency is varied from 0 to 1 MHz. Looking at the morphology of silver clusters and frequency dependent I-V behavior, we can deduce that the array of silver nanowires is showing a capacitive behaviour. The I-V curve depicts some a rectifying behaviour which needs to be studied further. We are trying to model the conductivity in these nano wire arrays as being a consequence of percolation mechanism and the grain boundaries are playing a major role in this behavior.

5.2.8 Conducting Carbon Nanowires patterning by ion irradiation

Amit Kumar^{1*}, L.D. Filip², J. D. Carey², J. C. Pivin³, A. Tripathi¹, D. K. Avasthi¹

¹Inter University Accelerator Centre, Aruna Asaf Ali Marg, New Delhi-110067

²Advanced Technology Institute, University of Surrey, Guildford GU2 7XH,

³CSNSM, Bâtiment 108, 91405 Orsay Campus, France

Ion beam methods are now emerging as a tool in nano-fabrication for structuring material and modification on the nanometer/atomic scale [1-2]. This work reports the formation of conducting carbon nanowires by ion irradiation and the effect of the density of energy transferred to the dimension and electrical. C_{60} films (200 nm) were deposited on 50 nm thick Au layers on Si substrate. The fullerene films were irradiated by 120 MeV Au, 180 MeV Ag and 55 MeV Ti ions at different fluences using 15MV Pelletron accelerator at Inter-University Accelerator Centre, New Delhi. The conducting AFM (C-AFM) measurements were performed on the pristine and irradiated samples using Nanoscope IIIa SPM. The field emission (FE) characteristics of pristine and irradiated films were examined using a sphere-to-plane geometry in which a 5 mm stainless-steel ball bearing is suspended 40 mm above.

The C-AFM image of the C_{60} film irradiated for 120 MeV Au ions at a fluence of 6×10^{10} ions/cm² were recorded to prove the nanowire regions in the irradiated fullerene film. The role of electronic density deposition on the nanowires has been investigated by irradiation of same thickness fullerene films by 120 MeV Au ($S_e = 13\text{keV/nm}$), 180 MeV Ag ($S_e = 11\text{keV/nm}$) and 55 MeV Ti ($S_e = 5\text{keV/nm}$) ions. The conducting paths (nanowires) are observed in the above irradiated films at 0.5 V, 2V and 9 V corresponding to the electronic energy deposition of 13 keV/nm, 11 keV/nm and 5 keV/nm. These values show that electronic energy deposition played main role in conducting track formation. The conductivity of these nano wires varies from $\sim 10^{-1}$ S/cm to $\sim 10^{-4}$ S/cm, depending on S_e [3].

Field emission properties have been studied on pristine and synthesized carbon nanowires by 180 MeV Ag ions at different fluences, as shown in figure 1 (a). The threshold voltage of about 13, 15, 17 V/mm has been observed for nanowires synthesized at 3×10^{11} , 3×10^{12} and 3×10^{13} ions/cm² fluence respectively, whereas pristine films show breakdown behavior at 51 V/ μm (shown in the inset of figure 1 (a)). The Fowler - Nordheim (F-N) plot [4] for field emission current of figure 1(a), $\ln(I/V^2)$ versus $1/V$ given in figure 1 (b). The inset of figure 1 (b) describe the simple form of the Fowler-Nordheim equation. The linear dependence of the plot indicates that the observed field emission from the carbon nanowires follow tunneling mechanism of F-N equation. The slope of the F-N plot can be given by, $-b(\phi^{3/2})/\beta$, where b is a constant with the value of

$6.83 \times 10^{-9} \text{ eV}^{-3/2} \text{ V/micron}$, ϕ is work function and β is field amplification/enhancement factor. We estimated the field enhancement factor (β) value with the hypothesis that the work function is similar to that of graphite ($\sim 5 \text{ eV}$) and found $\beta = 447, 343$ and 291 at $3 \times 10^{11}, 3 \times 10^{12}$ and $3 \times 10^{13} \text{ ions/cm}^2$ fluence, respectively.

These analyses show that field enhancement factor decreases with ion fluence. It is reported that at higher areal densities of carbon nanotubes field screening becomes a significant factor for emission properties, which leads to lower field enhancement factor [4]. In present case, lower field enhancement factor at higher fluence is due to the less inter-spacing between the nanowires or higher areal density.

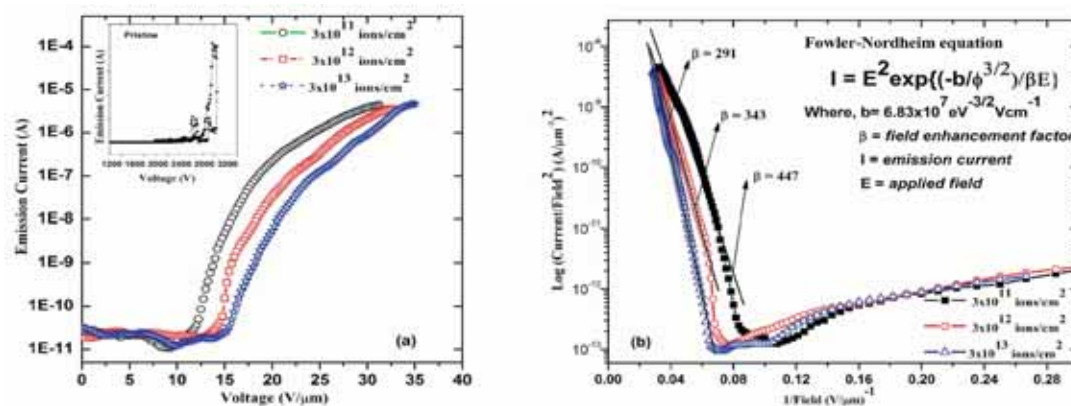


Fig. 1. (a) The emission current versus applied voltage of the synthesized carbon nanowires by ion irradiation. Inset shows the emission from the pristine fullerene film. (b) The F-N equation fitting of I-V measurement of the synthesized carbon nanowires.

REFERENCES

- [1] Amit Kumar, D.K. Avasthi, J.C. Pivin, A. Tripathi, and F. Singh, Physical Review B. 74, 153409 (2006).
- [2] Amit Kumar, Fouran Singh, J. C. Pvin, Journal of Physics D: Applied Physics 40, 2083 (2007).
- [3] Amit Kumar, D.K. Avasthi, A. Tripathi, D. Kabiraj, F. Singh, J.C. Pivin, Journal of Applied Physics 101, 014308 (2007).
- [4] L. Nilsson, O. Groening, C. Emmenegger, O. Kuettel, E. Schaller, L. Schlapbach, H. Kind, J.-M. Bonard, and K. Kern, Appl. Phys. Lett. 76, 2071 (2000).

5.2.9 Synthesis of Nanoscale Copper Nitride Thin Film and Modification of The Surface Under High Electronic Excitation

S. Ghosh¹, A. Tripathi², V. Ganesan³ and D. K. Avasthi²

¹Indian Institute of Technology Delhi, Hauz Khas, New Delhi-110 016

²Inter University Accelerator Centre, Aruna Asaf Ali Marg, New Delhi 110 067

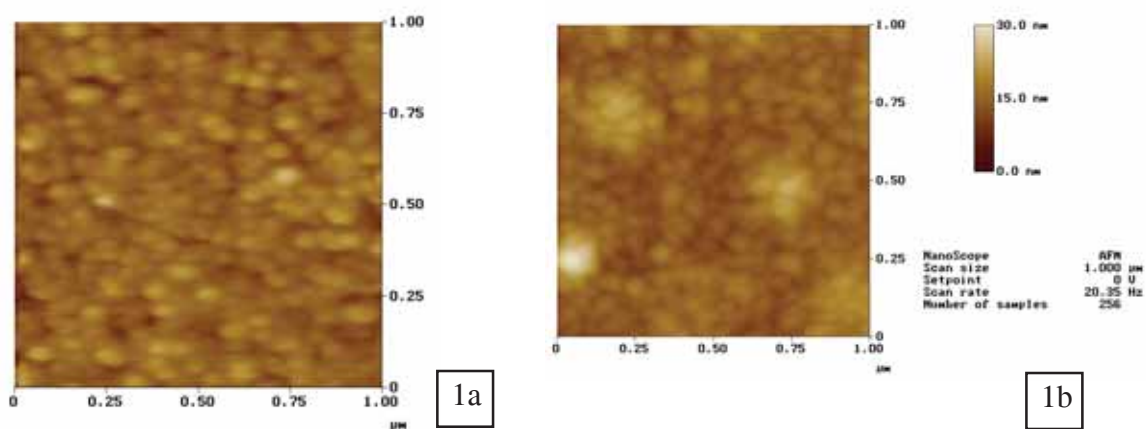
³UGC-DAE Consortium for Scientific Research, Khandwa Road, Indore-452017

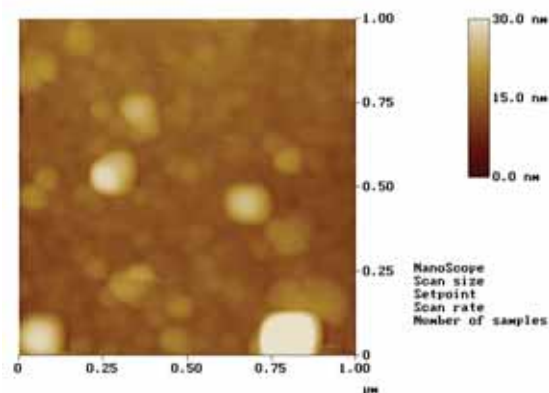
Electronic sputtering [1], or erosion of material under dense electronic excitation is another field of research. Evolution of nitrogen from copper nitride (Cu_3N) film due to impingement

of 200 MeV Au ion is one of the examples of electronic sputtering as studied by our group [2]. Formation of nanoscale metallic structures on thin Cu_3N films under 200 MeV Au ion irradiation is a consequence of electronic sputtering, which has been observed recently [2]. In the present study we irradiate Cu_3N films deposited on Si and glass substrates by 200 MeV Au^{15+} ions at different fluences and studied the surface morphology of the as deposited and irradiated films by atomic force microscopy (AFM). The results are explained on the basis of thermal spike mechanism [3].

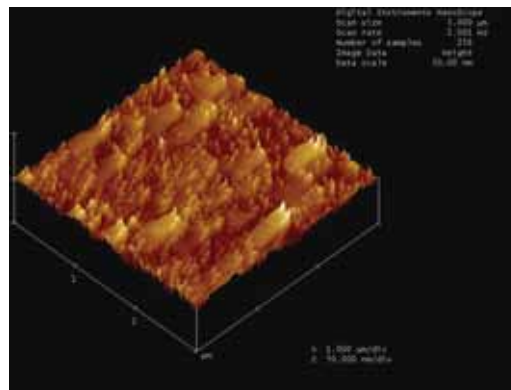
Copper nitride (Cu_3N) films are deposited on Si and borosilicate glass substrates by RF reactive sputtering technique in the reactive environment of nitrogen plasma in a similar manner as reported in our earlier study. Irradiation of the films is done by 200 MeV Au^{15+} ions at different fluences (maximum of 5×10^{12} ions/cm²) from the Pelletron accelerator of Inter University Accelerator Centre. Surface morphology of the as deposited and irradiated Cu_3N films was examined by atomic force microscopy (AFM), Nanoscope-III AFM (Digital Instruments Inc). Grain sizes along XY plane are determined from AFM images scanned for different areas.

AFM study of un-irradiated films shows the following surface morphologies: as deposited $\text{Cu}_3\text{N}/\text{Si}$ films have nanogranular surface with uniform distribution of grains having average diameter of ~ 90 nm (fig. 1a). In case of $\text{Cu}_3\text{N}/\text{glass}$ films an agglomeration of grains on the surface is observed (fig. 1b). After irradiation the following changes in the surface morphology are seen: (i) enhancement of grain size has been observed for both type of films irradiated with a fluence of 1×10^{12} ions/cm². This is evident from fig. 2a from which the average grain size was found to be ~ 120 nm for $\text{Cu}_3\text{N}/\text{Si}$ film. With increase in ion fluence (2×10^{13} ions/cm²) mass transport on the surface (fig. 2b) long the direction of incident ion for $\text{Cu}_3\text{N}/\text{Si}$ film is observed. However, in $\text{Cu}_3\text{N}/\text{glass}$ films the damage on the surface is different, non-uniform grain growth at some places and hillock structure on the surface is seen. At a fluence of about 2×10^{13} ions/cm² line-like features have been observed in $\text{Cu}_3\text{N}/\text{glass}$ films. The results [4] are understood on the basis of thermal spike formation in the lattice.





2a



2b

REFERENCES

- [1] R.E. Johnson and B. U. R. Sundqvist, Phys. Today, 305, March 1992.
- [2] S. Ghosh, V. V. Sivakumar, A. Tripathi, S. Khan, V. Ganesan, A. Gupta, A. Nath and D. K. Avasthi, Nucl. Instr. and Meth. In Phys. Res. B 248 (2006) 71.
- [3] M. Toulemonde, J. M. Costantini, Ch. Dufour, A. Meftah, E. Paumier and F. Studer, Nucl. Instr. And Meth. In Phys. Res. B 116 (1996) 37.
- [4] S. Ghosh, A. Tripathi, V. Ganesan and D. K. Avasthi, Oral Presentation in '3rd International conference on technological advances of thin films and surface coatings,' 11-15 Dec. 2006, Singapore

5.2.10 The effect of swift heavy ion irradiation on the phase transition of nanostructure manganite and ortho-ferrites and its comparison with hydrostatic pressure using Mössbauer Spectroscopy

Usha Chandra¹, Nisha Yadav¹, N.Lakshmi², K. Venugopal², K.Asokan³, Ravi Kumar and G.Parthasarathy⁴

¹ High-Pressure Physics Lab., Dept. of Physics, University of Rajasthan, Jaipur

² Department of Physics, M .L. Sukhadia University , Udaipur 313001

³ Inter-University Accelerator Centre, Aruna Asaf Ali Marg, New Delhi 110067.

⁴ National Geophysical Research Institute, Uppal Road, Hyderabad 500007

Complex perovskite manganites LaMnO_3 are particularly important since their properties could be tailored for specific purposes. Doping at La-site by divalent ions or by creating vacancy would give rise to ferromagnetism and semiconductor to metal transition due to double exchange mechanism in these systems [1]. Urushibara et al. found insulator- metal transition at 300K for polycrystalline bulk $\text{La}_{0.8}\text{Sr}_{0.2}\text{MnO}_3$ [2]. A variation in T_c due to change in Mn-O bond length as well as Mn-O-Mn bond angle was seen with the application of hydrostatic pressure [3].

Nanocrystalline samples $\text{La}_{0.8}\text{Sr}_{0.2}\text{Mn}_{0.8}\text{Fe}_{0.2}\text{O}_3$ (named as stoichiometric sample), $\text{La}_{0.9}\text{Mn}_{0.8}\text{Fe}_{0.2}\text{O}_{3.15}$ (named as La-deficient sample), $\text{La}_{0.86}\text{Sr}_{0.14}\text{Mn}_{0.8}\text{Fe}_{0.16}\text{O}_{2.91}$ (represented as Mn-deficient sample), synthesized by sol gel technique were characterized through XRD for phase purity and particle size determination [4]. Temperature dependent electrical resistivity measure-

measurements on stoichiometric sample showed insulating behaviour. High Pressure Mössbauer and electrical resistivity measurements on stoichiometric sample showed a first order transition at 0.52 GPa while another subtle phase transition was observed at 3.6 GPa.[5]. While the deficient sample show a sudden change in resistivity at 0.3 GPa. Further increase in pressure reduces the resistivity monotonically for La-deficient system up to 1.6 GPa while Mn-deficient system undergoes another sudden change in resistivity at 0.78 GPa. (Fig 1)

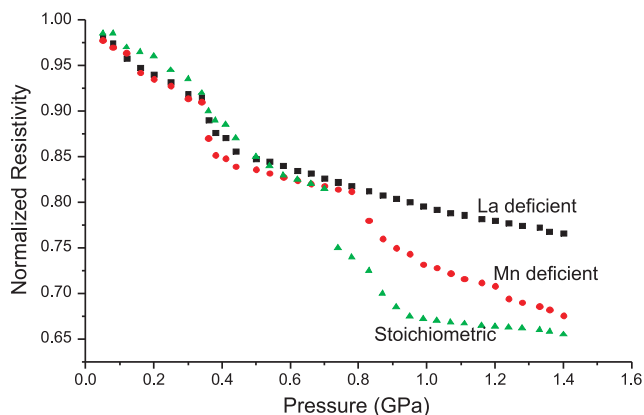


Fig.1. Normalized Resistivity (with reference to resistivity at room pressure and temperature) at various pressures up to 1.6 GPa of Stoichiometric as well as La and Mn deficient samples

The energetic ion beam has been used as an essential tool for controlled modification of materials, thus modifying their transport properties [6]. The effect of Swift Heavy Ions (SHI) irradiations on materials have been correlated with the effects produced by the hydrostatic pressure[7]. To study the correlation in above systems, the samples were irradiated at room temperature with 200 MeV Ag^{+16} ion beam using 15 MV Pelletron with fluences of 1×10^{13} , 5×10^{12} , 1×10^{12} , 5×10^{11} , 1×10^{11} ions/cm². The beam current was kept low to avoid heating of the sample. The area covered by ion beam for scanning was 10×10 mm². The irradiated samples were tested for oxygen stoichiometry by iodometric titration. No appreciable change was observed. Magnetic measurements ZFC and FC were done on these pristine and irradiated samples using vibration Sample magnetometer up to 20 K at 44 Gauss field.

Fig 2 (a) and 2(b) show magnetization versus temperature (M-T) curves for stoichiometric sample. For measurements in ZFC mode, sample is first cooled from 300 K down to 20 K in the absence of any external magnetic field then moment is recorded in the warming cycle with the field of 44 Gauss up to 300 K. In FC mode, the sample is cooled from 300K down to 20K in the presence of magnetic field and moment is recorded in the warming cycle. Magnetic properties seem to change under the influence of irradiation. Analysis on these measurements is under process. However the figure represents the influence of irradiation on one of the samples.

Our aim in the proposal is to correlate the effect of hydrostatic pressure with that of radiation pressure through Mössbauer Parameters which are highly sensitive to pressure [5]. Mössbauer as well as electrical resistivity measurements would be carried out on these samples.

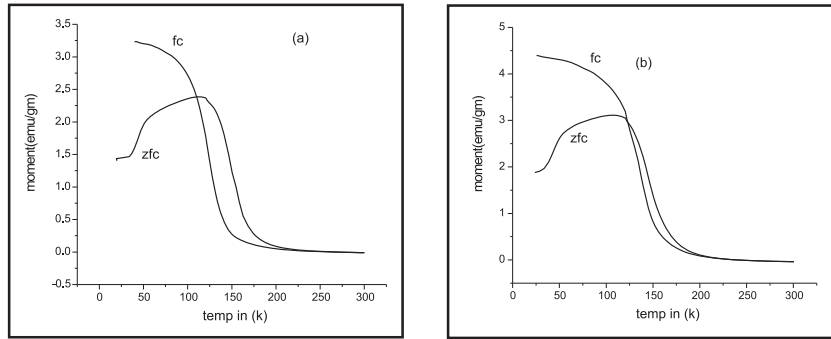


Fig. 2. Magnetization-temperature (FC/ZFC) curves of (a)pristine and (b)irradiated stoichiometric Sample $\text{La}_{0.8}\text{Sr}_{0.2}\text{Mn}_{0.8}\text{Fe}_{0.2}\text{O}_3$ with fluence 1×10^{13} ions/cm²

REFERENCES

- [1] C.Zener, Phys. Rev. 82(1951)403
- [2] A.Urushibara et al. Phys. Rev. B, 51 (1995)103
- [3] P.G.Radelli et al., Phys. Rev.B,56 (1997)8265
- [4] Manoj Kumar et al., Mat. lett.60(2006)2066
- [5] Usha Chandra et al. Hyp.Int. 163(2005)129
- [6] A.Sarkar et al. NIM.B 230(2005) 285
- [7] Ravi Kumar et al. NIM B 244(2006)110

5.2.11 The Effect of Ion Beam on PVDF/Layered Silicate Nanocomposites

B.B. Srivastava¹, P. Maiti¹, D. Pandey¹, P. K. Kulriya², D.K. Avasthi²

¹School of Materials Science and Technology, Institute of Technology, Banaras Hindu University, Varanasi 221 005

²Inter-University Accelerator Center, Aruna Asaf Ali Marg, New Delhi, 110 067

The nanocomposite was prepared by melt extrusion method using 4 wt % of nanoclay and pure PVDF and its copolymer (HFP). Extrusion was carried out in a twin-screw extruder. The mixing was done at a temperature of 205°C for 10 minutes under high shear rate. During melt mixing, the polymer chains diffuse into the galleries between the silicate layers. From earlier reports it is confirmed that the modified clay remains stable during the compounding step. Thin samples of approx 35 mm thickness are prepared by hot compression technique. Special care has been taken to produce air bubble free samples. It is clear from fig. 1 that the d_{001} peak of the clay has been shifted to lower angles corresponding to an increase in the d-spacing from 1.8nm (30B clay) to 2.9nm for the 4 wt % of the nanocomposite.

On irradiation of SHI (Si^{+7} ion, 80 MeV) on PVDF thin film, it becomes completely black and brittle indicating degradation of pure polymer at higher fluence ($>10^{12}$ ions/cm²). On the contrary, nanocomposites films become slight brown, showing minimum degradation of the matrix polymer. So, nanoclay, made of aluminosilicate layers, is shielding the polymer matrix from SHI irradiation. Upon irradiation these PVDF nanocomposites (PVDFNC) films exhibit the shifting of

d_{001} peak (corresponding the intergallery spacing) to lower angle with increase in fluence (Fig 2). The dotted line indicates the gallery spacing of nanocomposites before irradiation. Again, in case of PVDF the intensity of the three crystalline peaks d_{020} , d_{110} , d_{111} are decreasing showing amorphousization with increase of fluence.

PVDFNC exhibit b-phase and the intensity of two peaks d_{200} and d_{110} are decreasing but not as prominently as we find in PVDF, showing PVDFNC is resisting the ion irradiation (fig. 3 and 4). Visibly it is also clear that as at high fluence the PVDF thin film got black color showing a large amorphousization but PVDFNC4 thin film got only dark brown color showing protective-ness against ion irradiation.

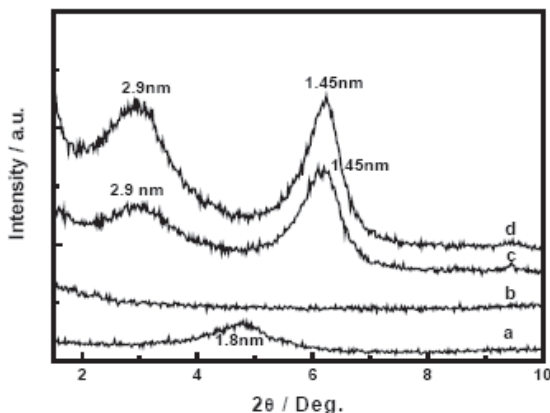


Fig. 1. XRD patterns of PVDF and PVDFNCs
a) Pure nanoclay(30B) b) Pure PVDF
c) PVDFNC4 d) PVDFNC8

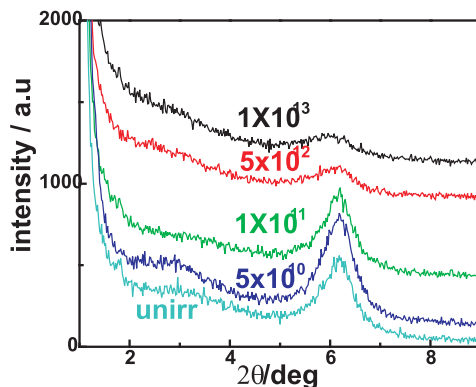


Fig. 2. XRD patterns of PVDFNC4 at different Fluence

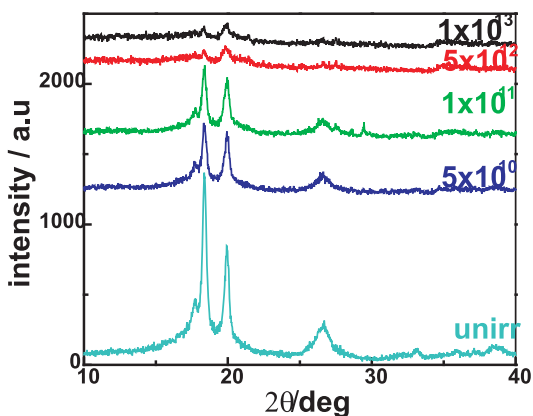


Fig. 3. XRD pattern of PVDF at various ion fluences

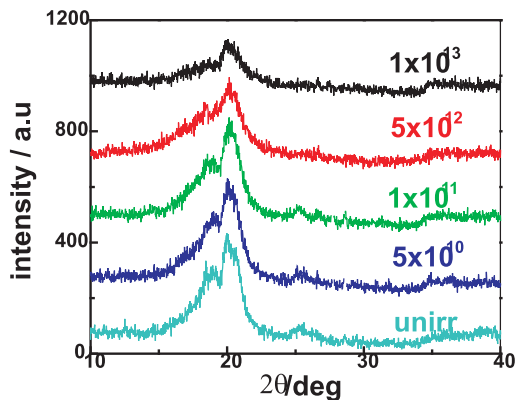


Fig. 4. XRD pattern of PVDFNC t various ion fluences

5.2.12 Ferromagnetic Carbon by Energetic Ion Irradiation

Amit Kumar¹, D. K. Avasthi¹, J. C. Pivin², R. M. Papaléo³, A. Tripathi¹, F. Singh¹

¹Inter-University Accelerator Centre, Aruna Asaf Ali Marg, New Delhi 110067

²CSNSM, IN2 P3-CNRS, Bâtiment 108, 91405 Orsay Campus, France

³Faculdade de Física - PUCRS, Porto Alegre- Brasil

In last few years, the possible existence of ferromagnetism in materials consisting solely of carbon has been studied experimentally [1-3] and theoretically [4]. A weak magnetic response has been reported for fullerenes after treatment under high-pressure and high-temperature conditions [1], proton irradiated graphite [2], N and C implanted nanocrystalline diamond [3] and other treated carbon materials. The driving force behind these studies was not only to create technologically important, light, non-metallic magnets with a Curie point well above room temperature, but also to understand a fundamental problem of the origin of magnetism in carbon phases, which traditionally has been thought to show diamagnetic behavior only. Recently, we reported the occurrence of ferromagnetism in ion irradiated fullerene thin films [5,6]. These report give strong support to the magnetism in carbon, which is mainly mediated by defects.

Fullerene thin films were deposited on Si (100) substrates in a vacuum of 1×10^{-6} torr. The irradiations with 90 MeV Au, 55 MeV Ti and 10 MeV O ion beam were performed at Inter-University Accelerator Centre (IUAC), New Delhi and the Porto Alegre HVEE 3 MV Tandatron accelerator, Brazil at different fluence. The electronic energy loss (S_e) by O, Ti and Au were 197, 630 and 1400 eV/(1×10^{15} atoms/cm²) respectively. The nuclear energy loss (S_n) by O, Ti and Au ions was 0.3, 1.1, 23.0 eV/(1×10^{15} atoms/cm²), respectively.

The curves of magnetization versus applied field recorded for the pristine fullerene film and Au ion irradiated films at different fluence, are shown in figure 1 (a). The hysteresis loop in irradiated films show the ferromagnetism in these films. The ferromagnetic contribution increases with the ion fluence. To investigate the effect of electronic energy loss, fullerene films were irradiated with 90 MeV Au, 55 MeV Ti and 10 MeV O ions. Figure 1 (a), (b) and (c) show the magnetization measurements for 90 MeV Au, 55 MeV Ti, and 10 MeV O ions irradiated fullerene films, respectively. The total electronic energy depositions ($S_e \times \phi$) for Au, Ti and O ions at highest fluence are about 84, 38 and 10 eV/atoms and the corresponding saturation magnetization is about 2.27, 0.72 and 0.55 emu/cc, respectively. These measurements show that the electronic energy density deposition play significant role for inducing the ferromagnetic signal in irradiated fullerene films.

Temperature dependent magnetic measurement and magnetic force microscopy measurements performed at room temperatures on irradiated films confirmed that the Curie temperature is higher than room temperature [5,6], which is very useful from ap-

plication point of view. It is also reported that the electronic excitation has higher efficiency for inducing the magnetic signal than that of the collision cascade [6]. The increase in the saturation magnetization with ion fluence and electronic energy density deposition prove the existence of ferromagnetism in ion irradiated films, which is mainly mediated by defect production, consisting of sp^2/sp^3 bonded carbon atoms. The oxygen attachment on the irradiated films may also be responsible for magnetic signal in ion irradiated fullerene films.

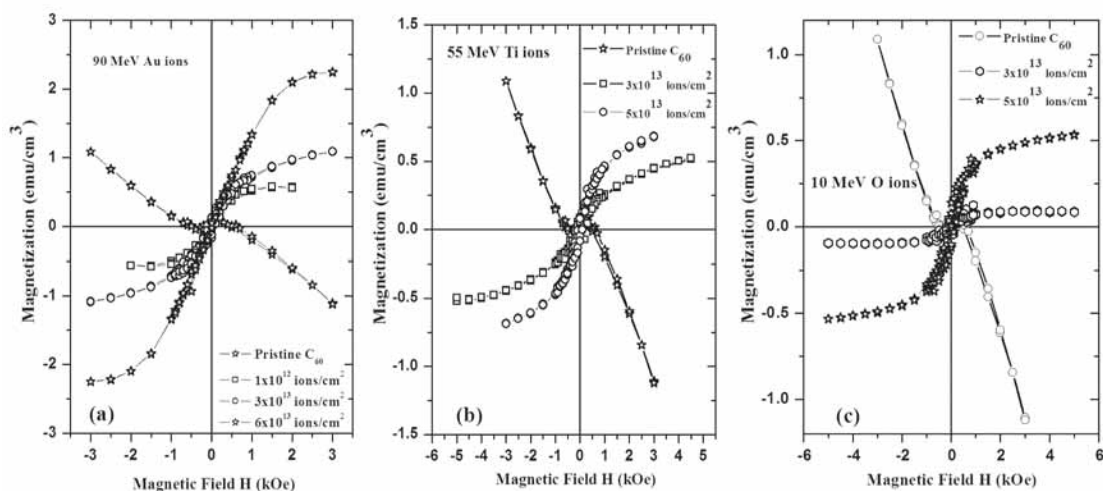


Fig. 1. The magnetization measurements of (a) 90 MeV Au, (b) 55 MeV Ti, and (c) 10 MeV O ion irradiated fullerene films at indicated fluences.

REFERENCES

- [1] T. L. Makarova B. Sundqvist, R. Höhne, P. Esquinaz, Y. Kopelevich, P. Scharff, V.A. Davydov, L.S. Kashevarova, and A.R. Rakhmanina, *Nature (London)* 413, 716 (2001).
- [2] P. Esquinazi, D. Spemann, R. Hohne, A. Setzer, K. H. Han, and T. Butz, *Phys. Rev. Lett.* 91, 227201 (2003).
- [3] S. Talapatra, P. G. Ganesan, T. Kim, R. Vajtai, M. Huang, M. Shima, G. Rmanath, D. Srivastava, S. C. Deevi, P. M. Ajayan, *Phys. Rev. Lett.* 95, 097201 (2005).
- [4] P. O. Lehtinen, A. S. Foster, Y. Ma, A. V. Krasheninnikov, and R. M. Nieminen, *Phys. Rev. B* 93, 187202 (2004).
- [5] Amit Kumar, D.K. Avasthi, J.C. Pivin, A. Tripathi, and F. Singh, *Physical Review B*, 74 (2006) 153409.
- [6] Amit Kumar, D. K. Avasthi, J. C. Pivin, A. Tripathi, F. Singh, I. Sulania, *Journal of Nanoscience and Technology* (2007) in press.

5.2.13 Development of Nano Pores Films of Cis 1, 4 Polyisoprene for Drug Delivery System

Nisha Sasi¹, Ambuj Tripathi², P.K. Bajpai³ and P.Predeep^{1,*}

¹ Condensed Matter Physics Laboratory, Sree Narayana College, Kollam, Kerala

² Inter-University Accelerator Centre, Aruna Asaf Ali Marg, New Delhi 110067

³ Department of Pure and Applied Physics, G.G. University, Bilaspur, India.

* Department Of Physics, National Institute Of Technology, Calicut, India.

A new concept for mechanically stable drug release system is to combine hydrogel with porous ion track membrane to have the advantage of high mechanical strength. Here remarkable and useful features of polymers swelling ability manifest itself when the swelling can be triggered by a change in the environment surrounding the controlled drug release system. The ion track etching technique based on irradiation of the film with swift heavy ions and subsequent chemical etching is used to prepare nano porous and micro porous films. The nano porous and the micro porous made in the polymer film can act as the delivery route. In this study micro meter and nanometer thick films of natural rubber (cis 1,4 polyisoprene) are prepared by spin coating and dip coating techniques and are irradiated with Au ions with energy 132 MeV at fluences of 10^{10} - 10^{11} ions/cm² with the aim of producing nano pores. However the high fluence of 10^{11} ion/cm², populated on the surface of the films largely and due to large density of ions, the surface are fully got ploughed.

The controlled permeation of asymmetrically shaped nano pores has recently attracted a big interest to novel studies of translocation of biomolecules [1]. The purpose behind controlling of the drug delivery is to achieve more effective therapies while eliminating the potential for both under and over dosing. Other advantage of using controlled delivery systems can include the maintenance of drug levels within a desired range.

The ideal drug delivery system should be inert, bio compatible, comfortable for the patient, capable of achieving high drug loading, safe from accidental release, simple to administer and remove, and easy to fabricate and sterilize[1].

A range of materials have been employed to control the release of drugs and other active reagents.

*Poly (urethanes) for elasticity

*Poly (ethylene) for toughness and lack of swelling

*Poly (vinyl alcohol) for hydrophilicity and strength etc.

Natural rubber is a biocompatible polymer which is one of the largest produce of our country. Its mechanical strength, flexibility and easy processability make them a potential candidate for drug delivery system once it could be proved that nanopores can be developed in them for the delivery of drugs. To prepare nano pores, ion etching technique based on irradiation of a film with swift heavy ions and subsequent chemical etching techniques are to be used.

Thin films of natural rubber prepared on glass substrates, at room temperature, by spin coating method from a solution of natural rubber in CCl₄. This film roll are irradiated by ¹⁹⁷Au ions at 132 MeV with ion fluence of 10^{10} - 10^{11} ion/cm².

The pores in the irradiated samples are generated by using etching technique. To etch the track, the irradiated membrane is clamped between the two chambers in the conductivity cell. Both the chambers are filled with the etchant (9M, NaOH) at room temperature[2]. In this technique etching starts from both sides and as soon as they reach the other side of the sample, a sudden increase of current is observed.

However, the Atomic Force microscopy pictures (fig.1) show that instead of

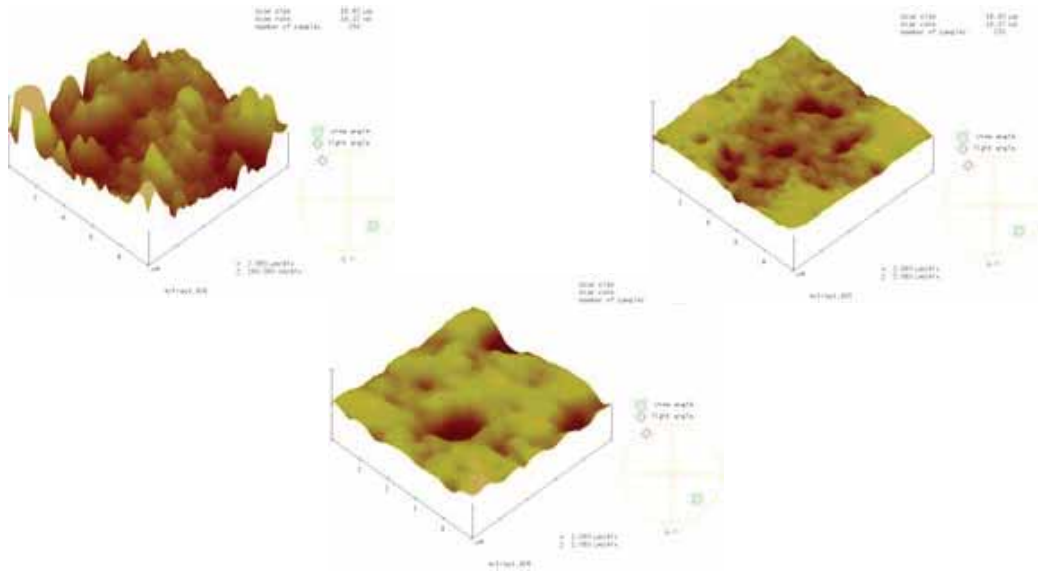


Fig. 1. AFM pictures of irradiated and etched rubber films

nano pores non uniform micro and larger sized holes and pits are formed. This had happened due to the use of large fluence of 10^{11} ion/cm². For nano pores only smaller fluences are to be used. The significance of this study is that a soft and flexible polymer like cis 1, 4-polyisoprene (natural rubber) can be successfully used for producing ion tracks by swift heavy ions even at energies of 132 MeV.

REFERENCES

- [1] Medical Plastics and Biomaterials Magazine (MPB Archive, Nov. 97)
- [2] Apel p. Korchev Y.E. Siwy Z. Spohr R. Yoshida M. Nucl. Instr Meth Phys Res B(2001); 184; 337-46

5.2.14 Structural and optical properties of C⁺⁶ ion (80 MeV) irradiated CdS:Mn system

Y.K. Vijay¹, Balram Tripathi¹, V. Kulshreshtha¹, K. Awasthi¹, N.K. Acharya¹, R.K. Mangal¹, D.K. Avasthi², F. Singh², P.K. Kulriya², S.A. Khan²

¹Department of Physics, University of Rajasthan Jaipur-302004

²Inter University Accelerator Centre, Aruna Asaf Ali Marg, New Delhi 110-067

Manganese doped CdS nanocrystals have been studied mainly due to their luminescence properties [1]. Nanocrystals of CdS: Mn is the most studied system among all the semiconductor nanocrystals. Emission from Mn⁺² ions has been reported at 600 nm. Interest in properties of chemically synthesized sulphide nanocrystals stem from their potential use in non-linear optical devices [2]. Synthesis of CdS:Mn by ion im-

plantation has been reported by Budai et al [3]. Grain fragmentation and grain evaporation have been observed in nanomaterials [4]. In this context ion impact on CdS:Mn is interesting due to suppression or generation of weak link boundaries in case of nanocrystals.

Figure 1, shows the X-ray diffraction (XRD) patterns of pristine and C^{+6} (1×10^{13} ions/cm²) irradiated CdS: Mn nanocrystals. The crystal structure of these nanocrystals is found to be in hexagonal phase having particle size distribution between the range of (18-20 nm). It is clear that C^{+6} ions irradiated samples shows the sharp reduction in intensity of the peaks. In this process it generates defects and resulting in a non-crystalline nature. Also, the intensity variation can be attributed to the creation of defects like surface tracks.

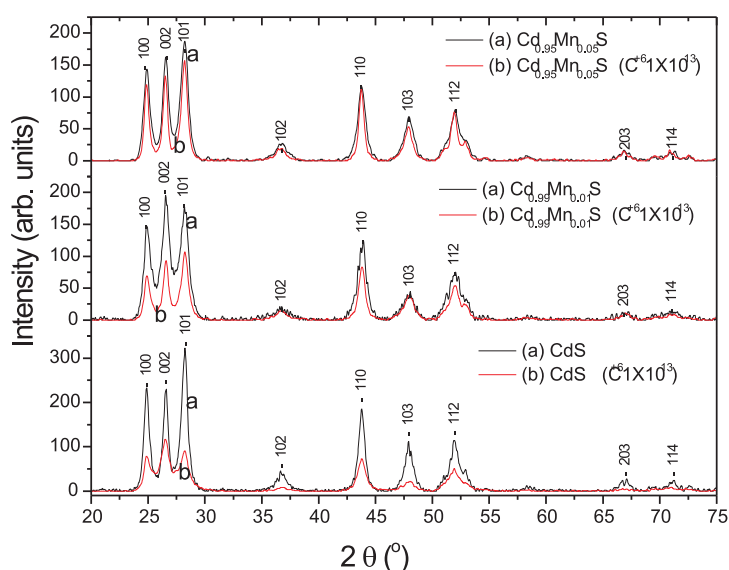


Fig. 1. X-Ray diffraction patterns for $Cd_{1-x}Mn_xS$ ($x=0-5\%$)

The PL spectrum consists of broad emission peaks for pristine CdS at 587.58 nm (28,775), 667.91 nm (14,259). For Mn =1% doped CdS there is an increase in PL intensity and also some shift in the wavelength has been observed 587.91 nm (37265), 668.22 nm (15054) respectively. For Mn =5% doped CdS only PL intensity is found to be increased. Both PL peaks exhibit significant shift with respect to absorption edge. Hence the luminescence bands can be identified with transitions involving donors, acceptors and surface states. It is observed that both PL bands shifts towards the higher wavelengths and there is sharp reduction in PL intensities, which confirms that the lattice disorder begins on the surface of the samples due to the high energy irradiation. This result suggests that defects created by the C^{+6} ions on CdS: Mn nanocrystals can act either as traps or as non-radiative recombination centres [5].

The optical absorption edge provides us a reliable estimate of the band gap of any system. It is clear from the absorption measurement that absorption edge shifts towards the longer wavelength on increasing the Mn concentration in host CdS and the band gap values lies between

(3.54 eV.- 3.01 eV.), as shown in Table 1.

The optical band gap values are given in table 1.

Table1: Optical band gap values for $Cd_{1-x}Mn_xS$ (x=0-5%)

Sample	Band gap (eV) (Unirradiated)	Band gap (eV) (Irradiated)
CdS	3.54	3.59
$Cd_{.99}Mn_{.01}S$	3.36	3.54
$Cd_{.95}Mn_{.05}S$	3.01	3.18

After SHI irradiation it is found that optical band gap values slightly increases in comparison to the pristine samples. This change in band gap due to SHI irradiation attributed to the shift in energy levels of the doped semiconductor nanocrystal.

REFERENCES

- [1] J. K. Furdyna, J. Appl. Phys., 64 (1988) R29.
- [2] D. J. Norris and M.G. Bawendi, Phys. Rev. B., 53 (1996) 16338.
- [3] J. D. Budai, C.W. White, S. P. Withrow, R. A. Zuhar and J. G. Zhu, Mater. Res. Soc. Symp. Proc., 89 (1997)452.
- [4] S. Berthelot, F. Hemon, E. Gourbilleaur and E. Paumier, Nucl. Instrum. & Meth. B, 146 (1998) 437.
- [5] J. Wagner, P. Koidl, K.H. Bachem, C. Uzan-Saguy, R. Kailash and M. Bruder, J. Appl. Phys.,73 (1993) 2739.

5.2.15 Synthesis of nanodimensional TiO_2 using energetic ion beam

Madhavi Thakurdesai¹, Y.Batra,² I. Sulania², P.K.Kulariya², A.Mahadkar³, V. Bhattacharyya¹, D. Kanjilal²

¹Department of Physics, University of Mumbai, Vidyanagri, Mumbai - 400 098

²Inter University Accelerator Centre, Aruna Asaf Ali Marg, New Delhi 110 067

³Tata Institute of Fundamental Research, Homi Bhabha Road Mumbai - 400 005

Objective of present investigation is to grow transition metal oxide nanocrystals on transparent insulating matrices. Currently many methods are used to prepare nanocrystalline structures but in most of the cases amorphous phase is formed and post deposition annealing is required for amorphous to crystalline phase transition [1]. This thermal treatment gives rise to clusters that nucleate and grow at different times and precipitate might undergo Ostwald ripening process leading to wide size distribution. These problems can be overcome if swift heavy ion (SHI) irradiation. SHI irradiation deposits large amount of energy to the target mostly through electronic energy loss leading to structural phase transformation in the system, eliminating the requirement of further thermal annealing [2]. The ion beam when passes through material creates a high temperature zone of a few nanometer radius along its trajectory. The material inside the cylindrical zone melts if track

temperature reaches above melting point of the material. This liquid phase is quenched immediately due to subsequent heat transfer to the surrounding lattice in a very short period of time. The cooling rate is extremely high ($\sim 10^{14}$ K/s) and the material within the track solidifies [3]. As short period of time is available for atomic diffusion, growth of crystalline phase is restricted to a few nanometers. Thus nanocrystalline phases are formed [4].

Amorphous thin films (200 nm) of TiO_2 are grown on fused silica substrate using thermal evaporation method. These films were subsequently annealed in oxygen atmosphere to achieve stoichiometrically correct oxide phase. TiO_2 thin films were later irradiated by 100 MeV Ag/Au ion beam using 16 MV Pelletron facility at IUAC, New Delhi, India. Ion beam was scanned on 10 mm \times 10 mm area on the sample surface for uniform irradiation using magnetic scanner. Ion flux was 10^9 ions. $\text{cm}^{-2}.\text{sec}^{-1}$. The ion fluence was varied between 10^{11} ions/ cm^2 and 10^{13} ions/ cm^2 .

Atomic force microscopy was done to observe nanostructure formation. Nanoprotrusions formed on the surface as a result of SHI irradiation. These protrusions are seen as hillocks in AFM images. In present experiment hillocks of nanometric dimensions are formed on the surface of irradiated films which are not visible in the pristine film. Fig 1 shows GAXRD spectra of unirradiated as well as irradiated films. The as deposited film is amorphous in nature. After irradiation mixed anatase ($2\theta = 37.99^\circ$) and rutile ($2\theta = 44.23^\circ$) phase of TiO_2 is formed.

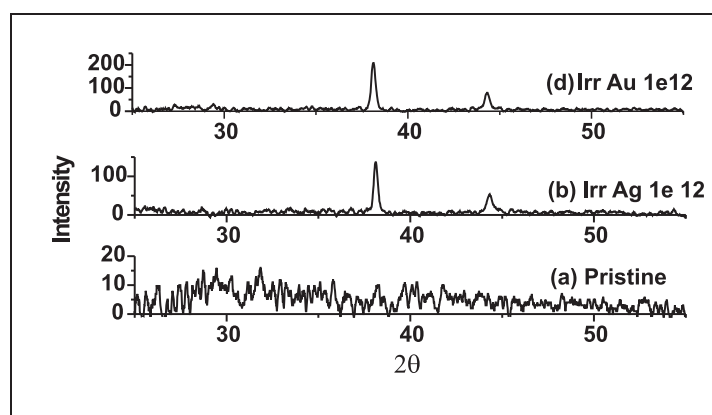


**Fig. 1. GAXRD spectra of (a) 200 nm as deposited film
(b) 200 nm film irradiated by Ag ion beam at fluence 1×10^{12} ions/ cm^2
c) 200 nm 200 nm film irradiated by Au ion beam at fluence 1×10^{12} ions/ cm^2**

The optical characterization was done by absorption measurement carried on UV-VIS double beam spectrophotometer CARY 5000. The quantum confinement effect increases the band gap of the semiconductor. Bandgap increase of 0.1-0.2 eV is observed. Particle size as calculated on the basis of increase in bandgap matches well with particle size as estimated by AFM.

Amorphous to nanocrystalline phase transition is achieved by SHI irradiation. Hillocks like nanoprotrusions of the size 10-12 nm are observed on the surface of irradiated films. Mixed rutile and anatase phase of TiO_2 is formed after irradiation. Increase in bandgap after irradiation indicates nanostructure formation.

REFERENCES

- [1] I.N.Kholmanov, E.Barborini, S Vinati, P Piseri, A Podesta, C Ducati, C Lenardi and P Milani Nanotechnology 14 (2003) 1168.
- [2] T Mohanty, A Pradhan, S Gupta and D Kanjilal Nanotechnology 15 (2004)1620.
- [3] G Szenes Phys. Rev. B Vol 51(1995) 8026
- [4] J. M. Constantini, F. Brisard, M. Toulemonde, F. Studer, Nuclear Instruments and Methods in Physics Research B 122 (1997) 514

5.2.16 KeV atoms induced nano ripples at surface

I. Sulania¹, A.Tripathi¹, D. Kabiraj¹, S. Varma², Matthieu Lequeux³ and D.K.Avasthi¹

¹Inter University Accelerator Centre, Aruna asaf Ali Marg, New Delhi 110067

²Institute Of Physics, Bhubaneswar

³Grenoble University, France

Ion/atom bombardment is known to enhance surface diffusion and affect the surface morphology to produce nanostructures[1]. The most common effect of ions on surface diffusion is related to direct transfer of the energy and momentum to the surface atoms by ion-atom collisions, changing the diffusion probability of an atom to diffuse one point to another. This behavior was first modeled by Bradley & Harper [2] who considered the deterministic competition between roughening induced by curvature dependent sputtering yield [3,4] and smoothing induced by thermal surface diffusion[5]. We have studied the changes in surface morphology and formation of ripples as a function of fluence. The angle dependence of morphological changes have also been studied. Sputtering due to the impact of energetic particles can both enhance and suppress surface diffusion[6].

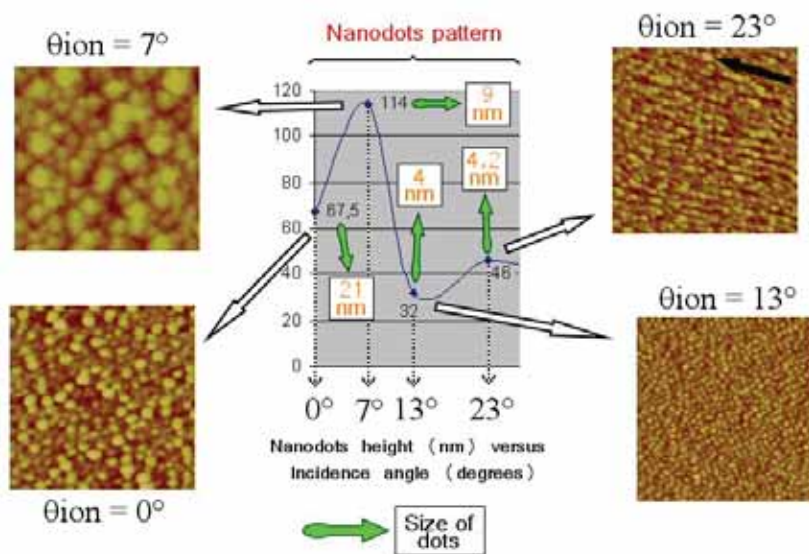


Fig. 1. The formation of nanodots as the angle of incidence of the atom beam is changed from normal to grazing incidence using the angles $q_{\text{atom}} = 0^\circ, 7^\circ, 13^\circ$ and 23° .

The fluence and angle dependent studies are done with 1.5keV Ar with a flux of 14.8 mA/cm² at IUAC, New Delhi. For fluence study, InP(100) semi-insulating samples were bombarded at an incidence angle of 45° to the normal at a base pressure of 1x10⁻³ torr at room temperature with fluence varying from 4x10¹⁶ to 3.2x10¹⁷ atoms/cm². For angle dependence study, the angle of incidence of the ions was changed from 0° to 83° with respect to the normal to the surface for 15min bombardment corresponding to a fluence of 8x10¹⁶ atoms/cm². The formation of ripples and dot structures on sputtered InP(100) were characterized with SPM Multimode IIIa using Si₃N₄ tip with radius of curvature ~10nm. An increase in the ripple wavelengths and roughness with the fluence has been observed. A transition from nanodots to ripples has also been observed. The formation of nanodots at lower angles of incidence is shown in Figure 1. The development of ripple structures at higher angles of incidence is shown in Figure 2.

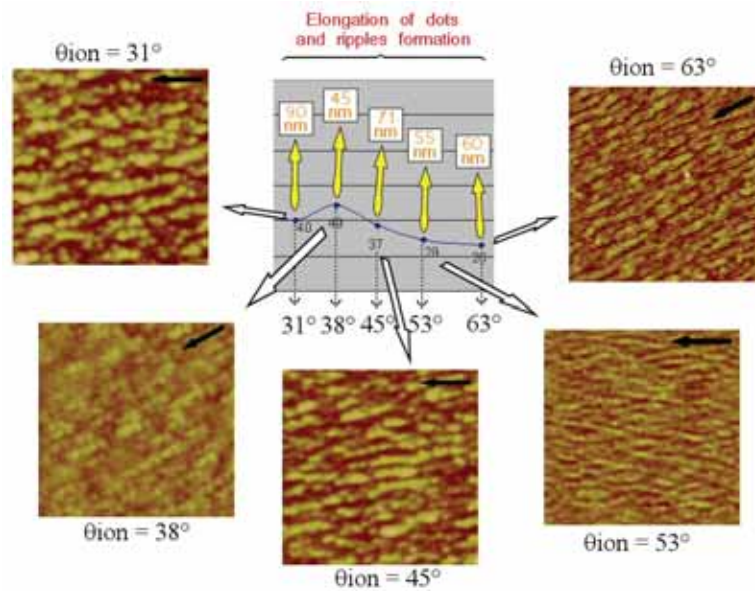


Fig. 2. The development of ripple structure as the angle of incidence of the atom beam is changed from 31° to 38°, 45°, 53° and 63°.

REFERENCES

- [1] J. Eriebacher, M.J.Aziz, Phys. Rev. Lett 82, 2330 (1999)
- [2] R.M.Bradley and J.M.E, Harper, J. Vac. Sci. Technol. A 6, 2390 (1998)
- [3] P.Sigmund, J. Mater. Sci. 8, 1545 (1993)
- [4] G.Carter, M.J.Nobes and R. P. Webb, J. Mater. Sci. 16, 2091(1981)
- [5] W. W. Mullins, J. Appl. Phys. 30, 77 (1959)
- [6] Sputtering by particle bombardment, edited by R.Behrish, Springer, 1981, 1983, Vols I-III

5.2.17 KeV ion beam induced self-structuring of 6H-SiC surfaces

Yashpal S. Katharria¹, Sandeep Kumar¹, A. T. Sharma², F. Singh¹, D. Kanjilal¹

¹Inter-University Accelerator Centre, Aruna Asaf Ali Marg, New Delhi 110 067

Self-organization of solid surfaces during ion bombardment has attracted considerable scientific attention due to its capability of spontaneously producing regular arrays of submicron scale structures (mainly dots and ripples). These structures have either been reported or predicted to find applications as varied as quantum dots, templates for producing a few other low dimensional structures (e.g. nano-rods, nano-wires etc.), and optical and x-ray gratings. At low ion energies (~a few keV/amu) elastic collisions of ions with atoms of the solid also termed as nuclear stopping result in surface sputtering. According to Bradley and Harper (BH) [1], an instability caused by local surface curvature dependent sputtering competes with surface relaxation processes tending to equilibrate the local chemical potential over the surface. Depending on certain experimental and materials parameters, this interplay and competition between the two operating phenomena of surface roughening and smoothening leads to the appearance of semi-periodic ripples morphology during a mono-directional ion irradiation. In the present study, we have investigated the temporal evolution of 6H-SiC (0001) surface under 100 keV Ar⁺ ion irradiation at oblique incidence ($\theta=60^\circ$ with respect to sample surface normal).

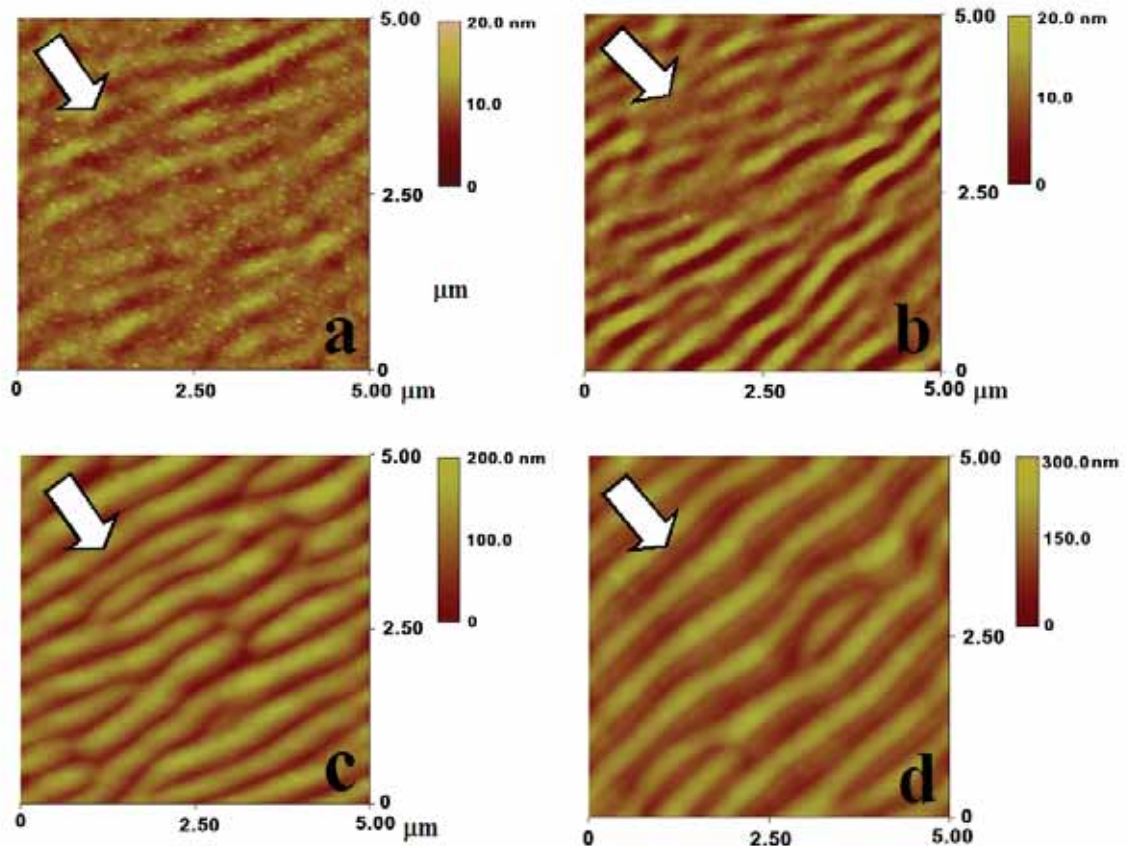


Fig.1. Surface morphology of 6H-SiC (0001) substrates resulted from off-normal irradiated 100 keV Ar⁺ ions at fluence of (a) $6 \times 10^{16} \text{ cm}^{-2}$ (b) $1.7 \times 10^{17} \text{ cm}^{-2}$ (c) $6 \times 10^{17} \text{ cm}^{-2}$, and (d) $1.2 \times 10^{18} \text{ cm}^{-2}$. Arrows represent the beam incidence direction.

A few AFM images representative of the 6H-SiC surface sputtered at different Ar⁺ ions fluences at an ion incidence angle $\theta=60^\circ$ are shown in the fig.1. At the lowest ion fluence ($\phi = 6 \times 10^{16} \text{ cm}^{-2}$) formation of mounds or nano-scale dots with an average diameter $30 \pm 4 \text{ nm}$ and height $\sim 4 \text{ nm}$, superimposed on the irregular wavy features on the surface could be clearly seen. As the sputtering proceeds, spatial regularity of the wavy surface features increases. At the same time, nano-dots seen at the early fluence are reduced in their size as well as density and finally disappear at $\phi = 3.5 \times 10^{17} \text{ cm}^{-2}$. At this stage, ripples with a well-defined period and the wave-vectorial orientation parallel to the ion beam direction start appearing on the surface. A similar work performed on Si (100) surfaces could be found in ref. [2].

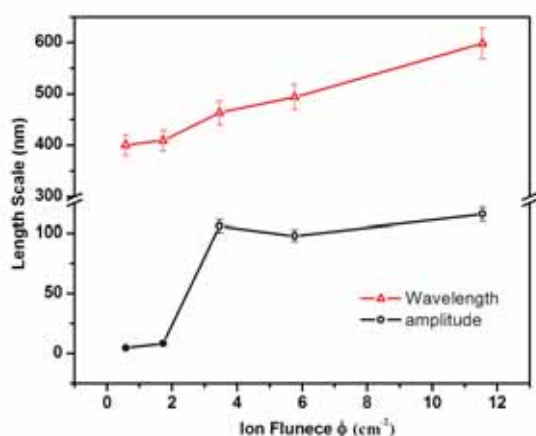


Fig. 2. Variation of ripple wavelength (λ) and ripple amplitude (R) with fluence (ϕ).

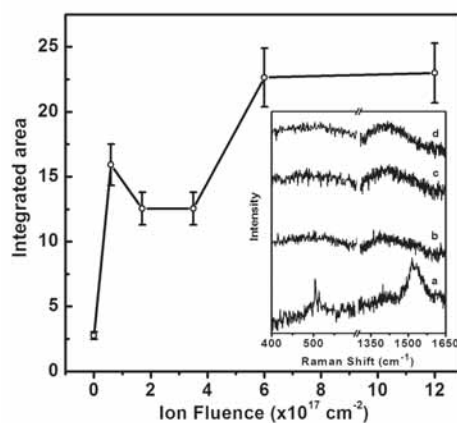


Fig. 3. Variation of C fraction of 6H-SiC with incident ion fluence (ϕ) of Ar⁺ ions. Inset shows Raman spectra of pristine and irradiated 6H-SiC wafer.

Fig.2 shows the variation of ripple amplitude (R) and wavelength λ with fluence ϕ . An initial exponential growth of amplitude following the prediction of linear BH model [1] is followed by a non-linear evolution where the amplitude is seen to undergo a level of saturation. For two initial fluences, λ does not vary significantly as the sputtering proceeds. However, a slow variation of wavelength ($\lambda \propto \phi^{0.15}$) seems to start at $\phi = 1.7 \times 10^{17} \text{ cm}^{-2}$. The results of micro-Raman measurements performed to investigate the structural changes introduced by Ar ions in near surface region of 6H-SiC wafers are shown in fig.3. An enrichment of surface in a-C with increasing ion fluence could also be seen from this fig., where the integrated area obtained from the Gaussian fit of the peak corresponding to a-C has been plotted with fluence. This enrichment is due to the difference in the sputtering yield of Si and C, which are approximated to be 4.42 and 3.26, respectively, using TRIM calculations.

REFERENCES

- [1] R.M. Bradley and J.M.E. Harper J. Vac. Sci Technol. A 6, 2390 (1988).
- [2] Yashpal S. Katharria, Sandeep Kumar, A Tarun Sharma, D Kanjilal, Appl. Surf. Sci. (2007) doi:10.1016/j.apsusc.2007.01.130.

5.2.18 Swift heavy ion irradiation effects on CdTe and CdZnTe crystal based gamma ray detectors

P. Veeramani¹, S. Moorthy Babu^{1*}, M. Haris¹, D. Kanjilal² and P. Sugathan²

¹Crystal Growth Centre, Anna University, Chennai-600 025, INDIA.

²Inter-University Accelerator Centre, Aruna Asaf Ali Marg, New Delhi 110 067

CdTe is a direct band gap II-VI compound semiconductor and used as a substrate material in radiation environments such as fusion reactors and space applications. Also it is useful as a substrate material for the growth of HgCdTe epitaxial layers required for the fabrication of advanced infrared detectors for satellite based surveillance, gamma ray detectors, solar cells and other important applications [1,2]. The fabricated detector were subjected to irradiation with 100 MeV Ag⁷⁺ ions by using the 15 UD Pelletron Accelerator at the IUAC, New Delhi. These studies were performed at liquid Nitrogen temperature in an experimental chamber under vacuum better than 10⁻⁷ torr. The beam was scanned over a 10mm x 10mm area on the sample using a magnetic beam scanner. The following fluences were used: 1x10¹⁰, 1x10¹¹, 1x10¹² and 1x10¹³ ions cm⁻². According to the calculations of Stopping and ranges of ions in matter [2], the projected range (R_p) of the 100 MeV Ag ion in Au/CdTe is 9.3 μm. Electronic flow characterization was analysed using Keithley's programmable voltage source (model 230) and a Pico ammeter (model 486).

The energy spectra of gamma rays obtained from ⁵⁷Co and ²⁴¹Am for the control and 100 MeV Ag⁷⁺ ion irradiated Schottky CdTe and CdZnTe detectors at 20°C were recorded. The applied bias voltages were chosen as 100 V for the CdTe and 300 V for the CdZnTe detector in order to obtain comparable leakage current. For the pure sample, the energy resolution of the ⁵⁷Co (122keV) line was 2.9% for the CdTe and 3.8% for the CdZnTe detector. The energy resolution of the ²⁴¹Am (59.5 keV) line was 8.1% for the CdTe and 8.2% for the CdZnTe detector. The spectra for irradiated detectors illustrate that the main photo peaks (59.5 keV for ²⁴¹Am and 122 keV for ⁵⁷Co) shift gradually towards the lower channels and there was gradual broadening of peaks as the irradiation fluence increases.

In Tables 1(a) and 1(b), the variation of the values of the energy resolution are presented together with the photopeak centroid position for the control and 100 MeV Ag⁷⁺ ion irradiated Schottky CdTe and CdZnTe detectors.

Table 1 (a) Energy resolution R(%) and photopeak centroid position C(ch) of Au/CdTe/In detectors before and after irradiation

Fluence (ions.cm ⁻²)	Au/CdTe/In			
	²⁴¹ Am (59.5 keV)		⁵⁷ Co (122keV)	
	R (%)	C (ch)	R (%)	C (ch)
control	8.1	292	2.9	611
1x10 ¹¹	9.3	289	5.5	606
1x10 ¹²	12.4	282	8.4	581
1x10 ¹³	17.8	260	14.6	568

Table 1 (b) Energy resolution R(%) and photopeak centroid position C(ch) of Au/CdZnTe/In detectors before and after irradiation

Fluence (ions.cm ⁻²)	Au/CdTe/In			
	²⁴¹ Am (59.5 keV)		⁵⁷ Co (122keV)	
	R (%)	C (ch)	R (%)	C (ch)
control	8.2	280	3.8	590
1x10 ¹¹	9.1	278	4.2	588
1x10 ¹²	9.3	277	4.5	585
1x10 ¹³	NA	262	NA	566

For CdZnTe detectors, there was linear relationship between the irradiation dose and the worsening of spectroscopic performance. This material shows a sudden transition for the high-fluence situation and to the complete degradation of the detector at a fluence of 10¹³ ions.cm⁻².

The effect of swift heavy ion irradiation on CdTe and CdZnTe substrate properties and Schottky diode structure based gamma ray detector performance were analyzed. From the results, the gamma spectrum illustrates that the main photo peaks (59.5 keV for ²⁴¹Am and 122 keV for ⁵⁷Co) shift gradually towards the lower channels and there was gradual broadening of peaks as the irradiation fluence increases. All spectroscopic capabilities were lost when the irradiation fluence range exceeds 10¹³ ions. cm⁻² value. Also these higher fluences induce a complete degradation of the transport properties that cannot be overcome even if a high bias voltage was applied.

REFERENCES

- [1] Guoqiang Li, Wanqi Jie, Hui Hua and Zhi Gu (2003), 'Cd_{1-x}Zn_xTe: Growth and characterisation of crystals for X-ray and gamma-ray detectors', Prog. in Crystal Growth and Characterization of Materials, Vol. 46, pp. 85-91.
- [2] Young-Hun Kim, Se-Young An, Ju-Young Lee, In Jae Kim, Ki-Nam Oh, Sun-Ung Kim and Mann-Jang Park (1999), 'Photoluminescence study on the effect of the surface of CdTe by surface passivation', J. Appl. Phys., Vol. 85/10, pp. 7370-7373.

5.2.19 Investigation of deep level defects in copper irradiated bipolar junction transistor

K.V. Madhu¹, Ravi Kumar², M. Ravindra³ and R. Damle¹

¹Department of Physics, Jnanabharati, Bangalore University, Bangalore-560 056.

²Inter-University Accelerator Center, Aruna Asaf Ali Marg, New Delhi 110 067.

³Components Division, ICG, ISRO Satellite Centre, Bangalore-560 017.

Bipolar junction transistors (BJTs) are being extensively used in space and other radiation rich environments. These devices are sensitive to high energy particle irradiation. In the present study, commercial bipolar junction transistor (2N 2219A, npn) planned for space application and

manufactured in an indigenous technology from Continental Device India Ltd. is irradiated with 150 MeV Cu^{11+} ions with fluence of the order 10^{12} ions cm^{-2} . I-V, C-V and Deep Level Transient Spectroscopy (DLTS) measurements are made before and after irradiation with three different fluences to study radiation induced transistor gain degradation and characteristics of deep level defects. Gummel plots show that the base current increases while the collector current decreases as the ion fluence increases. C-V characteristics show that there is a considerable degradation of junction capacitance after irradiation. The properties such as activation energy, trap concentration and capture cross section of deep level defects are studied by DLTS. Figure 1 exhibits the DLTS spectra of Cu-ion irradiated BJT for different ion fluences. The irradiated transistor is subjected to isothermal and isochronal (30 min) annealing. During isochronal (30 min) annealing, the temperature is varied from 100°C to 500°C in the steps of 50°C . After annealing at each temperature, I-V, C-V and DLTS measurements are made to monitor the annealing behaviour of deep level defects. I-V characteristics of the transistor as a function of annealing temperature show that the base current decreases with an increase in the annealing temperature whereas the collector current increases with an increase in the annealing temperature.

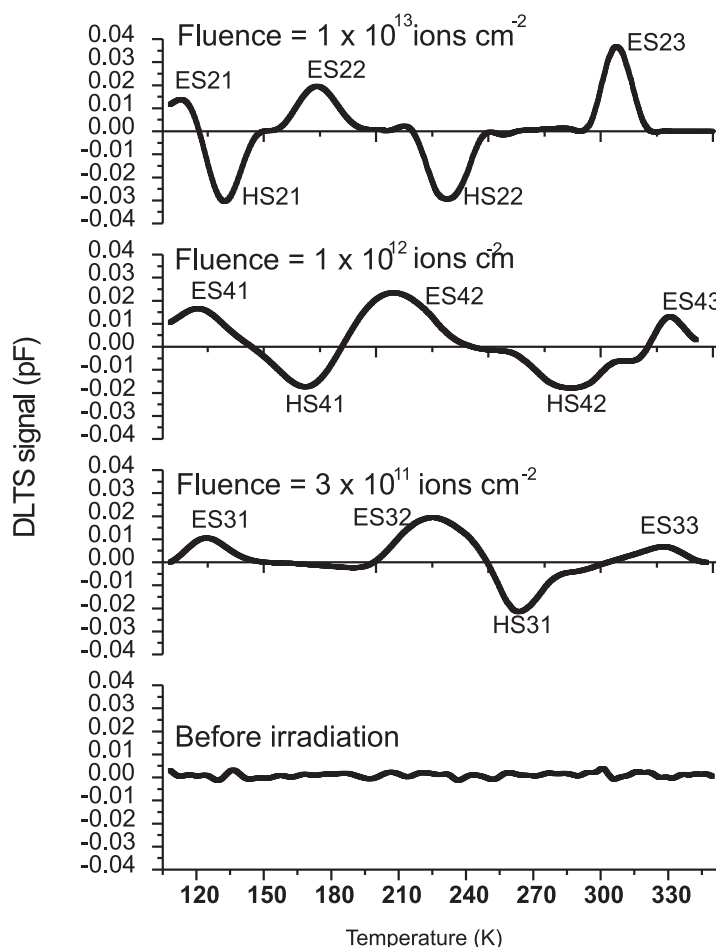


Fig. 1. DLTS spectra of Cu-ion irradiated transistor for three different fluences. Rate window is fixed at 127.9 s^{-1} .

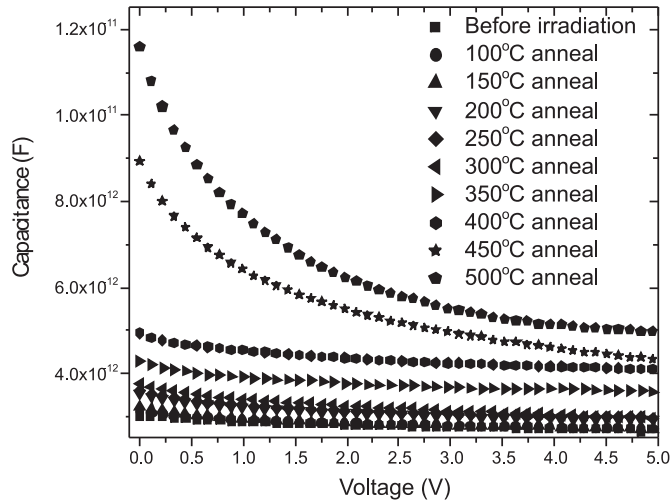


Fig. 2. C-V characteristics of the Cu-ion irradiated transistor at different isochronal annealing temperatures.

C-V characteristics of the transistor as a function of annealing temperature show that there is a major recovery in the capacitance of the base-collector junction after annealing at 350°C (Fig. 2). DLTS studies show that the defects anneal above 350°C. The defects $E_C-0.228$ eV and $E_V+0.203$ eV are identified as di-vacancies, $E_C-0.369$ eV as carbon-oxygen (C-O) complex, $E_V+0.504$ eV and $E_V+0.526$ eV as interstitial clusters, $E_C-0.188$ eV and $E_C-0.164$ eV as A-centers, $E_V+0.302$ eV as vacancy-oxygen-boron (V-O-B) complex, $E_C-0.340$ eV as M-center, $E_C-0.276$ eV as boron-oxygen (B-O) complex and $E_V+0.383$ eV as K-center. The levels $E_C-0.682$ eV, $E_C-0.695$ eV and $E_C-0.636$ eV are identified as new energy levels for defect clusters in silicon. A detailed analysis of the annealing behaviour of the defects reveals that the defects generated in the base region of the transistor by displacement damage appear to be responsible for an increase in base current upon irradiation through Shockley Read Hall (SRH) recombination and consequent transistor gain degradation.

5.2.20 MeV heavy ion beam induced epitaxial crystallization of buried Si_3N_4 layer

T. Som¹, B. Satpati¹, O.P. Sinha¹, J. Ghatak¹, N.C. Mishra², D.K. Avasthi³ and D. Kanjilal³

¹Institute of Physics, Sachivalaya Marg, Bhubaneswar 751 005

²Physics Department, Utkal University, Bhubaneswar 751 004

³Inter-University Accelerator Centre, Aruna Asaf Ali Marg, New Delhi 110 067

We have studied swift heavy ion beam induced epitaxial crystallization (SHIBIEC) of a buried Si_3N_4 layer at temperatures as low as 100-200°C, where the projectile ions lose their energy mainly by inelastic collision processes. 70 MeV O^{7+} , 70 MeV Si^{5+} ions, and 100 MeV Ag^{8+} were used (up to a fluence of 1×10^{14} ions cm^{-2}) to induce recrystallization in the thin Si_3N_4 layer, which was produced by N ion implantation at 300°C. It can be mentioned here that this is a typical silicon-on-insulator (SOI) structure consisting of an almost

defect-free device-worthy Si layer at the top, a good dielectric layer in the form of a buried silicon nitride/oxide layer, and two high-quality abrupt interfaces of the buried insulating layer with the top as well as the substrate Si.

Ultrasonically cleaned Si(100) samples were implanted with 100 keV N⁺ ions at 300°C up to a fluence of 8×10¹⁷ ions cm⁻². Later on, the N-implanted samples were irradiated by 70 MeV O⁷⁺, 70 MeV Si⁵⁺, and 100 MeV Ag⁸⁺ ions using a constant fluence of 1×10¹⁴ ions cm⁻² at different temperatures, viz. room temperature (RT), 100°, 150°, 200°, 250°, and 300°C. For all the ion species, the implanted species would penetrate deep (a few mm) into the Si substrate. The energy deposited by them were calculated by SRIM-2003 code. Systemic transmission electron microscopy (TEM) and selected area diffraction (SAD) patterns are used to examine the microstructure formed in the buried layer. To check the crystallinity of each layer, selected area diffraction (SAD) patterns were collected from three distinctly different regions. The SAD patterns clearly indicate that although the implanted layer is amorphous, the layer above it and the substrate Si are crystalline.

TEM study was performed for an implanted sample, which was further irradiated by 70MeV O⁷⁺, 70MeV Si⁵⁺, and 100 MeV Ag⁸⁺ ions at RT to the fluence of 1×10¹⁴ ions cm⁻². The SAD patterns (not shown) collected from all three layers indicate that the implanted layer still remains amorphous, while Si layers below and above it retain their single crystalline nature. It is expected because Si does not get amorphized under SHI irradiation [1,2]. We have obtained recrystallized Si₃N₄ layer due to irradiation by O, Si and Ag ions at 100°, 150° and 200°C, respectively (micrograph not shown) [3]. A possible mechanism of recrystallization is discussed on the basis of formation of vacancies along the track of the swift heavy ion and their migration at elevated temperatures during irradiation.[1,3,4]

In order to find out a possible correlation, the respective recrystallization temperatures are plotted against the S_e/S_n ratios (in the silicon nitride layer) of all the three ion species and are shown in Fig. 1. These data show an inverse linear relationship between the two and thus justify our argument that the recrystallization temperature decreases with an increasing S_e/S_n ratio. SHI induced recrystallization in amorphous Si also shows a similar trend where the higher S_e/S_n ratio causes a reduction in the activation energy and a higher regrowth rate for any given temperature [5]. It also shows the possibility of predicting the temperature at which the SHIBIEC sets in for the silicon nitride system. It may be mentioned that SHIBIEC in Si [6] and Si₃N₄ are the only works known to us and hence a lot needs to be done to have a clear understanding on the role of the S_e/S_n ratio.

REFERENCES

- [1] M. Levalois and P. Mary, Nucl. Instr. Meth. Phys. Res. B 156 (1999) 64 and references therein.
- [2] W. Wesch, A. Kamarou, and E. Wendler, Nucl. Instr. meth. phys. res. B 225 (2004) 111.

- [3] T. Som, B. Satpati, O.P. Sinha, D.K. Avasthi, and D. Kanjilal: Nucl. Instr. Meth. Phys. Res. B 245 (2006) 255.
- [4] T. Som, O.P. Sinha, J. Ghatak, B. Satpati, and D. Kanjilal: J. Appl. Phys. 101 (2007) 034912.
- [5] P. K. Sahoo, Ph.D Thesis, IIT, Kanpur, (2004)
- [6] P. K. Sahoo, T. Som, D. Kanjilal, and V. N. Kulkarni: Nucl. Instrum. & Meth. Phys. Res. B 240 (2005) 239.

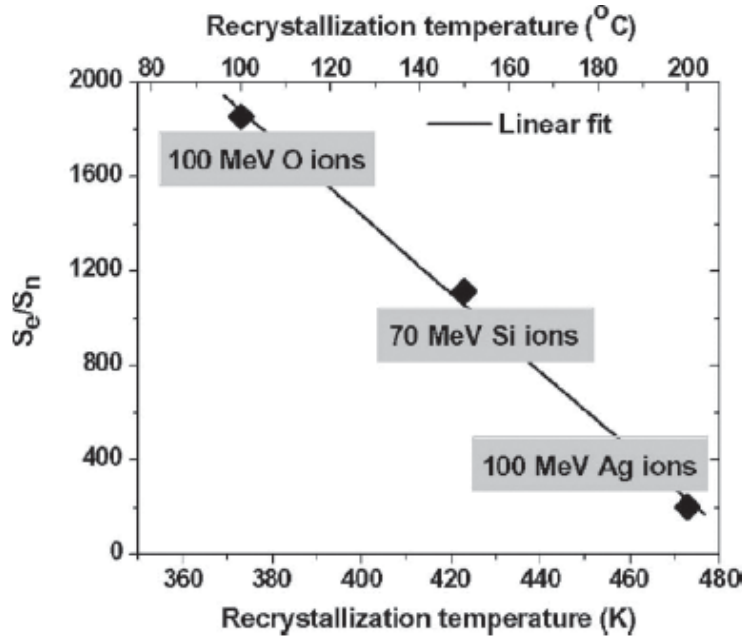


Fig. 1. Variation in the recrystallization temperature of the buried silicon nitride layer and the S_e/S_n ratio of different ions. All irradiations were performed at a fixed fluence of 1×10^{14} ions cm^{-2} .

5.2.21 ERDA studies of ion beam synthesized silicon oxynitride surface layers

A. D. Yadav¹, S. K. Dubey¹, Rucha H. Polji¹, Saif A. Khan² and D. K. Avasthi²

¹Department of Physics, University of Mumbai, Mumbai

²Inter University Accelerator Centre, Aruna Asaf Ali Marg, New Delhi 110067

The research interest in the area of high fluence ($\geq 10^{16}$ ions- cm^{-2}) ion-implantation is growing for producing materials with compositions and structures unattainable by conventional techniques. The synthesis of silicon oxynitride insulating layers using ion beam techniques has scope of potential application in future nanoscale silicon technology. In the present experiment, surface layers of silicon oxynitride ($\text{Si}_x\text{O}_y\text{N}_z$) were synthesized by high fluence dual implantation of molecular oxygen ($^{16}\text{O}_2^+$) and nitrogen ($^{14}\text{N}_2^+$) ions in different ratios into single crystal silicon wafers at 30 keV using low energy ion beam facility at the Department of Physics, Mumbai University. The total ion-fluences employed were 2×10^{18} atoms- cm^{-2} . The annealing of the ion beam synthesized surface layers was carried out at 500°C and 800°C in flow of dry nitrogen gas each for 30

min. The compositional depth profile analysis of the formed structures was carried out with heavy-ion Elastic recoil detection analysis (HI-ERDA) using 15 UD Pelletron accelerator facility at Inter University Accelerator Centre, New Delhi. The ERDA spectra were transformed into depth versus concentration profile using the SIMNRA simulation code.

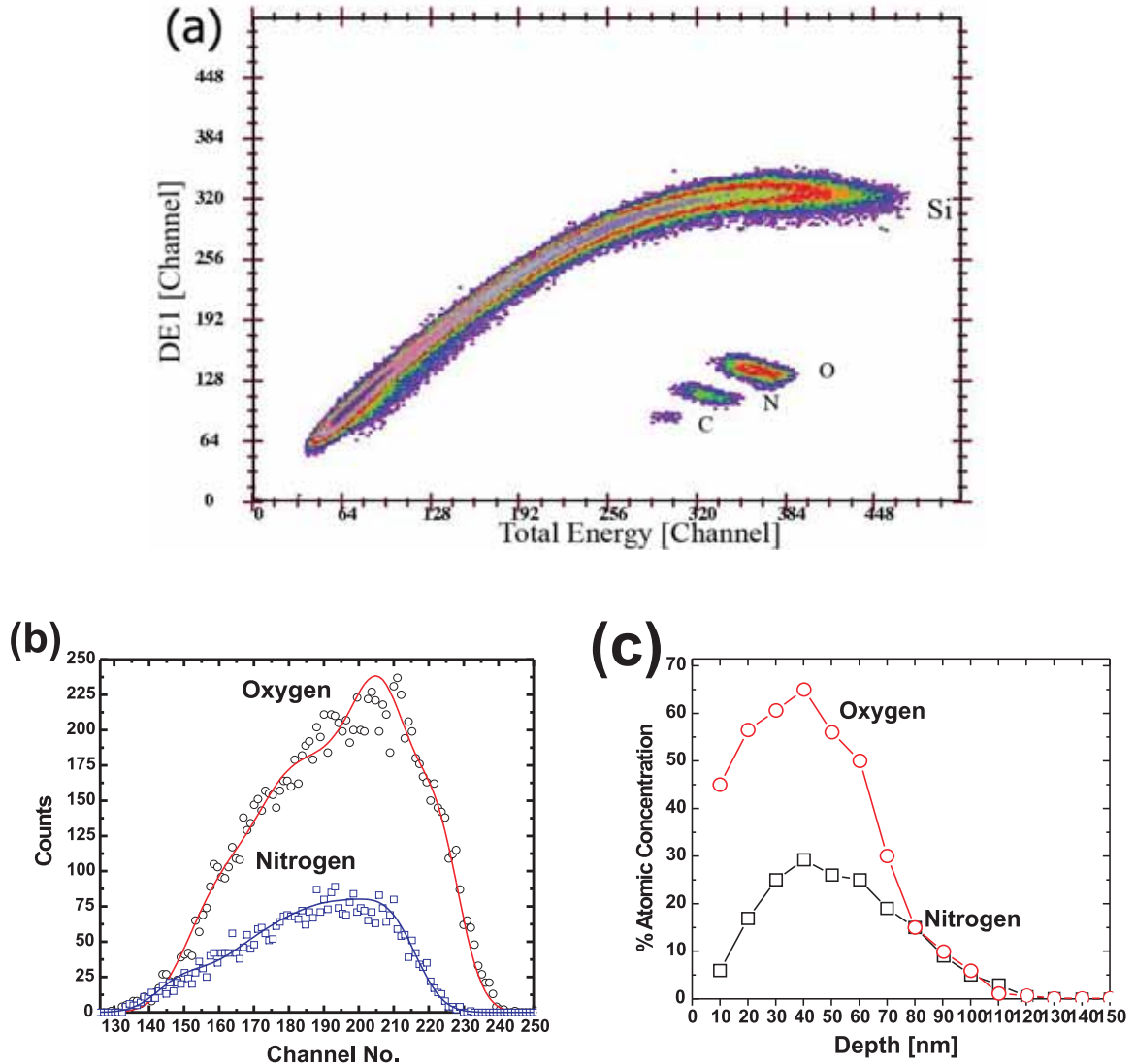


Fig. 1. HI-ERDA spectra of silicon sample implanted with O: N ratio 3: 1.

The annealing behaviour of oxygen and nitrogen implanted sample with O: N ratio 3:1 is shown in Fig. 2. It is seen that the peak of the nitrogen recoils at 65 nm shifts towards bulk and the oxygen peak at 35 nm shifts towards the surface. On annealing the sample, the oxygen distribution is found to get narrower and the nitrogen diffuses towards the bulk. These results imply that the redistribution of oxygen and nitrogen takes place on annealing.

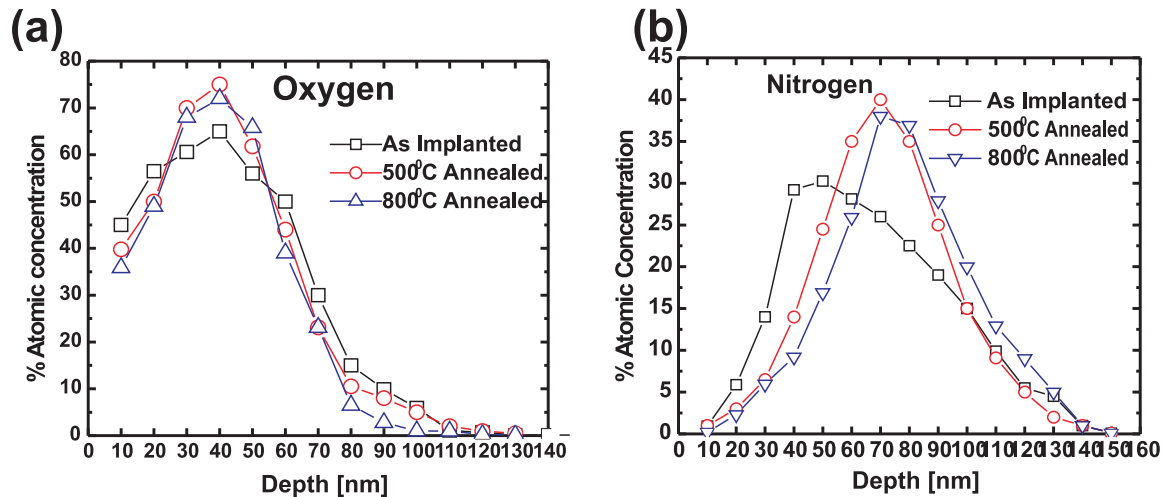


Fig. 2. Annealing behavior of silicon sample implanted with O: N ratio 3: 1.

REFERENCES

- [1] A. Ermolieff, P. Molle, S. Marthon, *Appl. Phys. Lett.* 56 (1990) 2672.
- [2] Y. Li, A. Kilner, R. J. Chater, A. Nejm, P. L. F. Hemment, T. J. Talte, *J. Appl. Phys.* 74 (1983) 82

5.2.22 In situ analysis of 180 MeV $^{107}\text{Ag}^{14+}$ Irradiated Au/n-Si Schottky Structures

Sandeep Kumar¹, Y.S. Katharria¹, V. Baranwal², A. T. Sharma³, D. Kanjilal¹

¹Inter-University Accelerator Centre, Aruna Asaf Ali Marg, New Delhi 110 067

²Department of Physics, University of Allahabad, Allahabad, 211 002

³Department of Physics and Astrophysics, University of Delhi, Delhi, 110 007

Schottky barrier diode (SBD) is the most simple and fundamental semiconductor device. The studies on the effect of swift heavy ion (SHI) irradiation on SBD are important for application as well as fundamental understanding of the phenomenon. These studies shed light on the basic ion-solid interaction process, and their influence on various properties of semiconductors. For further improvement in the understanding of the effect of irradiation on SBDs, a systematic I-V characterization of the SHI irradiated Au/n-Si SBD is carried out in-situ at various fluences on the same SBD keeping all other physical parameters like ion flux, sample temperature and vacuum environment identical.

The Schottky diode was fabricated using both side-polished n-type Si (100) sample of resistivity (0.5-1) $\Omega\text{-cm}$. To make Ohmic contact Aluminum was deposited by thermal evaporation method in high vacuum chamber followed by a temperature treatment at 525°C for 25 minutes in argon gas environment. Schottky contact was created by deposition of Au on the sample having Ohmic contact by thermal resistive heating technique in an ultra high vacuum chamber.

The irradiation was performed by 180 MeV $^{107}\text{Ag}^{14+}$ ion beam using the 15UD Pelletron accelerator facility at Inter-University Accelerator Centre, New Delhi. The current-voltage (I-V)

measurements were carried out during irradiation in a vacuum chamber at a vacuum of the order of 1×10^{-6} mbar.

The experimental data is fitted by the thermionic emission equation, which is given by [1]

$$I = I_0 \exp\left(\frac{qV}{nkT}\right) \left[1 - \exp\left(-\frac{qV}{kT}\right) \right] \quad (1)$$

where I_0 is the saturation current and n is the ideality factor. The saturation current I_0 is given by

$$I_0 = AA^*T^2 \exp\left(-\frac{q\Phi_{B0}}{kT}\right) \quad (2)$$

where A^* , A , and Φ_{B0} represents the Richardson constant, the contact area and zero-bias Schottky barrier height (SBH) respectively. From the slope of $\ln(I)$ versus V curve, the value of ideality factor is calculated. The I_0 is determined from the intercept of $\ln(I)$ versus V curve on the y-axis.

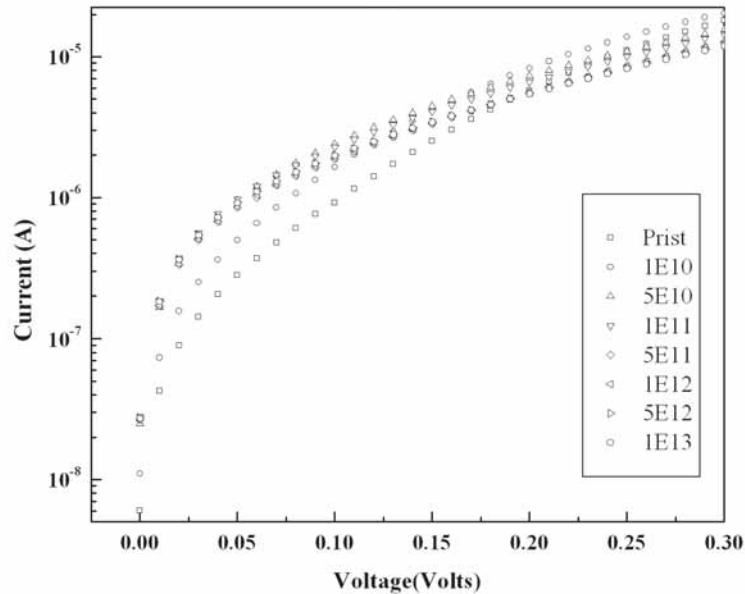


Fig. 1

Fig 1 shows the $\ln(I)$ versus V characteristics for pristine as well as irradiated Au/n-Si at different irradiation fluences. The values of ideality factor n and zero-bias barrier height F_{B0} of the diode were calculated and are plotted as a function of fluence in Fig.2. The ideality factor n exhibits an increasing trend while the zero-bias barrier height decreases with increasing irradiation fluence. The barrier height of Au/n-Si SBD shows an exponentially decrease with fluence. In this case experimental barrier height can be given by the equation

$$\Phi_{SBH} = \Phi_{sat} + \frac{nkT}{q} \exp\left(-\frac{\phi}{\phi_0}\right) \quad (3)$$

where ϕ_0 is the initial irradiation fluence; in this case its value is 1×10^{11} ions-cm⁻². If $\phi \rightarrow \infty$ then $\Phi_{SBH} \rightarrow \Phi_{sat} = 0.69$ in this case.

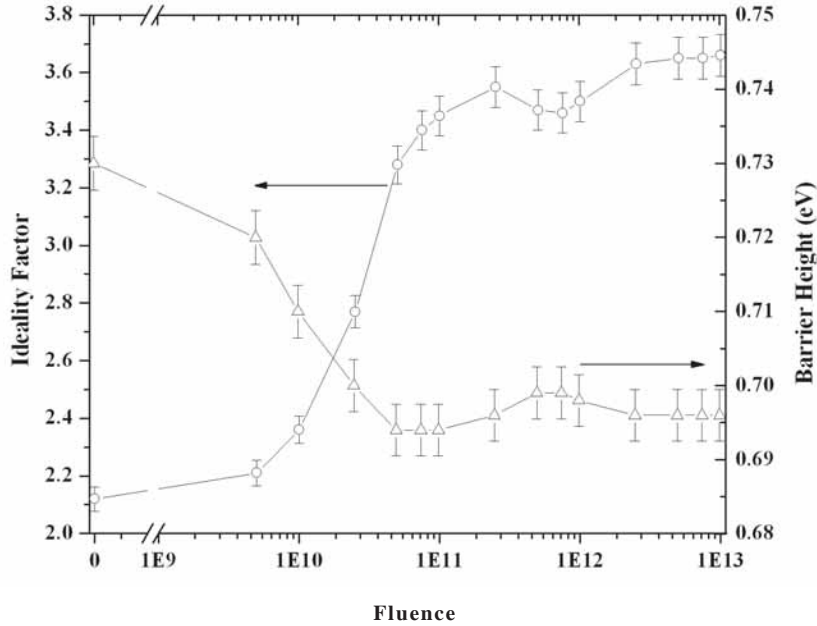


Fig. 2

This behavior of SBH with fluence of 180MeV ¹⁰⁷Ag¹⁴⁺ is due to the increased interface states density at the MS interface. It is well known that when a SHI penetrates through the MS interface, it loses the energy through nuclear and electronic energy loss mechanisms. The intense electronic excitation due to prominent inelastic collision of the SHI at the MS interface region leads to the production of vacancies, interstitials and complex defects, which results in the introduction of interface states at MS interface. For the pristine SBD the value of SBH is 0.73 eV, it means there is finite density of interface state, which decreased to 0.714eV after irradiation with fluence 1×10^{10} ions-cm⁻². It means that there is increase in interface state density and resultant orientation of the Schottky barrier more towards the Bardeen limit [2]. It shows that at the fluence 1×10^{11} ions-cm⁻², interface state density become so high that Fermi level gets pinned. When SHI irradiation induced defect concentration becomes more than the doping concentration then Fermi level will be pinned at the defect level. If we further increase the irradiation fluence then defect concentration will increase but the position of the Fermi level will remain the same. So barrier height will not change with the increased fluence.

REFERENCES

- [1] S. M. Sze, Physics of semiconductor devices. 2nd ed. (Wiley, New York, 1981).
- [2] J. Bardeen, Phys. Rev. 71(1947) 717

5.2.23 Effect of Swift ion beam on the electrical transport properties across Au/n-GaAs Schottky structure

Shahnawaz¹, A.T. Sharma¹, Sandeep Kumar², Y.S. Katharria², D.Kanjilal²

¹Department of Physics & Astrophysics, University of Delhi, Delhi 110007

²Inter-University Accelerator Centre, Aruna Asaf Ali Marg, New Delhi 110067

GaAs is a direct band gap semiconductor and has great technological importance due to its applications in detectors, high speed semiconductor devices and in optoelectronics. Metal-semiconductor (M-S) interfaces form an integral part of any semiconductor device and thus their study attracts a lot of research interests. Study of high energy ion beam modifications is helpful in simulating the performance of semiconductor devices in space and radiation environments. There are some reports on such studies with M-S contacts [1, 2].

In our study the effect of effect of swift ion beams ($72.5\text{MeV } ^{58}\text{Ni}^{6+}$, $180\text{MeV } ^{107}\text{Ag}^{15+}$, and $80\text{MeV } ^{16}\text{O}^{6+}$) on the transport properties of Au/n-GaAs Schottky structures is investigated through an in-situ Current-Voltage (I-V) characterization technique. The sample was prepared by deposition of Au Schottky contact on n-GaAs (Si-doped), and Au-Ge eutectic alloy was used for preparation of Ohmic contact. During experiment, the irradiation fluence was carefully varied from 5×10^9 to 5×10^{13} ions cm^{-2} , and I-V characterization was performed at close intervals in order to make a detailed study of ion beam induced modifications on the electrical transport behaviour.

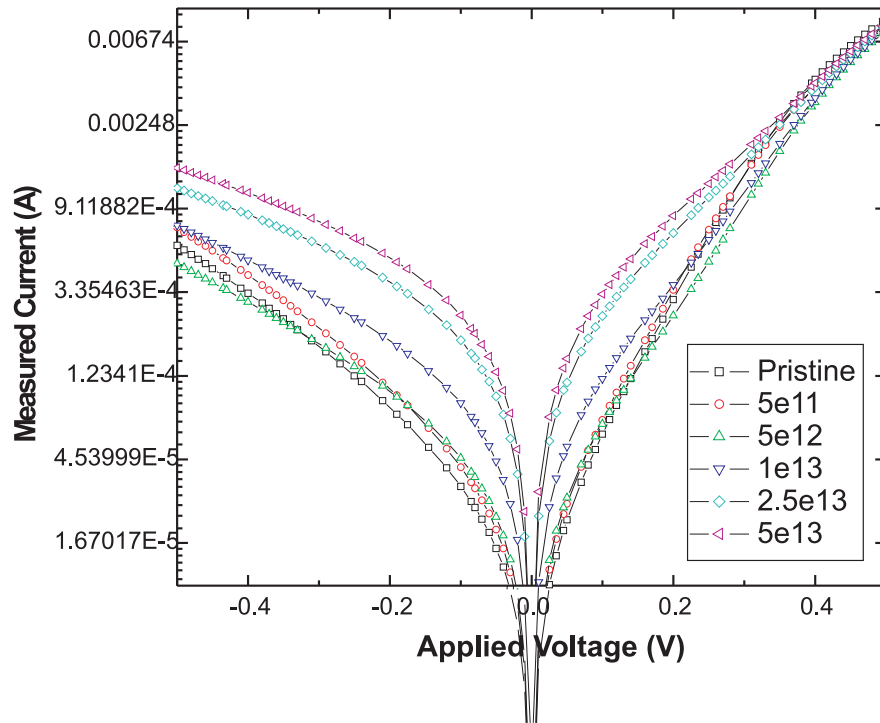


Fig. 1.

Fig.(1) shows the I-V characteristics of the pristine diode and also under various fluences of irradiation with 72.5MeV $^{58}\text{Ni}^{6+}$ ions, where only few selected fluences are shown for clarity. From analysis of I-V data, it was observed that the diode properties like Schottky Barrier height (SBH), ideality factor (n) and reverse leakage current (I_R) vary as a function of ion irradiation fluence [Fig. (2)]. The swift heavy ion loses energy as it enters the target and leads to modification in characteristics of the M-S interface and formation of various types of defects at the interface. This alters the nature and density of states at the M-S interface which is very significant in determining the transport characteristics across the barrier. The nature and degree of modification was found to vary with the species of the ion depending on its mass and ratio of electronic and nuclear energy losses.

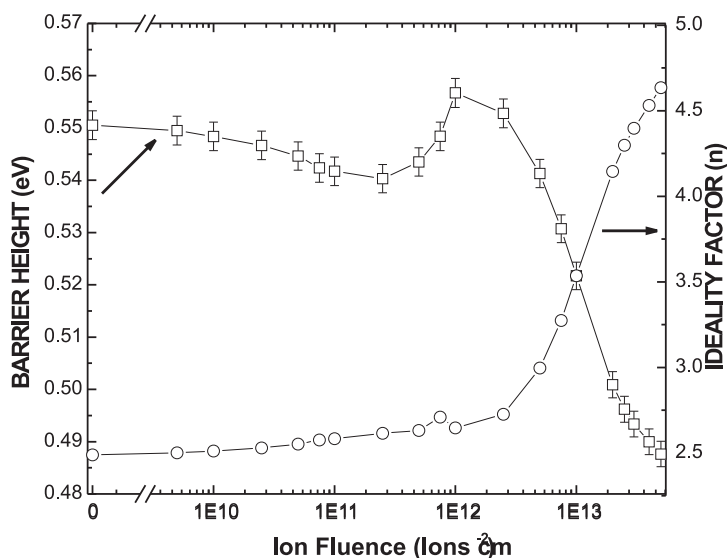


Fig.2.

REFERENCE

- [1] R.Singh, S.K. Arora, J.P. Singh, D. Kanjilal, Radiat. Eff. Def. Solids 157 (2002) 367.
- [2] S.Kumar, D.Kanjilal, Nucl. Ins. and Meth. B 248 (2006) 109

5.2.24 Band-structure, interface and surface modification of InGaAs/InP MQWs

S Dhamodaran¹, A P Pathak¹, A Turos², S A Khan³, D K Avasthi³, R Kesavamoorthy⁴ and B M Arora⁵

¹School of Physics, University of Hyderabad, Hyderabad - 500 046

²Institute of Electronic Materials Technology, Warsaw, Poland

³Inter University Accelerator Centre, Aruna Asaf Ali Marg, New Delhi 110 067

⁴Materials Sc. Division, Indira Gandhi Centre for Atomic Research, Kalpakkam

⁵Tata Institute of Fundamental Research, Mumbai - 400 005

Quantum well intermixing (QWI) is of interest from the band structure engineering point of view. Among the III-V semiconductors, $\text{In}_x\text{Ga}_{1-x}\text{As}/\text{InP}$ is a key material used in longer wave-

length optical communications. In literature high energy ion beam induced modification of semiconductor quantum wells has not been reported to our knowledge. The basics of such high energy interaction with multilayers are also of high interest. Here we attempt to understand the modification induced by swift heavy ions (energy > 1 MeV/nucleon). The ion induced modifications have been characterized using photoluminescence (PL), High Resolution XRD (HRXRD), Raman spectroscopy and Atomic Force Microscopy (AFM).

The InGaAs sample was grown on (001) oriented semi-insulating InP substrates using MOCVD. The MQWs consist of 15 periods of InGaAs/InP with a nominal layer thickness of 20nm each. The Indium composition of the layer have been chosen to be $x=0.55$ which is nearly lattice matched to the InP substrate. The irradiation was performed at room temperature by 150 MeV Ag¹²⁺ ions with a fluence of 1×10^{13} ions/cm² and 200 MeV Au¹³⁺ with a fluence of 7×10^{12} ions/cm² from Pelletron accelerator. As-grown and high energy irradiated InGaAs/InP multi quantum wells were annealed using proximity capping at 500 and 700°C for 60s in N₂ (1000 SCCM) atmosphere. The sample identifications are M-U, M-I1, M-I2, M-U-A5, M-U-A7, M-I1-A5 and M-I1-A7 for as-grown, Ag irradiated, Au irradiated, 500 deg annealed as-grown, 700 deg annealed as-grown, 500 deg annealed Ag irradiated and 700 deg annealed Ag irradiated samples respectively.

From the PL studies, we could identify thickness variations in the MQW sample which has been resolved by recording the PL as a function of temperature and power. Three distinct peaks were observed in the PL spectra recorded at 18K. The intense peak corresponds to the heavy hole (hh) -electron transition and two more peaks at higher and lower in energy than the main peak were observed. The intensity and width of the high energy peak increased whereas the low energy peak vanished as a function of temperature. As a function of power, all the three peaks intensity increased linearly indicating no defect related luminescence. PL spectra of irradiated plus annealed samples were indicating a band-gap shift of about 25nm. HRXRD and Raman analysis indicate interface mixing and formation of quaternary alloy at the interface. Also the satellite peaks in HRXRD spectra vanished at high temperature annealing of irradiated samples. The Au ion irradiated samples show stronger interfacial degradation than the Ag ion irradiation. Raman spectra show GaP in the irradiated samples which were not observed in the as-grown sample. Surface morphology of these samples indicates damage overlapping regions and hence high density of craters at the surface. The surface roughness increases from 0.2nm to as high as 6nm. The crater sizes and densities were also increasing as a function of irradiation, irradiation plus annealing and also for Au and Ag ion irradiations. The PL, HRXRD, Raman and AFM images are given in Fig.1 (a), (b), (c) and (d) respectively.

The band structure, interface and surface modifications have been analyzed using, PL, HRXRD, Raman and AFM. The concurrent use of these techniques was useful in getting detailed information regarding the modifications. The modifications indicate that high fluence is more effective than high electronic energy of the incident ions. The analysis indicates irradiation of compressively strained InGaAs/InP MQWs increases the interfacial strain.

REFERENCE

[1] S Dhamodaran, A P Pathak, A Turos, S A Khan, D K Avasthi, R Kesavamoorthy, B M Arora, (Communicated).

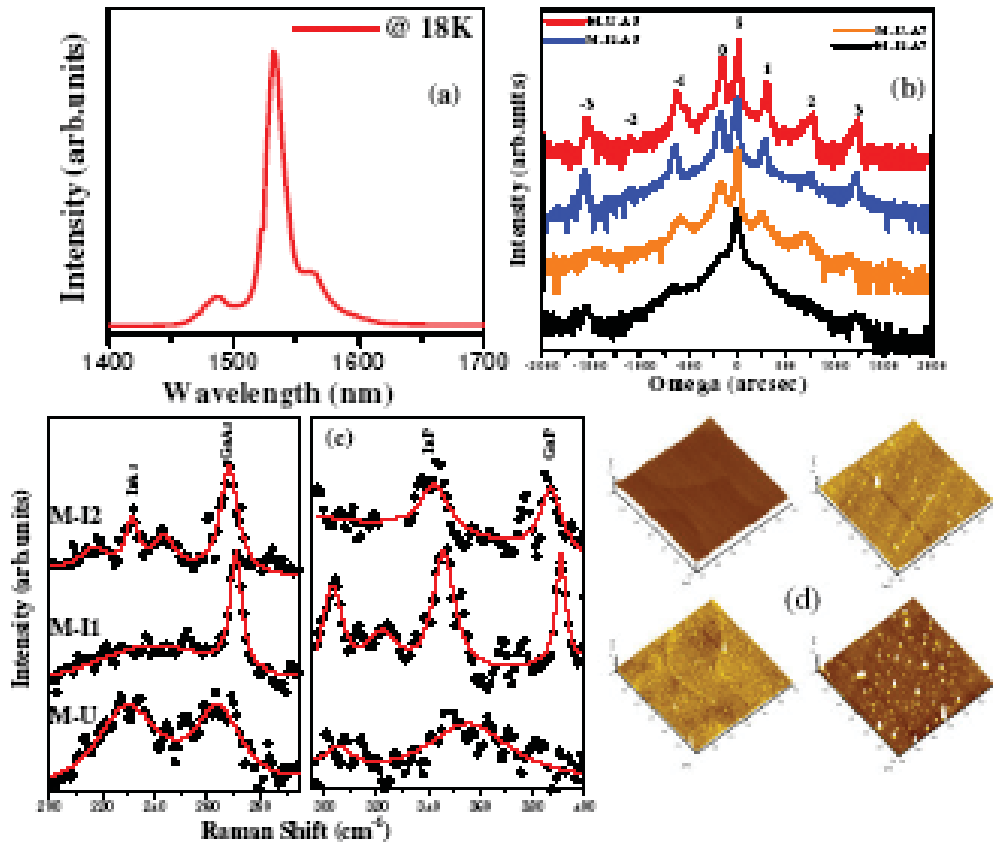


Fig.1. (a) PL spectra of as-grown sample recorded at 18K, (b) HRXRD of as-grown, annealed and irradiated samples (c) Raman spectra of as-grown and irradiated samples and (d) AFM of as-grown and irradiated samples.

5.2.25 Photoluminescence study of 100 MeV gold swift heavy ion irradiated copper sulfide thin films

Abhay A. Sagade², Fouran Singh¹ and Ramphal Sharma²

¹Inter University Accelerator Centre, Aruna Asaf Ali Marg, New Delhi 110 067

²Thin Film and Nanotechnology Laboratory, Dept. of Physics, Dr. Babasaheb Ambedkar Marathwada University, Aurangabad 431 004

The Cu_xS is well known material because of its opto-electronic properties. Although there are number of reports, it is still in interest due to variation in properties depending on $x = 1$ to 2. The opto-electronic and solar control properties of chemically deposited Cu_xS thin films have been studied experimentally. These films exhibit low IR transmittance and higher IR reflectance coupled with low visible reflectance and high visible transmittance. These optical characteristics enable Cu_xS solar control films to cut off more heat radiation in the IR region and allow sufficient

illumination in the interior of buildings.

Recently it was also reported that, Cu_xS could also be used for the detection of the traces of ethanol, acetone and some gaseous molecules, which include the (NH) n - group. The Cu_xS sensors were working at room temperature rather than at high temperatures. The response and recovery times were also within tenths of seconds.

The $\text{Cu}_{1.4}\text{S}$ thin films were prepared by economic solution growth technique (SGT) at room temperature. The AR grade copper sulfate (hydrous) and thiourea were used as precursor chemical for the Cu^+ and S^- ions, respectively. The films of area $1 \times 1 \text{ cm}^2$ were deposited on to the precleaned glass slides. The redish coloured films with 70% transmittance in optical region were deposited within 90 mins.

Numerous experiments and theoretical calculations of Szenes [1] showed that above certain threshold values of the electronic stopping power S_{et} ($1 \text{ keV}/\text{\AA}$) high energy heavy ions are capable of changing the physical properties of the material. Taking this point of view and using SRIM-2003 [2] calculations the energy loss of the 100 MeV Au ions in the copper sulfide was carried out. Electronic energy loss ($S_e = 2.38 \text{ keV}/\text{\AA}$) is the dominant mechanism of energy loss in the copper sulfide amorphous matrix. Next, the films have been irradiated at room temperature (300 K) using 15UD Pelletron accelerator at IUAC, New Delhi. The films were exposed to the ion beam for fluence of 10^{11} , 10^{12} and $5 \times 10^{12} \text{ ions cm}^{-2}$. The angle of incidence of SHI was 90° with plane of samples. The vacuum of 10^{-7} Torr was maintained during the irradiation [3].

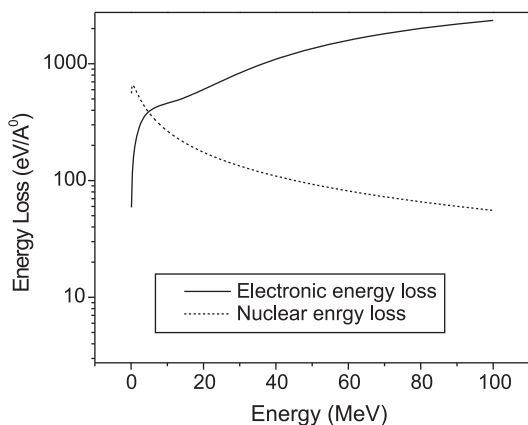


Fig. 1

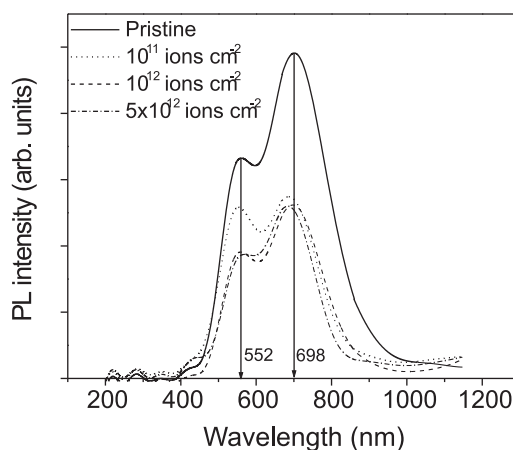


Fig. 2

Fig. 1 shows the energy loss of the SHI in the copper sulfide matrix. The nuclear energy loss is feeble in comparison with the electronic energy loss. Also, the Bragg peak is nowhere in the picture. Fig. 2 shows the Photoluminescence (PL) of copper sulfide thin films irradiated with different fluence. PL measurements were carried out by using He Cd laser with 320 nm excitation. It is observed that there are two peaks at 552 and 698 nm. The first peak is attributed to the formation of copper oxide (Cu_2O) on the surface of the films and the second one is due to the defect

state below the conduction band edge. As the fluence increases, the luminescence intensity of both the peaks decreases and there is no shift in the peak position for all fluences.

REFERENCES

- [1] Szenes G 2002 Phys. Rev. B 65 45206; Szenes G 1996 Nucl. Instr. and Meth. B 116 141.
- [2] Ziegler J F, Biersack J P, Littmark U 1985 The Stopping and Ranges of Ions in Solids (Pergamon: New York); www.srim.org.
- [3] Abhay A. Sagade et. al. 2007 Radiation Effects and Defects and Solids 162 77.

5.2.26 Understanding of Radiation Induced Defects in ZnO and Their Role on Transport and Optical Properties

Sreetama Dutta¹, S. Chattopadhyay², A. Sarkar³, F. Singh⁴, P. K. Kulriya⁴, D. Jana¹

¹Department of Physics, University of Calcutta, 92 A.P.C. Road, Kolkata 700009

²Department of Physics, Taki Government College, Taki 743429

³Department of Physics, Bangabasi Morning College, 19 R.C. Sarani, Kolkata

⁴Inter University Accelerator Center, Aruna asaf Ali Marg, New Delhi 110067

Over the decades, radiation damage is a widely used technique for controlled modification of physical properties of different systems [1]. This is possibly the most suitable one for tuning structural, electrical and optical properties of different materials through controlled production of defects and disorder [2,3] induced by ion-beam irradiation. Zinc Oxide (ZnO) is a wide band gap II-VI semiconductor with immense potential for its use in next generation electro-optic devices [4]. We have already studied the effect of annealing on the structural and optical properties and defect generation in ZnO [5,6]. A proper understanding of the ion beam irradiation induced modifications in band gap, grain size, surface morphology in ZnO is a requirement for its utilization in technological application.

In the present report, main thrust has been on the systematic plan of our experiments to study the role of irradiation-induced defects and disorder on physical properties of the system. As-supplied high purity ZnO (purity 99.9 % from Sigma-Aldrich, Germany) powder has been palletized and annealed at 300 °C and 500 °C for 18 hour followed by slow cooling (30 °C/h) in air. The two sets of sample were irradiated by 100 MeV Si⁸⁺ ions with different fluence starting from 5×10^{12} to 1×10^{14} ions/cm² using the Pelletron accelerator at Inter-University Acceleration Centre (IUAC), New Delhi.

After irradiation, X-ray diffraction (XRD) and Photoluminescence (PL) measurements were done on both sets of samples at IUAC to study the effect of irradiation on their structural and optical properties. The FWHM values of (101) peak (shown in Table 1), observed from XRD spectra, reveal that the effect of irradiation on crystallinity is sample-dependent. We have found a broad green-yellow PL band that can be interpreted on the basis of transition from deep level to valence level and this deep level emission is generally associated with the presence of structural defect and impurities [3]. The phonon-assisted transition may cause the broadening of visible light emission spectra [7]. We have also observed that the enhancement of fluence causes the depletion of the defect level due to the antisite oxygen (Ozn) that causes the lowering of intensity of PL

spectra [4]. Further supporting experiments and data analysis are in progress for drawing more conclusive features in this system and will be communicated in future.

Table 1. FWHM of pristine and irradiated samples

Sample	pristine	1×10^{13} ions/cm ²	6×10^{13} ions/cm ²	1×10^{14} ions/cm ²
Annealed at 300 °C	0.186°	0.185°	0.183°	0.181°
Annealed at 500 °C	0.186°	0.175°	0.158°	0.173°

REFERENCES

- [1] D.C. Look et al., Appl. Phys. Lett. 82 (1999) 811
- [2] W. S. Shi et al., J. Appl. Phys. 91 (2002) 5640
- [3] P. M. Ratheesh Kumar et al., J. Appl. Phys. 97 (2005) 013509
- [4] D.C. Look et al., Phys. Rev. Lett. 82 (1999) 2552
- [5] S. Dutta et al., J. Appl. Phys. 98 (2005) 053513
- [6] S. Dutta et al., J. Appl. Phys. 100 (2006) 114328
- [7] D. C. Reynolds et al., Solid State Commun. 101 (1997) 643

5.2.27 Controlled growth of Au nanoparticles induced by SHI irradiation: An in-situ X-ray diffraction study

Y. K. Mishra¹, D. K. Avasthi¹, P. K. Kulriya¹, F. Singh¹, D. Kabiraj¹, A. Tripathi¹, J. C. Pivin², I. S. Bayer³ and A. Biswas³

¹Inter University Accelerator Centre, Aruna Asaf Ali Marg, New Delhi 110067

²CSNSM, IN2P3-CNRS, Batiment 108, F-91405, Orsay Campus, France.

³Office of Electronic Miniaturization, University of Alaska, Fairbanks, U.S.A.

Noble metal nanoparticles (NPs) are of interest because of the quantum confinement of electrons, which controls many physical and chemical properties. These properties can be tuned by varying their size, shape and the embedding environment by different available fabrication techniques. The present work is an attempt to examine the possibility of using the swift heavy ions (SHI) to tailor the size of metal NPs. Investigation by in-situ XRD at the irradiation chamber is performed to monitor the growth of average particles size with ion fluence. In this report, we reveal the growth of Au NPs induced by 90 MeV Ni ions [1]. Generally there are variations from sample to sample in synthesis of NPs in a matrix and the effect of ion irradiation is dependent on the pristine state of the sample. Therefore it becomes desirable that the ion fluence dependence study should be performed on the same sample. The incidence angle in the grazing incidence X-ray diffraction (XRD) experiments cannot be perfectly reproduced in case of set of different samples, as it depends on the gluing of the sample on the holder. The in-

situ XRD facility in the beam line of IUAC, allows studying the XRD of the same sample after irradiation at various ion fluences.

Thin films of silica (thickness of about 140nm of XRD and optical absorption experiments) embedding Au NPs, were deposited on quartz by atom beam co-sputtering [2]. Rutherford backscattering spectrometry (RBS) was used for the quantification of metal fraction in SiO₂ matrix. The films were irradiated with 90 MeV Ni ions having an electronic and nuclear stopping power of 7.2 and 0.014 keV/nm respectively. The irradiation fluence was varied from 1×10^{13} - 1×10^{14} ions cm⁻². The vacuum inside the XRD chamber was maintained at $\sim 10^{-5}$ torr during irradiation and the irradiation was performed at normal incidence. UV-visible absorption spectra were recorded using Hitachi U3300, dual beam spectrophotometer. Transmission electron microscope (TEM) measurements were carried out using a JEOL JEM-3010 300 kV machine with a LaB₆ electron source.

RBS analysis of the Au-SiO₂ co-sputtered film, confirms Au with atomic fraction of $\sim 19.6\%$ in silica film of 140 nm thickness. Optical absorption spectra of pristine and irradiated co-sputtered film (shown in figure 1 (a)) reveal the presence of Au NPs with a SPR peak at ~ 520 nm. XRD spectra of pristine and irradiated samples are shown in figure 1 (b). The decrease in the FWHM of the (111) Au peak with the increasing ion fluence indicates the growth of the Au NPs. The growth is initially rapid but beyond a critical fluence the growth rate decreases. From the optical absorption spectra, it can be clearly seen that the NPs grow with increasing fluence since the full width at half maximum (FWHM) of the SPR peak decreases.

Ion beam induced growth of Au nanoparticles was confirmed by the TEM measurements. The TEM results closely match with the observations and interpretations made from the UV-VIS and in-situ XRD data on the Au NPs growth.

In-situ XRD spectra shows a regular shift in the diffraction peak of the Au (111) towards larger angle with increase in fluence, which indicates a decrease in lattice constant. This decrease could be attributed to the known decrease in surface tension of any kind of NPs with the increasing size.

The present work demonstrates that SHI can be used for tailoring the size of particles and hence the optical properties of metal NPs.

REFERENCES

- [1] Y. K. Mishra, D. K. Avasthi, P. K. Kulriya, F. Singh, D. Kabiraj, A. Tripathi, J. C. Pivin, I. S. Bayer and Abhijit Biswas, *Appl. Phys. Lett.* 90 (2007) 073110.
- [2] Y. K. Mishra, S. Mohapatra, D. Kabiraj, B. Mohanta, N. P. Lalla, J. C. Pivin and D. K. Avasthi, *Scripta Materialia* 56 (2007) 629.

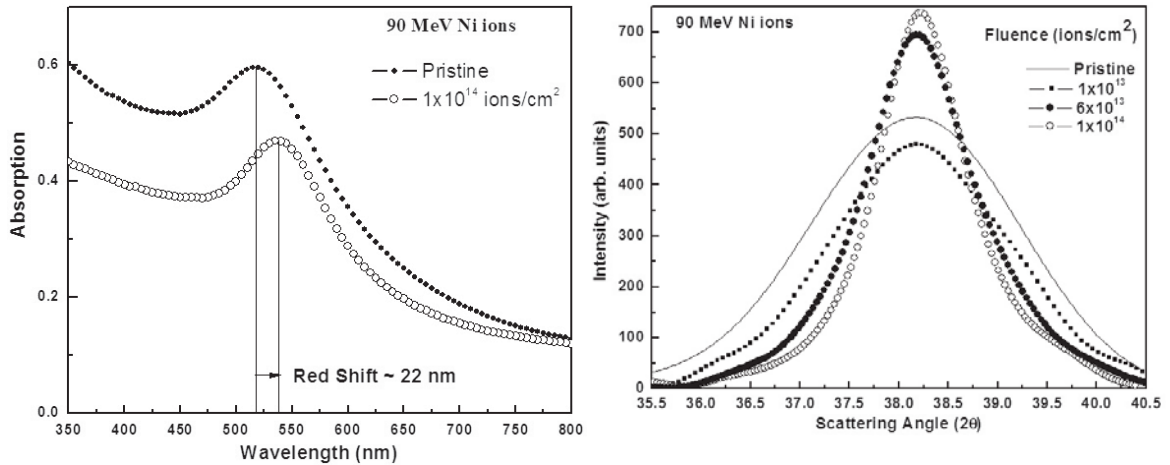


Fig. 1.(a) Optical absorption and (b) XRD spectra of pristine and irradiated samples

5.2.28 SPM Studies of Cobalt Thin Films Irradiated With Swift Heavy Ions

A. Tripathi, Indra Sulania, D. Kabiraj and D. K. Avasthi

Inter University Accelerator Centre, Aruna Asaf Ali Marg, New Delhi 110 067

The surface growth mechanism and magnetization studies of Co thin films (2-10 nm) are undertaken in the present study. The films are deposited on n-type Si(100) substrates after depositing a 5 nm thick layer of SiO₂ by electron beam evaporation technique at a base pressure of $\sim 10^{-6}$ torr. The samples have been irradiated by 120 MeV Ag and Au ions with fluence varying from 1×10^{11} to 1×10^{14} ions/cm². The unirradiated and irradiated films have been characterized using Digital Nanoscope IIIa Multimode SPM in AFM/MFM mode. The MFM measurements [1] are done using the single crystal Si tip with Co-Cr coating and at a lift height of 10-40 nm.

The AFM study of film with 2 nm nominal thickness shows formation of nano-islands of dimension 200 nm x 500 nm x 30nm. This may be attributed to the formation of Co droplets over silica which act as nucleation centres leading to surface diffusion process induced cluster formation [2]. The MFM images show a high degree of magnetization in unirradiated films. The irradiated films show that at first the bigger cobalt clusters break up into smaller fragments. As the fluence is further increased ion beam induced clustering takes place. The AFM study of 2 nm film shows the formation of uniform granular film with average grain size of 40 nm after irradiation with 120 MeV Ag ions at a fluence of 1×10^{14} ions/cm². (Fig. 1)

The AFM study shows that continuous films are obtained for films with thickness beyond 4 nm. However, irradiation shows formation of uniform granular film are obtained for 4 nm and 10 nm films also, a result similar to 2 nm film. The MFM images for a 10 nm film with increasing fluence is shown in Figure 2.

The MFM results show a decrease in magnetization signal after irradiation. The results indicate two possibilities: First a complete amorphization of the Co film and second is complete mixing between the layers of Co and SiO₂.

REFERENCES

- [1] R. D. Gomez et.al., J. Appl. Phys., 80 (1), 342 (1996).
- [2] J. A. Venables et.al., Rep.Prog.Phys, Vol 47, pp399-459 (1984).

5.2.29 Formation self-affine nanostructures on the surface of ZnO thin film under swift heavy ion irradiation

D. C. Agarwal¹, D. K. Avasthi², S. A. Khan², I. Sulania², D. Kabiraj² and R. S. Chauhan¹

¹Department of Physics, R. B. S. College, Agra, 282 002

²Inter-University Accelerator Centre, Aruna Asaf Ali Marg, New Delhi, 110 067

³CSNSM, IN2P3-CNRS, Batiment 108, F-91405, Orsay Campus, France

Ion irradiation at normal incidence or off-normal incidence accompanied by substrate rotation is reported to result in the production of ordered nano-dots on various materials. Moreover, off-normal irradiation has also been seen to result in the formation of periodic height modulation in the form of ripples with a submicron length scales [1-3]. Bradley and Harper (BH) theory [4] and its refinements based on the surface instability caused by local surface curvature dependent sputtering is frequently used to explain the formation of ordered structures during the ion bombardment. There are many reports of surface evolution in the low energy regime and a few reports are available in high-energy regime. Here, we report the formation of various types of self-affine nanostructures on the surface of ZnO thin film under swift heavy ion irradiation.

ZnO thin films of 120 nm thickness were deposited on Si substrate by e-beam evaporation technique. The films were irradiated at room temperature with Ag 100 MeV ions in the fluence range from 1×10^{10} to 3×10^{13} ions.cm⁻² from Pelletron Accelerator at the IUAC, NewDelhi. The surfaces of the post-irradiated samples were characterized by Atomic force microscopy (AFM) Nanoscope III.

AFM image of the pristine sample shows that the features on the surface are randomly distributed. They do not show a regular or periodic behaviour. When films are irradiated at low fluence value upto 7×10^{12} ions/cm², the surface morphology of ZnO films is dominated by an almost uniformly distributed nanoscale, self-affine pattern. Deposition of energy in the surface region of films and subsequent changes in surface free energy induce the formation of these structures. The shape (as well as size) of these structures changes with ion fluence.

At spatial frequencies greater than the correlation length (k_0), the Power spectral density (PSD) function follows the relation: $PSD = q^{-n}$ (1)

The exponent 'n' is a real number and may define the mechanisms contributing to the surface evolution. According to this relation, the value of 'n' could be obtained from a linear fit of the end of frequency range tail of the PSD function. The slope of PSD function (n) is increased from 2.25 to 4.1 up to the ion fluence 1×10^{12} ions- cm^{-2} and after that is decreased. The value of roughness exponent α is determined from the slope of PSD function. The roughness of the ZnO film increases upto the critical value of fluence of 1×10^{12} ions/ cm^2 and follow the equation $w \sim \phi^\beta$ with a growth exponent $\beta=0.24$. In this regime, nonlinear effects eventually stabilizing the surface. The surface relaxes by surface diffusion with Edwards - Wilkinsons (EW) [6] value of β .

At higher fluence value beyond the critical fluence, the roughness decreases. It is shown in Figure 1. Eklund et.al. [7] Studied the diffusion dominated surface structures, which lead to a q^{-4} dependence for large spatial frequencies (q) in PSD. The value of roughness exponent is determined and it lies between 0.8 to 1.0. The observed value of $\alpha=0.90 \pm 0.1$ shows self-affine nature of the structures and reveals that the surface diffusion is dominant in the evolution of surface structures.

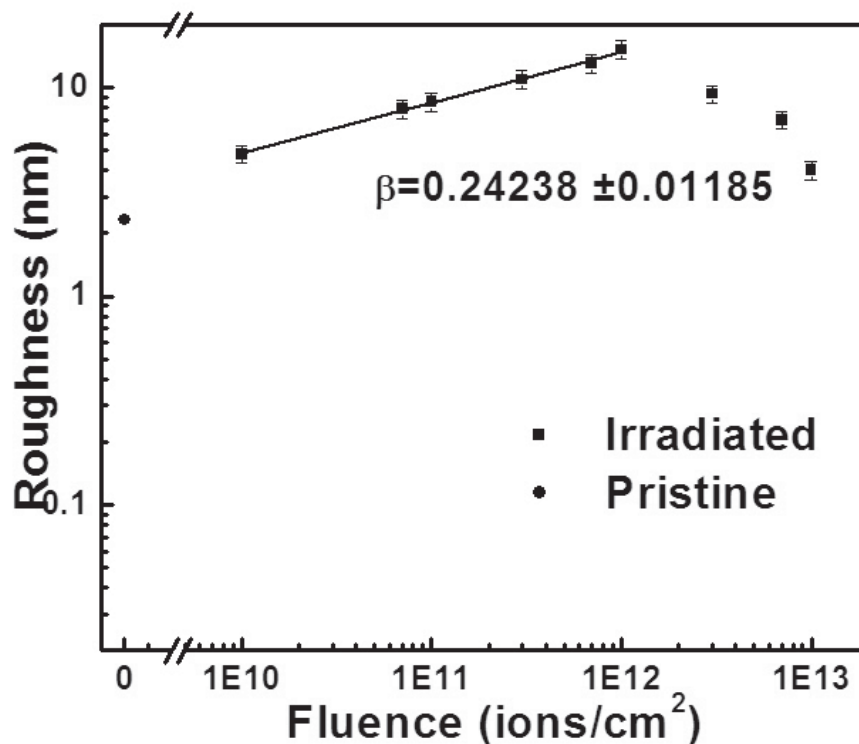


Fig. 1. Variation of roughness with ion fluence

REFERENCES

- [1] Facsco et al., Science 285, 1551 (1999).
- [2] Gago et al. Nanotechnology 13, 304 (2002).
- [3] Fan et al. Nanotechnology 16, 1526 (2005).

- [4] Bardley et al. J. Vac. Sci. Technol. A 6, 2390 (1988).
- [5] D.C. Agarwal et.al., J. Appl. Phys.99, 123105 (2006)
- [6] S.F.Edwards, D. R. Wilkinson, Proc. R. Soc. London A 381(1992)17
- [7] Eklund et.al. Surf. Sci. 285, 197 (1993)

5.2.30 Ion beam induced phase separation of Ge nanocrystals in GeO₂ matrix

Y. Batra, D. Kabiraj, S. Kumar and D. Kanjilal

Inter University Accelerator Centre, Aruna Asaf Ali Marg, New Delhi 110 067

Recently, Si and Ge nanoparticles have attracted a lot of research interest. This is because of their excellent optical and electronic properties, which can be utilized for applications in the field of optoelectronic devices. Si and Ge nanoparticles have been extensively investigated as promising candidates for the charge storage in nanocrystal gate memories. However, Ge is rather attractive candidate due to its smaller band gap than that of Si and therefore has faster write and erase speeds.

Embedded Ge nanoparticles have been mainly synthesized by various techniques such as ion implantation, oxidation of SiGe alloys and solution synthesis process. However phase separation is another process of synthesis of nanoparticles in sub-stoichiometric oxide. In this work, SHI (Swift Heavy Ion) irradiation has been used as a tool for phase separation process in GeO_x matrix.

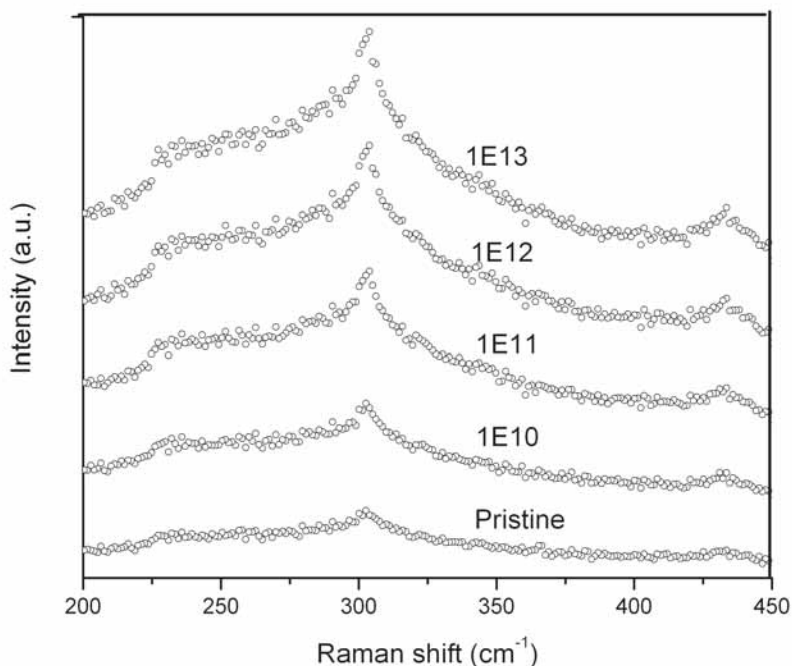


Fig.1. Micro-Raman spectra of pristine and irradiated thin films of GeO_x

Films of sub stoichiometric GeO_x were grown on Si substrate by electron beam evaporation. Thickness of the films was kept 100 nm. Further, irradiation of these films was carried out using 100 MeV Au for various fluences. After irradiation, films were characterized by micro-Raman spectroscopy. Raman spectra of the films (Fig.1.) clearly show the presence of Ge nanoparticles in the irradiated films. With increasing fluence, an increase in the intensity of the characteristic Raman peak of Ge nanoparticles is observed.

Surface morphology of GeO_x thin films were studied by atomic force microscopy (AFM).

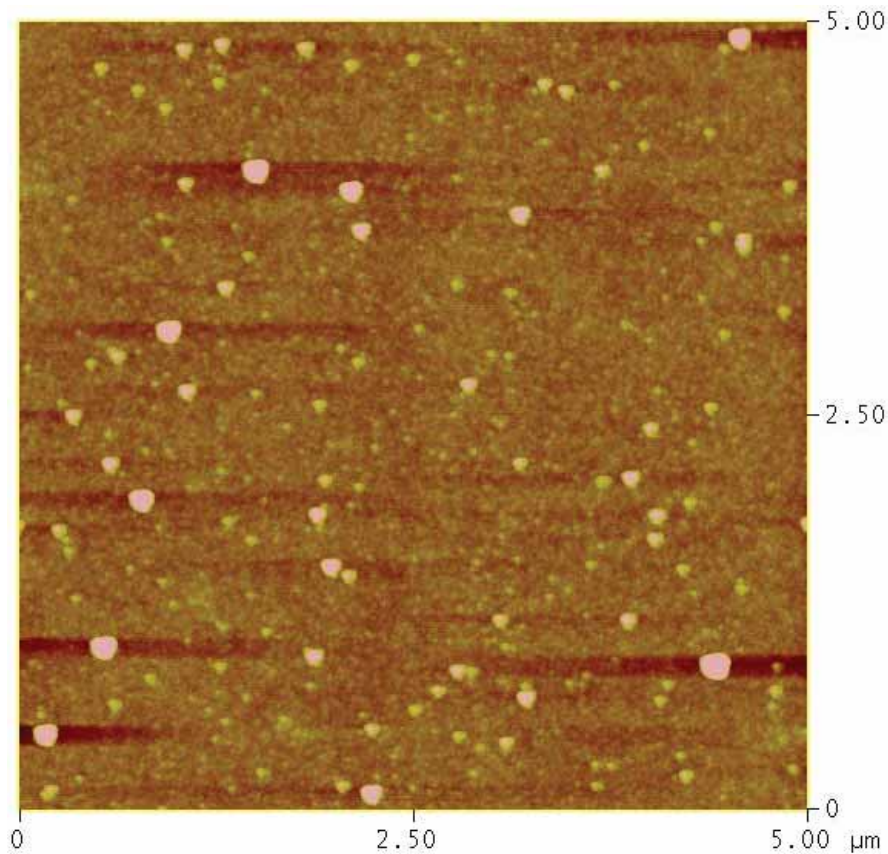


Fig.2. AFM image of pristine GeO_x film

After irradiation at various fluences it was observed that initially, the rms roughness of the films increased from a fluence of 1×10^{10} to 1×10^{11} ions/cm². Afterwards, it decreased for the fluence of 1×10^{12} ion/cm² and transforming into uniform granular film for 1×10^{13} ions/cm².

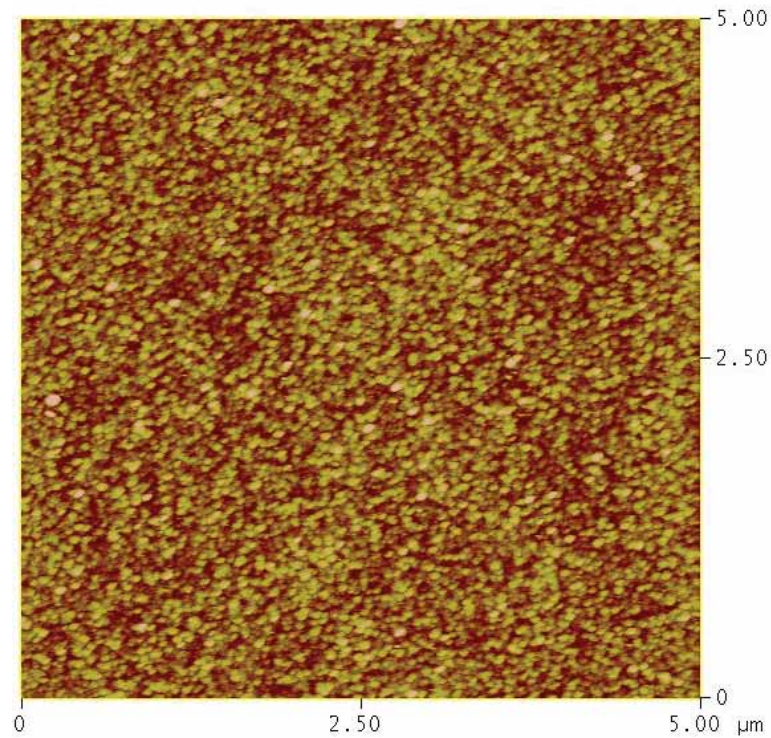


Fig. 3. AFM images of irradiated films of GeO_x for fluence of 1×10^{13} ions/cm²

We have investigated ion beam induced formation of Ge nanoparticles embedded in GeO_2 matrix as a result of phase separation. Surface morphology of pristine as well as irradiated films is studied using AFM. These are our preliminary results. More characterizations are to be done for detailed study of the system.

5.2.31 Nano-structuring and Gas Sensing Studies of Swift Heavy Ion Irradiated Metal Oxide Thin Films

¹Sanju Rani, ²N. K. Puri, ²Somnath C Roy, ¹M C Bhatnagar and ³D Kanjilal

¹Thin Film Laboratory, Dept. of Physics, Indian Institute of Technology, Delhi

²Amity School of Engineering, Amity University, NOIDA Campus, 201301

³Inter University Accelerator Centre, Aruna Asaf Ali Marg, New Delhi 110 067

Tin oxide is a wide band gap semiconductor, widely used as a base material for gas sensors. The microstructure and defect chemistry of pure tin oxide is modified by different techniques (such as doping etc) to enhance sensitivity and selectivity for any particular target gas [1]. However, the effect of Swift Heavy Ion irradiation on the gas sensing properties of tin oxide has never been studied. In this work, an experiment has been performed on 15 UD Pelletron facility at the Inter University Accelerator Centre (IUAC), New Delhi to study the effect of ion irradiation on pure and Fe doped SnO_2 thin films. Our previous work has shown that Fe doping in SnO_2 films enhances selectivity for the CO gas [2]. The 100 nm thick pure and Fe doped SnO_2 thin films were deposited on glass, silicon and fused quartz substrates by sol-gel dip coating. These films were irradiated by 75

MeV Ni ion with fluences ranging from 10^{11} ions/cm² to 3×10^{13} ions/cm². Structure, microstructure and surface morphology of the irradiated films was characterized by x-ray diffraction (XRD), transmission electron microscopy (TEM) and atomic force microscopy (AFM). The XRD results show increased crystallization and strain with increase in fluence from 10^{11} to 1×10^{13} ions/cm². However, at higher fluence of 3×10^{13} ions/cm² crystallinity decreases along with the appearance of additional peaks corresponding to mixed phases. The TEM diffraction revealed ring patterns up to a fluence of 1×10^{12} ions/cm², while spot patterns are observed for a fluence of 1×10^{13} ions/cm² indicating a very high degree of crystallinity. The TEM micrographs showed crystallite size of the order of 20 nm and the size distribution becomes more uniform with increase in ion fluence up to 1×10^{13} ions/cm². The AFM images revealed increase in surface roughness and densification with increasing ion fluence. Optical transmittance measurements have been carried out to estimate the band gap of the irradiated films, which is found to decrease with increasing ion fluence. The gas sensing studies on irradiated pure SnO₂ films and structural characterization of Fe doped films are currently underway.

REFERENCES

- [1] G. Korotcenkov, Gas response control through structural and chemical modification of metal oxide films: state of the art and approaches, *Sens. Actuator B* 107 (2005) 209- 232.
- [2] Sanju Rani, S.C. Roy and M.C. Bhatnagar, Effect of Fe Doping on the Gas Sensing Properties of Nano-crystalline SnO₂ Thin Films, *Sens. Actuator B* 122 (2007) 104- 110

5.2.32 Investigation of Swift Heavy Ion Effects on the Optical Properties of Titanium Dioxide

Aadesh P. Singh¹, Saroj Kumari¹, Ambuj Tripathi³, P. Kulariya³, Rohit Shrivastava², Sahab Dass², Vibha R. Satsangi¹

¹Department of Physics & Computer Science, Dayalbagh Educational Institute, Dayalbagh, Agra -5,

²Department of Chemistry, Dayalbagh Educational Institute, Dayalbagh, Agra -5,

³Inter University Accelerator Centre, Aruna Asaf Ali Marg, New Delhi 110 067

The use of nanostructured metal oxide semiconductors in photoelectrochemical (PEC) splitting of water is an exciting area of the research with immense possibility of finding a viable solution to the alarming fossil fuel crisis by producing hydrogen using solar energy and water. TiO₂ have a unique set of properties that makes it most promising candidate for photoelectrode in the PEC cell e.g. long term chemical stability, low cost and high oxidizing power. An important property of TiO₂ which makes it most suitable for solar splitting of water is its band edges matching with the redox level of the water, which facilitate easy transfer of charge carrier at semiconductor/ electrolyte junction in PEC cell. But the disadvantage with TiO₂ as a photoelectrode is its high band gap energy ~ 3.2 eV lying in the UV region which allows it to absorb only $\sim 4\%$ of incoming solar radiation falling on it [1]. Thus to have an efficient PEC system for solar hydrogen production, it is essential to reduce the bandgap of TiO₂ photoelectrode for efficient water splitting.

In the present study swift heavy ion induced modification on titanium dioxide (TiO₂) thin films have been studied with respect to photoelectrochemical splitting of water. Nanoparticles of TiO₂ were prepared by sol-gel method. Thin films from the gel were deposited on Indium doped

conducting glass substrate ($\text{SnO}_2:\text{In}$) using spin coating unit and sintered at $500\text{ }^\circ\text{C}$ for 2 hours. These films were later irradiated by 120 MeV Ag^{9+} beam with fluence range from 5×10^{11} to 1×10^{13} ions/ cm^2 from the 15 MV Pelletron at the IUAC, New Delhi. Swift heavy ion induced modifications were studied by X-ray diffraction, UV-Vis Spectrophotometry, optical absorption and atomic force microscopy.

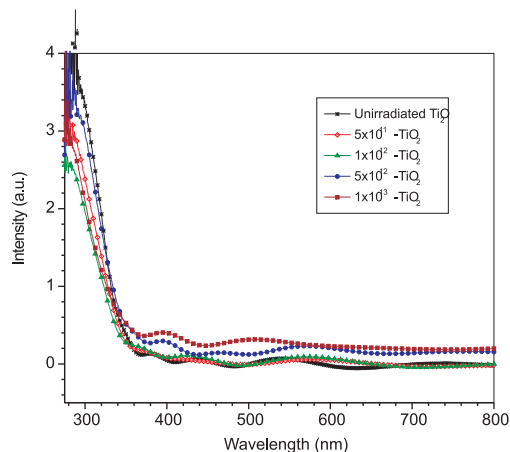


Fig. 1. Absorption spectra of unirradiated and 120 MeV Ag^{9+} ion irradiated TiO_2 thin films at different fluence deposited on conducting glass plate

As the SHI beam induces structural modification in the samples, phase and particle size of TiO_2 film were investigated before and after irradiation by XRD data. From the XRD spectrum, it was observed that unirradiated film exhibits feature characteristics of the anatase TiO_2 crystallographic phase. Apparently, this sample also contains some peaks of rutile phase. No change in the phase of the material were observed on irradiation. After irradiation by 120 MeV Ag^{9+} ion beam, the crystalline nature of the samples decreases on increasing the fluence. The average particle size as calculated from the XRD data using Scherer's equation was found to be 23 nm in unirradiated TiO_2 and was decreased down to 11 nm in samples irradiated at a fluence 1×10^{13} ions/ cm^2 .

UV-Vis spectra of the irradiated samples show that on increasing the fluence, the absorption edge was shifted in the visible region of the solar spectrum (Fig. 1). From the absorption data it was observed that on increasing the fluence, the band gap energy decreases from 3.17 eV for unirradiated sample to 3.08 eV for sample irradiated with fluence 1×10^{13} ions/ cm^2 .

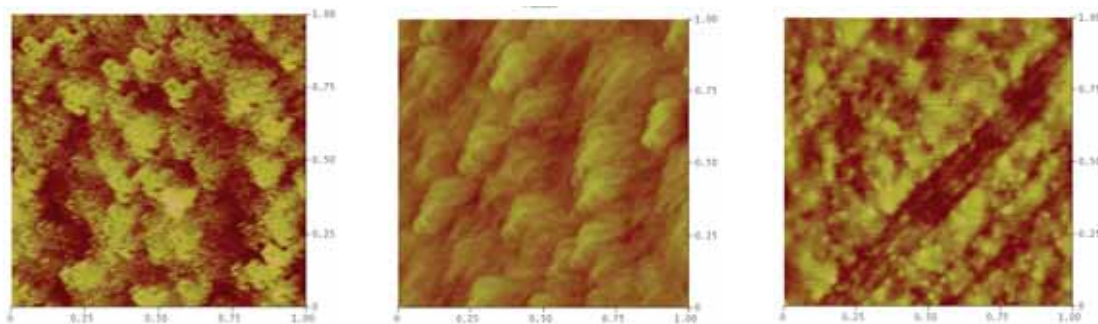


Fig. 2(a) Unirradiated

2(b) 1×10^{12} ion/ cm^2

2(c) 1×10^{13} ion/ cm^2

AFM micrographs of the unirradiated and irradiated samples were recorded. The representative AFM images of the TiO₂ surface of unirradiated and irradiated with 1x10¹² ions/cm₂ and 1x10¹³ ions/cm² fluences are presented in Figs 2(a), 2(b) and 2(c) respectively.

Unirradiated sample showed a smooth micrograph with root means square (rms) roughness of 0.4 nm. After irradiation, the roughness was found to 0.7 and 1.3 nm at the fluences 1x10¹² ions/cm² and 1x10¹³ ions/cm² respectively. Particle size calculated from AFM data supports to the values obtained from XRD. The work regarding the use of irradiated and unirradiated TiO₂ films in Photoelectrochemical cell is under progress.

REFERENCE

- [1] Lindgren, T., Mwabora, J.M., Avendano, E., Jonsson, J., Hoel, A., Granqvist, C.-G. and Lindquist, S.-E., J. Phys. Chem. B, 2003, 107, 5709-5716.

5.2.33 Modifications in physical, optical and electrical properties of tin oxide by swift heavy Au⁸⁺ ion bombardment

N. G. Deshpande¹, Y. G. Gudage¹, A. A. Sagade¹, A. Ghosh¹, D. Y. Vyavahare¹, J. C. Vyas², F. Singh³, A. Tripathi³ and Ramphal Sharma¹

¹Thin film and Nanotechnology laboratory, Department of Physics,
Dr. Babasaheb Ambedkar Marathwada University, Aurangabad

²Technical Physics and Prototype Engineering Division, BARC, Mumbai

³Inter University Accelerator Centre, Aruna Asaf Ali Marg, New Delhi 110067

Ion beam effect on the material depends on the ion energy, fluence and ion species. The interaction of the ion with material is the deciding factor in the ion beam induced material modification [1]. In the present investigation we tried to deposit tin oxide (SnO₂) thin films on glass substrate by using M-SILAR technique. The as-deposited films were annealed in oxygen atmosphere for 1h at 500°C. The annealed films were further irradiated using Au⁸⁺ ion with energy 100 MeV using different fluencies 1×10¹¹, 1×10¹², 5×10¹² and 1×10¹³ ions/cm² using tandem Pelletron accelerator. Electronic stopping power of 100 MeV Au⁸⁺ ions in SnO₂ thin film is 2.24 keV/Å, while nuclear stopping power is 50.45 eV/Å. Hence, in our case the electronic energy loss is dominant. The annealed and irradiated films were characterized for structural, optical and electrical properties. The results obtained are explained by considering the energy deposited due to the electronic energy loss upon irradiation with heavy ions, which modifies the properties of the material.

XRD studies showed formation of tin oxide with tetragonal structure. α-SnO phase was also detected. However, due to heavy ion bombardment, many peaks vanish, while some decreases with respect to intensity. The low intensity XRD peaks indicate that the films consist of coarsely fine grains (nanocrystalline) and/or are amorphous in nature.

AFM revealed uniform deposition of the material with increase in grain size after irradiation. While dealing with SHI, heavy ion noticeably changes material proper-

ties in a narrow cylindrical region around its trajectory. The SHI losses major amount of energy in interaction with atoms through electron-ion interaction. This causes local material heating known as thermal spike, resulting from energy and momentum transfer from the excited electrons to the lattice in the cylindrical region. As the fluence i.e. number of ions/cm², increases they will impinge on the surface in the neighbourhood of each other. As a consequence, the generated melted region may coalesce with each other forming larger grains and hence the grain size increases. Decrease in band gap from 3.51 eV to 2.82 eV was seen with increases in fluence. The high-energy irradiation induced lattice damage creates defect energy levels below conduction band and hence the band gap decreases [2]. A decrease in PL (fig.1) intensity, and an additional peak was observed after irradiation. I-V (fig.2) measurements showed a decrease in resistance with fluency. This might be attributed due to increase in grain size.

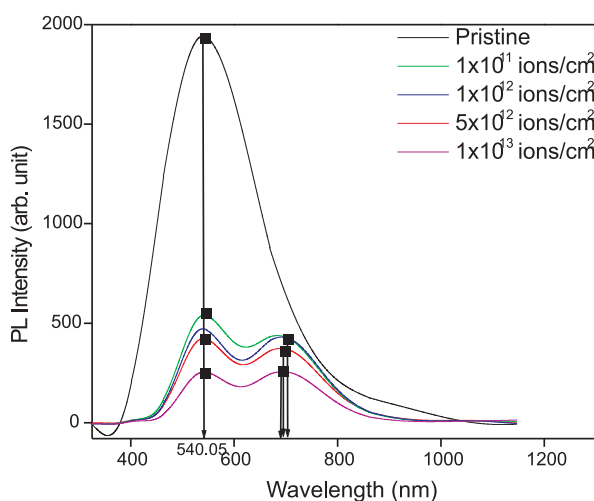


Fig.1. PL spectra of pristine and Au irradiated tin oxide samples

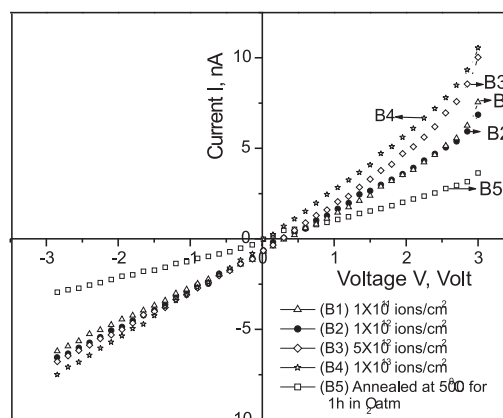


Fig.2. I-V plot of pristine and Au irradiated tin oxide samples

REFERENCES

- [1] D. K. Avasthi, Current Science, 78 (11) (2000) 1297.
 [2] K. L. Narayanan, K. P. Vijayakumar, K. G. M. Nair, and N. S. Thampi, Physica B, 240 (1997) 8.

5.2.34 Swift heavy ion induced Structural Modification in NiO thin films

P. Mallick¹, D.C. Agarwal², Chandana Rath³, R.Biswal⁴, D. Behera⁵, D.K. Avasthi⁶, D. Kanjilal⁶ and N.C. Mishra⁴

¹Department of Physics, North Orissa University, Baripada 757 003

²Department of Physics, R.B.S. College, Agra 282 002

³School of Material Science & Technology, Institute of Technology, BHU, Varanasi

⁴Department of Physics, Utkal University, Bhubaneswar 751 004

⁵Department of Physics, NIT, Rourkela 769 008

⁶Inter-University Accelerator Center, Aruna Asaf Ali Marg, New Delhi 110 067

Generation of uncompensated spins on the surface of antiferromagnetic (AF) nanoparticles leads to evolution of ferromagnetism and even superparamagnetism at the expense of antiferromagnetism [1]. Such magnetic characteristics make the AF nanoparticles more interesting as compared to their ferro and ferrimagnetic counterparts. NiO is an antiferromagnetic Mott-Hubbard insulator. In the nanoparticle form NiO has found interest due to its potential device application in solar cell [2], spin valve [3], Capacitor, memory devices [4,5] etc. Ion beams in the past have played a very crucial role in the formation, modification and characterization of nanoparticles [6,7]. The present study explores the evolution of NiO nanoparticles under swift heavy ion irradiation.

NiO thin films of 100 nm thickness were deposited on Si substrate by e-beam evaporation technique. The films were sintered at 500°C for half an hour. The annealed films were irradiated at room temperature with Au 120 and 200 MeV ions in the fluence range from 3×10^{10} to 3×10^{13} ions.cm⁻² from Pelletron Accelerator at the IUAC, New Delhi. The electronic energy loss, S_e for Au ions of both 120 (31.58 keV/nm) and 200 MeV (40.75 keV/nm) ions exceeds the threshold, S_{th} (30keV/nm) value for track formation in NiO. The structural changes due to the high density electronic excitation are studied by XRD for various fluences of irradiation.

XRD of annealed NiO films shows peaks due to (111) and (200) planes (Fig. 1) and indicates the formation of FCC phase and texturing of the films. Fig. 1 and 2 also show the evolution of XRD pattern with 120 and 200 MeV Au ion irradiation. Ion irradiation can effect the XRD peak position as well as the full width at half maximum (FWHM) of the peaks. The former arises due to changes in lattice parameter and the later due to amorphization. To study both the aspects, the XRD peaks shown in Fig.1 were normalized separately at (111) and at (200) peak position. Both the peaks shift towards higher angles with increasing fluence for both 120 MeV and 200 MeV Au irradiation. The shifting is more prominent in the (200) direction than along (111) direction and also is more prominent for 200 MeV than for 120 MeV ion irradiation. The shifting of the peaks to higher angles indicates smaller lattice spacing, which may arise due to radial pressure around the latent tracks.

The FWHM at both peak positions broadens with the irradiation fluences and finally split in the fluence range 3×10^{12} to 3×10^{13} ions.cm⁻². We discuss the origin of increase in XRD peak width with irradiation fluence in relation to track formation.

We report structural modification of NiO/Si films sintered at 500°C when irradiated by 120 MeV and 200 MeV Au ions. The pristine films show XRD peaks along (111) and (200) directions indicating grain orientation. The FWHM at both the peak positions increases with the increase of ion fluences. This can be explained by the formation of ion tracks.

REFERENCES

- [1] S.D. Tiwari and K.P.Rajeev, Thin Solid Films 505 (2006) 113.
- [2] J. Bandara and H. Weerasinghe, Sol. Energy Mater. Sol. Cells 85 (2005) 385.
- [3] M. Pinarbasi, S. Metin, H. Gill, M. Parker, B. Gurney, M. Carey and C. Tsang, J. Appl. Phys. 87 (2000) 5714.

- [4] Y. Lin, J. Wang, L. Jiang, Y. Chen and C. Nan, Applied Physics Letters 85 (2004) 5664.
 [5] J. Wu, C. Nan, Y. Lin and Y. Deng, Physical Review Letters 89 (2002) 217601.
 [6] E. Valentin, H. Bernas, C. Ricolleau and F. Creuzet, Phys. Rev. Lett. 86(2001) 99.
 [7] T.Mohanty, A. Pradhan, S. Gupta and D. Kanjilal, Nanotechnology, 15 (2004) 1620.

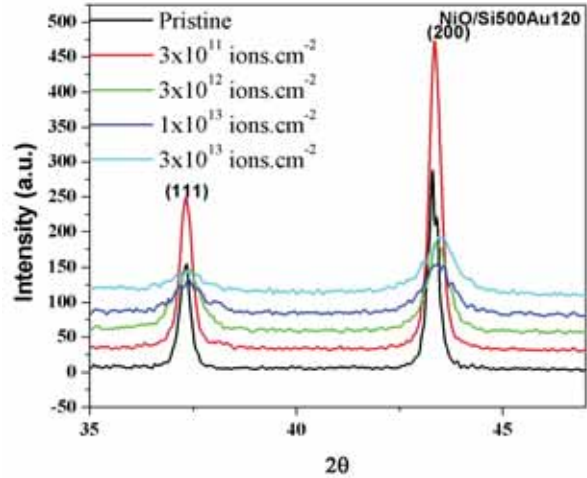


Fig.1. XRD pattern of NiO thin films of Unirradiated and irradiated with 120 MeV Au ion.

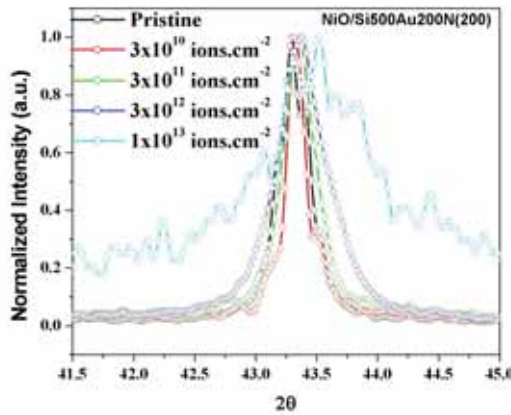


Fig. 2. The evolution of Normalized Intensity at (200) of NiO film irradiated with 200 MeV Au ion at different fluences.

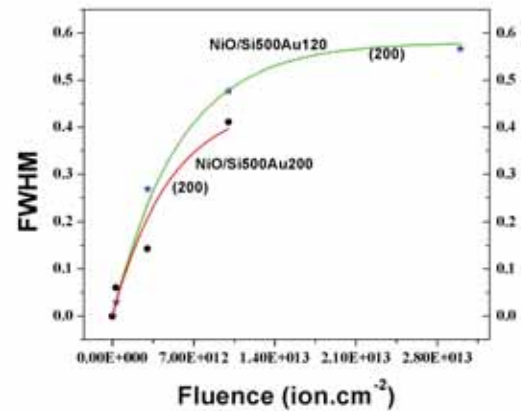


Fig. 3. The variation of FWHM at (200) peak with irradiation fluences of NiO film irradiated with both 120MeV (upper) and 200MeV (lower) Au ion.

5.2.35 Thermoluminescence and Photoluminescence studies in 100 MeV Si⁷⁺ irradiated aluminum oxide

K.R. Nagabhushana¹, B.N.Lakshminarasappa¹ and Fouran Singh²

¹Department of Physics, Jnanabharathi Campus, Bangalore University, Bangalore

²Inter University Accelerator Center, Aruna Asaf Ali Marg, New Delhi 110067

Various modifications in insulating materials have been observed due to irradiation with energetic heavy ions. The high value of the electronic stopping power (dE/dx) induces a high density of the electron-hole pairs surrounding the ion path. Luminescence produced in solid samples by the impact of MeV-energy heavy ions is the recent subject of investigations [1]. Thermoluminescence (TL) and Photoluminescence (PL) behavior of 100 MeV Si^{7+} ion irradiated polycrystalline aluminum oxide phosphor have been studied and the results are reported here. The combustion synthesized polycrystalline aluminum oxide is heat treated for 3 hours at 900°C in a muffle furnace. The pellets of 8 mm diameter and ~1 mm thickness are irradiated with 100 MeV Si^{7+} ions for various fluences. The electron energy loss (Se) and nuclear energy loss (Sn) of 100 MeV Si^{7+} ions in Al_2O_3 are calculated using SRIM 2003 program and the values are found to be 4.4 keV nm^{-1} and 0.003 keV nm^{-1} respectively. The PL measurements are carried out under 325 nm He-Cd laser excitation. TL is carried by PC based automated TL reader.

The thermoluminescence glow curves of heat treated polycrystalline aluminum oxide pellets irradiated with 100 MeV Si^{7+} ions for the fluence in the range 1×10^{11} to 2×10^{13} ions cm^{-2} are recorded. A single prominent glow with peak at 546 K is observed in all samples. It is observed that the TL intensity increases up to 1×10^{13} ions cm^{-2} and thereafter decreases. The luminescence efficiency is found to be reduced either by large defect complexes or stress introduced by implantation at higher fluences [2]. Further, we performed PL measurements. The PL spectrum indicated the emission at ~544 nm besides a sharp emission with peak at ~695 nm [3]. It is observed that the PL intensity at ~544 nm increases up to 1×10^{13} ions cm^{-2} and there after it decreases. At the fluence of 2×10^{13} ions cm^{-2} the 544 nm peak is absent while a broad emission in the range ~540-603 nm is observed.

The trap parameters are calculated using Q-basic program. The activation energy and the frequency factor for 1×10^{13} ions cm^{-2} for example are found to be 0.67 eV and 2.2×10^5 s^{-1} respectively.

REFERENCES

- [1] Horowitz, Y.S., Avila, O. and Villafuerte, M. R. 2001, Nucl. Instr. and Meth. B 184 85.
- [2] Al Ghamdi, A and Townsend, P.D. 1990. Nucl. Instrum. and Meth.. B 46, 133.
- [3] Dalmaso, C., Iacconi1, P., Beauvy, M., Lapraz1, D., Balan, E. and G. Calas 2006 Radiat. Protec. Dosim.119, 222

5.2.36 SHI Induced Grain Fragmentation in Lithium Fluoride Thin Films

M. Kumar¹, S. A. Khan², F. Singh², A. Tripathi², D. K. Avasthi² and A. C. Pandey¹

¹Department of Physics, University of Allahabad, Allahabad 211 002, India

²Inter-University Accelerator Centre, Aruna Asaf ali Marg, New Delhi 110 067

Nanometer sized films of LiF (160 nm thin) were irradiated with 120 MeV Ag ions to study SHI induced grain fragmentation in these films. Reduction in the grain size of the films due to irradiation with fluence was observed by atomic force microscopy as shown in figure 1 for (a) pristine and fluences of (b) 5×10^{11} , (c) 1×10^{12} and (d) 1×10^{13} ions/ cm^2 . The grain size decreases from about 46 nm for the pristine sample to a minimum of about 15 nm for high fluence irradiation.

The reduction in the grain size is attributed to the strain induced fragmentation of the grains. So far, the inelastic thermal spike has been used to describe the strain in the grains by SHI. According to the thermal spike model, the energy is deposited by the projectile ions in the electronic subsystem of the target. This energy is shared among the electrons by electron-electron coupling and transferred subsequently to the lattice atoms via electron-lattice interactions leading to a large increase in the temperature along and in the vicinity of the ion path. Pressure waves develop due to the temperature spike and cause strain in the grains. This strain leads to the fragmentation of grains [1].

The thermal evolution in lattice subsystem of LiF is analyzed within the framework of inelastic thermal spike model. If there is no volume expansion, the increase in the pressure, ΔP can be correlated with temperature rise ΔT in terms of linear thermal expansion coefficient α and adiabatic compressibility χ as [2]:

$$\Delta P = \beta P \Delta T = \frac{\alpha}{\chi} \Delta T$$

where β is volumetric thermal expansion coefficient. So the increase in the pressure can be calculated as long as lattice remains in the solid for which these coefficients will be constant and the values of α and χ are $13.3 \times 10^{-6} \text{ K}^{-1}$ and $1.435 \times 10^{-11} \text{ Pa}^{-1}$, respectively. The pressure was calculated by using $\Delta P = P(r,t) - P_0$ and $\Delta T = T(r,t) - T_0$ where P_0 and T_0 are initial conditions. $T(r,t)$ was estimated by thermal spike code [3] using the parameters of LiF irradiated with 120 MeV Ag ions. Figure 2 shows pressure and temperature evolution with respect to radial distance r to the ion path in the lattice at $4 \times 10^{-14} \text{ s}$ for which the lattice temperature is highest during the irradiation. The pressure is not uniform as it depends on the radial distance, r , resulting in large shear forces responsible for destruction of solids. The whole grain is composed of highly strained region resulting in fragmentation of big grains in smaller grains due to explosion.

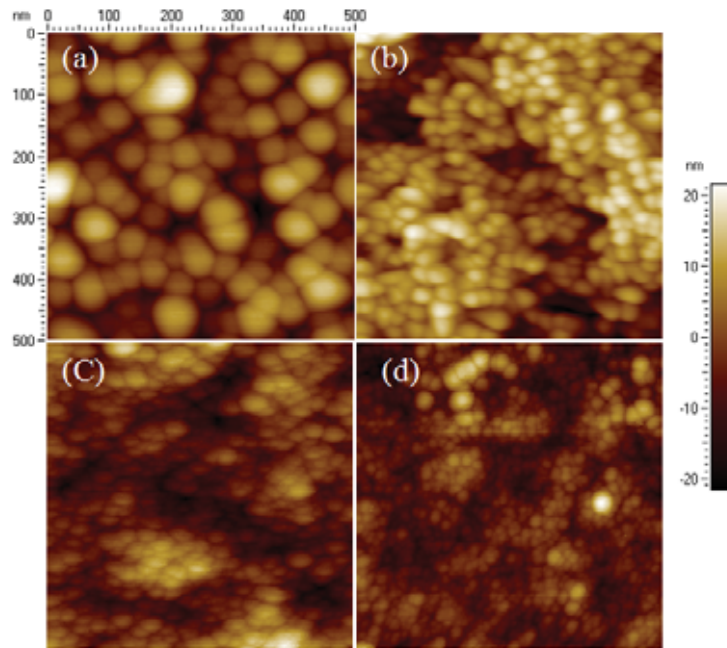


Fig. 1. AFM images of (a) pristine and (b, c, d) 120 MeV Ag irradiated LiF films.

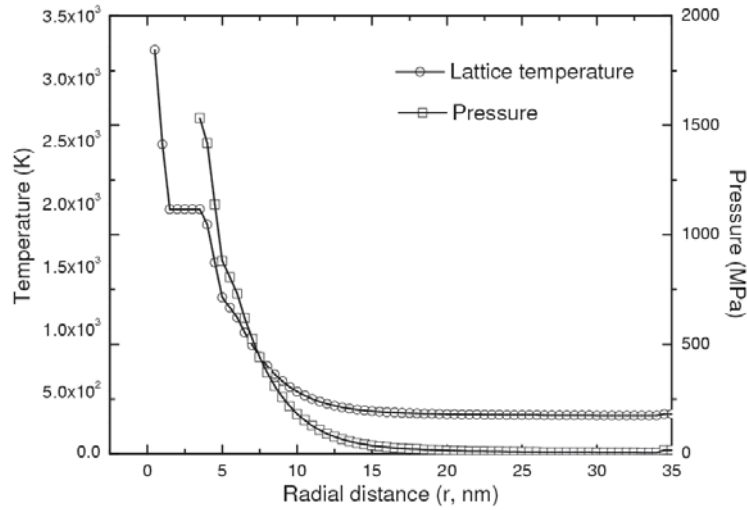


Fig. 2. Atomic temperature and pressure as functions of radial distance r to the ion path at a time of 4×10^{-14} s.

REFERENCES

- [1] M. Kumar et al., J. Phys. D: Appl. Phys. 38 (2005) 367 & 39 (2006) 2935.
- [2] A. Berthelot et al., Nucl. Instrum. Meth. B 146 (1998) 437.
- [3] M. Toulemonde, Ch. Dufour and J. Stoquert, TSpoke, version 0.1, Copyright 2001.

5.2.37 Materials Modification by SHI Induced Low Energy Electrons

R. Biswal¹, J. John², D. Behera³, P. Mallick⁴, Sandeep Kumar⁵, D. Kanjilal⁵, T. Mohanty⁶ and N.C. Mishra¹

¹Department of Physics, Utkal University, Bhubaneswar 751004

²Tata Institute of Fundamental Research, Mumbai 400005

³National Institute of Technology, Rourkela 769008

⁴Department of Physics, North Orissa University, Baripada 757003

⁵Inter University Accelerator Center, Aruna Asaf Ali Marg, New Delhi 110067

⁶School of Physical Sciences, Jawaharlal Nehru University, New Delhi 110067

In the present study we report defect production by secondary electrons induced during 200 MeV Ag ion irradiation. Ion irradiation was undertaken on 150 nm thick $\text{YBa}_2\text{Cu}_3\text{O}_{7-x}$ (YBCO) thin films prepared by pulsed laser deposition (PLD) technique on LaAlO_3 substrates. YBCO was chosen since it can accommodate a wide range of defects at the oxygen sites, which can influence its superconducting properties. To prevent sample heating during irradiation and to acquire in-situ resistance data in the low fluence regime, a low ion beam current (0.027-1 pA) was maintained. The in-situ $R(T)$ data was taken right after irradiation in heating cycle up to a maximum temperature of 150 K. Details of experimental procedure can be found elsewhere [1,2]. In these measurements, the sample temperatures were thus kept well below room temperature to avoid annealing of irradiation-induced point defects as discussed later.

Fig. 1(a) shows the evolution of the temperature dependent resistance, $R(T)$ characteristics with varying fluence from 1×10^9 ions. cm^{-2} to 1.1×10^{13} ions. cm^{-2} . Superconducting transition was seen up to a fluence of 6.2×10^{12} ions. cm^{-2} . Zero resistive state however, could only be achieved above the lowest temperature (82 K) of the target ladder up to a fluence of 1.71×10^{11} ions. cm^{-2} . At the highest fluence of 1.1×10^{13} ions. cm^{-2} used in the present study, the $R(T)$ showed a semiconducting behaviour. Fig. 1(b) shows the fluence dependence of the mean field transition

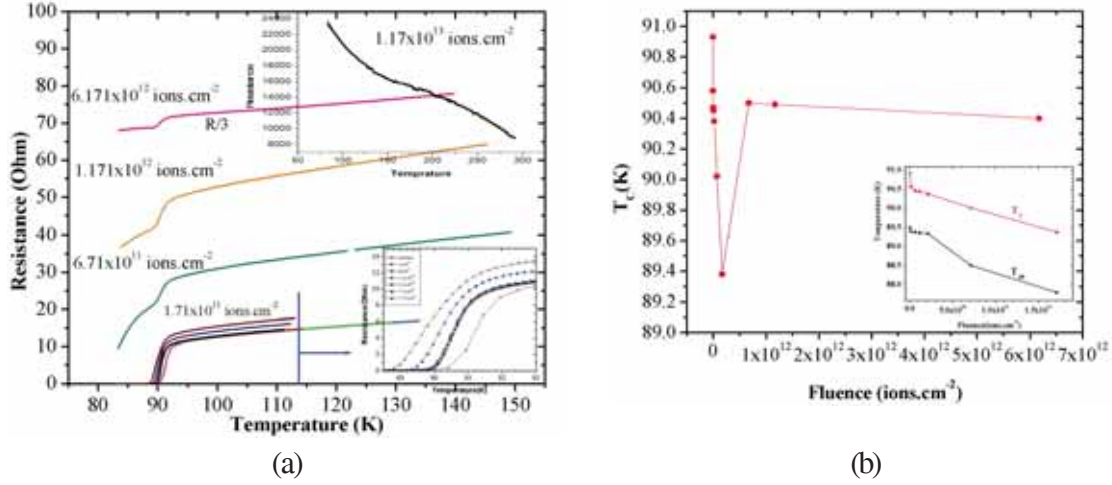


Fig. 1. (a) Resistance vs Temperature at different fluences. (b) T_c , T_{c0} variation with fluence [Inset show variation at low fluence regime]

temperature, T_c . The inset in Fig. 2 shows the variation of T_c and T_{c0} in the low fluence regime. Both T_c and T_{c0} continuously decrease with fluence up to 1.7×10^{11} ions. cm^{-2} , beyond which T_c showed an increase of ~ 1.1 K in the fluence interval 1.7×10^{11} and 6.71×10^{11} ions. cm^{-2} . Further increasing fluence up to 6.17×10^{12} ions. cm^{-2} leads to only a slight decrease of T_c within 0.1 K.

The electronic energy loss, S_e , nuclear energy loss, S_n , and range of 200 MeV Ag ions in YBCO calculated from SRIM 2006 are $25.18 \text{ keV.nm}^{-1}$, 70.95 eV.nm^{-1} and $12.66 \mu\text{m}$ respectively. Since the thickness of the sample is much less than the range of the ion beam, energy deposited in the film is uniform and is mostly due to electronic energy loss. Confining S_e to values greater than S_{eth} (14.4 keV.nm^{-1}), where amorphized latent tracks are created, Bourgault et al (1989) have shown that in the low fluence regime where tracks do not overlap, the T_c onset remains almost constant due to availability of percolating paths for supercurrent conduction [3]. Increasing the fluence further eventually leads to T_c suppression due to track overlap. Our study however shows that T_c decreases by about 0.35-1.55K in thin film of YBCO when irradiated by 200MeV Ag ions at 82K in a fluence regime, which is three orders of magnitude less than that required for track overlap.

The unexpected suppression of T_c in the low fluence regime suggests that along with the latent tracks there must be a large concentration of defects created at low temperature irradiation, which contributes to $R(T)$ data. These point defects are in fact created by the secondary electrons resulting from ionising collision of the SHI with electrons of the stopping medium. Previous studies

have shown that these point defects are annealed out at room temperature [4, 5].

In fig. 1, we encounter three regimes of fluence with varying nature of $R(T)$. In the low fluence range ($\leq 1.71 \times 10^{11}$ ions.cm⁻²), low concentration point defects are distributed homogeneously, which leads to a global decrease in T_c . In the mid fluence range (6.71×10^{11} to 6.17×10^{12} ions.cm⁻²), the high concentration of point defects undergo defect-defect interaction, clustering of defects and phase segregation. This fluence range marks the occurrence of superconducting transition within localized regions, which are connected to each other through regions with higher defect concentration. The resistance here shows a rapid increase with irradiation fluence. Insulating behavior with different activation energies in different temperature interval was observed at the highest fluence of 1.1×10^{13} ions.cm⁻².

REFERENCES

- [1] R. Biswal, J. John, D. Behera, P. Mallick, S. Kumar, D. Kanjilal and N.C. Mishra (Communicated)
- [2] R. Biswal, J. John, D. Behera, P. Mallick, S. Kumar, D. Kanjilal and N.C. Mishra Proceedings of the DAE Solid State Physics Symposium vol. 51 (2006) 645
- [3] D. Bourgault, S. Bouffard, H. Toulemonde, D. Groult, J Provost, F. Studer, N. Nguyen and B. Raveau Phys. Rev. B 39 (1989) 6549
- [4] D. Behera, T. Mohanty, S. K. Dash, T. Banerjee, D. Kanjilal, N.C. Mishra, Radiation Measurements 369 (2003) 125
- [5] A. Iwase, N. Ishikawa, Y. Chimi, K. Tsuru, H. Wakana, O. Michikami, and T. Kambara Nucl. Instr. Meth. B 146 (1998) 557

5.2.38 Effect of 90 MeV O-ion irradiation on La_{0.7}Pb_{0.3}MnO₃ single crystals

M. Ramesh Babu¹, K.Asokan², Ravikumar² and R.Jayavel¹

¹Crystal Growth Centre, Anna University, Chennai-600025

²Inter-University Accelerator Centre, Aruna Asaf Ali Marg, New Delhi 110067

Single crystals of La_{0.7}Pb_{0.3}MnO₃ were grown by high temperature solution growth method using PbO-PbF₂ as a solvent. Recent studies have shown that swift heavy ion (SHI) irradiations induces significant modification in the electronic transport and magnetic properties because of their extreme sensitivity to the lattice distortion and defect concentration [1]. In order to understand the effect of SHI in magnetic single crystals, we have carried out the present study using 90 MeV O ions at various fluences ranging from 10¹¹ to 10¹⁴ ions/cm². The surface and transport properties have been studied as function of ion fluences. The change in the surface morphology of both unirradiated and irradiated single crystals was investigated by Atomic Force Microscopy (AFM) as shown in the figure 1. As evident from the figure, irradiated samples show increase in the surface roughness compared to unirradiated crystals due to the creation of point defect produced by O ion beam irradiation. For higher fluences, it produces more point defects it will increase the roughness of the single crystals. Irradiated samples with 1×10^{12} ions/cm² possess higher surface roughness value of 54.2 nm compared to un-irradiated sample whose roughness is 31 nm. This is attributed to the defects created by irradiation [1]. It is clearly revealed that the irradiation increases the surface roughness of the single crystals.

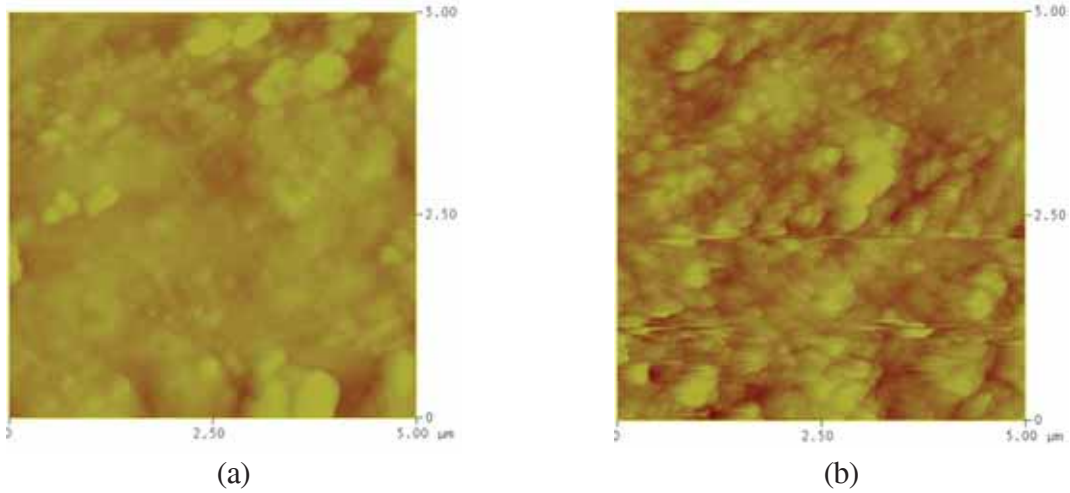


Fig.1. AFM images of the single crystals of $\text{La}_{0.7}\text{Pb}_{0.3}\text{MnO}_3$ were grown by high temperature solution growth (a) unirradiated crystal (b) 90 MeV O irradiated crystal.

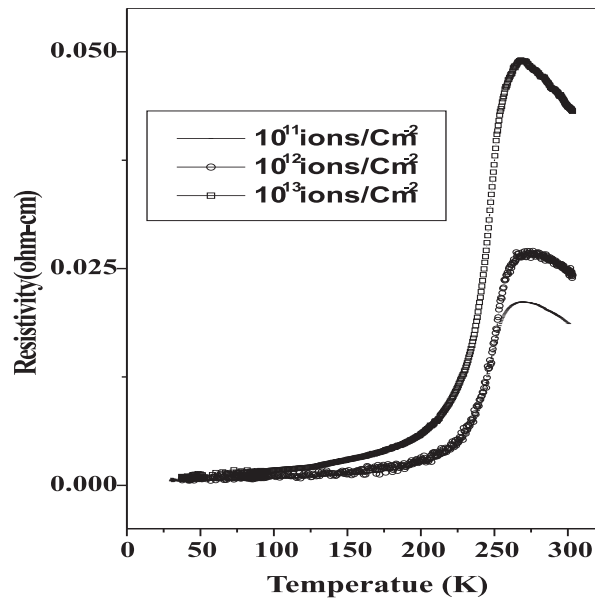


Fig.2. Transport measurement showing the variation of resistivity and metal-insulator transition temperature. Note that the 90 MeV O ion beam irradiation induces the sharp transition especially in the higher fluences.

Fig.2 shows the transport measurement of irradiated crystals. A systematic variation in the Metal-Insulator transition temperature has been observed in our transport measurements. It is also observed the irradiation increases resistivity of the single crystals. However the broad nature of M-I transition is remarkably reduced as the fluence is increased. Such sharp transitions will be of special interest for application of these materials in devices. For the low fluences, the resistivity of the single crystals slightly increases due to the strain relaxation in the lattice and as the fluence increases, it is likely to change the hopping of electrons between the Mn ions via O ions [2]. It is

reported that O ion beam irradiation mostly modifies the oxygen site rather than La, Pb, Mn sites[3]. Replacement of oxygen induces interstitial defects and also has significant effect in the physical properties of these materials. The defect concentration increases for the higher fluences and also increases the resistivity of the materials.

REFERENCE

- [1] R.J. Choudhary, Ravi kumar, S.I. Patel, Shahid Housain, J.P. Srivastava and S.K. Maalic. J.Appl.Phys.Letter 86,(2005) 222501.
- [2] Ravi Kumar, R.J. Choudhary, S.I. Patel, Shahid Housain, J.P. Srivastava, S.P. Sangal and S.E. Lofland. J.Appl.Phys. 96(2004) 7383.
- [3] S.Chattopadhyay, a.Sarkar, A. Banerjee, S.Karmakar, D. Banerjee, R. Kumar and B.K. Chaudhuri

5.2.39 Swift Heavy Ion Beam Induced Modifications in Ferroelectric Single crystals and in Ceramics

P.K. Bajpai¹, C.R.K. Mohan¹, Deepak Shah¹ and V. Shiv Kumar² and Ravi Kumar²

¹Department of Pure & Applied Physics, Guru Ghasidas University, Bilaspur

²Inter University Accelerator Centre, Aruna Asaf Ali Marg, New Delhi 110067

The ion beam interaction and surface modification in crystals having long range order and switchable dipoles such as ferroelectric materials are studied scantily. We have studied the effect of SHI irradiation on the single crystals of pure and doped TGS-a ferroelectric most suitable for the pyroelectric detection of IR radiation and in ceramic samples $Ba_{1-x}Sr_xTiO_3$ (BST). TGS crystals were grown and irradiated with 100 MeV Oxygen ion beam on (010) cleavage surface. Dielectric studies were performed on as grown and irradiated crystals. Optical spectra were obtained and indirect band gap transition edge energy was calculated as a function of irradiated energy fluence. Hysteresis loop parameters were measured. Atomic force microscopy was used to study the surface micro relief of irradiated crystals. XRD and dielectric measurements were performed on irradiated crystals

The ferroelectric hysteresis loop becomes asymmetric and spontaneous polarization decreases with irradiation. The asymmetry increases with increasing fluence. This shows that internal bias field develops in the crystals due to SHI irradiation. The asymmetric loops in irradiated crystals, however, become more symmetric. Peak dielectric constant associated with PE to FE phase transition decreases with increasing fluence in all SHI irradiated crystals and dielectric loss also decreases. However, the transition temperature does not shift with irradiation. The transition becomes diffuse phase transition.

Dielectric dispersion curve changes with doping. The negative slope with increasing frequency, is typical for ferroelectrics. Doping tries to stabilize mono domain situation that is reflected in decreasing slope. As the crystals are irradiated, the slope changes drastically for that crystal which was multi domain. However, not much change is observed in those which were poled due to doping. The change in slope is taken as the degree of measurement of multi-domain state of crystal.

The origin of these changes lies in the thermally generated electric field (TGEF) coming from the thermal gradient. The associated electric field developing in the crystal due to SHI irradiation is calculated in the model developed [1].

Optical spectra shows no additional band observed due to donor levels/ defect states in irradiated crystals. The absorption band centered around 258 nm appears in irradiated crystal. This indicates that some charge transfer processes are induced due to irradiation.

The calculated absorption coefficient follows Urbach rule. Energy band gap using Urbach formulation for direct and indirect band transitions shows that the indirect allowed transition band gap decreases with irradiation. This shows increase in disorder in irradiated crystals. The disorder, however, decreases with increased fluence. In cobalt doped crystals, the additional absorption band centered around 258 nm due to charge transfer within the octahedral bisglycino-cuppe(II) chelate compound which is formed by the doping Co^{2+} ions, is observed. With irradiation this absorption peak disappears.

$(\alpha h\nu)^{1/2}$ Vs energy near the absorption edge is plotted and is used to calculate the band gap energy of indirect allowed transition in TGS. The obtained value for band gap (E_g) are 4.96 eV in unirradiated and 4.33 and 4.55 eV in irradiated crystals with ion fluence 5×10^{10} and 10^{11} ions/cm², respectively.

Atomic force microscopic image analysis in the topography mode (contact mode) has been performed for all samples. The smooth surface of pure TGS shows pits and protrusions when irradiated with SHI beam. The height and dimensions of this micro-relief vary with ion beam fluence as well as on doping. Observed micro-relief is analyzed considering the lamellar domain structure of TGS. The results are explained considering the domain movement induced by the internal bias field created due to irradiation results into piezoelectric compression and stretching forming these features on the surface. The number of micro-relief features is invariably less than the total number of ions hitting the surface. Thus the observed features are due to multi ion impact. It has been shown that under controlled conditions of fluence and doping, almost regular nano size micro-reliefs could be observed on the irradiated surface. This demonstrates that swift heavy ion beam irradiation could be used as a tool to modify the surface Nano structures.

Barium strontium titanate (BST) ceramic pellets shows no structural change as observed in XRD pattern due to irradiation with 100 MeV oxygen beam. The XRD peaks width increases showing the material becomes less crystalline. The dielectric response also decreases with small shift in transition temperature.

REFERENCE

- [1] P.K. Bajpai, Deepak Shah, Ravi Kumar, Nuclear Instruments and Methods in Physical Research B 244, 264 (2006).

5.2.40 Ag^+ and Au^+ Swift Heavy Ion Induced Lithium-Zinc-Silicate Glass photoluminescence Studies

Mahantappa. S. Jogad¹, Fouran Singh². Aravind H. Dyama, Lingappa A. Udachan¹

¹Sharanabasaveshwar College of Science Gulbarga - 585 103, Karnataka,

²Inter-University Accelerator Centre, Aruna Asaf Ali Marg, New Delhi 110067

Recently considerable attention has been focused on the development of new glass-ceramics (GC). With the advancement of science of materials, disordered systems like glasses and glass-ceramics have received considerable attention, because of their some unusual thermo-physical properties. GCs are essentially polycrystalline solids in the matrix of residual glass phase. In this respect, glass-ceramics are different from usual ceramics.

Photoluminescence (PL) studies have been carried out on Lithium zinc silicate (LZS) glass samples having the nominal composition $55\text{SiO}_2\text{-}15\text{xLiO}_2\text{-}5\text{Na}_2\text{O-}19\text{B}_2\text{O}_3\text{-}(27\text{-x})\text{ZnO-}2\text{P}_2\text{O}_5$ where $1 \leq x \leq 23$, bombarded with 100 MeV swift heavy Ag^+ ions. LZS glass samples are prepared using conventional melt-quench technique. Samples of different thickness are bombarded with Ag ions having fluence in the range of $10^{11}\text{-}10^{14}$ ions/cm², using 15UD Pelletron accelerator. The samples are irradiated at room temperature in the vacuum chamber, which is evacuated to about 3.6×10^{-6} Torr. PL measurements are carried out using Mechelle 900 spectrograph with charged coupled device (CCD) array as detector. Excitation is carried out using Kimmon He-Cd laser (442 nm).

Also Photoluminescence (PL) studies have been carried out on Lithium zinc silicate (LZS) glass samples bombarded with 120 MeV swift heavy AU^+ ions.

The PL intensity is found to increase with increase of ion fluence. This may be attributed to irradiation induced crystallization in LZS glasses. The crystallization is expected to reduce non radiating recombination centers, thereby increasing the PL intensity. Further detailed work on the identification of resulting phases and luminescent centers is going on. It will be discussed at the presentation of paper.

5.2.41 Effect of 100 MeV energy silver ions on the Optical Properties of Borosilicate glass

V.S. Jadhav¹, S.D.Dhole¹, D.Kanjilal², Indra Sulania² and V.N.Bhoraskar¹

¹Department of Physics, University of Pune

²Inter University Accelerator Centre, Aruna Asaf Ali Marg, New Delhi 110067

Few borosilicate glass samples were irradiated with 100 MeV Ag ions at the fluence level ranging from 1×10^{11} to 5×10^{13} ions/cm². The optical properties have been characterized using UV Visible, Photoluminescence, and FTIR spectroscopies. Their respective results are shown in figure 1,2 and 3 respectively. Figure 1 shows the UV Visible absorption spectra for irradiated Borosilicate glass. It is observed from the figure that the absorption at 4.5eV is occurring mainly due to B₂ band, which arises from oxygen deficiency in SiO_2 structure. The intensity of the absorption peak also found to be increased with increase in ion fluence. This attributes due to the concentration of

paramagnetic positively charged oxygen vacancies which increases with increase in ion fluence. Figure 2 shows PL spectra for irradiated Borosilicate glass. It is observed that two peaks at 2eV and 3.25eV are observed due to non bridging oxygen hole centers (NBOHC) and Si-O-Si dangling bonds respectively. Whereas there is no change in the intensity at 2eV peak, but marginal change is observed in the peak at 3.25eV for higher ion fluence level. This is because the generation of the defects and the respective concentration is very small. However, two new peaks at 2.71eV and 2.57eV are introduced at the fluence level of 1×10^{13} to 5×10^{13} ions/cm². This may be due to formation of peroxy radicals. Figure 3 shows FTIR transmission spectra for irradiated borosilicate glass. It is found from the figure that two peaks are observed at 2259cm⁻¹ and 3673 cm⁻¹, their respective intensity decreases with increase in the ion fluence. The peak at 3673 cm⁻¹ corresponds to Si-OH bonds and the peak at 2259 cm⁻¹ corresponds to Si-O-Si bonds. These bonds are responsible for the change in paramagnetic defects. Therefore the decrease in the transmission intensity is mainly due to scission of Si-O-Si bonds. It is also observed from the FTIR spectra that the peak positions of these two peaks are not shifted with increase in the ion fluence. This indicates that there is no change in Si-O-Si bond angle and it is highly stable against 100MeV Ag ion irradiation.

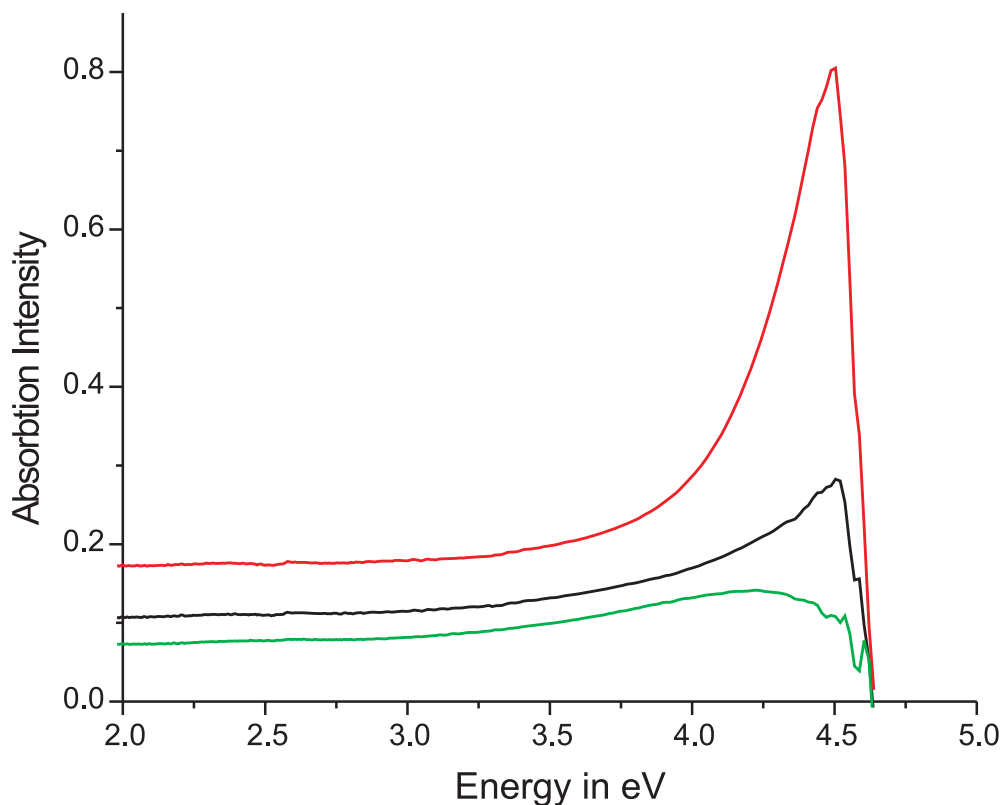


Fig. 1. UV Visible absorption spectra for 100 MeV Ag ion irradiated Borosilicate glass.

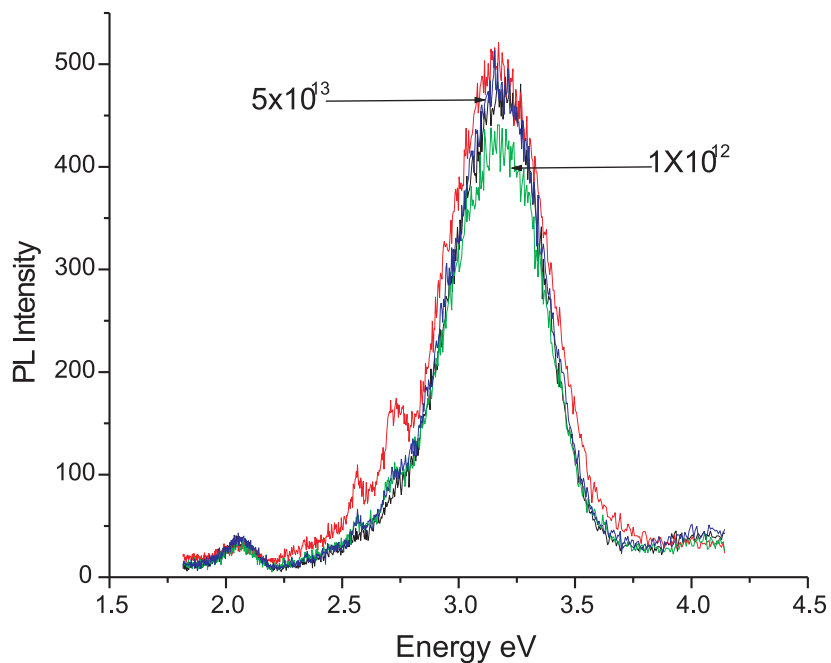


Fig. 2. PL spectra for 100 MeV Ag ion irradiated borosilicate glass.

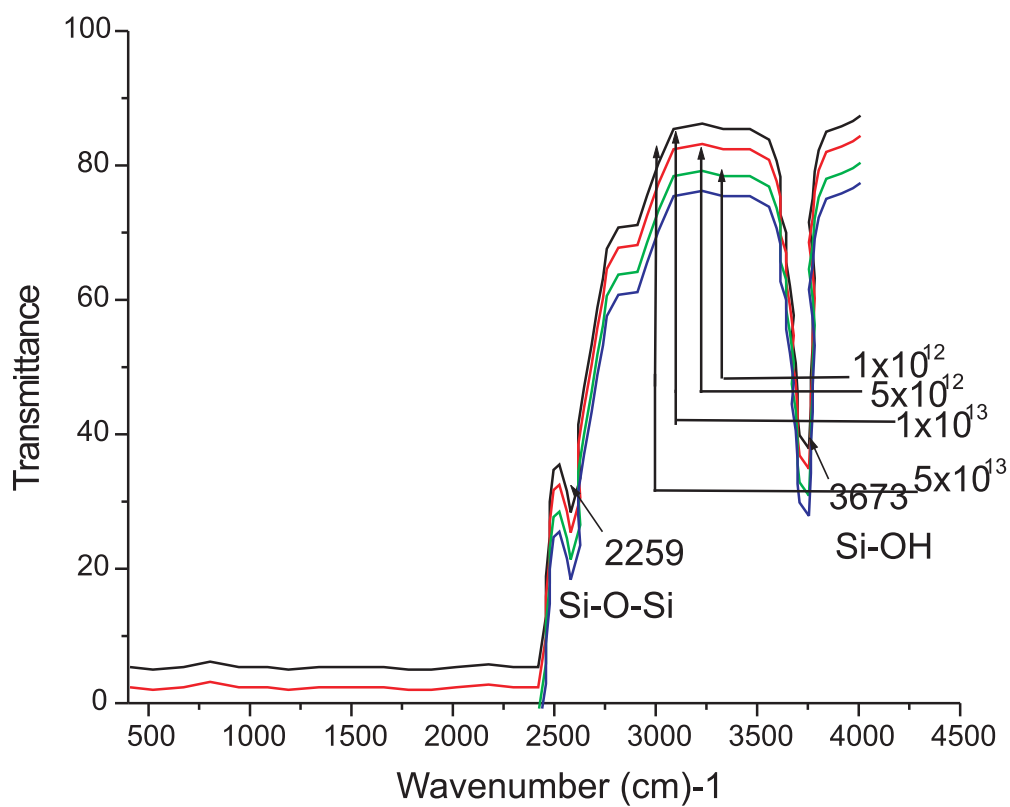


Fig. 3. PL spectra for 100 MeV Ag ion irradiated borosilicate glass.

REFERENCES

- [1] Stevens-Kalceff M A 2001 Appl.Phys.Lett.79 3050
- [2] Skuja L and Guttler B 1996 Phys.Rev.Lett.77 2093
- [3] Satio K and Ikushima A J 2002 J.Appl.Phys.91 4886
- [4] Hosono H, Mizuguchi M, Kawazoe H and Ogawa T 1999 Appl.Phys.Lett.74 2755

5.2.42 Swift heavy ion irradiation induced amorphization in ThGeO₄

M. K. Patel¹, V. Vijayakumar¹, D. K. Avasthi², P. Kularia², S. Kailas⁴ and A. K. Tyagi³

¹High pressure physics division, Bhabha Atomic Research Centre, Mumbai 400 085

²Inter-University Accelerator Center, Aruna Asaf Ali Marg, New Delhi 110 067

³Solid State Chemistry Division, Bhabha Atomic Research Centre, Mumbai 400 085

⁴Nuclear Physics Division, Bhabha Atomic Research Centre, Mumbai 400 085

ThGeO₄ is a member of the ABO₄ class of compounds and shows dimorphism. Under ambient conditions it is zircon type (ZrSiO₄) and transforms to scheelite type (CaWO₄) under high pressure. Interestingly the latter transforms back to zircon upon increasing the temperature. Swift heavy ions (SHI) passing through materials deposit energy mainly in the electronic stopping regime. This deposition of energy causes highly non-equilibrium temperature and pressure conditions along the ion tracks, leading to structural modifications along the tracks. Thus in the present work the structural progression of the two polymorphs of ThGeO₄ under SHI irradiation is investigated in order to understand the kinetics impeded structural modifications that these phases may undergo. We show that x-ray diffraction can be employed to look at how a particular structure progresses towards various phase transformation or amorphization as well as to extract information on the track radius.

SHI irradiations were carried out on zircon type tetragonal ThGeO₄ (Z-) using 93 MeV Ni⁷⁺ ions with various fluences using the 15UD Pelletron at IUAC, New Delhi. In-situ XRD characterizations were carried out at various fluences within small intervals. Similar irradiations were also carried out on scheelite type ThGeO₄ (S-), however the characterization for the same was done ex-situ.

In-situ XRD was performed on z-ThGeO₄ at various fluences. It is observed that with an increase in the fluence from 1×10^{12} to 6×10^{13} ions/cm² there is an exponential decrease in the area of the Bragg peaks. Interestingly, with an increase in fluence the peak positions shift towards higher values of 2θ (Fig 1), indicating compression of the lattice. The crystallite size, estimated from Scherrers formula, also decreases from 78 to 20 nm. Finally an amorphous like pattern is observed at higher fluences. Assuming that this amorphization takes place along the ion trajectory in a cylindrical region, the evolution of the relative area, $A(\phi)$, was fitted with an exponential expression [$A(\phi) = A_D \exp(-\pi r^2 \phi) + A_s$ where A_D & A_s are constants and r the track radius] to obtain a track radius of 3.7 nm. The x-ray powder pattern of the sample irradiated with highest fluence does not resemble usual glassy amorphous pattern. Thus there appears to be some intermediate range ordering or the material may be similar to nano phase material. The XRD patterns of s-

ThGeO₄ also show a decrease in the intensity and relative area with an increase in the fluence. However, no shift in peak positions was observed on either sides of the original 2θ position. Finally complete amorphization was observed at higher fluences.

Passage of SHI through materials causes large temperature and pressure conditions in very short time intervals. We expected that under SHI irradiation that z-ThGeO₄ would transform to s-ThGeO₄ which is a high pressure polymorph and s-ThGeO₄ would transform to z-ThGeO₄ which is high temperature polymorph. However, progression towards amorphization was observed in z-ThGeO₄ via compression of the lattice and neither compression nor expansion of the lattice was observed during the amorphization in s-ThGeO₄.

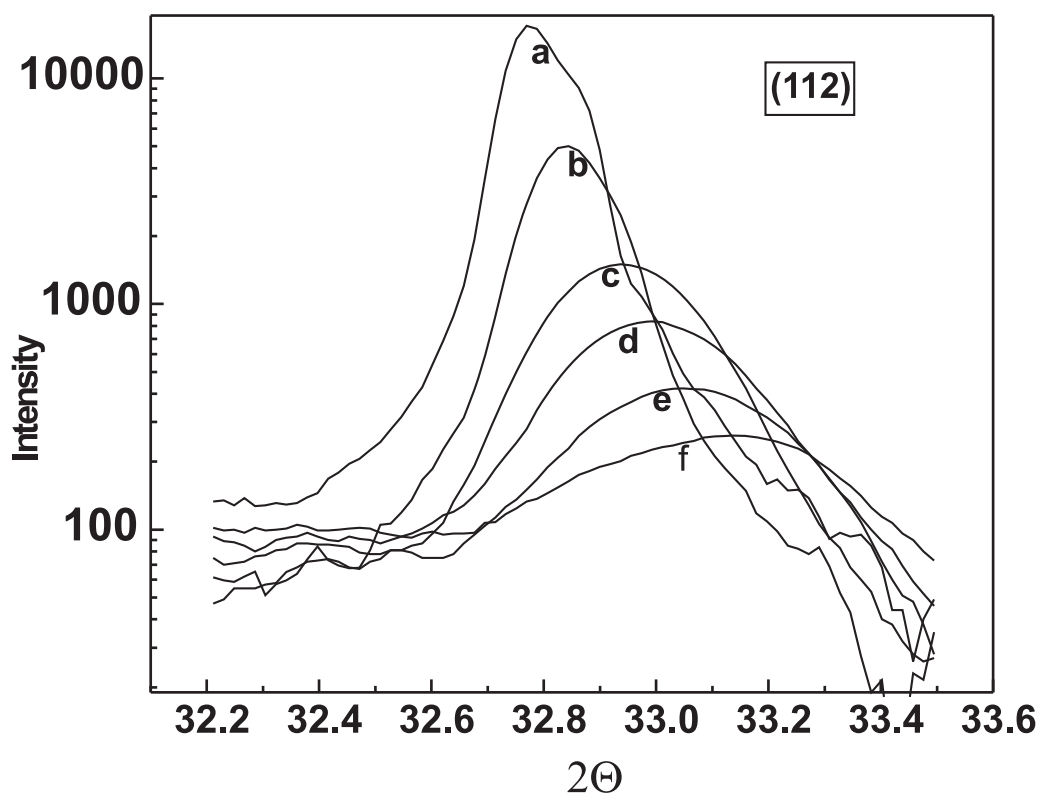


Fig.1. The (112) diffraction peak for zThGeO₄ irradiated with (a) 1×10¹² (b) 2×10¹² (c) 4×10¹² (d) 6×10¹² (e) 8×10¹² (f) 1×10¹³ ions/cm²sc

5.2.43 Development of NLO Devices from Stoichiometric Lithium Niobate

P.Kumar¹, S.Moorthy Babu¹ and D.Kanjilal²

¹Crystal Growth Centre, Anna University, Chennai-600 025.

²Inter University Accelerator Centre, Aruna Asaf Ali Marg, New Delhi 110067

Lithium niobate (LiNbO_3) is one of the technologically important oxide single crystals. It has an unusual combination of ferroelectric, electro-optic, acousto-optic and piezoelectric properties. It has been extensively studied because of its high potential in device application. These include electro-optical modulators, second harmonic generators, surface acoustic wave filters, waveguide lasers etc.

Ferroelectric lithium niobate (LiNbO_3) single crystals, oriented in (001) direction, grown by czhoralski melt growth technique were investigated in this project. Wafers were taken from shoulder, middle and bottom portions of the crystal boule and cut and polished (on both sides). Pure stoichiometric LiNbO_3 (SLN) and Ti doped congruent LiNbO_3 (CLN) samples of dimensions of $\sim 10 \times 5 \times 0.8$ cm were used for proton ion implantation with energy of 120 keV and Li ion beam irradiation with energy of 50 MeV. Various fluences of 1×10^{15} , 1×10^{16} , 1×10^{17} ions were used for implantation and 1×10^{11} , 1×10^{12} , 5×10^{12} and 1×10^{13} were used for irradiation by keeping the current value constant as ~ 0.5 pA to avoid local heating. The surface modifications and defects created on the polished surface after ion implantation and irradiation processes have been investigated by various experimental techniques.

X-ray diffraction analysis (XRD), Fourier Infrared analysis (FTIR) and Atomic Force Microscopy (AFM) analysis were performed for ion implanted/ irradiated LiNbO_3 samples.

X-ray diffraction studies were carried out for implanted/ irradiated CLN samples using Bruker AXS diffractometer. For comparison, we carried out XRD analysis on virgin sample. It is known that in high energy ion irradiation, the electronic energy loss is dominating compared to the nuclear energy loss. XRD patterns show variations in peak intensity and increase in spectral width (FWHM) with increase of fluence range indicating that the crystalline nature turned into amorphous at surface.

Since the crystals of LiNbO_3 were grown in air by the Czhoralski melt growth technique, H^+ ion always present in the crystal. It is assumed that H is incorporated into the crystal from the humidity of surrounding atmosphere. We have implanted 120 keV H^+ ions with fluences of 1×10^{15} , 1×10^{16} and 1×10^{17} . Hence our FT- IR analysis shows O-H bond formation caused by infrared (IR) absorption due to vibronical excitation. This OH- stretching vibration is sensitive to a change of the ion environment. After ion implantation and irradiation the absorption coefficient of O-H stretching vibration further increases.

The AFM studies reveal that the surface roughness value is 1.12 nm which increases with 120 keV H^+ ion implantation and Li^{3+} ion irradiation to 5.6 nm and 4.7 nm respectively.

5.2.44 Studies on the effect of SHI on the optical and electrical properties of organic nonlinear optical Benzimidazole (BMZ) Crystals

T.Kanagasekaran¹, P.Mythili¹, P.Srinivasan¹, N.Vijayan², P.K.Kulriya³, D.Kanjilal³, R.Gopalakrishnan¹ and P.Ramasamy⁴

¹Department of Physics, Anna University, Chennai -600 025, India

²Materials Characterization Division, National Physical Laboratory, New Delhi

³Inter University Accelerator Centre, Aruna Asaf Ali Marg, New Delhi 110067

⁴SSN College of Engineering, Kalavakkam, India.

The bulk single crystals of BMZ have been successfully grown by Bridgman technique using glass ampoule of length 22cm with wall thickness 1.2 mm (approximately) and necked portion is less than 1.5 mm in diameter. The cut and polished BMZ crystals have been irradiated by 70 MeV Ag ion beam delivered from 15MV pelletron Accelerator at IUAC, Delhi. Optical absorption studies were performed on 70 MeV Ag ion irradiated BMZ crystals. The electronic structure of BMZ crystals thus can be visualized from the study of UV-Vis spectra. The UV-Vis spectra of virgin and irradiated crystals were recorded using shimadzu UV-Vis spectrometer. The unirradiated BMZ crystals show its characteristic peak at around 305 nm, which is a $\Pi - \Pi^*$ transition of the heteroatomic benzene ring. The characteristic peaks at 312 nm and 318 nm are observed for irradiated BMZ crystals at fluences of 5×10^{11} ions/cm² and 5×10^{12} ions/cm², respectively. The increase in absorbance of irradiated BMZ crystals can be explained by decrease in absorption coefficient (α) on increasing the radiation fluence.

The dielectric studies were carried out on BMZ crystal using a Hioki (3535) LCR meter before and after irradiation at various temperatures (35 °C to 95 °C) and frequencies ranging from 20Hz to 5 MHz. A small cylindrical furnace whose temperature was controlled by a Eurotherm 818p controller with an accuracy of +0.1 °C was used to house the sample. The dielectric constant (ϵ') was calculated from C and using the equation (1)

$$\epsilon' = \left(\frac{Ct}{\epsilon_0 A} \right) \quad (1)$$

where ϵ_0 is the permittivity of free space, t is the thickness of the sample, A is the area of cross section and C is the capacitance of the sample. The dielectric loss is given by ϵ'' ($\tan \delta$), where δ is the dissipation factor.

The effect of angular frequency ω on the dielectric constant (ϵ') at temperatures 35 to 95 °C is studied for pristine and irradiated BMZ crystals. Initially ϵ' increases and reaches a maximum, and then decreases with the frequency for both the pristine and irradiated BMZ crystals. The large value of dielectric constant at low frequency is due to the presence of space charge polarization. The decrease in the values of ϵ' with the frequency takes place when the jumping frequency of electric charge carriers cannot follow the alternation of the ac electric field applied beyond a certain critical frequency. The dielectric constant was found to increase by a factor of nearly 5.3, after SHI irradiation of fluence of 5×10^{11} ions/cm². The drastic increase in dielectric constant due to ion irradiation may be correlated to the defects created along the ion tracks and structural modifications induced in the surrounding regions. Incident heavy ions get embedded in the crystal, lose energy by both the inelastic collisions that dominate near the end of the irradiated ions and elastic collisions. The increase in dielectric constants for irradiated samples may be attributed to the disordering of the crystal lattice by the ion beam. When the fluence is 5×10^{11} ions/cm² the damaged regions are isolated from each other as the ion produces a region of amorphous material surrounded by regions containing defects. As we increase the fluence to 5×10^{12} ions/cm², more ions are activated with the lattice disorderness and causing more activation of interaction between

the ions thus increases the capacitance hence the dielectric constant increases.

5.2.45 Contrast in the ^{57}Fe Mössbauer spectroscopic signature of Swift Heavy Ion Irradiated Ti-substituted Li-Al and Li-Cr ferrites

M. C. Chhantbar¹, Ali Yousif², Ravikumar³ and H. H. Joshi¹

¹Department of Physics, Saurashtra University, Rajkot-360 005

²Department of Physics, Sultan Qaboos University, Muscat, OMAN

³Inter University Accelerator Centre, Aruna Asaf Ali Marg, New Delhi 1110067

The iron Mössbauer spectroscopy is an important microscopic probe for ferrites to study the hyperfine interaction parameters, magnetic structure or to reveal coexisting magnetic phases and to deduce unambiguously the distribution of Fe^{3+} ions among the two antiferromagnetically coupled sublattices tetrahedral(A) and octahedral(B) of spinel lattice. There are reports on the elucidation of paramagnetic centres through Mössbauer spectroscopy in Li-Al ferrites [1] and inherent tendency of Ti^{4+} ions to induce short range magnetic clusters [2] in ferrites with the higher magnetic dilution. The present communication clearly brings out the contrast in the influence of the SHI irradiation on the magnetic behaviour of the $\text{Li}_{0.5(1+x)}\text{Ti}_x\text{Al}_{0.1}\text{Fe}_{2.4-1.5x}\text{O}_4$ (LTAF) and $\text{Li}_{0.5(1+x)}\text{Ti}_x\text{Cr}_{0.1}\text{Fe}_{2.4-1.5x}\text{O}_4$ (LTCF) for $x = 0.0$ to 0.3.

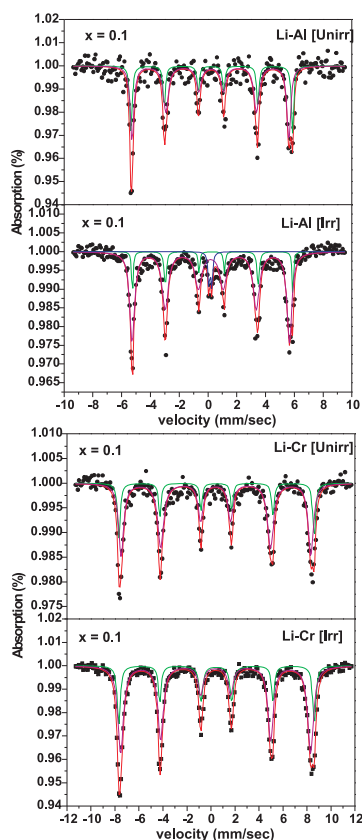


Fig. 1 Mössbauer spectra at 295K

The polycrystalline samples of the systems were synthesized by double sintering ceramic technique. The EDAX has ascertained the compositional purity of the specimens. The details of the irradiation and Mössbauer experiments have been described elsewhere [3]. The specimens were irradiated in vacuum with 50 MeV Li^{3+} ions with fluence of 5×10^{13} ions/cm² using 15 UD Pelletron accelerator at IUAC, New Delhi. The Mössbauer spectra were analyzed using NORMOS computer software using non-linear least square minimization [4]

The XRD patterns for all the samples confirmed the formation of single phase spinel structure. The Mössbauer spectra at 295K for all the specimen exhibit two superimposed asymmetric A and B-site Zeeman sextets. The spectra for irradiated samples of LTAF system exhibit central paramagnetic doublet superimposed on magnetic sextet which is attributed to the partial formation of paramagnetic centres and rearrangement of the cations in the lattice due to SHI.

No appreciable influence of SHI has been observed in the Mössbauer spectra of LTCF ferrites. The hyperfine interaction parameters deduced through Mössbauer spectra are given in the Table 1. The iron distribution parameter $\delta = \text{Fe}^{3+}(\text{A}) / \text{Fe}^{3+}(\text{B})$ derived through XRD intensity analysis and Mössbauer Lorentzian area ratio are in good agreement. It is known that the electronic energy loss threshold (S_{eth}) required for producing amorphization is of the order of 103 eV / Å, therefore it is difficult to comprehend the creation of columnar amorphization at the value of electronic energy loss (S_e) ~ 12 eV / Å. Moreover, the amorphization is not reflected in the XRD patterns of both the systems. In case of LTAF system, the generation of point /clusters of defects inhibits the long range ferrimagnetic order through redistribution of cations in the localized defected regions leading to the formation of paramagnetic centres giving rise to the central paramagnetic doublet.

In contrast, the Mössbauer spectra of the irradiated samples of LTCF system with the same fluence as used for the LTAF do not show any sign of central paramagnetic doublet. This suggests that the presence of magnetic ion Cr^{3+} (3 μB) in the lattice seems to play an important role of keeping the long range order intact in spite of SHI induced defected regions/rearrangement of the cations while the coexistence of non-magnetic cations Al^{3+} and Ti^{4+} gives rise to SHI induced localized paramagnetic centres.

In conclusion, the contrast in the role of Ti^{4+} in the presence of Al^{3+} and Cr^{3+} causing the formation of paramagnetic centres through SHI induced cation rearrangement has been revealed through the comparative Mössbauer signatures of both the systems.

REFERENCES

- [1] S.K.Kulshreshtha, J.Mater. Sci. 5 (1986) 638
- [2] C.R.K.Murty and N.G. Nandikar, Pramana, 13 (1979) 413
- [3] M.C. Chhantbar et al, Nucl. Instr. and Meth. B 244, (2006) 124.
- [4] J. R. Gabriel, S. L. Ruby, Nucl. Instr. And Meth 36 (1965) 23.

Table 1 - Mössbauer parameters at temperature 295K: Hyperfine field (Hnf), Isomer shift (I.S), and Iron distribution parameter $\delta = \text{Fe}^{3+}(\text{A})/\text{Fe}^{3+}(\text{B})$ for unirradiated and irradiated samples of $\text{Li}_{0.5(1+x)}\text{Ti}_x\text{Al}_{0.1}\text{Fe}_{2.4-1.5x}\text{O}_4$ and $\text{Li}_{0.5(1+x)}\text{Ti}_x\text{Cr}_{0.1}\text{Fe}_{2.4-1.5x}\text{O}_4$ systems

$\text{Li}_{0.5(1+x)}\text{Ti}_x\text{Al}_{0.1}\text{Fe}_{2.4-1.5x}\text{O}_4$								
Content (x)	Sample	Hnf (kOe)± 2 kOe		I.S (mm/sec)± 0.03		δ		I_d %
		A-site	B-site	A-site	B-site	XRD	Moss	
0.0	Unirr	332	342	0.21	0.31	0.68	0.66	---
	Irr	329	349	0.21	0.28	0.71	0.69	4.5
0.1	Unirr	320	339	0.19	0.29	0.73	0.71	---
	Irr	321	344	0.22	0.32	0.76	0.75	11.6
0.3	Unirr	309	338	0.24	0.35	0.72	0.77	----
	Irr	308	342	0.22	0.32	0.81	0.82	9.1
$\text{Li}_{0.5(1+x)}\text{Ti}_x\text{Cr}_{0.1}\text{Fe}_{2.4-1.5x}\text{O}_4$								
Content (x)	Sample	Hnf (kOe)± 2 kOe		I.S (mm/sec)± 0.03		δ		I_d %
		A-site	B-site	A-site	B-site	XRD	Moss	
0.0	Unirr	493	506	0.38	0.45	0.71	0.68	Absent
	Irr	494	508	0.40	0.43	0.73	0.71	
0.1	Unirr	490	504	0.40	0.46	0.72	0.72	
	Irr	485	502	0.37	0.42	0.76	0.77	
0.3	Unirr	465	489	0.40	0.43	0.77	0.74	
	Irr	462	487	0.35	0.41	0.81	0.80	

5.2.46 Swift heavy ion induced damage in pyrochlores

M. K. Patel¹, B. P. Mandal², Vinita Grover², D. K. Avasthi³ and A. K. Tyagi²

¹High pressure physics division, Bhabha Atomic Research Centre, Mumbai 400 085

²Chemistry Division, Bhabha Atomic Research Centre, Mumbai 400 085, India.

³Inter-University Accelerator Center, Aruna Asaf Ali Marg, New Delhi 110 067

Pyrochlores are being contemplated as potential host lattices for future applications in nuclear technology. Example for hosting minor actinides to be used in ADSS for accommodating plutonium as inert matrix fuels [1, 2]. Pyrochlores have the general formula $\text{A}_2\text{B}_2\text{O}_6$ where, A is the larger cation and B is the smaller one. Mostly A is a trivalent rare-earth ion and B is tetravalent 3d transition metal. The ordered pyrochlore

belongs to the Fd-3m space group and is a superstructure of the ideal defect fluorite structure (Fm-3m space group) with exactly twice the lattice constant. The A and B cations occupy the 16c and 16d sites, respectively. The O and O' anions occupy the 48f and 8a site respectively. A symmetrically identical anion site, 8b, is vacant. The structural phase transition from the Fd-3m pyrochlore structure to the Fm-3m ideal defect fluorite structure involves the randomization of the anions among the 48f, 8a, and 8b sites and the cations between the 16c and 16d sites [3]. An IMF or transmutation target, in a radiation environment will experience large damage due to neutrons, fission fragments (FF), α -particles and recoils caused by α -particles (α -recoils). Accelerated SHI beams can advantageously simulate damage caused by fission fragments. SHI is mainly deposit energy via. excitation and/or ionization of target atoms, termed as electronic energy loss and cause amorphization or phase transformation in materials

Three pyrochlores $Gd_2Zr_2O_7$, $Gd_2Ti_2O_7$ and $Nd_2Zr_2O_7$ were prepared by standard solid state route, grinding appropriate reactants in stoichiometric proportions and subsequently subjecting them to various heat treatments. The XRD patterns of final products were analyzed by comparing with the reported ones. The powders were then compacted into pellets of 8mm diameter and 2mm thickness. The beam time experiments carried out at the Inter-University Accelerator Center (IUAC), New Delhi are summarized in the table bellow. Each of the three pyrochlores were irradiated with three ion beams at three fluences i.e. 1×10^{13} , 5×10^{13} and 1×10^{14} ions/cm²

Table 1. Radius ratio (r_A/r_B), Cation antisite defect energy ECA (eV) [2] and 48f oxygen 'x' parameter:

Sample	r_A/r_B	E_{CA} (eV)	48f 'x' parameter
$Gd_2Zr_2O_7$	1.46	3.20-3.60	0.345
$Nd_2Zr_2O_7$	1.54	4.00-4.40	0.334
$Gd_2Ti_2O_7$	1.75	5.60-6.00	0.326

After SHI irradiations XRD measurements were made ex-situ using the Bruker D8 - Advance diffractometer. Cu Ka ≈ 1.5406 Å radiation was used at 40 kV and 40 mA. Position sensitive Ventic-1 detector at IUAC, New Delhi was used to detect the diffracted beam scanning and the 2θ angle between 10° to 80° with 0.02 step size.

XRD measurements indicate an order disorder phase transformation from pyrochlore to defect fluorite, finally amorphization was observed. It is observed that the susceptibility towards SHI induced amorphization increases with increase in r_A/r_B . Hence, pyrochlore with highest r_A/r_B ($Gd_2Ti_2O_7$) readily amorphizes while the one with least r_A/r_B ($Gd_2Zr_2O_7$) does not amorphize even at S_e of 22.2 keV/nm. However, recrystallization was observed in $Gd_2Zr_2O_7$. The damage in the present case is caused in the electronic stopping regime unlike many studies in the past which have been studying the stability of pyrochlores in the nuclear stopping regime. Thus the damage is

strongly dependent on S_e .

Ordered Pyrochlores exist within r_A/r_B ratio ranging from 1.2 to 1.6. $Gd_2Zr_2O_7$ with $r_A/r_B = 1.46$, under ion irradiation induced disorder the two cations can undergo randomization of A and B cations. The structure in this case tends to release the excess energy by undergoing a phase transformation to defect fluorite instead of amorphization. This renders higher radiation stability to $Gd_2Zr_2O_7$. As the r_A/r_B increases i.e. for $Nd_2Zr_2O_7$ and $Gd_2Ti_2O_7$, the radius of the two cations become distinctly different and under ion irradiation induced disorder, the randomization is hindered. Thus the excess energy cannot be released and the only means to do so is to undergo a structural transformation from crystalline to amorphous state. Thus $Nd_2Zr_2O_7$ and $Gd_2Ti_2O_7$ undergo amorphization faster than $Gd_2Zr_2O_7$. Complete amorphization was seen in the case of $Nd_2Zr_2O_7$ and $Gd_2Ti_2O_7$ while $Gd_2Zr_2O_7$ did not amorphize even at the maximum S_e and fluence and recrystallization was observed.

Finally, $Gd_2Zr_2O_7$ and $Nd_2Zr_2O_7$ amorphizes via compression of the lattice indicating a dominating pressure induces transformations caused by SHI.

REFERENCES

- [1] R.C. Ewing, W. J. Weber and J. Lian, J. App. Phys. 95 (2004) 5949.
- [2] K.E. Sickafus, L. Minervini, R.W. Grimes, J.A. Valdez, M. Ishimaru, F. Li, K. J. McClellan and T. Harimann, Science 289 (2000) 748.
- [3] M.A. Subramanian, G. Aravamudan and G.V. Subba Rao, Prog. Solid. State. Chem. 15 (1983) 55.

5.2.47 Irradiation Effects of 100 MeV Oxygen Ions on Hydroxyapatite

S. Prakash Parthiban¹, R.V. Suganthi¹, E.K. Giriya¹, K. Elayaraja¹, P. Kulariya², Y. S. Katharria², F. Singh², I. Sulaniya², A. Tripathi², K. Asokan², D. Kanjilal², S. Yadav³, T.P. Singh³, S. Narayana Kalkura¹

¹Crystal Growth Centre, Anna University, Chennai - 600025

²Inter University Accelerator Centre, Aruna Asaf Ali Marg, New Delhi -110067

³Department of Biophysics, All India Institute of Medical Sciences, New Delhi

Hydroxyapatite (HAP, $Ca_{10}(PO_4)_6(OH)_2$) is the main mineral constituent of bones and teeth. Bone contains carbonated-HAP crystals in the form of plates and needles, which are about 40-60 nm long, 20 nm wide, and 1.5-5 nm thick. Therefore from the point of view of biocompatibility, synthetically prepared HAP seems to be the most suitable ceramic material for hard tissue replacement implants [1-4]. Pure HAP is highly stable and can withstand temperatures up to 1600°C without undergoing any phase transition. Apatites (mainly, fluoroapatite and HAP) could be used as matrix for storing nuclear waste elements like Sr, I, Np, Pu, etc. The effect of swift heavy ion irradiation on fluoroapatite pellets was carried out by Miro et al. to explore its properties for nuclear waste storage [5]. There are also reports of low energy irradiation of hydroxyapatite composites [6] and ion beam densification of HAP [7].

The method of preparation of HAP plays a significant role in its bulk and surface properties. For this purpose, HAP was prepared using different routes like wet-chemical-hydrothermal (WCH), silica gel matrix (SGM), sol-gel-hydrothermal (SGH), and microwave (MW) treatments.

Pellets of these HAP powders (8 mm in diameter and about 1 mm in thickness) were subjected to irradiation by oxygen ion at energy of 100 MeV (fluences 1×10^{12} , 1×10^{13} , 1×10^{14} particles/cm², current 4 pA). Glancing angle X-ray diffraction (GXRD), atomic force microscopy (AFM), photoluminescence spectra (PL), scanning electron microscopy (SEM), dynamic light scattering (DLS), and in vitro bioactivity test using simulated body fluid (SBF) were carried out on the irradiated samples. A summary of the significant results and observations are given below.

Significant improvement in crystallinity and reduction in particle size was seen for samples by SGM, WCH, SGH, MW and SGH. XRD of silicon doped HAP by SGH (sintered to 300 °C) showed excellent enhancement in crystallinity when irradiated with a fluence of 1×10^{12} particles/cm² [fig. 1].

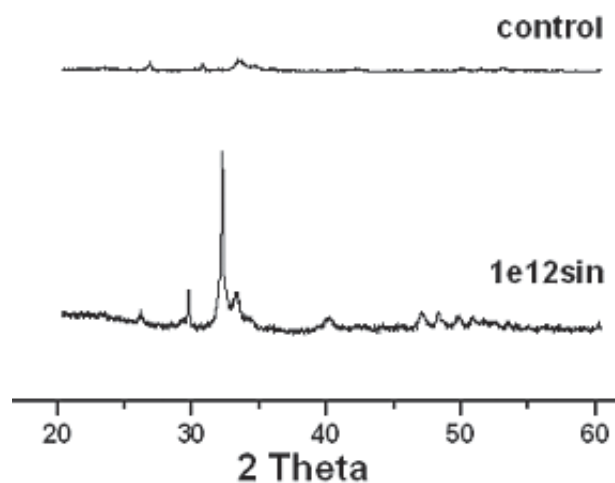


Fig. 1. XRD of sintered silicon doped HAP by SGH showing excellent crystallinity.

AFM pictures of WCH confirmed the reduction in particle size from 1.008 μm (control) to 53.40 nm (fluence 10^{14} particles/cm²). Pores were induced in all samples after irradiation. Their average size was in the range of 4-6 μm . The particle size reduction was also further confirmed by DLS for these samples.

Surface analysis of some of the irradiated samples showed significant changes in its morphology. HAP prepared by microwave method (MW) showed platy morphology when irradiated with a fluence of 10^{12} particles/cm². There was also increase in the aspect ratio of the particles, which would make them more protein adsorbant.

Ionoluminescence was observed in all samples during irradiation. Presence of phosphorus in HAP is likely to be the origin of ionoluminescence. Photoluminescence spectra were taken to investigate this property. SGM showed excellent ionoluminescence compared to other samples. The PL spectra showed peak shift towards higher wavelength region (when fluence increases) with broadening of the peaks.

Reduction in the particle size and pore formation was observed in all the irradiated samples. Reduction in particle size leads to better bioactivity and biocompatibility. The pores formed will

allow the circulation of physiological fluids and further helps in bone ingrowths . This is the first report of irradiation on pure HAP with high-energy ions and it showed excellent bioactivity and improvement of its surface properties which makes it a better biomaterial.

REFERENCES

- [1] M.P. Ginebra et al., J. Cont. Release 113 (2006) 102-110.
- [2] J.R. Woodard et al., Biomaterials 28 (2007) 45-54.
- [3] T. Kawasaki, J. Chromatography 544 (1991) 147-184.
- [4] M.P. Mahabole et al., Bull. Mater. Sci. 28(6) (2005) 535-545.
- [5] S. Miro et al., Nucl. Instr. and Meth. B 227 (2005) 306-318.
- [6] E. Suljovrujic et al., Rad. Phy. Chem. 67 (2003) 375-379.
- [7] C.M. Lopatin et al., Nucl. Instr. and Meth. B 145 (1998) 522-531.

5.2.48 Studies of Effect of Irradiation on Structure, Conductivity and Charge Storage Properties of Polyaniline Composites

Pratima Jaiswal¹ and Rajiv Prakash¹

¹School of Materials Science and Technology, Institute of Technology, BHU

Electronically conducting polymers are suitable electrode materials for high performance supercapacitors, for their high specific capacitance and high dc conductivity in the charged state. Recently, polyaniline (PANI) and its derivative have been considered as a promising material for the energy storage devices [1, 2] and are used in electrochemical capacitor as electroactive material with high faradic pseudo capacitance [1] due to the existence of several oxidation states [2]. However, the poor processability and mechanical properties are the major limitations in the device fabrication. The effect of ion beam (energy > 1 MeV) irradiation on the conducting polymers is studied to enhance or alter the properties like conductivity, density, chain length and solubility. The primary phenomena associated with ion beam and polymer interactions are cross-linking, chain scission and emission of atoms, molecules and molecular fragments [3, 4]. Recently, effect of Swift Heavy Ion (SHI) irradiation (>80 MeV) on polypyrrole and polyaniline was studied, however, no considerable improvement was achieved in the redox properties and capacitance of these polymers [5-7]. In this project processable polyaniline composites are synthesised and the effect of high-energy irradiation on their structure, conductivity and charge storage properties is studied.

A redox capacitor was developed using PANI-PAA composites based on parallel plate assembly. The processable composite film was coated over ITO glass plates (one side conducting) by solvent evaporation technique. Electrical connections from each ITO plates were taken by soldering a wire with silver paint. Similarly redox capacitor was developed using PANI-PVC composites also. Composite coated ITO plates were assembled in a small glass cell using Teflon separator and filled with 0.1M NaClO₄-PC electrolyte in case of PANI-PAA composites and 0.1N HCl with 0.5 NaClO₄ electrolyte for PANI-PVC composites. The geometrical area of the capacitor was main-

tained as 1 cm^2 .

Polyaniline composites coated ITO plates or glass plates were irradiated with 100 MeV Si^{+8} ion at Pelletron Accelerator, N. Delhi with fluences 10^{12} , 3×10^{12} and 10^{13} ions/ cm^2 .

The dc conductivity of the polymer composites were measured using four probes technique. A decrease in the conductivity was observed in irradiated samples in comparison to unirradiated samples. The UV visible spectra of irradiated PANI-PVC composite showed two peaks at 461nm, which was also observed in unirradiated sample along with a new peak at 531nm. Similarly, UV visible spectra of irradiated PANI-PAA composite showed two peaks at 448 nm, which was also observed in unirradiated sample along with a new peak at 540nm. The appearance of the new absorption peaks above 500nm is a clear indication of quinoid formation or doped states formation in the composites. The carboxylic groups present in the insulating polymer chains showed an acid-base reaction with NH group of PANI, which enhanced due to irradiation.

The FTIR studies of the irradiated and unirradiated polymer composites did not show any considerable shift in the peaks; however, N-H peak stretching of the PANI diminished in the irradiated samples, which also supported the interaction of carboxylic group of insulating polymers to N-H group of PANI on irradiation.

The structural study of the composites was carried out using XRD technique. Two new peaks appeared at 2Θ of 32° and 34.5° in both the irradiated polymers with disappearance of two broad PANI characteristic peaks. The appearance of two new sharp peaks indicating more ordered geometry. The disappearance of PANI or amorphous polymer characteristic humps is probably due to chain scissoring and formation of short length chains during the irradiation. It is also supported as a loss of electroactivity was observed in the irradiated composites at higher fluence.

The impedance analysis was done using parallel plate assembly of two polymer composite coated ITO electrodes in propylene carbonate having 0.1M sodium perchlorate in the frequency range 0.01 to 1×10^4 Hz. The various parameters viz. geometrical capacitor, solution resistance, impedance of the PANI electrolyte interface, bulk faradic impedance, Warburg diffusion impedance, ionic charge-transfer resistance at the PANI-electrolyte interface, electron-transfer resistance of the redox transitions, double-layer capacitance and bulk faradic pseudo capacitance were calculated based on equivalent-circuit model for the PANI-coated electrode using Zim Impedance software. The composites irradiated at 10^{12} fluence showed higher double-layer capacitance and Warburg diffusion impedance in comparison to the unirradiated composites; however, no improvement was observed in bulk faradic pseudo capacitance. Moreover, composites irradiated at 10^{13} fluence showed nearly same or some time lower capacitance value. The capacitance was calculated based on equivalent-circuit model and obtained of the order of 5 F per gram of total composite weight.

From this study we can conclude that SHI irradiation is a good technique to

enhance the interactions of two components in the composite materials as we observed a better interaction of the PANI with carboxylated insulating polymers viz. PVC or PAA. The chain alignment and order is also improved after irradiation and polymers showed better stability in comparison to the unirradiated polymer composites.

REFERENCES

- [1] C.C. Hu & C.H. Chu. *J. Electroanal. Chem.* 503 (2001) 105
- [2] C.C Hu. & C.H. Chu. *Mater. Chem. Phys.* 65 (2000) 329
- [3] M. Mastragostino. C. Arbizzani and F. Soavi *Solid State Ion.* 148 (2002) 493
- [4] R. Mishra. S. P. Tripathy. D. Sinha. K. K. Dwivedi. S. Ghosh. D. T. Khathing. M. Muther. D Fink & W H Chung. *Nucl. Instrum. Methods B* 168 (2000) 59
- [5] A. M. P. Hussain. A. Kumar. F. Singh & D K Avasthi. *J. Phys. D: Appl. Phys.* 39 (2006) 750
- [6] A.M.P. Hussaina and A. Kumar. *Eur. Phys. J. Appl. Phys.* 36 (2006) 105
- [7] A.M.P. Hussain. D. Saikia. F. Singh. D.K. Avasthi. A. Kumar. *Nuclear Instruments and Methods in Physics Research B* 240 (2005) 834

5.2.49 SHI Irradiation Induced Electrochemical Stability Enhancement in Poly (3-Methylthiophene) Conducting Polymer Electrodes

A. Kumar¹, A.M.P. Hussain¹, F. Singh² and D.K. Avasthi²

¹Dept. of Physics, Tezpur University, Napaam-784028, Assam

²Inter University Accelerator Centre, Aruna Asaf Ali Marg, New Delhi-110067

Intrinsic conducting polymers (ICPs) have emerged as promising electrode materials for redox capacitors because of high capacitive energy storage, low cost as compared to other alternative electrode materials e.g., activated carbon and noble metal oxides, easily synthesizable and store charge throughout their volume [1] but they suffer from the disadvantage of lower cycle-life and slow kinetics of ion transport because the redox sites in polymer backbone are not sufficiently stable for many repeated redox processes [2]. Swift heavy ion (SHI) irradiation of polymers has been found to produce useful modifications in their physical and chemical properties. Increase in hardness, strength and wear resistance, electrical conductivity, density, chain length, crystallinity, solubility and improvements in the optical transmission properties of the polymers have been reported. In the present work all-polymer redox supercapacitors are fabricated with PVDF-HFP(20w/o)- PMMA(10w/o)- LiCF₃SO₃(10w/o)-PC+DEC(57w/o)- SiO₂(3w/o) polymer gel electrolyte sandwiched between [CH₃(CH₂)₃]₄NBF₄ doped poly(3-methylthiophene) conducting polymer and 120 MeV Si⁹⁺ ion irradiated electrodes with a view to improve the performance, particularly cycle life, of the supercapacitors.

The dc conductivity study measured by four probe method shows increase in conductivity in the poly(3-methylthiophene) polymer films upon SHI irradiation, which can be attributed to the energy transfer by electronic stopping mechanism. Ion irradiation produces large number of charged and active chemical species, cations, anions,

radicals and electrons along the ion track [3]. XRD studies show increase in the degree of crystallinity upon SHI irradiation. The redox nature of the conducting polymer electrodes, remains unaffected upon SHI irradiation as observed in the cyclic voltammograms of the poly (3-methylthiophene) conducting polymer films before and after irradiation in Fig 1. The figure shows that the redox peaks occur at the same potential but the current is slightly increased with the increase in fluence. This indicates slight improvement in the charge storage capacity of the electrodes.

The electrochemical stability of the supercapacitors is tested for 10,000 charge-discharge cycles. The capacitance values are calculated after every 1000 cycles and presented in the stability plots in Fig. 2. The figure shows that the capacitance of the supercapacitor with unirradiated electrodes goes on decreasing whereas that of the supercapacitors with irradiated electrodes becomes stable after about 5000 cycle and does not decrease further, even though the capacitance value is slightly lower. The initial decrease in the capacitance values observed in the stability plots may be attributed to the irreversible faradic reaction occurring at the electrode surface due to the presence of volatile surface groups e.g. OH^- , CN^- etc. which cause loss of charge at the electrode. Upon SHI irradiation, the stabilization of the surface groups may occur due to cross-linking induced by huge energy deposition by electronic energy loss mechanism. The volatile surface groups may also evaporate due to energy transfer upon SHI irradiation. Thus the cycle life stability is improved.

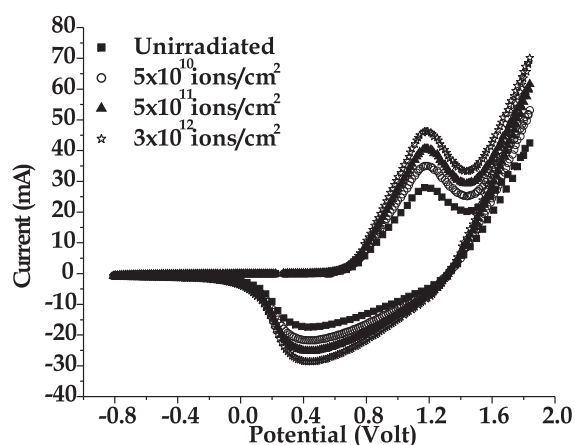


Fig. 1. Cyclic voltammograms of 120 MeV Si^{9+} ion irradiated poly(3-methylthiophene) conducting polymer at three different fluences of 5×10^{10} , 5×10^{11} and 3×10^{12} ions/cm².

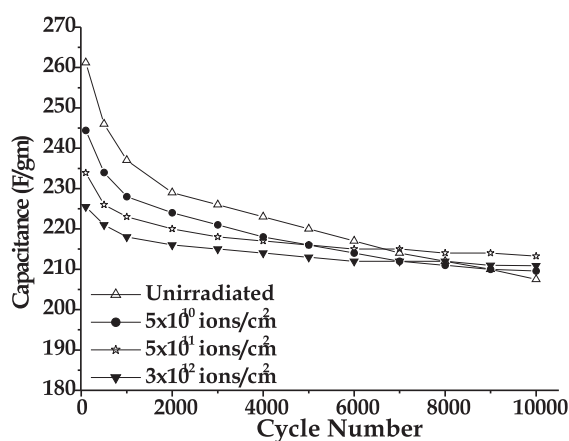


Fig.2. Stability plots of supercapacitors with $[\text{CH}_3(\text{CH}_2)_3]_4\text{NBF}_4$ doped poly(3-methylthiophene) electrodes before and after SHI irradiation.

REFERENCES

- [1]. A. Rudge, J. Davey, I. Raistrick, S. Gottesfeld and J.P. Ferrarist, *J. Power Sources* 47 (1994) 89.
- [2]. J.H. Park, J.M. Ko, O.O. Park and D.W. Kim, *J. Power Sources* 105 (2002) 20.
- [3]. E.H. Lee, *Nuclear Instruments and Methods B* 151 (1999) 29.

5.2.50 FTIR Analysis of Pristine and Ion Irradiated Polymers

JK Quamara¹, Anu Sharma¹, Geetika Goyal¹, Y. Sridharbabu¹ and Maneesha Garg¹

¹Department of Applied Physics, National Institute of Technology, Kurukshetra

The Fourier transform infrared absorption spectroscopy (FTIR) provides precise information about orientation of specific functional groups within the polymer film. In infrared spectroscopy the frequency region of 4000-650 cm^{-1} is mainly investigated for polymer characterization. In the present investigations FTIR analysis of thin film polymers have been done which were homogeneously damaged in the bulk by high energy heavy ion irradiation.

The polymers were irradiated with different ions viz Oxygen, Nickel and Lithium (energy: 50-80 MeV and fluence: 5×10^4 to 1.5×10^{14} ions/ cm^2) using PELLETRON facility at IUAC, New Delhi. The FTIR analysis of pristine and irradiated samples was done using ABB Bomem spectrometer (MB 104E) with the ATR (attenuated total reflection) in the 4000- 500 cm^{-1} range. Few representative FTIR spectrum of pristine and ion irradiated polymers are illustrated in figs 1-3. The FTIR spectra of pristine kapton-H (fig. 1) reveals the characteristic bonds around 717, 1079, 1160, 1230, 1367, 1494, 1601, 1703 and 1770 cm^{-1} assigned respectively to the C=O bending, C-O-C stretching, C-C bending, C-N stretching (two peaks i.e. 1230, 1367 cm^{-1}), aromatic C=C ring stretch (two peaks i.e. 1494, 1601 cm^{-1}), C=O symmetrical stretching and C=O asymmetrical stretching.

The FTIR spectra of 75 MeV O ion irradiated (fluence: 1.8×10^{14} ions/ cm^2) kapton-H polyimide (fig 1) shows the reduction in the intensity of typical bands in the FTIR spectra indicating that certain morphological changes have occurred in the polymer due to irradiation.. A very broad band between 2500-3500 cm^{-1} which is absent in case of pristine samples has been observed. This broad band has been associated to the presence of absorbed water in irradiated samples.

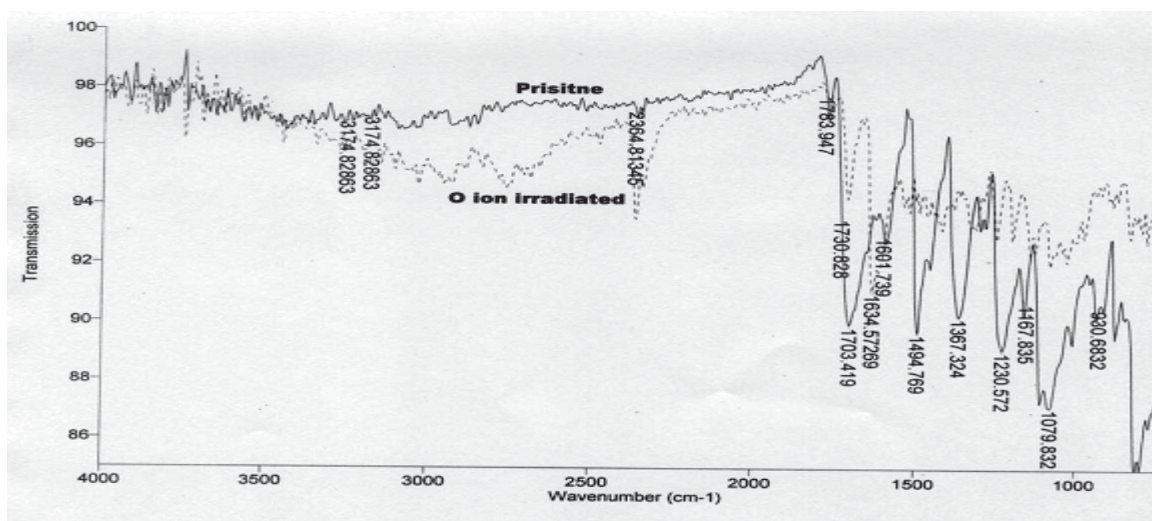


Fig. 1. FTIR spectra of pristine and 75 MeV O ion irradiated (fluence: 1.8×10^{14} ions/ cm^2) irradiated kapton-H polyimide.

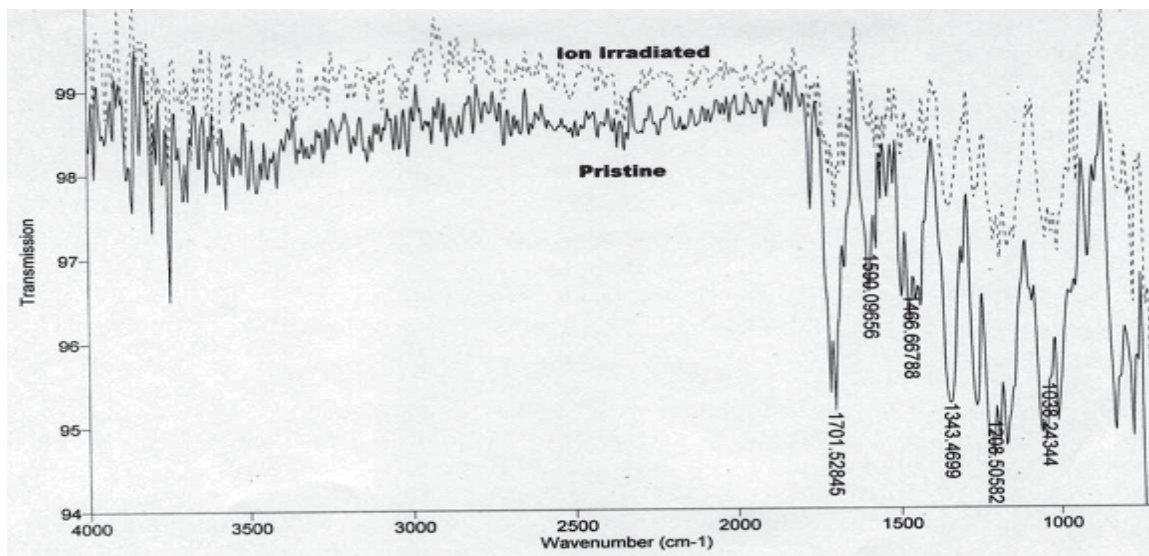


Fig. 2. FTIR spectra of pristine and 75 MeV O ion irradiated (fluence: 1.2×10^{13} ions/cm²) irradiated polyetherimide.

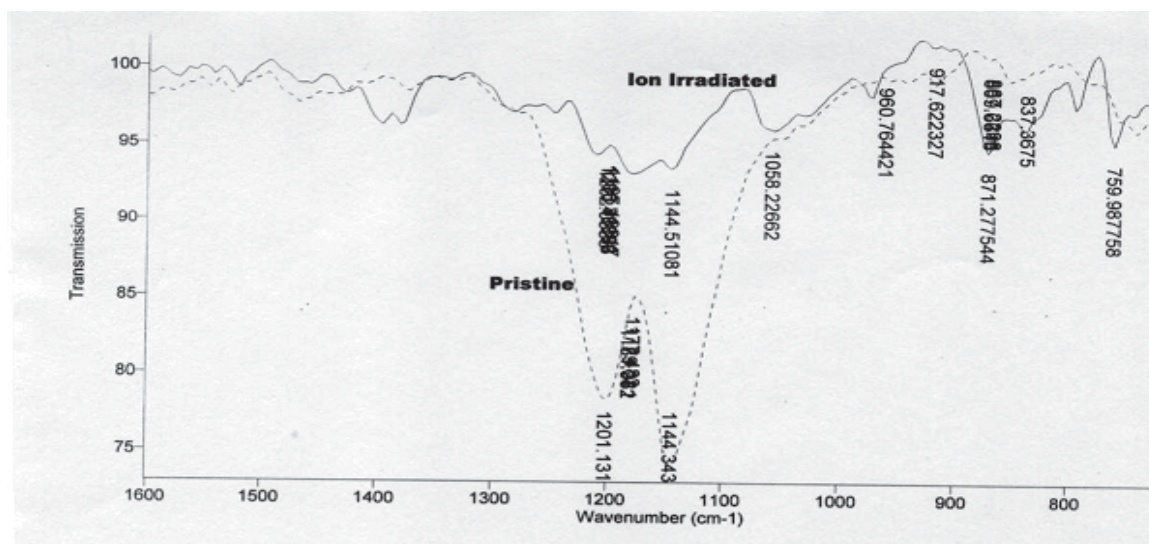


Fig. 3. FTIR spectra of pristine and 75 MeV O ion irradiated (fluence: 1.2×10^{12} ions/cm²) irradiated Teflon.

Demerization of carbonyl groups in polyimides is one of the major consequences of high energy ion irradiation [1]. A decrease in the intensity of the band around 1703 cm^{-1} in irradiated samples shows the decrease in the number of carbonyl groups.

The FTIR spectra of kapton-H polyimide irradiated with 80 MeV Ni and 50 MeV Li ions is almost similar to that of oxygen ion irradiated polyimide (not shown). A moderate shift in the frequency of the characteristic bands is due to different LETs of different ions.

The FTIR spectra of pristine Polyetherimide (fig 2) show the characteristic bonds around 707, 1038, 1140, 1701 and 1760 cm^{-1} assigned respectively to the C=O bending, C-O-C stretching, C-C bending, C=O symmetrical stretching and C=O asymmetrical stretching. Two peaks around 1208, 1343 cm^{-1} corresponds to C-N stretching and 1466, 1590 cm^{-1} to the aromatic C=C ring stretch. The peaks in the wave number region 1100 and 1200 cm^{-1} indicates the presence of carbon fluorine bonds which is consistent with the known structure of Teflon. After irradiation, we find the peaks corresponding to these wave numbers but with considerable decrease in the peak magnitude.

REFERENCE

- [1] Garg Maneesha and Quamara J.K., Nucl. Instrum. Methods. Phys. Res. B., 2001,179: 389

5.2.51 SHI induced modification of polymer composites

N.L.Singh¹, Anjum Qureshi¹, Sejal Shah¹, V.V. Sivakumar², A. Tripathi², F. Singh² and D.K. Avasthi²

¹Department of Physics, M. S. University of Baroda, Vadodara

²Inter University Accelerator Centre, Aruna Asaf Ali Marg, New Delhi 110 067

There is an increasing interest in the polymer-matrix composites prepared by mixing two or more constituents to make up some disadvantages in single material [1,2]. We have prepared metal doped polymer composites by two methods. i) Chemical method ii) RF sputtering method.

Ferric oxalate was used as organometallic fillers in polyvinyl chloride to form polymer matrix composite films at different concentration of filler. These films were irradiated with 80 MeV O^{6+} ions at the fluence of 10^{11} and 10^{12} ions/ cm^2 . The radiation induced modifications in dielectric properties, microhardness, surface morphology and surface roughness of polymer composite films have been investigated at different concentration (i.e. 5%, 10% and 15%) of filler. It was observed that hardness and electrical conductivity of the films increase with the concentration of the dispersed ferric oxalate and also with the fluence. From the analysis of frequency, f , dependence of dielectric constant, it has been found that the dielectric response in both pristine and irradiated samples obey the Universal law given by $\epsilon \propto f^{-n-1}$. The dielectric constant/loss is observed to change significantly due to irradiation. This suggests that ion beam irradiation promotes (i) the metal to polymer bonding and (ii) convert the polymeric structure into hydrogen depleted carbon network. The irradiation makes polymer harder and more conductive. AFM images shows that average roughness of the irradiated films is lower than that of unirradiated films. Surface morphology of irradiated polymer composite films is observed to change. Scanning Electron microscopy results show that partial agglomeration of fillers in the polymer matrix.

Another set of composites with Fe doped PI has been prepared by RF sputtering. Thin film was formed by co-sputtering of polymeric film and Fe foil. The assembly contains a target holder acting as cathode and a substrate holder acting as anode. Substrates are kept on the anode at a distance of 5 cm from the cathode. The cathode is connected to RF power supply. The anode and the rest of the system are properly grounded electrically insulated height adjustable table. The

process was done at room temperature at the pressure of 2×10^{-2} torr. Thin film of metal dispersed polymer (thickness ~ 200 nm) was formed on glass and silicon substrate. Using RBS measurement the concentration of Fe in the composite is found to be 0.5%, 0.9% and 5% for three different deposition conditions.

These films have been irradiated by 120 MeV Ni^{10+} ions using Pelletron facility at IUAC, New Delhi. The fluence of the beam was taken 10^{11} , 10^{12} , 5×10^{12} ions/cm². The change in surface morphology before and after irradiation was studied by AFM. Surface roughness is observed to decrease after irradiation but it increases with metal compound concentration. The increase in roughness with metallic concentration may be attributed to increase of density and size of metal particles on the surfaces of the polymeric film [2]. The magnetic behavior of the Fe doped PI films has been studied by MFM. Result shows that the magnetization decreases after irradiation. Optical characteristic of the pristine and irradiated samples have been studied by UV-Vis Spectroscopy for the range of 250-900 nm by U-3000/U-3300 Spectrophotometer (Hitachi). It is observed that the band gap decrease with increase in metal concentration.

REFERENCES

- [1] B. Russell, V. Valerity, et al., Science 292 (2001) 2469
- [2] T. Pan, J. P. Huang, Z. Y. Li, Phys. B 301 (2001) 190
- [3] X. Yan, T. Xu, S. Xu, X. Wang and S. Yang, Nanotechnology 15, 1759 (2004)

5.2.52 Effect of Li^{3+} ion irradiation on L-threonine amino acid single crystals

G. Ramesh Kumar¹, S. Gokul Raj¹, V. Mathivanan¹, Thenneti Raghavulu¹, M. Kovendhan¹, A. Tripathi², D. Kanjilal², K. Asokan², I. Sulaniya², R. Mohan¹

¹Department of Physics, Presidency College, Chepauk, Chennai 600 005

²Inter University Accelerator Centre, Aruna Asaf Ali Marg, New Delhi 110 067

L-threonine is an optically active crystallizes in non-centrosymmetric $P2_12_12_1$ space group of an orthorhombic system. Its second harmonic generation efficiency has been found to be greater than that of potassium dihydrogen phosphate (KDP) single crystals [1,2]. We are interested to adopt different processing methods to enhance the electrooptic and SHG properties of amino acid single crystals. Ion beam irradiation is an efficient tool to modify the bulk properties of the single crystal. In the present work, we have made an attempt to study the effect of Li^{3+} ion irradiation on structural, optical and dielectric properties of L-threonine single crystals.

L-threonine single crystal was grown by low temperature solution growth and the crystals were well polished using Alumina paste. Polished samples were subjected to 50 MeV Li^{3+} ion irradiation at various fluences ranging from 1×10^{10} - 1×10^{12} ions/cm². The beam current used was around 2 pA.

The structural characterization using X-ray diffraction has been recorded for pure and irradiated L-threonine single crystals. The wavelength of the X-ray irradiation used was $\text{CuK}\alpha$ (1.5408 Å). It has been observed that there is a reduction in the peak intensities of the peaks with the increase in the ion fluences. At higher fluences, the surface of the crystal

becomes amorphous. As we have used Bragg Brentano parafofocussing geometry, the radiation induced amorphization depth has been estimated to be around 840 nm which is twice that of range of Li^{3+} ions in L-threonine single crystals [4].

Dielectric study was performed on pure and irradiated samples of L-threonine using Solartron impedance analyzer in the frequency range 100 Hz - 10 MHz at room temperature. It was found that dielectric constant of L-threonine decreases for lower frequencies (10^{10} , 10^{11}) due to irradiation induced electronic defects in the crystals. At the higher fluence, there is a sudden rise in the dielectric constant due to the surface amorphization. The dielectric constant of L-threonine for the ion fluence 1×10^{12} was found to be 200. Electro-optic coefficient of any non-centrosymmetric crystal depends on the dielectric constant. The increased dielectric constant of irradiated specimen favours the crystal to be feasible in using them in Pockel's devices [5]. Thermal strength of the virgin and irradiated crystals was found out using NeTZSCH - Geratebau GmbH thermal analyzer in the temperature range 30° - 400° C in nitrogen atmosphere. Same heating rate was applied to both irradiated and unirradiated crystals. From simultaneous TGA-DTA studies, it was found that irradiated L-threonine was thermally stable up to 278.6° C, whereas the virgin L-threonine sample decomposes at 265.2° C. Thermal stability of the crystal has increased substantially on Li^{3+} irradiation.

REFERENCES

- [1] J.J.Rodrigues Jr., L.Misoguti, F.D.Nunes, C.R.Mendonca, S.C.Zilio Opt. Mater. 22 (2003) 235.
- [2] G Ramesh Kumar, S. Gokul Raj, R. Mohan, R. Jayavel, Cryst. Growth & Des. 6 (200) 1308.
- [3] B.E. McCandless, Mat. Res. Soc. Symp. Proc., 856 (2005) F4.1.1.
- [4] J. F. Zeighler, J.P. Biersack, U. Littmart., (1985), Stopping ranges of ions in solids., Vol.1 (New York: Pergamonn)
- [5] P. Sreemana Aithal, H.S. Nagaraja, P. Mohan Rao, D.K. Avasthi, Asati Sharma., J. Appl. Phys., 81(11) (1997) 1526

5.2.53 Heavy ion testing of LMFS memory devices

S B Umesh¹, A R Khan¹, G R Joshi¹, M.Ravindra¹, Saif A Khan²

¹ISRO Satellite Centre, Bangalore

²Inter University Accelerator Centre, Aruna Asaf Ali Marg, New Delhi 110 067

All major spacecraft subsystems use LMFS (Lockheed Martin Federal Systems, presently BAe systems) memory devices in critical applications. These devices are being planned for its usage in LEO and GEO missions. These devices are procured to the QML 'V' level, in Rad hard version with a minimum TID of 100Krad (Si), SEL immune and have high immunity to single event upsets.

Even though these devices are designed for radiation hardness, as a part of evaluation, it is required to conduct the radiation tests on samples to verify the manufacturer test data. As a part of the radiation verification testing, these devices were subjected to Heavy ion testing to the maximum available LET value of 45 MeV-cm²/mg. The test conditions and results are

given below.

The three devices types were tested for heavy ions and the test details are given below.

The details of the devices tested are tabulated below.

S.No.	Device type	Function	Quality level	TID Krads (Si)	LET _{in} SEL (MeV - cm ² /mg)	LET _{in} SEU (MeV - cm ² /mg)
1.	197A807 - 144T	32K x 8 PROM	QML V	300K	>110	>120
2.	182A934-235	32K x 8 SRAM	QML V	100K	>120	>120
3.	190A325-134	128K x 8 SRAM	QML V	300K	>120	>60

The devices were tested in IUAC (Inter University Accelerator Centre), New Delhi for Heavy ions. The details of Heavy ions and protons are tabulated below.

S.No.	Ion type	Energy (MeV)	LET (MeV - cm ² / mg)	Flux (ions/cm ² /sec)	Fluence (ions/cm ²)	Facility
1.	¹⁰⁷ Ag ⁸⁺	100	45.27	700	1 x 10 ⁶	IUAC, New Delhi

SRAMS: During irradiation a Checker board pattern AAh and its compliment 55h are written into all the memory locations. The data is read continuously and compared with the known written data. If an upset occurs, there will be a mismatch in the read data and an error counter is updated and the count is displayed and recorded.

After all the locations are read, all memory locations are again refreshed and the procedure is repeated.

PROM: Similar to RAM a checker board and its compliment are written in all the locations and it is one time programmable. During irradiation, the data is read continuously and in case of any mismatch in the read data, error counter is updated and the count is displayed and recorded.

For both the device types supply current is continuously monitored.

Ion	Flux	Device type	Function	Result
$^{107}\text{Ag}^{8+}$ LET _{th} 45.27 MeV - cm ² /mg	700ions/cm ² /s Equivalent TID= 0.5 rads/s	197A807 -	32K x 8	No failures observed and No variation in supply current
		144T	PROM	
		182A934-235	32K x 8	No failures observed and No variation in supply current
		190A325-134	128K x 8	No failures observed and No variation in supply current
			SRAM	

The test conducted for the heavy ions with silver ion $^{107}\text{Ag}^{8+}$ with an LET of 45.27 MeV - cm²/ mg does not have any effect on the devices. This is expected as the LET thresholds for SEU and the Latch up are greater than 100 MeV - cm²/ mg.

The working of the LMFS devices is satisfactory for Heavy ions. No major anomalies were observed during irradiation.

5.3 RADIATION BIOLOGY RESEARCH

The experiments conducted in this field involved an ongoing research project on the germination properties, biochemical properties etc. on ion beam irradiated mustard seeds by users from MDU Rohtak, which utilised 50 MeV ^7Li beam. The other project for which the beam time has been utilised involved study of chromosome aberration and cell cycle kinetics on CHO cell line with manipulation of endogenous glutathione level. For this 85 MeV ^{12}C and 50 MeV ^7Li beam was used. Beam time has also been utilised to study high LET radiation action on endogenous hormonal levels and protein profile in cotton using 45 MeV ^7Li ions.

5.3.1 High LET Radiation induced cellular damage in CHO cells with regard to endogenous GSH status

G. Pujari¹, A. Sarma², A. Chatterjee³

¹Department of Zoology, North Eastern Hill University, Shillong

²Inter University Accelerator Centre, Aruna Asaf Ali Marg, New Delhi 110067

³Department of Biotechnology and Bioinformatics, NEH University, Shillong

Intracellular Glutathione (GSH) is the most important subsets of the endogenous cellular sulfhydryls regarding the modification of cellular responses to both ionizing radiation and chemotherapeutic agents [1, 2]. Studies have shown that chemical agents that act as a radiomodifier against low LET radiation are less effective in changing sensitivity with high LET radiation [3, 4].

Therefore, in order to study the role of endogenous GSH in the high LET irradiated cells, an approach is taken to manipulate intracellular GSH concentrations by treating with Buthionine sulfoximine (BSO). BSO blocks GSH synthesis by selectively blocking the enzyme gamma glutamine cysteinesynthetase [5]. The experiment was performed with the following objectives-

1. To evaluate the role of GSH on high LET induced chromosome aberrations.
2. To evaluate the pattern of delay in cell proliferation after irradiated with high LET radiation and the role of GSH in it.

Cell Culture: Chinese hamster CHO cells were routinely cultured in 90 mm cell culture petriplates (Tarson) in Dulbecco's Modified Eagle's Medium (JRH Biosciences) supplemented with 10% Foetal calf serum (Biological Industries, Israel) and kept at 37°C in humidified atmosphere with 5% CO_2 . In order to deplete GSH, BSO (Sigma, USA) was used at a concentration of 200 μM for 5hrs. before irradiation. GSH was used at a concentration of 2mM for 4hrs. Cell culture was set up in the presence of 5-bromodeoxyuridine BrdU, (Sigma, USA). Colcemid (Gibco) is added to arrest the cells at metaphase.

Irradiation : Heavy ion irradiation ^{12}C of LET 271 Kev/ μm and ^7Li of LET 60 KeV/ μm was carried out using Radiation Biology Beam Line of 16 MV 15 UD Pelletron at Inter University Accelerator Centre (IUAC), New Delhi. Cells were seeded 12 hrs prior to irradiation in Petriplates of 35 mm diameter. The Cells were irradiated under sterile condition, at atmospheric pressure and were exposed to ions through polypropylene film. Cells were irradiated with two fluence of 2.3×10^6

and 6.9×10^6 particles/cm² in the case of Carbon Beam and 1.1×10^7 and 3.2×10^7 particles/cm² in the case of Lithium Beam. These fluences are equivalent to 1 and 3 Gy respectively. Fresh medium was added after irradiation and culture was set in the presence of 6 µg/ml BrdU in order to differentiate between 1st, 2nd and subsequent metaphase. Cells were given 2hrs Colcemid treatment and harvested at 14, 28 and 42 hrs.

Results:

Chromosome Aberration:

- Carbon Beam of LET 271 KeV/µm showing more aberrant metaphase percentage compared to Lithium beam of LET 60KeV/µm (Fig:1).
- With the course of harvest time, there is increase in the aberrations (Fig:1).
- Spectrum of aberration is dominated by deletions.
- Carbon Beam irradiated cells showed high percentage of exchanges than lithium irradiated cells. This may be due to more DNA lesions caused by carbon beam and thus the probability of rejoining is high (Table 1& 2).
- In both the cases exogenous addition of GSH is increasing the exchange aberrations (Table 1& 2).
- GSH is not showing any protection against high LET radiation.
- BSO addition is reducing exchanges and drastically increasing deletion percentage.

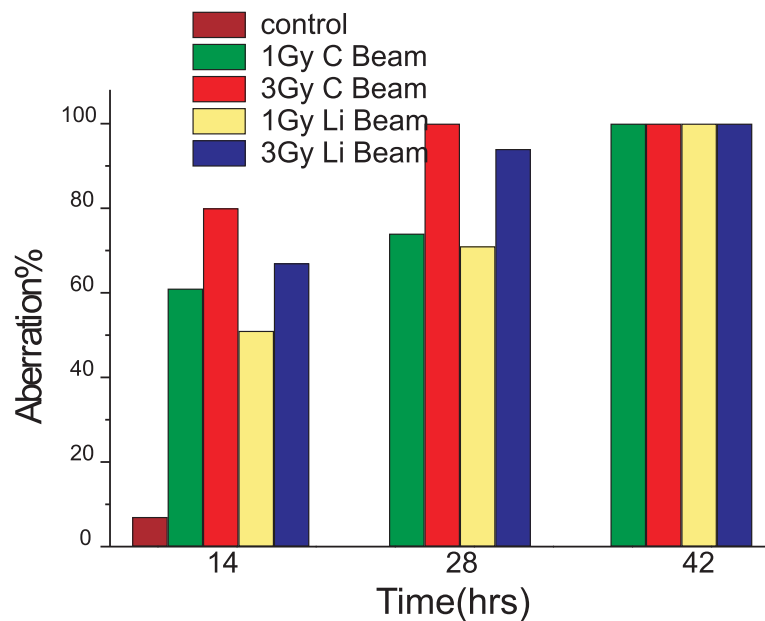


Fig. 1. Aberrant metaphase percentage in Carbon and Lithium Beam irradiated CHO cells.

Table 1: Chromosomal Aberration induced by ^{12}C beam of LET 271KeV/ μm in CHO cells harvested at 14 and 28 hrs.

Exptal Condn.	Total metaphase	Aberrant metaphase%	chrom. Exch. %	Ctd Exch%	Del %	Ctd. bk%
14 hours						
Control	109	7	0	0	7	2
1 Gy	120	61	18	8	75	24
3 Gy	119	80	32	11	103	20
GSH + 1 Gy	203	66	29	14	68	30
GSH + 3 Gy	151	77	40	15	90	32
BSO + 1 Gy	102	67	10	7	96	18
BSO + 3 Gy	110	76	29	6	127	33
28 hours						
1 Gy	81	74	25	12	105	13
3 Gy	50	100	34	20	146	20
GSH + 1 Gy	46	74	36	13	91	15
GSH + 3 Gy	38	97	39	18	155	26
BSO + 1 Gy	46	78	17	9	168	9
BSO + 3 Gy	32	100	28	16	200	19

Table 2: Chromosomal Aberration induced by ^7Li beam of LET 60KeV/ μm in CHO cells harvested at 14 and 28 hrs.

Exptal Condn.	Total metaphase	Aberrant metaphase%	chrom. Exch. %	Ctd Exch%	Del %	Ctd. bk%
14 hours						
Control	120	7	0	0	7	3
1 Gy	109	51	14	6	61	18
3 Gy	127	67	24	9	80	18
GSH + 1 Gy	92	62	24	3	64	14
GSH + 3 Gy	117	74	29	16	87	8
BSO + 1 Gy	107	55	9	9	98	8
BSO + 3 Gy	109	71	18	9	114	15

28 hours

1 Gy	21	71	19	0	110	5
3 Gy	51	94	27	14	159	27
GSH + 1 Gy	26	77	27	0	100	8
GSH + 3 Gy	36	97	33	9	169	9
BSO + 1 Gy	33	70	17	7	128	12
BSO + 3 Gy	43	91	23	2	212	23

Cell Cycle kinetics:

- We could observe delay in cell cycle after high LET Irradiation.
- Carbon Beam irradiated cells showed more delay compared to Lithium beam irradiated cells (Fig 2).
- Exogenous addition of GSH is further increasing cell cycle delay at 28 hrs harvest but at 42 hrs harvest does not show any such effect (Fig: 3 & 4).

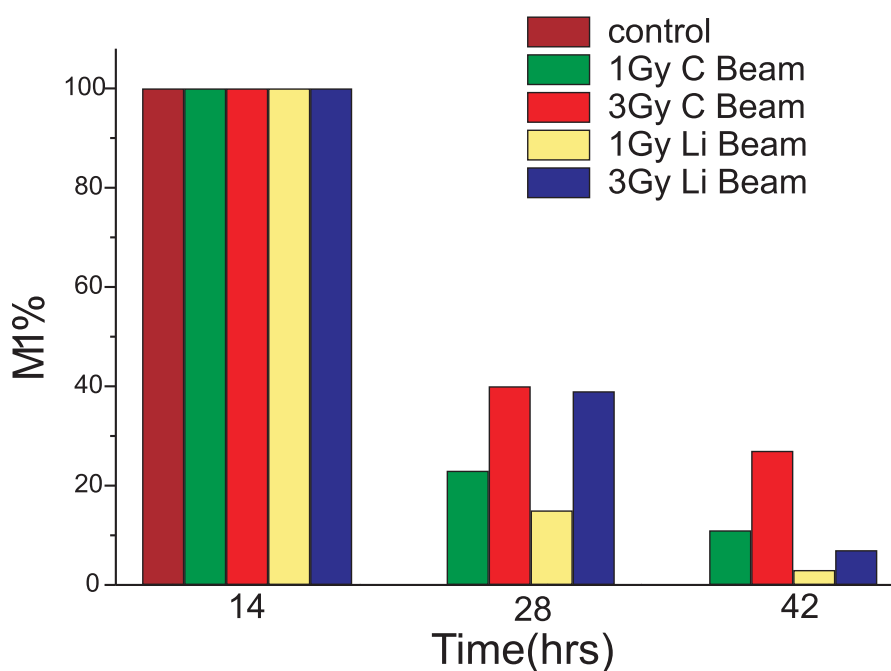


Fig. 2. Cell cycle kinetics of CHO cells irradiated with Carbon (271 KeV/ μ m) and Lithium Beam(LET 60 KeV/ μ m).

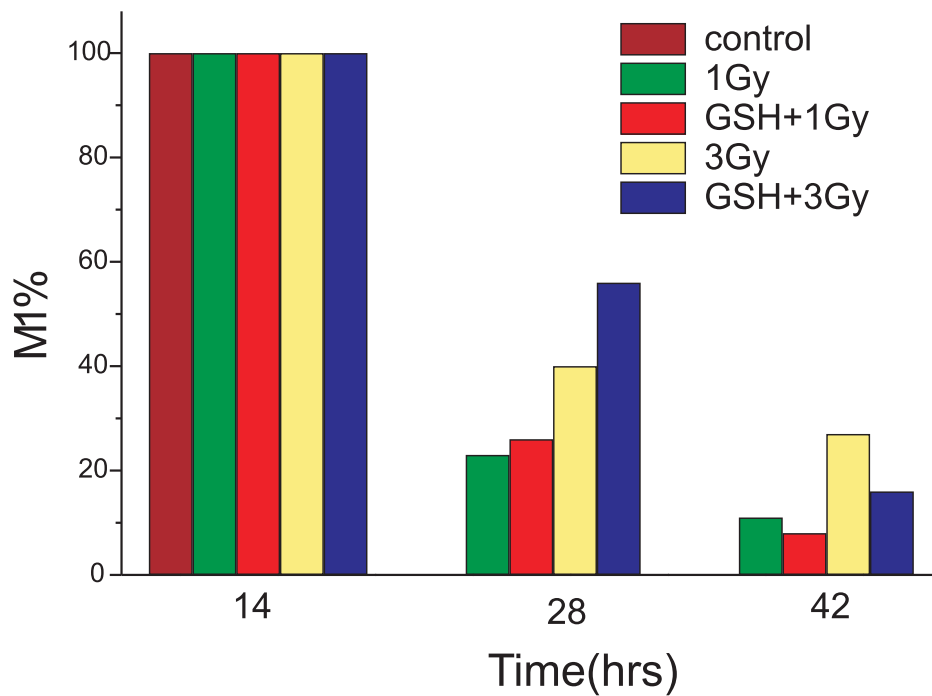


Fig. 3. Cell cycle kinetics of CHO cells with or without GSH in carbon beam Irradiated cells.

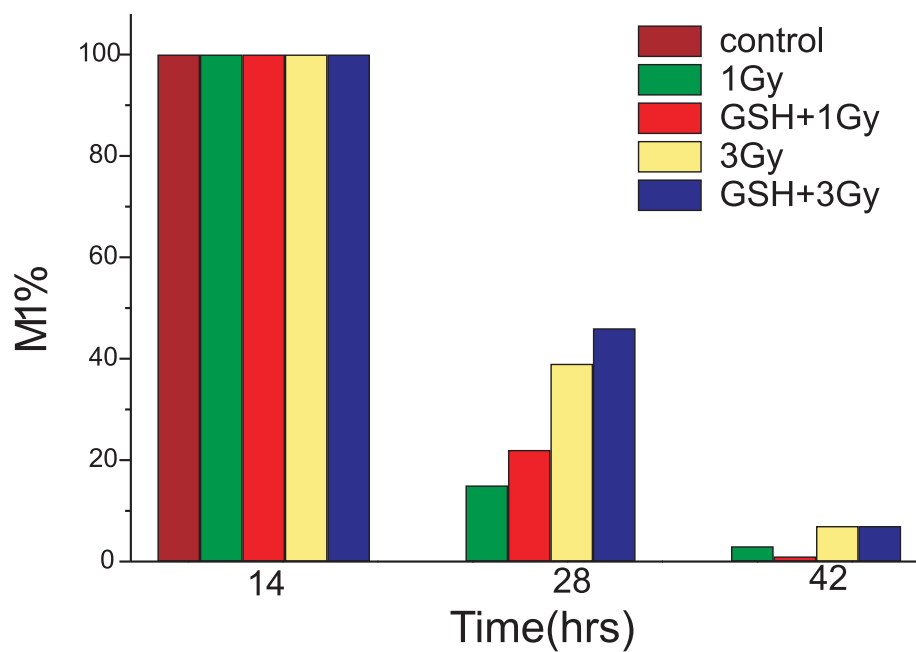


Fig. 4. Cell cycle kinetics of CHO cells with or without GSH in Lithium beam Irradiated cells.

The experiment indicates that percentage of aberrant metaphase increases with increase in LET and with sample time. A LET- and time- dependent expression of chromosomal damage can be related to differences in energy deposition of radiation types. The exposure of cells to particles results in an inhomogeneous energy deposition per cell. The inhomogeneity is determined by different number of particle hit per cell nucleus and by non uniform dose distribution inside the particle track. Cells with low number of particle traversals and correspondingly low chromosomal damage enter mitosis earlier than cells with a high number of hits and more chromosomal damage.

We can infer that GSH acting as a radioprotector against low LET radiation does not have any appreciable role to play against high LET radiation. Observed increase in exchange type of aberration in GSH treated cells explains that GSH has a role to play in DNA double strand break rejoining. Since BSO treatment to the cells is reducing exchange type of aberrations and increasing deletions, it can be concluded that GSH has role to play in DNA double strand break rejoining of the lesions produced by high LET radiation.

REFERENCES

- [1]. Clark.E.P(1986) Thiol-induced biochemical modification of chemo- and radioresponses. *Int J Radiat Oncol Biol Phys*; 12: 1121-1126.
- [2] Chattopadhyay.A.,Deb.S and Chatterjee. A. (1999) Modulation of the clastogenic activity of g-irradiation in buthionine sulfoximine mediated glutathione depleted mammalian cells. *Int J radiat Biol*; 75: 1283-1291.
- [3] Barendsen.G.W, Koot C.J, Van Kersen, Bewley D.K., Parnell C.J., Field S.B.,(1966) The effect of oxygen in impairment of the proliferative capacity of human cells in culture by ionizing radiation of different LET. *Int. J. Radiat. Biol*; 10, 317-327.
- [4] Todd P (1967) Heavy- ion irradiation of cultured human cells. *Radiat. Res; Suppl. 7*, 196-207.
- [5] Griffith, O. W. and Meister.A. (1979) Translocation of intracellular glutathione to membrane bound g-glutamyl transpeptidase activities. *Proc.Natl.Acad.Sci USA*;76,268-272.

5.4 ATOMIC PHYSICS RESEARCH

The Atomic physics research at IUAC is pursued with the ion beams from the Pelletron and the multiply charged ions from the Low Energy Ion Beam Facility.

For beam foil spectroscopy experiments with the Pelletron, the Doppler tuned spectrometer (DTS) have been tested successfully off line as well as on line in general purpose scattering chamber (GPSC). Results obtained from off line test are given in section 4.6. Back Gammon structure of cathode needs to be modified for appropriate use with the experiments. Foil translation system as well as absorber foil changing mechanism without breaking the vacuum have been installed in the GPSC. All these systems viz., DTS, foil translational system and absorber foil changing mechanism can be dismantled and reinstalled easily to facilitate other experiments in the chamber.

Atomic physics beam line as mentioned in 4.6 has been renovated so that experiments on hyperfine structure effects on K x-ray production cross section can be done in better way. Experimental set up and targets are being prepared to carry out experiments in collaboration with Panjabi University, Patiala. Charge-state fraction measurement setup using the position sensitive parallel plate avalanche counter will also be very efficient. Experiments may start as soon as users are available.

1 M normal incidence spectrometer has been made ready for optical spectroscopy experiments in the PKDELIS laboratory. We are planning to make a program for carrying out measurements relevant to astrophysics with users.

Atomic and molecular physics experiments in the low energy ion beam laboratory are in full swing. Position sensitive multi-hit time-of-flight measurement system is used to study the fragmentation dynamics of complete and incomplete fragmentation process as presented below.

5.4.1 Experimental signature on selective high-lying Rydberg states: A possible origin of Radio Recombination lines in interstellar medium

T. Nandi², Nissar Ahmad¹ and Ranjeet K. Karn²

¹Physics Dept., AMU, Aligarh

²Inter-University Accelerator Centre, Aruna Asaf Ali Marg, New Delhi 110067

Intensity plot of any transitions with time shows exponential decrease and the trend somewhat varies depending upon the complicated cascades and line-blending present in the experiment. However, appearance of a cusp-shaped structure, as normally observed in the forward scattered electron spectra in the ion-solid collisions, in the middle of a decay is beyond the current knowledge of physics. In the series of the experiments using the reliable experimental set up [1] we consistently observe such a structure (Fig. 1). Origin of the cusp-shaped structure is found to be successive cascading from the specific high-lying Rydberg levels possibly populating from the interaction of electron in the continuum with the projectile ion and the quasi free electron residing at the exit surface of the target foil. Experimental data have been analyzed in the light of a cascade model derived on the basis of ladder-like de-excitation chain and the Bethe and Salpeter hypoth-

esis on the transition probabilities. Present observations may find important implications on the origin of radio recombination lines observed from interstellar spaces.

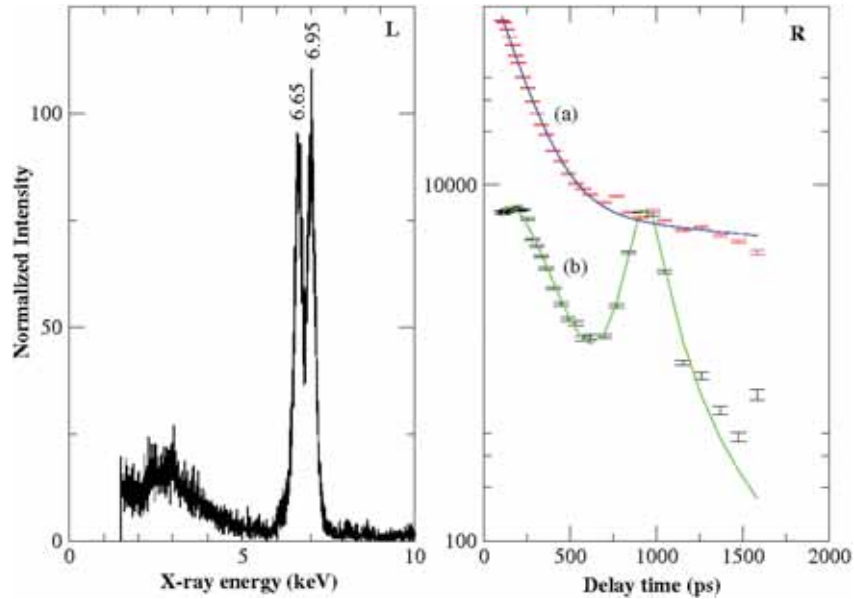


Fig. 1. L: X-ray spectrum of 164 MeV Fe beam on C foil at 946 ps delay. R: X-ray photo peak intensity plot as a function of delay times: (a) the 6.65 keV peak intensity fitted with two-exponential function and (b) the 6.95 keV peak intensity fitted with the equation having two exponential and one Lorentzian terms. The Lorentzian term represents the cusp structure.

REFERENCE

- [1] Nissar Ahmad et al Rev. Sci. Instru. 77, (2006) 033107.

5.4.2 A novel cascade model to explain the cusp structure in the decay curve

T. Nandi and Ranjeet K. Karn

Inter-University Accelerator Centre, Aruna Asaf Ali Marg, New Delhi 110067

In the series of beam-foil experiments we consistently observe a few x-ray lines appearing in the spectra that grow with time after the interactions. Intensity plot of such transitions as a function of time exhibits cusp structure on the long lived component of the decay curve.

These structures have been treated as Lorentzian profile. The centroid of such a Lorentzian profiles in Fig.1 of earlier article, gives a measure of time taken for the electrons to cascade down from the high Rydberg states in corresponding ions to low lying excited states from which emission is x-ray; viz., H-like $2p\ ^2P_{1/2, 3/2}$ states and He-like $1s2p, 2s2p, 2p^2$ and $2s^2$ levels. We have tried to estimate the quantum numbers of the high Rydberg states in H- and He-like ions in a novel way.

Within the frame work of non relativistic dipole approximation the mean lifetime for an electronic state (n and $l, l \neq 0$) in a H-like ion of nuclear charge Z [1] is given by

$$\tau(n,l) = \tau_0 \times n^3 l(l+1) / Z^4 \quad (1)$$

where $\tau_0 = 3\hbar / (2\pi\alpha^5 \mu c^2) = 93.42$ ps and μ is the reduced mass of the nucleus and an electron. Lifetime values for some high-Rydberg levels with $l=1$ are found to be close to the centroid of the Lorentzians. If such levels are populated they can end up in the ground state as large Δn transitions are more favored. However, we never observe such an x-ray line in the spectra, rather we observe $2s \ ^2S_{1/2}$ and $2p \ ^2P_{1/2,3/2}$ states decaying to the ground state. These facts suggest us that some high Rydberg states populated in our experiment are characterized by not only high n but high l also as $\Delta l > 1$ is forbidden. Hence the levels with high n and high l decay through ladder-like de-excitation chain. Beiersdorfer et al. [2] have observed already that the transition corresponding to $\Delta n \gg 1$ is negligible in the interaction of low-energy, bare, and hydrogen-like ions from EBIT with neutral gases. These facts lead us to propose a cascade model which assumes that the high (n,l) levels cascade down in succession and also satisfies the Bethe and Salpeter hypothesis [3]. Summing up the $\tau(n,l)$ values up to the final state which can emit x-ray; viz., $\tau(n=2,l=1)$ or $\tau(n=3,l=1)$ or $\tau(n=2,l=0)$ for H-like ions with the condition that $\Delta n = \Delta l = 1$, we obtain the total cascading time, $T(n,l)$ as follows:

$$T(n,l) = \sum \tau(i,j) \quad (2)$$

The $\tau(i,j)$ values for possible principal and angular momentum quantum numbers i, j have been taken from equation (1). $\tau(i,j)$ value for high (i,j) is order of magnitude greater than that for low (i,j) ; hence inaccuracy with $\tau(i,j)$ for low (i,j) does not introduce considerable error in the calculation of $T(n,l)$. It may be worth noting that only the levels with $n,l=n-1$ and $n,l=n-2$ can satisfy the above criterion and $n,l=n-1$ levels may finally end up to ground state via the $2p \ ^2P_{1/2,3/2}$ state and $n,l=n-2$ levels via the $2s \ ^2S_{1/2}$ state in the H-like ions. Similarly, this procedure has been applied to the He-like ions by assuming that the Rydberg electron is in the field of the nucleus of charge $Z-1$.

REFERENCES

- [1] Hermann Marxer and Larry Spruch, Phys. Rev. A 43 (1991) 1268.
- [2] P. Beiersdorfer et al., Astrophys. J., 549 (2001) L147.
- [3] Quantum Mechanics of one- and two-electron atoms, Eds. H.A. Bethe and E.E. Salpeter, A Plenum/Rosetta Edition, 1977. Bethe and Salpeter hypothesis states that the Einstein's A co-efficients are numerically much smaller when Δn and Δl are in opposite sense than when they are in same sense.

5.4.3 A novel technique to study atomic processes using projectile like nuclear reaction products

T. Nandi², Nissar Ahmad¹ and Ranjeet K. Karn²

¹Physics Dept., AMU, Aligarh

²Inter-University Accelerator Centre, Aruna Asaf Ali Marg, New Delhi 110067

The delayed appearance of the 6.95 and 8.06 keV peak in the beam-foil spectra with MeV ions of Fe and Ni, respectively, confirmed that these transitions are originated in the flight. Further, the beam energy used in the experiments are above the Coulomb barrier (135 MeV for

Fe on C and 149 MeV for Ni on C) and existence of the projectile-like nuclear products have been observed in the x-ray as well as the γ -spectra. Therefore, signature of the projectile-like nuclear reaction products has been observed in the x-ray as well as the γ -ray spectra [1]. The K-x-ray method [2] has been used to study heavy-ion nuclear reactions. However, the x-rays from nuclear reaction products have not yet been used to study any atomic phenomena. In the current study we have made an attempt to use such x-ray lines for the confirmation of the cusp-shaped structure in the decay curve. Typical x-ray spectra of the projectile-like ions originating from nuclear reactions of Fe at 164 MeV and Ni-experiments at 170 MeV have been shown in the Fig.1(a) and 1(c). Both the spectra clearly display a structure at the higher x-ray energy side compared to characteristic projectile x-ray lines.

Intensity of this structure in each experiment was plotted as a function of time as shown in Fig. 1(b) and 1(d). The data set in Fig.1(b) shows a few humps on the exponential curve

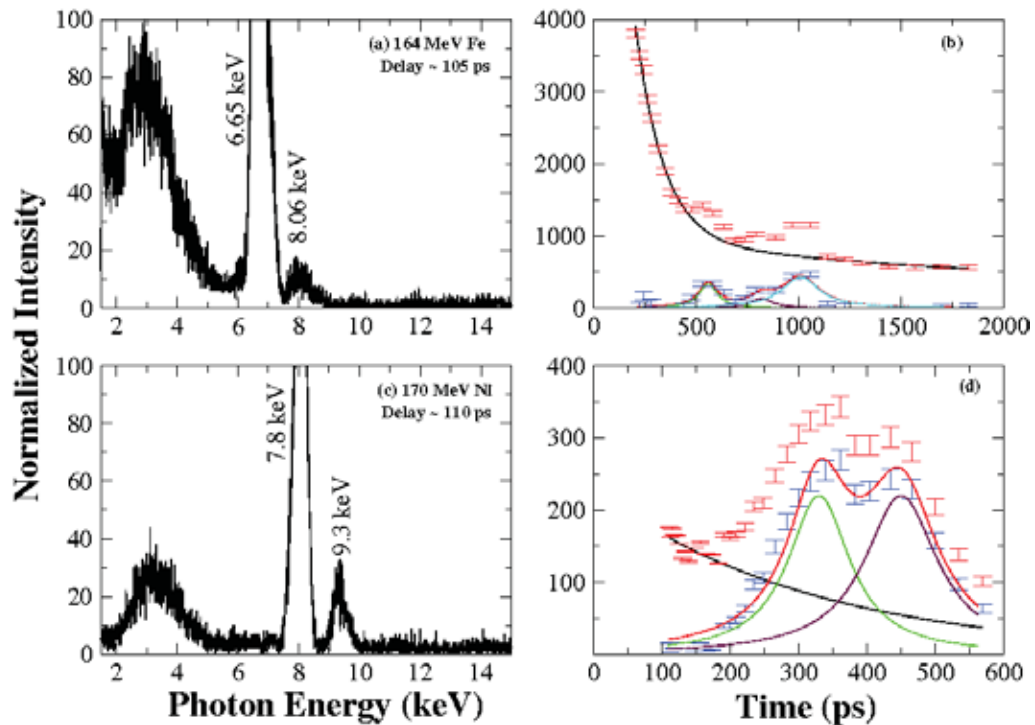


Fig. 1. Data from projectile like nuclear products: (a) X-ray energy spectrum of C-foil excited 164 MeV Fe beam. (b) Integrated counts of the broad peak from 7.5-9 keV as a function of time are shown with magenta colour and fitted with an exponential function as shown with green curve. The blue data points have been obtained by subtracting the contribution of exponential curve from the data points with magenta colour and they are fitted with an equation similar to equation (2) having three Lorentzian terms. (c) X-ray energy spectrum of C-foil excited 170 MeV Fe beam, (d) integrated counts of the broad peak from 8.6-10 keV as a function of time as shown with magenta colour and background is fitted with an exponential function as shown with green curve. The blue data points have- been obtained by subtracting the contribution of exponential background from the data points with magenta colour and they are fitted with equation (2).}

representing the decay of Paschen- β M2 and Lyman- β M1 x-ray lines. The lifetimes for the corresponding upper states found are 137 ± 7 and 3.09 ± 0.3 ns, respectively. By subtracting the exponential curve shown with solid line gives a structure which has been fitted with an equation consisting of three Lorentzian terms to obtain the centroids. Similar procedure has also been applied on the time spectra obtained in the Ni experiments. Decay curve of this peak shows two cusp-shaped structures, which is fitted with two Lorentzian terms. The centroids obtained have been listed in Table I.

Table I: Assignment of the high-lying Rydberg states which originate the final x-ray transitions.

Ion Beam	Peak (keV)	Ionic Levels	Decay Channel	Observed Centroid (ps)	Theory T(n,l) ps	Binding Energy (eV)
164 MeV ^{56}Fe	8.06	Ni^{27+}	(M1) Ly α	820 ± 82	826 (18,16)	32.9
	8.6	Cu^{28+}	(E1) Ly α	560 ± 56	586 (17,16)	39.6
156 MeV ^{58}Ni	9.3	Zn^{29+}	(E1) Ly α	345 ± 35	357 (16,15)	47.8
160 MeV ^{58}Ni	9.3	Zn^{29+}	(E1) Ly α	355 ± 35	357 (16,15)	47.8
163 MeV ^{58}Ni	9.3	Zn^{29+}	(E1) Ly α	340 ± 34	357 (16,15)	47.8
170 MeV ^{58}Ni	9.3	Zn^{29+}	(E1) Ly α	350 ± 35	357 (16,15)	47.8

Although x-ray energy spectrum shown in Fig.1(a) does not resolve the structure at 8-8.7 keV, the time spectrum exhibits three humps on an exponential curve. This implies that the composite structure belongs to three different lines. Using theoretical transition energies [3] and the centroid of the humps we attribute the structure consists of three peaks at 8.1, 8.25 and 8.6 keV for Ly- α in H-like Ni, Ly- β in H-like Fe and Ly- α in H-like Cu, respectively. Ni and Cu ions are products from nuclear reactions of Fe on C. Centroids obtained for each hump has been listed in table I and we assign the original high-lying Rydberg levels using the cascade model simulation. Similarly, the feature at 9-9.8 keV in the x-ray energy spectrum at 170 MeV Ni shows two humps in the time spectrum (above article). Accordingly, the structure is assigned to 9.3 and 9.59 keV lines attributing to Ly- α in H-like Zn and Ly- β in H-like Ni, respectively. Table I shows the centroids of these two humps and most probable origin of these two x-ray lines.

REFERENCES

- [1]. Nissar Ahmad, Ranjeet K. Karn, Pan Marketos and T. Nandi, Peculiar time dependence of unexpected lines in delayed beam-foil X-ray spectra of V, Fe and Ni, Nucl. Instr. Meth. B 233 191 (2005).
- [2]. Wilschut H.W. et al, Selection of heavy ion reaction channels via particle K X-ray coincidences, Phys. Lett. B123 173 (1983).
- [3] <http://physics.nisit.gov/cgi-bin/ASD/lines.ph>.

5.4.4 Atomic and Molecular Physics Experiments at LEIBF

C P Safvan, Sankar De, Jyoti Rajput and A. Roy

Inter-University Accelerator Centre, Aruna Asaf Ali Marg, New Delhi 110067

Using the low energy ion beam facility, experiments were conducted to study the dissociation dynamics of multiply charged molecules. The investigations studied several aspects of ion induced fragmentation, including target excitation and Auger emission, intramolecular bond rearrangements and vibrational flopping in dissociating molecules. The experiments used the time of flight apparatus coupled with position sensitive detectors and post collision charge state analyser to determine the fragmentation patterns and dynamics.

Target molecules, in the form of an effusive gas jet were made to interact with multiply charged Ar projectiles. The fragmented molecular ions were detected with a position sensitive time of flight mass spectrometer and event by event analysis coupled with coincidence map techniques were used for data interpretation. From the time of flight spectra, the following observations have been made:

- (i) Target excitation and Auger emission in N_2 : Signature of target excitation and Auger emission was discovered in the collision of Ar ions with Nitrogen targets. The kinetic energy releases in the fragmentation of Nitrogen molecules indicate that N_2^{5+} ions are formed in core excited states.
- (ii) Intra molecular bond rearrangement has been studied in methanol where the formation of H_3^+ from CH_3OH has been observed. Coupled with ab-initio potential energy surface calculations have explained the formation mechanism.
- (iii) In the dissociation of multiply charged acetylene, we have detected signature of vibrationally excited multiply charged acetylene ions that show a bent structure of (normally linear) acetylene before dissociation.

From the TOF spectrum of methanol molecules (fig.1), a wide range of dissociation products starting from undissociated molecular ions (CH_3OH^+), fragments losing a hydrogen atom due to breakage of C-H and O-H bonds (CH_2OH^+ , $CHOH^+$, COH^+ , CO^+) to complete rupture of C-O skeleton producing charged atomic species like C_q^+ and O_q^+ (where q varies from 1 to 3) were observed. The breakage of one or many of the C-H bonds or the O-H bond in the multiply ionized methanol results in the formation of H, H_2^+ , and H_3^+ . It is observed that H_3^+ is ejected from doubly charged methanol ions through two-body Coulomb explosion process ($CH_3OH^{2+} \rightarrow H_3^+ + COH^+$) after rearrangement has taken place. On the other hand, H_2^+ is formed due to both two-body ($CH_3OH^{2+} \rightarrow H_2^+ + CHOH^+$) and three- (or more) body ($CH_3OH^{2+} \rightarrow H_2^+ + COH^+ + H$) dissociation pathways.

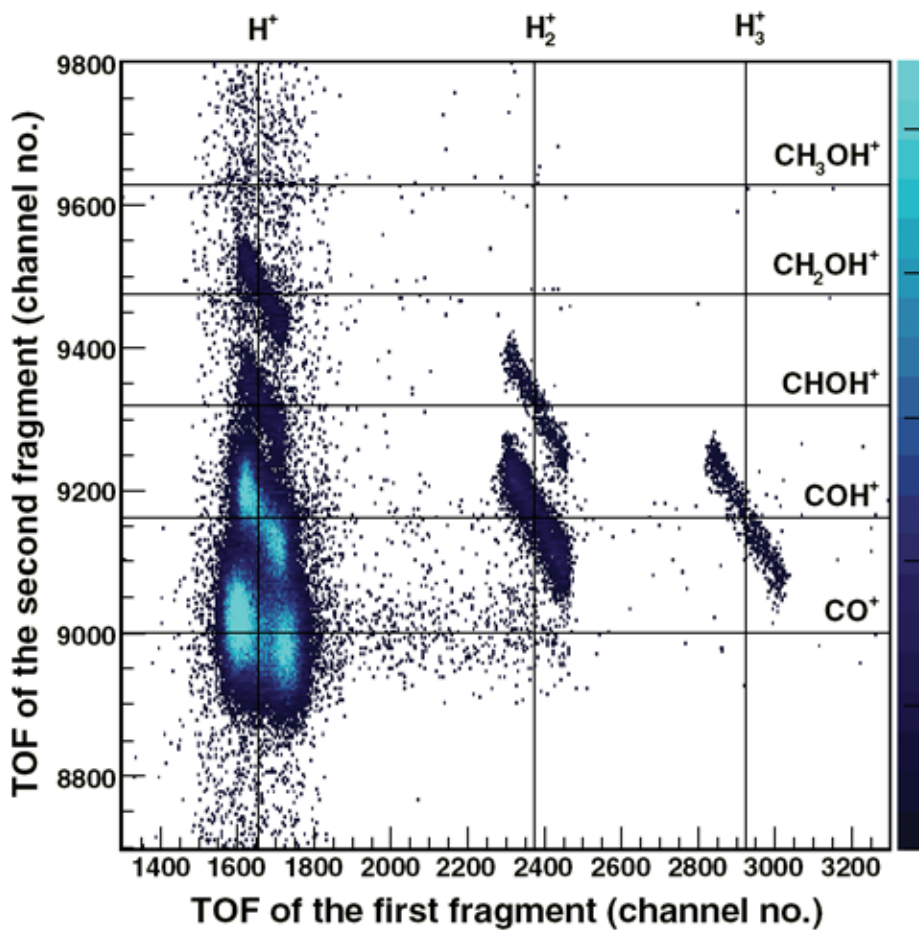


Fig. 1. Coincidence map corresponding to the fragmentation pathways $\text{CH}_3\text{OH}^{2+} \rightarrow \text{H}_m^+ + \text{CH}_{(3-m)}\text{OH}^+$ ($m = 1-3$): formation of H_2^+ and H_3^+ .